EXPERIMENTAL INVESTIGATIONS ON ELECTRO DISCHARGE SURFACE MODIFICATION OF DIE STEEL P20+Ni

A Thesis submitted to Gujarat Technological University

for the Award of

Doctor of Philosophy

in

Mechanical Engineering

by

Ramdatti Jayantigar Lakhmangar

Enrollment No. 149997119023

under the supervision of

Prof. A. V. Gohil

GUJARAT TECHNOLOGICAL UNIVERSITY

AHMEDABAD

December, 2020

EXPERIMENTAL INVESTIGATIONS ON ELECTRO DISCHARGE SURFACE MODIFICATION OF DIE STEEL P20+Ni

A Thesis submitted to Gujarat Technological University

for the Award of

Doctor of Philosophy

in

Mechanical Engineering

by

Ramdatti Jayantigar Lakhmangar

Enrollment No. 149997119023

under the supervision of

Prof. A. V. Gohil

GUJARAT TECHNOLOGICAL UNIVERSITY

AHMEDABAD

December, 2020

DECLARATION

I declare that the thesis entitled **"Experimental Investigations on Electro Discharge Surface Modification of Die Steel P20+Ni"** submitted by me for the degree of Doctor of Philosophy is the record of research work is carried out by me during the period from **2014** to **2019** under the supervision of **Prof. A. V. Gohil, Professor and Head, Production Engineering Department, Shantilal Shah Government Engineering College, Bhavnagar, Gujarat** and this has not formed the basis for the award of any degree, diploma, associateship, fellowship, titles in this or any other University or other institution of higher learning.

I further declare that the material obtained from other sources has been duly acknowledged in the thesis. I shall be solely responsible for any plagiarism or other irregularities if noticed in the thesis.

Signature of the Research Scholar:  Date: 05/12/2020

Name of Research Scholar: Ramdatti Jayantigar Lakhmangar (Enroll. No. 149997119023)

Place: Bhavnagar

CERTIFICATE

I certify that the work incorporated in the thesis **"Experimental Investigations on Electro Discharge Surface Modification of Die Steel P20+Ni"** submitted by **Ramdatti Jayantigar Lakhmangar (Enrollment No. 149997119023)** was carried out by the candidate under my supervision/guidance. To the best of my knowledge: (i) The candidate has not submitted the same research work to any other institution for any degree/diploma, Associateship, Fellowship or other similar titles (ii) The thesis submitted is a record of original research work done by the Research Scholar during the period of study under my supervision, and (iii) The thesis represents independent research work on the part of the Research Scholar.

Signature of Supervisor:  …… Date: 05/12/2020

Name of Supervisor: Prof. A. V. Gohil

Place: Bhavnagar

Course-work Completion Certificate

This is to certify that **Mr. Ramdatti Jayantigar Lakhmangar** enrollment no. **149997119023** is a Ph. D. scholar enrolled for the PhD program in the branch **Mechanical Engineering** of Gujarat Technological University, Ahmedabad.

(Pleases tick the relevant option(s))

☐ He has been exempted from the course-work (successfully completed during M. Phil Course)

☐ He has been exempted from Research Methodology Course only(Successfully completed during M. Phil Course)

[✓] He has successfully completed the PhD course work for the partial requirement for the award of PhD Degree. His/ Her performance in the course work is as follows-

Grade Obtained in Research Methodology (PH001)	Grade Obtained in Self-study Course (Core Subject) (PH002)
BC	AB

Supervisor's Sign: 

Name of Supervisor: **Prof. A. V. Gohil**

Originality Report Certificate

It is certified that PhD Thesis titled **"Experimental Investigations on Electro Discharge Surface Modification of Die Steel P20+Ni"** by **Ramdatti Jayantigar Lakhmangar (Enrollment No. 149997119023)** has been examined by us. We undertake the following:

a. The thesis has significant new work/knowledge as compared already published or is under consideration to be published elsewhere. No sentence, equation, diagram, Table, paragraph or section has been copied verbatim from previous work unless it is placed under quotation marks and duly referenced.
b. The work presented is original and own work of the author (i.e. there is no plagiarism). No ideas, processes, results or words of others have been presented as Author own work.
c. There is no fabrication of data or results which have been compiled/analyzed.
d. There is no falsification by manipulating research materials, equipment or processes, or changing or omitting data or results such that the research is not accurately represented in the research record.
e. The thesis has been checked using **Turnitin** (copy of originality report attached) and found within limits as per GTU Plagiarism Policy and instructions issued from time to time (i.e. permitted similarity index <=25%).

Signature of the Research Scholar:  Date: 05/12/2020

Name of Research Scholar: **Ramdatti Jayantigar Lakhmangar**

Place: **Bhavnagar**

Signature of Supervisor:  …… Date: 05/12/2020

Name of Supervisor: **Prof. A. V. Gohil**

Place: **Shantilal Shah Engineering College, Bhavnagar**

turnitin

Digital Receipt

This receipt acknowledges that Turnitin received your paper. Below you will find the receipt information regarding your submission.

The first page of your submissions is displayed below.

Submission author:	Jl Ramdatti
Assignment title:	LHSU
Submission title:	EXPERIMENTAL INVESTIGATIONS..
File name:	JLR_thesis.pdf
File size:	15.15M
Page count:	205
Word count:	60,481
Character count:	285,972
Submission date:	22-Jul-2019 10:13PM (UTC+0530)
Submission ID:	1154075457

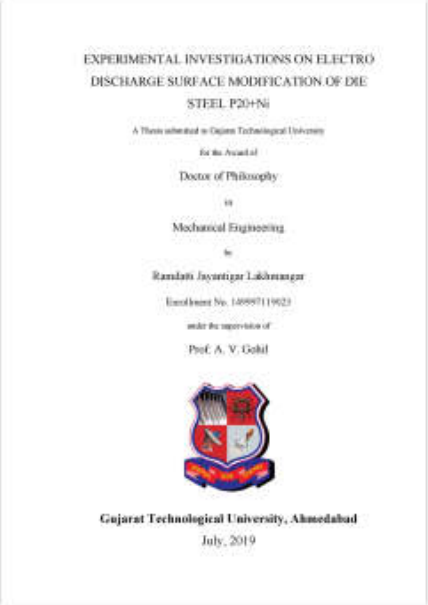

EXPERIMENTAL INVESTIGATIONS ON ELECTRO DISCHARGE SURFACE MODIFICATION OF DIE STEEL P20+Ni

A Thesis submitted to Gujarat Technological University

for the Award of

Doctor of Philosophy

in

Mechanical Engineering

by

Ramdatti Jayantigar Lakhmangar

Enrollment No. 149997119023

under the supervision of

Prof. A. V. Gohil

Gujarat Technological University, Ahmedabad

July, 2019

EXPERIMENTAL INVESTIGATIONS ON ELECTRO DISCHARGE SURFACE MODIFICATION OF DIE STEEL P20+Ni

ORIGINALITY REPORT

10%	4%	6%	10%
SIMILARITY INDEX	INTERNET SOURCES	PUBLICATIONS	STUDENT PAPERS

PRIMARY SOURCES

1	"Advanced Engineering Optimization Through Intelligent Techniques", Springer Science and Business Media LLC, 2020 Publication	3%
2	ethesis.nitrkl.ac.in Internet Source	1%
3	Submitted to Symbiosis International University Student Paper	1%
4	baadalsg.inflibnet.ac.in Internet Source	1%
5	Submitted to Pacific University Student Paper	1%
6	Submitted to IIT Delhi Student Paper	1%
7	pubs.sciepub.com Internet Source	1%

Exclude quotes	On	Exclude matches	< 1%
Exclude bibliography	On		

PhD THESIS Non-Exclusive License to

GUJARAT TECHNOLOGICAL UNIVERSITY

In consideration of being a PhD Research Scholar at GTU and in the interests of the facilitation of research at GTU and elsewhere, I **Ramdatti Jayantigar Lakhmangar** having (Enrollment No**: 149997119023**) hereby grant a non-exclusive, royalty-free and perpetual license to GTU on the following terms:

a) GTU is permitted to archive, reproduce and distribute my thesis, in whole or in part, and/or my abstract, in whole or in part (referred to collectively as the "Work") anywhere in the world, for non-commercial purposes, in all forms of media;
b) GTU is permitted to authorize, sub-lease, sub-contract or procure any of the acts mentioned in paragraph (a);
c) GTU is authorized to submit the Work at any National / International Library, under the authority of their "Thesis Non-Exclusive License";
d) The Universal Copyright Notice (©) shall appear on all copies made under the authority of this license;
e) I undertake to submit my thesis, through my University, to any Library and Archives. Any abstract submitted with the thesis will be considered to form part of the thesis.
f) I represent that my thesis my original work, does not infringe any rights of others, including privacy rights, and that I have the right to make the grant conferred by this non-exclusive license.
g) If third party copyrighted material was included in my thesis for which, under the terms of the Copyright Act, written permission from the copyright owners is required, I have obtained such permission from the copyright owners to do the acts mentioned in paragraph (a) above for the full term of copyright protection.
h) I retain copyright ownership and moral rights in my thesis and may deal with the copyright in my thesis, in any way consistent with rights granted by me to my University in this non-exclusive license.
i) I further promise to inform any person to whom I may hereafter assign or license my copyright in my thesis of the rights granted by me to my University in this nonexclusive license.

j) I am aware of and agree to accept the conditions and regulations of PhD including all policy matters related to authorship and plagiarism.

Signature of the Research Scholar: 

Name of Research Scholar: **Mr. Ramdatti Jayantigar Lakhmangar**

Date: 05/12/2020 Place: Bhavnagar

Signature of Supervisor: 

Name of Supervisor: **Prof. A. V. Gohil**

Date: 05/12/2020 Place: Shantilal Shah Engineering College, Bhavnagar

Seal:

Thesis Approval Form

The viva-voce of the PhD Thesis submitted by **Mr. Ramdatti Jayantigar Lakhmangar** (Enrollment No. **149997119023**) entitled "**Experimental Investigations on Electro Discharge Surface Modification of Die Steel P20+Ni**" was conducted on **19/12/2020 (Saturday)** at Gujarat Technological University.

(Please tick any one of the following options)

[✓] The performance of the candidate was satisfactory. We recommend that he be awarded the PhD degree.

☐ Any further modifications in research work recommended by the panel after 3 months from the date of first viva-voce upon request of the Supervisor or request of Independent Research Scholar after which viva-voce can be re-conducted by the same panel again

(Briefly specify the modifications suggested by the panel)

☐ The performance of the candidate was unsatisfactory. We recommend that he should not be awarded the PhD degree.

(The panel must give justifications for rejecting the research work)

Supervisor: Prof. A. V. Gohil

External Examiner 1: Prof. Dixit Garg

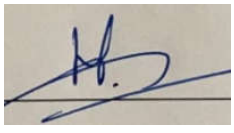

External Examiner 2: Prof. Vimlesh Soni

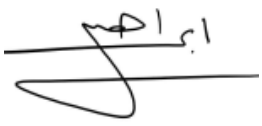

External Examiner 3: Prof. Ibrahem Maher

ABSTRACT

Electrical discharge machine (EDM) has proven itself as one of the most popular, widely accepted and versatile unconventional machining for die making, automobile, toolmaking, marine and defence industries. EDM is also used for developing complex profile in a electrically conductive materials irrespective of hardness. The process is versatile for machining a very thin and fragile sections without contact between tool and work material.

Though EDM is mainly used for machining "difficult to machine" metals particular in the mould and die making industries, some characteristics of it indicate its ability in the area of surface modification. The discrete electrical discharge between tool and work material generates very high temperature (8000 to 12000 °C), able to melting and vaporize work material and partially electrode material. The finding of optimum levels of process parameters helps to transfer tool material and carbon element from hydrocarbon dielectric to work surface. This surface alloying ability of EDM can be used to deposit desired electrode elements on the work material. These transfer tool elements were observed either in free form or in carbide form. The carbide formation can be occur due to bonding between tool elements and dissociated carbon from hydrocarbon dielectric at high temperature. The favorable chemical composition on machined surface leads to deliver desired mechanical and physical properties.

No work related to surface modification of P20+Ni die steel using EDM has been observed during the rigorous study of literature. Similarly, no work reported previously with comperable compositions and compaction pressure of P/M electrode. The experiments were performed on P20+Ni steel, which is mainly used as die and mould material for composite plastic products. The electrodes used for experimentation were manufactured through powder metallurgy (P/M) process. Electrodes were manufactured using three metallic powders such as copper (75% of wt), tungsten (23% of wt) and silicon (2% of wt). The present experimental work has been carried out to investigate favorable machining conditions, which enables to deposit tool elements on work surface.

The process parameters, which greatly influence the performance are selected on the bases of results of pilot experiments. Experimental matrix for pilot study was derived using Taguchi's L9 orthogonal array. Cutting parameters such as compaction pressure, peak current, and pulse on time are used to study its effects on output measures. To confirm material migration from electrode and variation in compositions of machined surface,

selected samples were analyzed using SEM, EDS and XRD. Levels of parameters for pilot experimentations were decided based on regorous literature review. Further use of EDM Handbook and results of several trial runs also considered for fixing levels of pilot experiments. The levels of input variables for the main experiments were decide based on the results of pilot experiments.

The main experiments were designed as per second-order central composite rotatable design (CCD) using response surface methodology. The total 30 number of experiments were performed according to the design matrix. Variations in input process parameters such as compaction pressure (C_p), peak current (I_p), pulse on time (T_{on}) and duty cycle (τ) were used to measure its effects on material removal rate (MRR), tool wear rate (TWR), surface roughness (SR), and microhardness (MH). The results of responses were analyzed using statistical software design expert 10. ANOVA for MRR, TWR, SR, and MH was performed to find contributions of individual parameters. Peak current was observed most significant parameters for all responses. More than 300% improvements in microhardness of machined surface was observed with P/M electrode. The scanning electron microscope was used to study the microstructure of selected machined samples. Results of SEM indicates defects free multi-layered recast surface. A very few microcracks were observed at high peak current and pulse on time. EDS and XRD analysis confirm the migration of electrode elements on the work material. Formation of various phases such as WC, W_2C, and SiC was observed during XRD analysis. Improvement in carbon percentage of machined surface was due to pyrolysis of hydrocarbon oil. Formation of carbide and an increase in carbon percentage on the machined surface will lead to significant improvement in microhardness.

Objectives of responses (maximize MRR and MH with minimum TWR and SR) were conflicting in nature, hence multi-objective optimization technique "composite desirability" approach is used to obtain a single set of input parameters. Predicted result of responses were confirmed with the experimental result.

Finally, it is concluded that the efforts to modify the surface of P20+Ni steel using EDM is technically feasible. Significant improvement in surface compositions and hence surface properties is possible with P/M electrode without any major alterations in the machine. Improvements in surface hardness of machined surface shall lead to the maximum working life of die and press tool.

Acknowledgments

I express my deep sense of gratitude and thanks to my revered guide **Prof. A. V. Gohil,** Professor and Head of Production Engineering Department, S. S. Engineering College, Bhavnagar, Gujarat, for his sincere and invaluable guidance, suggestions and sympathetic attitude which inspired me to submit this thesis report in the present form. His deep insights into the problem and ability to provide guidance and solutions have been of immense value in improving the quality of my research work at all stages.

I would like to extend gratitude to my DPC members, **Dr. K. G. Dave** and **Dr. R. L. Jhala**, for their deep involvement, invaluable help, guidance, and words of inspiration at every stage of this work.

I am indebted to the college authorities of Government Engineering College-Bhavnagar for providing me a workshop, laboratory and computer facilities required for this work. I am grateful to **Mr. A. G. Kunte** (Head of Production Engineering Department, GEC-Bhavnagar) who was always so willing to help me in various activities related to this thesis work. Special thanks to **Mr. L. D. Siddhpura** and **Mr. D. V. Rathod** for helping me during operating the EDM machine and supporting for various experimental works.

I express my love and gratitude to my wife **Sonal** and Son **Viraj** for their affectionate, patience and personal sacrifices, which enabled me to pursue my studies. I take this opportunity to express my respect and thankfulness to my parents who actually taught me how to learn.

A special thanks also to my dear friend **Mr. D. N. Gamit** and **Mr. S. R. Vaghasiya** for his continuous technical support and contribution to make the quality of the work better. I am also thankful to the Managing Director, TCR Advanced Engineering Pvt Ltd, Vadodara, for extending their utmost cooperation during the different metallurgical testing.

At last but not least, I would like to thank Almighty for not letting me down at the time of crisis and showing me the silver lining in the dark clouds.

List of Contains

List of Abbreviations

EDM	Electrical Discharge Machining
ANOVA	Analysis of Variance
DC	Direct Current
R-C	Resister-Capacitance
HAZ	Heat Affected Zone
RSM	Response Surface Methodology
MRR	Material Removal Rate
TWR	Tool Wear Rate
SR	Surface Roughness
MH	Microhardness
DOE	Design of Experiments
F-test	Lack of Fit Test
MSD	Mean Square Deviation
CCD	Central Composite Design
P/M	Powder Metallurgy
SS	Sum of Squares
OA	Orthogonal Array
S/N	Signal-to-Noise Ratio
SEM	Scanning Electron Microscope
EDS	Energy Dispersive Spectrometry
XRD	X-ray Diffraction
MS	Mean Square (Variance)
RSM	Root Mean Square
df	Degree of Freedom
DX 10	Design Expert 10

List of Symbols

Symbol	Contain
C_p	Compaction pressure, kg/cm^2
I_p	Peak current, Ampere
T_{on}	Pulse on time, μs
τ	Duty cycle, %
VHN	Vickers hardness number
R_a	Average surface roughness value, μm
OA	Orthogonal array
A	Compaction pressure, kg/cm^2
B	Peak current, Ampere
C	Pulse on time, μs
D	Duty cycle, %
P/M	Powder metallurgy
Cu	Copper
W	Tungsten
Si	Silicon
SS	Sum of squares
CCD	Central composite design
Wt%	Weight percentage
ρ	Density, kg/m^3
V	Discharge voltage
T_{off}	Pulse off time, μs
W_{bm}	Weight of workpiece before machining in gm
W_{am}	Weight of workpiece after machining in gm
T_m	Total machining time in minutes
W_{tb}	Weight of tool before machining in gm
W_{ta}	weight of tool after machining in gm
λ	Wavelength of the x-ray
θ	Scattering angle of the x-ray
ε	Fitting error for ith observation
D	Composite desirability
T_i	Target value for ith response

L_i	Lowest acceptable value for i^{th} response
H_i	Highest acceptable value for i^{th} response
d_i	Desirability for i^{th} response
w_i	Weight of desirability function of i^{th} response
WC	Tungsten carbide
SiC	Silicon carbide

List of Figures

List of Tables

List of Appendices

CHAPTER – 1

INTRODUCTION

Since the last decade use of high strength high temperature (HSHT) alloys in various engineering application has been continuously increasing. Further, day to day advancement in various technologies have been demanding to develop hard and difficult to machine materials [1]. The shaping of such alloys is a challenging task for manufacturing industries. Various un-conventional machining processes such as EDM, WEDM, ECM, AJM, USM, etc have been widely used for machining hard metals and alloys in industries. Electrical discharge machining (EDM) is one of the most popular and widely used un-conventional machining processes particularly for die and tool making industries [2]. During the production of components from hard alloy on press tool, the surface of the die and punch exposed severe conditions due to high temperature, pressure and abrasion wear. Hence, the enhancement of die and punch life is very essential for manufacturing industries. Various secondary surface treatments such as physical vapour deposition (PVD), chemical vapour depositions (CVD), electroplating, plasma arc coating etc have been carried out to enhance die and press tool life. However, these secondary surface treatments are very costly and time consuming with several limitations [3-4].

Besides the EDM process is capable of shaping difficult to machine material, attempts have been made by various researchers to explore EDM has a surface modification process. Researchers are continuously exploring different ways to modify/alter worksurface during EDM to create a hard layer on the surface and enhance the working life of die and press tool [5]. During the shaping of hard alloys on press tool retention of dimensional accuracy and surface qualities at very high temperature is most important. Further, in different application like aerospace, it is decided to have different surface properties at different locations of components [6]. The main purview of surface alloying/modification may be:

1. Modify the surface characteristics of work material by just changing the process parameters without altering the existing process.

2. Improve the microstructure of work surface due to the changing rate of melting and cooling.
3. Formation of hard constituents such as carbide, nitride on work surface.

Discrete electric discharge between electrode and work material generate the high-intensity spark which is capable to remove material from a workpiece. Various electrically conductive materials such as copper, copper-tungsten, graphite etc are used as EDM electrode. The process is capable to generate cavity as the shape of the electrode. There is no physical contact between tool and electrode and hence the process is capable of machine very hard and fragile components. Very high temperature (8000-12000 °C) at point of discharge is capable to melt and vaporize work material, tool electrode and dielectric. The process is performed in the presence of the dielectric. Variation in input process parameters have a greater impact on surface qualities and dimensional accuracy obtained during machining [7-8].

Due to a very high temperature in the area of discharge, the process is capable to melt and vaporize electrode material also with the work material. Most of the eroded material is flushed away by a dielectric; however, few of them get deposited back on the work surface as well as on the electrode surface. Presence of electrode elements on the work surface and vice versa has been observed by various researchers during surface analysis. Migration of electrode constituents and dissociated carbon elements from dielectric have been observed on the machined surface during the process performed at appropriate conditions [9]. Improvements in carbon percentage of the machined surface have been reported due to migration of dissociated carbon elements from dielectric either in free or carbide form [10].

1.1 NEED FOR SURFACE MODIFICATION

Geometrical and physical aspects of dies are playing a vital role in qualities and dimensional accuracies of components produced. The working condition of die not only influences the appearance and surface qualities of products but also is greatly concerned with the input process parameters of the manufacturing process. Therefore surface alloying/surface coating is very necessary to enhance the working life of die [11]. In simple words, surface modification may be defined as to develop new surface over a conventional surface with desired surface properties. It is also termed as variation in physical, chemical or biological characteristics of the material which completely differs from original surface metallurgy. The modified surface layer has greater metallurgical

similarities as compared to the surface coating on the metal substrate [12]. The surface alloying process is helpful to:

- Develop wear resistance, indentation and erosion resistance.
- Improve lubrication qualities and minimize friction of the surface.
- Develop corrosion and oxidation resistance.
- Develop fatigue resistance.

A larger number of engineering components has been failed due to abrasion, wear, corrosion and fatigue. Improvements in working life of such components are possible due to selecting an appropriate surface modification phenomenon. The vast choice is available to improve surface qualities mechanically for various mechanically operated components. Selection of appropriate surface alloying techniques depends on several input factors such as performance requirements of components, types of failure mechanism, types of material and working environments [13]. It is necessary to introduce desired alloying elements in free form or phase on the machined surface only rather than base material because of the following reasons:

1. It is important to enhance physical and mechanical properties at the point of contact rather than the whole mass, which will substantially increase the material cost.
2. The presence of alloying elements such as Mn, Cr, W, Mo, V and Ti in base material greatly affects the performance of the heat treatment process. The process of conversion of pearlite to austenite during heat treatment became slow. Larger proportions of austenite due to improvement instability is observed in place of martensite, hence it is desired to introduce required alloying elements after completion of the heat treatment process.
3. It is very difficult or sometimes not possible to add desired alloying elements during a molten state of the whole mass.

There are various surface modification processes such as physical vapour deposition (PVD), chemical vapour deposition (CVD), plasma spraying, nitriding, carburizing, electroplating, etc used in mould and die making industries. Figure 1.1 represents a categorized view of various conventional surface modification processes.

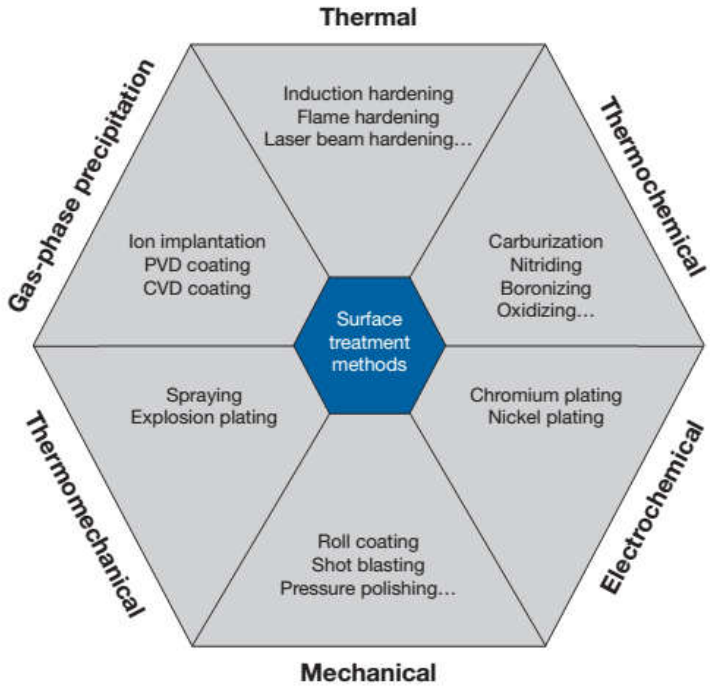

Figure 1.1 Different conventional methods for surface modification treatments [14]

However, all these processes are secondary surface treatment processes and it will perform on finished components. A substantial amount of cost and time will need to perform secondary surface treatments. There is a number of limitations in the various surface modification process. Electroplating can be applied for certain metals only as well as ample time is required for the process. Physical vapour deposition process performed under vacuum condition only; hence it is viable only for small-size components. In chemical vapour deposition process sometimes chemical reaction between the heated metal substrate and gases are poor and hence more time required completing the process. Laser coating also covers a very small area as well as it is a very costly process. Hence, if a surface modification can be possible during machining of die on EDM, it will reduce a substantial amount of cost and time particularly for small scale industries [15-16].

1.2 BASICS OF ELECTRICAL DISCHARGE MACHINING PROCESS

EDM is an advanced non-traditional machining process mainly used for hard and difficult to machine materials. The process is helpful for machine electrically conductive materials. The process is mainly used in tool and die making industries to produce complex and intricate shape which is difficult to produce using conventional machining processes. Metals such as hardened tool-steels, Kovar, Inconel and titanium are easily machined using EDM [17].

Electrical discharge machine is categorized under thermoelectric advanced machining process. Material is removing due to high heat deliver from sparking action. The process is capable to generate a replica of the tool on the work surface without physical contact. The process is performed under submerged conditions in dielectric [18]. The working layout of EDM is shown in Figure 1.2.

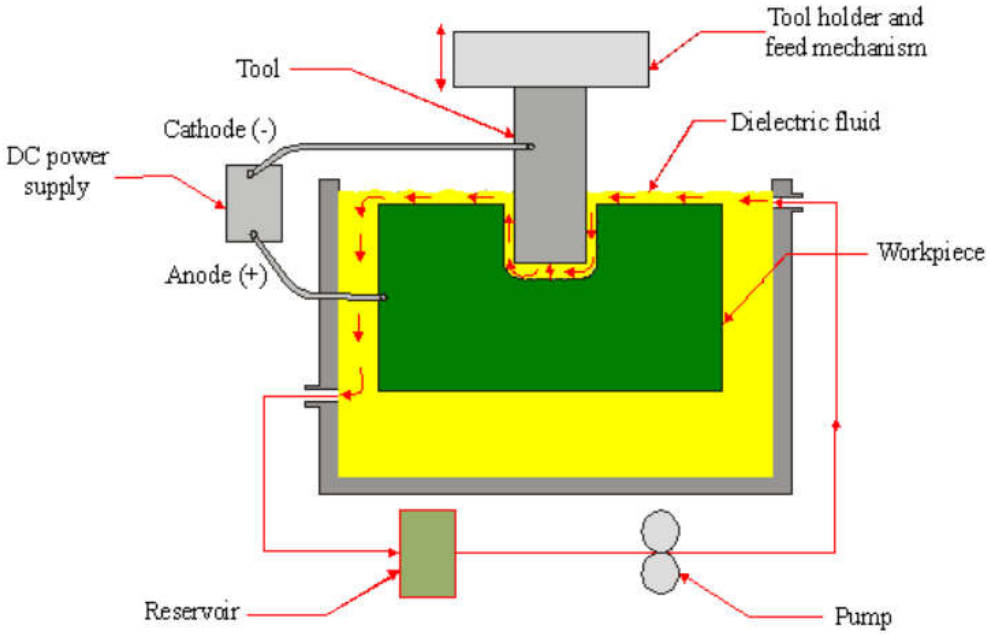

Figure 1.2 Basic principle of EDM [18]

The discrete electric discharge is occurring between the electrically conductive electrode and work material at the level of breakdown voltage. A very small gap (0.01 to 0.02 mm) between tool and work is maintained using a servo system. High temperature (8000 to 12000 °C) of spark has the ability to melt and vaporize the work material. The erosive action of spark is disposed of a tiny particle of work material known as debris. Disposed work material is flushed away by a dielectric. Recently conventional EDM process is modernized using computerized numerical control, automatic tool changer, wire cut EDM, rotating electrode EDM, Dry EDM. These all futures of EDM have made a very attractive and efficient machining process particularly for die and tool making industries [19].

1.3 MATERIAL REMOVAL MECHANISM IN EDM

To understand the mechanism of material removal process in EDM is very important. Transfer of elements from an electrode or dielectric can take place under specific

machining condition only. Different stages of material transfer mechanism are as follow [20-21]:

Stage 1: Electrode brought very near (0.01 to 0.02 mm) to work material in the presence of dielectric. High voltage applied to electrode, movement of free electron from cathode to anode has ability to ionize insulator type dielectric. Dielectric becomes a good conductor and hence plasma channel creates between the electrode and work material. The strong electric field produces at the point of least distance between electrode and work material.

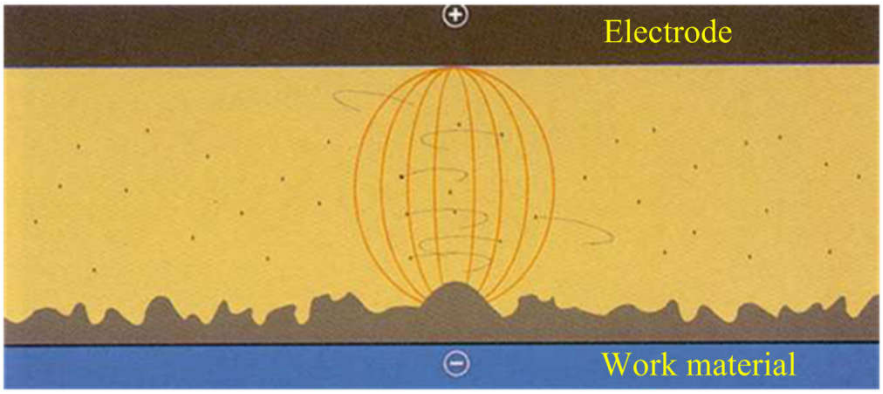

Figure 1.3 (a) Stage 1: Develop appropriate inter-electrode gap [22]

Stage 2: continuously ionisation process of dielectric will lead to increasing numbers of ions in the narrow channel. Dielectric presence in-between tool and work will become electrically conductive due to the high stream of ions.

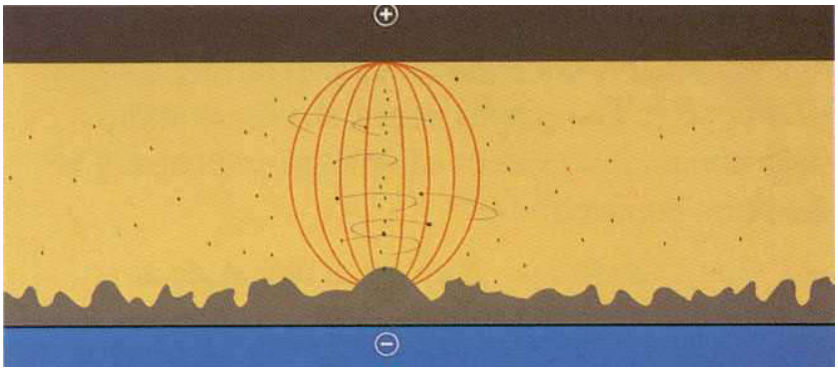

Figure 1.3 (b) Stage 2: Rapidly increase of ionized particles [22]

Stage 3: Due to the conversion of dielectric from insulator to conductor current is initiated and voltage is continuously reducing resulting in an increase in current.

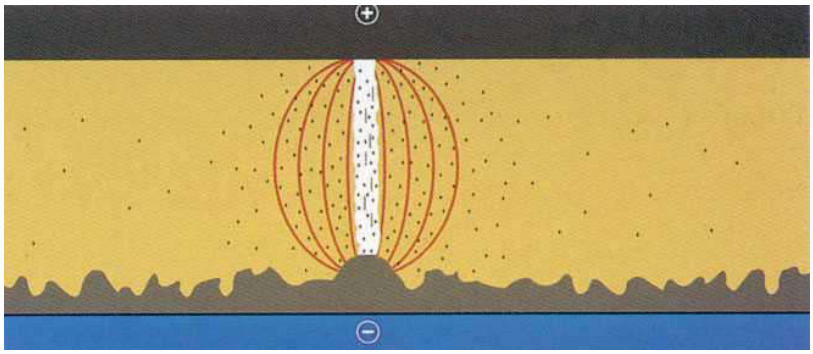

Figure 1.3 (c) Establishment of current [22]

Stage 4: Rapidly increase in current with a decrease in voltage during pulse on-time duration will lead to generating tremendous heat. The high amount of heat is capable to melt and vaporize work material, tool, and dielectric. Continuous plasma channel is produced between tool and electrode.

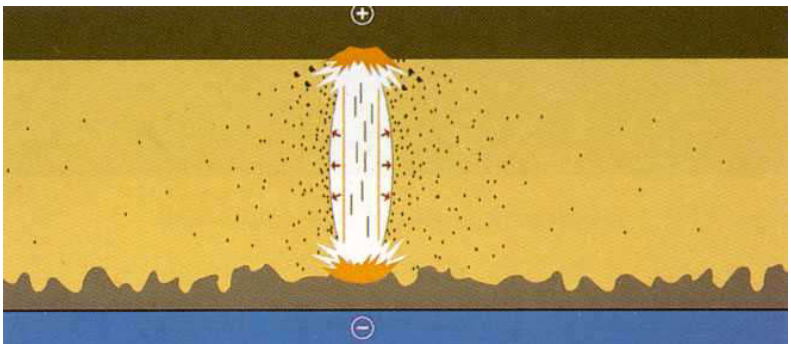

Figure 1.3 (d) Initiation of the discharge channels [22]

Stage 5: Combinations of high heat with a stream of discharge will create a vapour bubble. Expansion of the vapour bubble is limited by the flow of ions toward the discharge channel. Ions are attracted by a strong magnetic field that has been built up. Further current continuously increases with drop-down voltage.

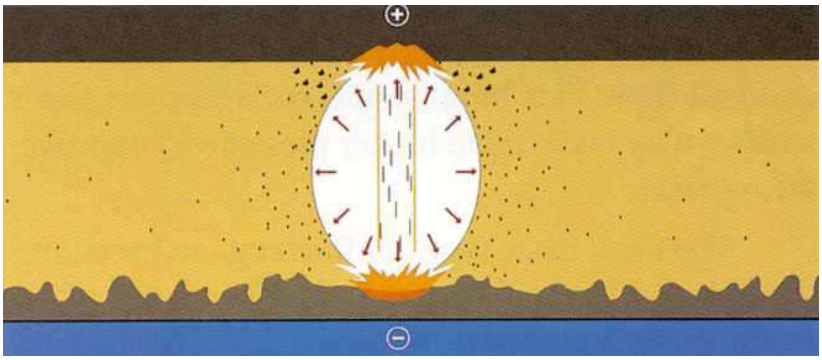

Figure 1.3(e) Attraction of ions toward the electromagnetic field [22]

Stage 6: Near the completion of the on-time duration, peak current and discharge voltage have stabilized, heat and pressure within the vapour bubble have reached their maximum and some metal is being removed. The molten metal pool is creating in the area of discharge and molten metal is remaining stable under the pressure of the vapour bubble. Formation of superheated plasma channel is observed due to the presence of vaporized metal of work material and electrode with dielectric and carbon element dissociated from pyrolysis of the dielectric. Presence of work material, electrode material and carbon in plasma channel will enhance the intensity of current in plasma channel [22].

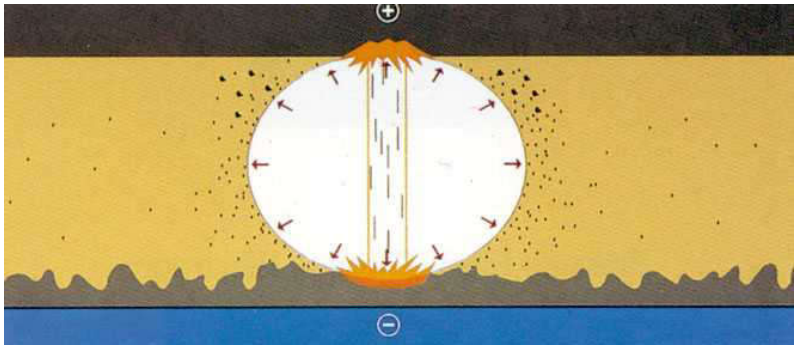

Figure 1.3 (f) Superheated plasma channels [22]

Stage 7: Pulse off time stage will begin after the end of the pulse on time. Current and voltage drop down towards zero at the initiation of pulse off time stage. Sharply reduction in temperature with the collapse in the vapour bubble is observed during off time. Decomposed metal particles are expelled from the work surface.

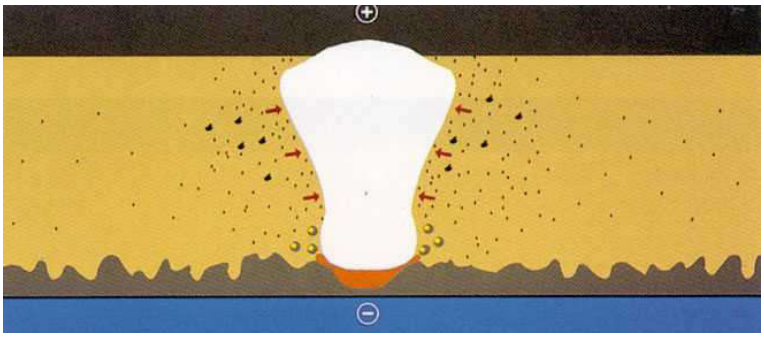

Figure 1.3(g) Initiation of pulse off time [22]

Stage 8: Due to collapse vapour bubble fresh dielectric is rush towards the inter-electrode gap. The flow of fresh dielectric is flush away debris and resolidified unexpelled molten metal which is known as the recast layer.

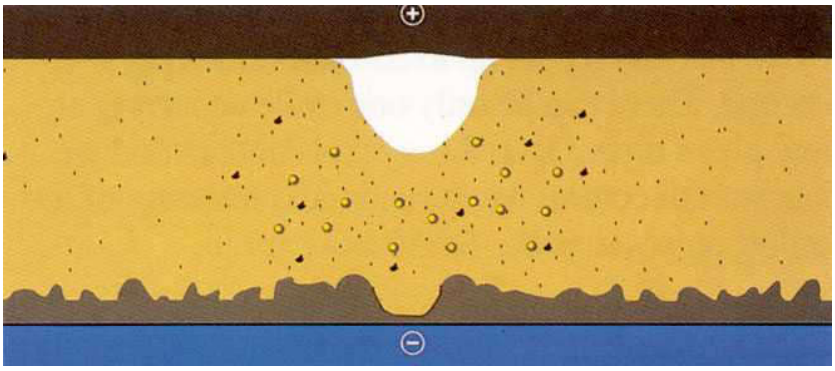

Figure 1.3(h) Flush away debris [22]

Stage 9: The expelled work materials solidified into small tiny particles and disperse in the dielectric. If sufficient pulse off time is not provided than debris is concentrated and hence there is unstable sparking action. This situation is responsible to produce DC arc which can damage the workpiece and electrode.

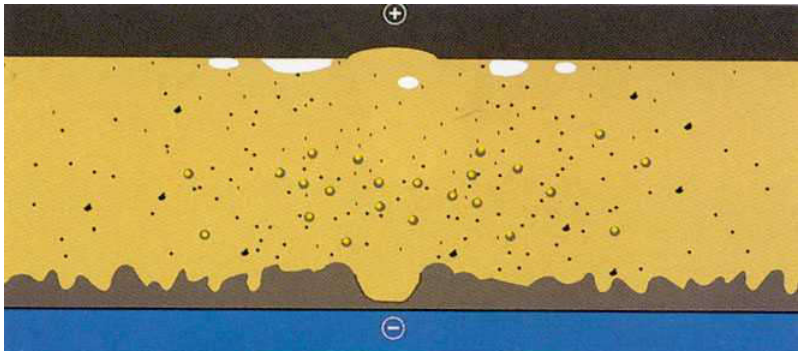

Figure 1.3(i) Solidification of expelled particles [22]

1.4 SELECTION OF WORK MATERIAL

For the present experimental work, one of the most popular and widely used tool and die steel P20+Ni was considered. Generally, plastic components die for high-pressure injection moulding and frame of pressure die were manufactured from P20+Ni steel. It is also used to manufacture large size plastic mould, home appliances, car accessories, electronic equipment, boaster plates of presses, shoe block for drop hammers etc. The chemical composition of P20+Ni steel is represented in below table 1.1.

Table 1.1 Composition of P20+Ni steel

Element	C	Si	Mn	P	S	Cr	Mo	Ni	Cu	V	Fe
Wt %	0.36	0.27	1.25	0.01	0.006	1.86	0.17	0.95	0.071	0.065	Balance

P20+Ni steel exposed to higher strength and toughness and hence machining of this steel on the conventional machine is very difficult. It is categorized under difficult to machine materials. The various physical and chemical properties are given in below Table 1.2.

Table 1.2 Physical and Mechanical properties of P20+Ni steel

Physical/Mechanical Properties	Value
Density	7861 Kg/m^3
Specific Gravity	7.86
Modulus of Elasticity	190- 207 GPa
Poisson's Ratio	0.27-0.30
Thermal Conductivity	41.5 w/m/°k
Tensile Strength (Ultimate)	965-1030 MPa
Tensile Strength (Yield)	827-862 MPa
Compressive Strength	862 MPa
Electrical Conductivity	$2.17x10^6$ S/m at 20 °C

1.5 OBJECTIVES AND SCOPE OF THE PRESENT INVESTIGATION

P20+Ni die steel is mainly used for manufacturing high pressure die for composite plastic products. Plastic mould has to be exposed to complex conditions during working. The main reasons for the failure of plastic moulds are to high pressure, temperature, wear, abrasion, and friction during working. An enhancement of die life is very important for economical productions [23].

Properties of work material are greatly influenced due to heating and cooling the work surface by a dielectric. Variation in chemical compositions of the machined surface might be possible due to depositions of elements from electrode and carbon elements from hydrocarbon dielectric. Die material must possess mechanical and physical properties such as strength, toughness, hardness, abrasion resistance and wear resistance [24]. These all desired properties can be improved by adding various elements like copper, tungsten and silicon from electrode or dielectric. Tungsten is helpful to improve the mechanical and physical properties of the work surface. Presence of tungsten is increase hardness and toughness of work material. It has a strong affinity with carbon and hence the formation of tungsten carbide can help to increase the abrasion resistance of work surface. Up to 2% presence of silicon intensifies the influence of chromium, manganese and molybdenum. Improvements in hardness and oxidation resistance of work surface are observed due to the

presence of silicon. Copper is helpful to increase the corrosion resistance of steel. Improvements in thermal and electrical conductivity are observed due to additions of copper, which is desirable for EDM operation [25].

The key objective of the present experimental work is to modify the surface of P20+Ni die steel using EDM. Experiments were performed using EDM electrode manufactured through powder metallurgy process. Experimental results were analyzed to investigate optimum levels of input process parameters which are able to transfer elements from electrode and dielectric to modify the work surface of P20+Ni die steel. Input levels of process parameters for main experimentations are decided based on the results of pilot experiments. Design matrix for the main experimentations was obtained using response surface methodology. SEM, EDS, and XRD analysis have been carried out to confirm the migration of material from the electrode to the work surface. The main objectives of the present experimental work are summarised as follow:

1. To develop a hard and modified surface layer on P20+Ni die steel machining on EDM using powder metallurgy (P/M) composite electrode.
2. To investigate the combined effects of P/M electrode and EDM parameters on the responses such as material removal rate (MRR), tool wear rate (TWR), surface roughness (SR) and microhardness (MH) as an aspects of the surface modification phenomenon.
3. To perform ANOVA, develop three-dimensional response surface plots and statistical regression equations for MRR, TWR, SR and MH using Response Surface Methodology (RSM).
4. Perform the multi-objective optimization using composite desirability approach to obtain the optimum set of parameter enables the best possible machining conditions for surface modification.
5. Detail study of micro-structure and composition of machined surface with changes occur due to variation of levels of parameters such as compaction pressure (C_p), peak current (I_p), pulse-on time (T_{on}) and duty cycle (τ) has been investigated using Scanning Electron Microscope (SEM), Energy Dispersive Spectrometry (EDS) and X-Ray Diffraction (XRD) techniques.

1.6 DIFFERENT PHASES OF EXPERIMENTATION

To fulfil desired objectives present experimental works have been divided in following different phases:

- Elaborate the literature available related to surface modification using Electrical Discharge Machining.
- Based on the literature review decide effective parameters which greatly contribute to the surface modification process.
- Perform numbers of a trial run to investigate levels of parameters for pilot experimentation. Consider variation in single factor at a time to finalise parameters for pilot experimentation.
- To optimize results of pilot experiments using Taguchi techniques for finding effects of selected parameters on qualities characteristics such as MRR, TWR, SR, and MH.
- Carried out SEM, EDS and XRD analysis of selected machined samples of pilot experiments to confirm migration of electrode elements on the work surface.
- Based on result analysis of pilot experiments decide different process parameters and their levels for main experimentation.
- Develop a design matrix for main experimentation based on a second-order rotatable central composite design using response surface methodology.
- Analyse results of main experiments using Design Expert 10 statistical software.
- Develop mathematical/regression model for MRR, TWR, SR, and MH using Response surface methodology. Perform ANOVA for all responses to find the contribution of individual parameters. Plot the 3-D surface plot for all responses to study the effects of parameters.
- Investigate surface morphology of machined surface using SEM, EDS, and XRD analysis.
- Carried out multi-objective optimization using composite desirability approach.
- Decide optimal set of input parameters which fulfil the combined objective of responses.
- Validate predicted results of responses with results obtained during the performance of experiments on EDM.

1.7 STRUCTURE OF THE THESIS

The total works of the thesis have been elaborated in different six chapters. The contents included in each chapter are summarised below:

Chapter – 1: Need for surface modification, Basics of the electrical discharge machining process, Material transfer phenomenon in EDM, Selection of work material, Objectives and scope of the present investigation, Different phases of experimentation.

Chapter – 2: Introduction, History of electrical discharge machine, Working principle of EDM, EDM process variables, Layers in EDMed surface, Effects of alloying elements in die and tool steel, Surface modification using powder metallurgy electrode, surface modification by powder mixed in dielectric, Multi-objective optimization of surface modification process using EDM, Gaps in literature.

Chapter – 3: Introduction, Machine tool, Work material, Properties of powder metallurgy electrode, Measurement of responses, Surface morphology, Identification of various phases, Experimental design strategy for pilot experiments, Selection of orthogonal array for pilot experiments, Signal to noise ratio for responses, Selected input parameters for pilot experimentation, Result analysis of material removal rate, Result analysis of tool wear rate, Result analysis of surface roughness, Result analysis of microhardness, Scanning electron microscopy, Energy dispersive spectrometry analysis, X-ray diffraction analysis.

Chapter – 4: Introduction, Response surface methodology, Experimental results, Analysis and discussion of MRR results, Selection of adequate model for MRR, Analysis of variance (ANOVA) for MRR, Effects of machining parameters on MRR, Analysis and discussion of TWR results, Selection of adequate model for TWR, Analysis of variance (ANOVA) for TWR, Effects of machining parameters on TWR, Analysis and discussion of SR results, Selection of adequate model for SR, Analysis of variance (ANOVA) for SR, Effects of machining parameters on SR, Analysis and discussion of MH results, Selection of adequate model for MH, Analysis of variance (ANOVA) for MH, Effects of machining parameters on MH,

Chapter – 5: Introduction to composite desirability approach, Multi response optimization using composite desirability, Optimization of MRR and TWR, Optimization of SR and MH, Optimization of MRR, TWR and SR, Optimization of MRR, TWR, SR and MH

(equal weight and important), Optimization of MRR, TWR, SR and MH (different weight and important).

Chapter – 6: lists down the conclusions of this research work. Recommendations for future work in this area have also been given.

This chapter is followed by references and appendices.

CHAPTER – 2

LITERATURE REVIEW

2.1 INTRODUCTION

Technologically well-developed industries like aerospace, automobile, nuclear reactors, etc. have been demanding materials/alloys which are able to deliver high strength to weight ratio. The trend towards to develop material which has high hardness, toughness, strength, and other improved properties. Hence, to machining such hard and tough alloy demanding improved cutting tool properties to maintain productivity and surface integrity [26]. It seems to be very difficult to develop tool materials, able to machining different HSTR alloys and very hard materials like tungsten, tantalum, titanium, etc. On the other side, traditional machining processes could not able to produce complex and intricate shapes with the required accuracy. These all concerned factors are forced to develop different non-conventional machining processes which are able to fulfil the needs of recent manufacturing industries [27].

Electrical discharge machining (EDM) has become one of the versatile processes particularly in automobile, tool room, production shop floor, die room, turbine, and similar manufacturing industries. The following factors contributing to enhancing its popularities:

- No need to create physical contact between electrode and work materials and hence very thin and fragile section can be easily machined.
- Parts can be produced without distortion. The process has the ability to maintain dimensional accuracy and precisions.
- There is no cutting force between electrode and work material.
- The process is capable of machining “difficult-to-machine” category material easily.
- A complex internal cavity can be easily produced, which seems very difficult or impossible using conventional machining methods.
- The process is almost burr-free.

The numbers of research works have been carried out by various researchers throughout the globe to enhance the process capabilities of the electrical discharge machine. These

research works include the use of different types of electrode material, dielectric, flushing techniques and to combine EDM with different unconventional machining like ECM, AJM, and USM, etc. Further literature related to improvements in EDM efficiency due to varying different process parameters is also available. Since the last decades, researchers have been exploring different ways to use EDM as a surface modification process in tool and die making industries. Two different methods have been explored by researchers which able to alter the compositions of work material during machining. Machining of work material has been carried out on EDM either using powder metallurgy (P/M) electrode or mixing different metallic powders in the dielectric. This chapter includes a summary of literature available related to surface modification of different die steel using EDM [28-29].

2.2 HISTORY OF ELECTRICAL DISCHARGE MACHINE

The present form of the electrical discharge machine began its journey from 1770. The English scientist Joseph Priestly observed the loss of small mass (erosive effect) from electrical conductor during the spark. First time in the 1930s, efforts were made to machine metals and diamonds using electric discharge. Erosive action between tool and work was established using the DC power supply. Intermittent arc was produced between tool and electrode. The process was not considered as accurate because of the overheating of the machining area. The process was named as arc machining in place of spark machining [30].

During 1943, at the time of world war-II, Two Russian scientist B.R. Lazarenko and N.I. Lazarenko from Moscow University developed a controlled material removal process using sparking action between two electrically conductive materials. Later on in 1950, the R-C (resistance-capacitance) circuit was invented, which was capable to develop controlled sparking time between tool and electrode. It was also capable to maintain an appropriate distance between tool and electrode automatically. After 1950, successively different development was done in the R-C circuit and technology of EDM [31].

Three American employees claimed the use of electrical discharges to remove the drill and broken taps from hydraulic valves. This work was considered as a base for the development of vacuum tube type electrical discharge machine and an electronic circuit for servo system, which was capable to maintain appropriate inter-electrode gap automatically without contact between tool and electrode. In the 1980s, EDM has been advanced using

computerized numerical control system (CNC EDM) which has greater efficiency with different advanced futures. Continuous developments in EDM technology have been resulting recent version of EDM which has the ability to machine any of electrically conductive material irrespective of hardness with greater accuracy [32].

2.3 Working principle of EDM

EDM is categorized under thermoelectric type advanced machining processes in which heat energy obtained by sparking action is used to erode the work material. Both work material and electrode material must be electrically conductive. Spark is initiated between electrode and work material (Figure 2.1), when very small (0.01 to 0.02 mm) gap is maintained between them. The duration of the complete cycle is only a few microseconds. The spark is initiated with very high frequencies (per second thousands of spark). The intensity of spark is concentrated in a very small area, which able to partial melting and vaporizes work and electrode material. EDM work using pulsed DC power supply of 80-100 V, with very high frequencies (approx 5 kHz). After individual discharge of spark, the capacitor will further be charged by the DC power source through a resistor (Figure 2.2). Material from work surface is eroded in the form of tiny particles known as debris. Cavity generates in work materials due to erosive actions is a replica of the electrode. A large amount of material is eroded from the work surface as compared to the electrode material. Servo system is used to maintain the optimum inter-electrode gap. The electrode will continuously move downward by the servo system as per the amount of material eroded from the work surface [33].

The dielectric helps to concentrate the generated discharge energy in a very small area. In EDM different types of hydrocarbon oil such as kerosene, transformer oil, lubricating oil, paraffin oil, and deionized water are used as the dielectric. Dielectric must possess very high dielectric strength means it will remain insulator until the levels of break down volt attained. Further, it helps to cool down electrode and work material. Dielectric helps to flush away debris from the inter-electrode gap which is necessary to avoid arcing during operation [34].

The use of Lazarenko R-C circuit in EDM is not able to deliver a high material removal rate. Maximum MRR is obtaining as a cost of surface finish only. The greater portion of machining time is consumed for charging the capacitor (Figure 2.3).

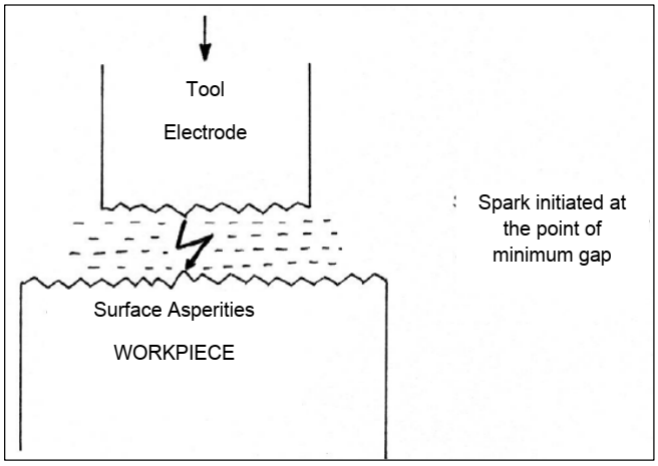

Figure 2.1 Initiation of spark in EDM [3]

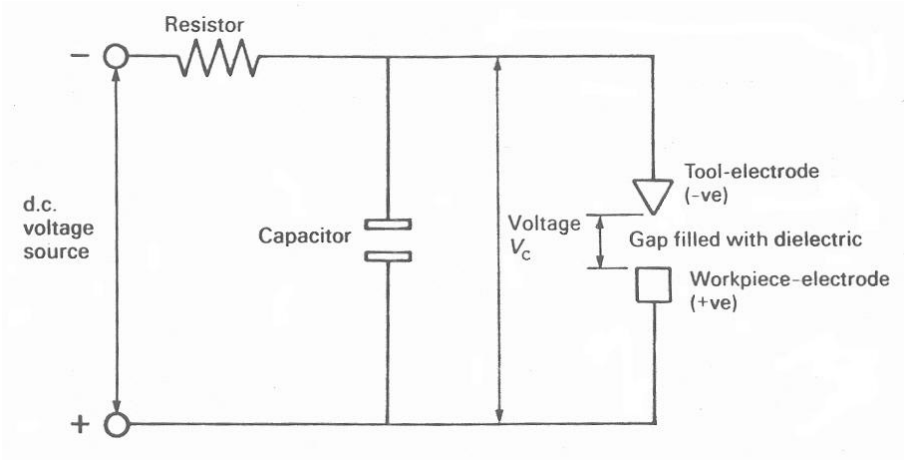

Figure 2.2 Lazarenko Resister-Capacitance (R-C) circuits [35]

A very high value of peak current is required to initiate spark while using R-C circuit. These higher value of peak current sometimes hamper the thermal properties of the EDM electrode. Thermal damage of electrode will lead to deteriorating the EDM performance.

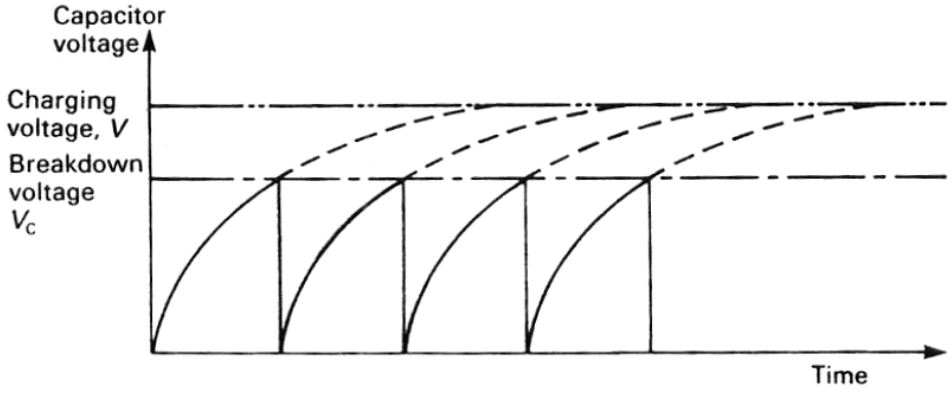

Figure 2.3 Graph of variation in capacitor voltage Vs time in R-C circuit [35]

It is a fact, if machining is performed with lower peak current and high spark duration, it will result in improved machining efficiency with minimum tool wear. The controlled pulse generator is employed in place of the R-C circuit. Waveform obtained using controlled pulse generator is shown in Figure 2.4. Controlled pulse generator performed with lower peak current and small idle time results in larger pulse duration as compared to R-C circuit.

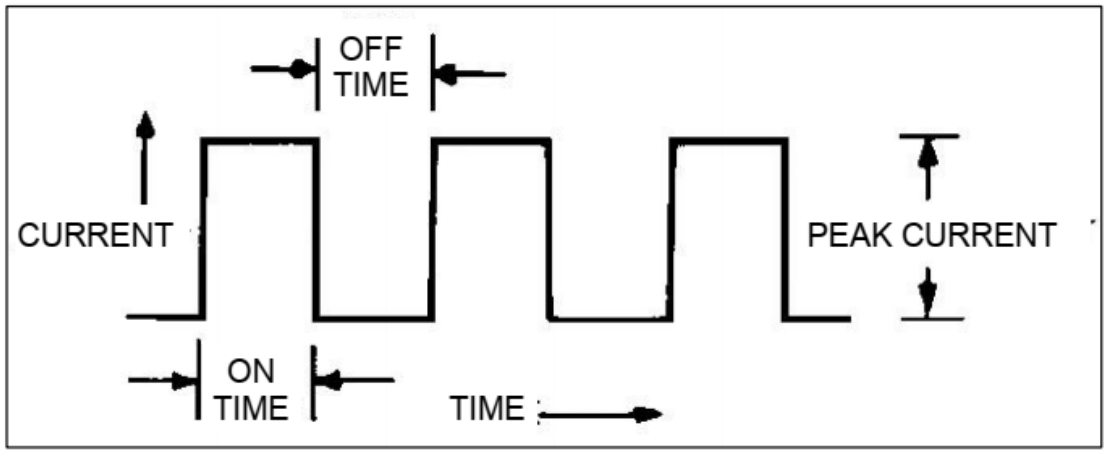

Figure 2.4 Pulse waveform of a controlled pulse generator [8]

The amount of total energy release from spark depends on the value of peak current and pulse on time (discharge duration). So, finally, a selection of levels of different input process parameters such as peak current, pulse on time, pulse off time, and gap voltage depends on the quality of the surface to be produced. In the open-circuit condition, the amount of voltage is increasing up to100 volt before discharge. The high potential between electrode and work material could be ionized the dielectric and hence voltage breaks down from 100 V to 35V. Variation in current and voltage with respect time during a single cycle is shown in Figure 2.5. In Figure 2.5 ‘a’ indicates a span of ionization time, ‘b’ indicates a span of discharge time, ‘c’ indicates deionization time and, ‘d’ represents the total idle time for one cycle. Mainly wear in EDM tool is occurring during the ionization process. The negative polarity is preferred for EDM employed with R-C circuit while positive polarity is always preferred for EDM employed with advanced pulse controlled generator [36].

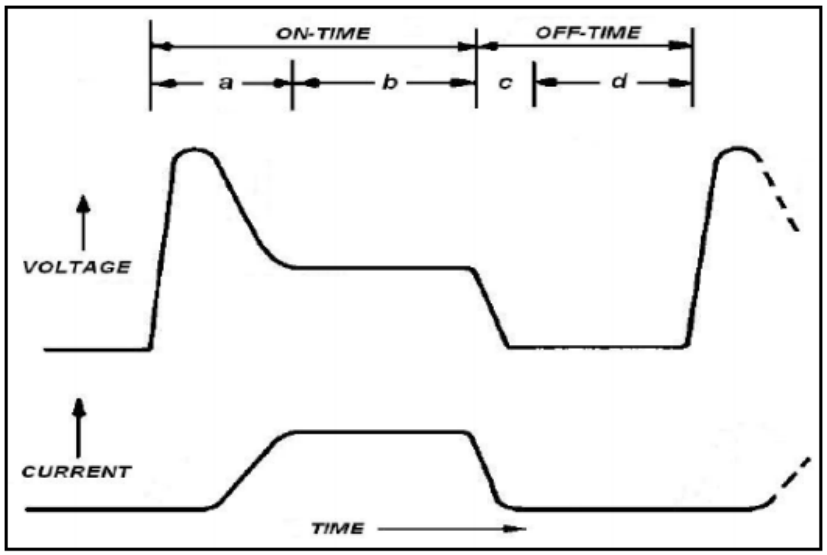

Figure 2.5 Actual graph for a single EDM cycle [35]

The amount of energy release from spark is combined contributions from peak current, pulse on time and gap voltage. However, the individual variation in any parameter is not contributing straight forward to remove material from a workpiece. Generally, it is observed that the width of the crater is proportional to the value of peak current and depth of the crater is proportional to pulse on time. Three-dimensional plots for EDM spark is shown in Figure 2.6.

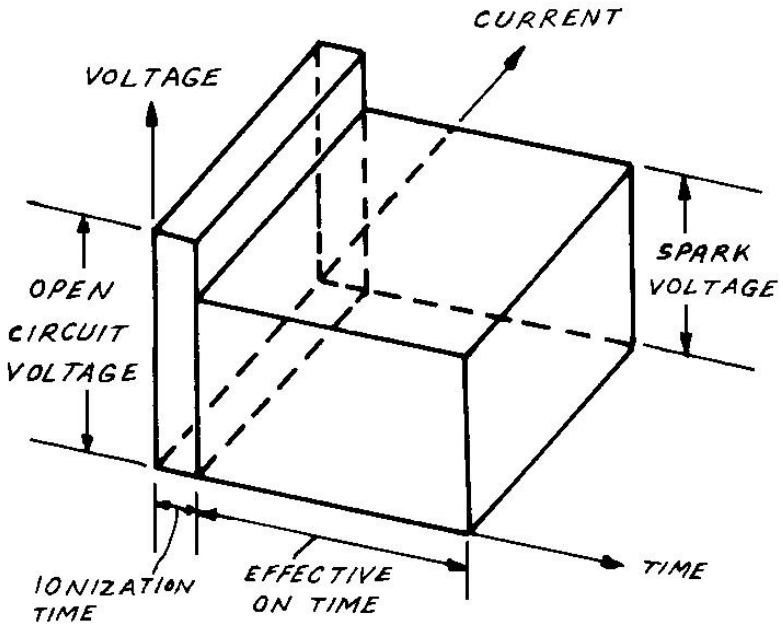

Figure 2.6 Three-dimensional plot of EDM spark [1]

2.4 EDM PROCESS VARIABLES

The selection of optimum levels of process parameters is playing an important role to enhance EDM efficiency. Required surface qualities can be obtained only when the process performed with optimum levels of parameters. Important process parameters and its effects on process performance are summarized below:

Peak Current (I_p): It is one of the important process parameters to govern the machining process. At initial stage-discharge current is zero and voltage start to increase continuously which leads to ionization of dielectric. Spark is initiated once the voltage is reaching its break down level with enough potential between electrode and work material. With the beginning of spark, the voltage starts reducing and became zero while current increases continuously during spark on time, which is considered as peak current. Values of peak current to be selected for machining is mainly depends on different factors such as the cross-sectional area and material of the electrode, work material, etc. The appropriate value of peak current is selected using a machine handbook. The high value of peak currents lead to maximize material removal rate but at the cost of poor surface finish with high electrode wear. Large values of peak current also produce adverse effects on dimensional accuracy. Graphite electrode was found most suitable with high peak current for maximizing MRR with least effects on SR and TWR.

Discharge Voltage (V): the level of discharge voltage is selected based on the inter-electrode gap required and breaking strength of dielectric. When the electrode is set very near to work material (0.01 to 0.02 mm) voltage is increasing continuously until it will reach up to the preset level. When voltage is attained break down level ionization of dielectric able to initiate sparking action. During sparking action peak currents are increased and voltage drop till the spark is stabilized. The large inter-electrode gap is required with the setting of maximum discharge voltage, which is a favorable condition to flush away debris and hence less possibility of arcing. The high value of discharge voltage is increased material removal rate, tool wear rate, and surface roughness. However, no impact of high-value voltage on microhardness is observed after machining.

Pulse on Time (T_{on}): It is the duration of spark for one complete cycle. EDM cycle comprises a span of pulse on-time and pulse off time in microseconds. The thermal energy is (heat) released during spark on time only. The material removal rate is always proportional to the amount of heat energy generated during spark on time. Total heat

energy obtains during a cycle is the product of peak current and pulse on time. Longer pulse duration means energy applied for a longer span and hence wide and deeper crater produce with extended on time. The further high value of energy is creating thick recast layer and deeper heat-affected zone. Hence selection of the optimum value of pulse on time is important for EDM operation. The appropriate value of pulse on-time is able to alloy the work surface, which is the desired condition for surface modification.

Pulse off Time (T_{off}): Timespan between the end of previous spark and beginning of next spark is considered as pulse off time. Optimal duration of pulse off time able to provides stable cutting operation. The lower value of off-time will increase the speed of the EDM operation. However, if the pulse off time is too short than eroded material not flush away properly and hence unstable machining. Further too short off-time unable to ionization of dielectric properly, which affects the efficiency of EDM. The total duration of pulse off time must be greater than the ionization-time of the dielectric to attain ideal machining condition. In modern EDM setup, one can select values of pulse off time independently ranging from 2 to 1000 μs. Sometimes EDM pulses fail to generate spark because of not selecting required levels of pulse on-time and pulse off-time.

Duty Cycle (τ): It is defined as the ratio of pulse on time to the total cycle time. The total cycle time is combinations of pulse on-time and pulse off time. In EDM sometimes the knob for setting the duty cycle is provided with a pulse on-time knob and hence desired level of pulse off time is obtained from duty cycle. The high value of duty cycle indicates a longer pulse on time and hence maximum MRR. High duty cycle means longer spark duration and hence maximum machining efficiency. The duty cycle can be represented as:

$$\tau = \frac{T_{on}}{T_{on} + T_{off}} \, X \, 100$$

Polarity: EDM can be operated with either straight or reverse polarity. In straight polarity tool is negative and work positive while in reverse polarity tool is positive and work negative. If EDM is operated with straight polarity than the very fast reaction of electron able to deliver more energy at work surface (anode) and hence significant MRR. However, the flow of high mass of electron with straight polarity will lead to maximizing the erosion of electrode particularly with longer pulse duration. Selection of polarity for EDM operation is governed by various factors such as electrode material, work material, pulse duration, and current density. Recent power supply system of EDM incorporated with

"swing pulse" facility to prevent arcing and hence one swing pulse is produced with every fifteen standard pulses.

Dielectric Fluid: Types of dielectric used during EDM operation is play an important role in performance. EDM is used thermal energy for melting and evaporate the work material. The EDM operations must be performed under the absence of oxygen to prevent oxidation and govern the process well. The dielectric helps to concentrate the generated discharge energy in a very small area. In EDM different types of hydrocarbon oil such as kerosene, transformer oil, lubricating oil, paraffin oil, and deionized water are used as the dielectric. Dielectric must possess very high dielectric strength means it will remain insulator until the levels of break down voltage attained. Further, it helps to cool down electrode and work material. Dielectric also helps to flush away the debris from the inter-electrode gap which is necessary to avoid arcing during operation.

Inter Electrode Gap (IEG): In EDM operation appropriate inter-electrode gap play vital role to stabilize spark as well as to flush away debris. Inter electrode gap stability and speeds of reaction are very important factors to maintain steady EDM performance. The servo mechanism is used to maintain required inter-electrode gap automatically. The system is equipped with a DC stepper motor and electro-hydraulic system to maintain the inter-electrode gap.

Electrode Material: The materials used for the EDM electrode should possess well electrical conductivity, thermal conductivity, and thermal stability. It should possess a low wear rate against impingements of positive ions. Electrode material should have a high density with a high melting point. Further material should be easily converted into the required shape and there are no chances of scarcity. Generally, copper, graphite, copper-tungsten, and brass are used as an EDM electrode.

Flushing Pressure and Types of Flushing: Effective flushing is very important to flush away debris produce through sparking action. Proper flushing during EDM operation is helpful to stabilize the spark. Flushing helps to carry away heat generated during sparking action. The proper flushing system helps to bring fresh dielectric in the inter-electrode gap. There are different types of flushing system used in EDM. Sometimes effective flushing can't maintain with deeper cavity and hence initiate arcing which deteriorates surface quality and dimensional accuracy. The gap flushing system is used to circulate the dielectric between the inter-electrode gap. High flushing pressure in the inter-electrode gap

helps to enhance EDM performance. Pressure flushing is a mode of flushing in which dielectric is forced through a hole drilled either electrode or work material. Quantity of dielectric flow during unit time is more important as compared to flushing pressure. Suction flushing is used for precise work in which eroded particles are sucked through flushing pipe. The suction flushing system is used with a very smaller inter-electrode gap. In interval flushing, the erosion process is interrupted for a while and the electrode is retracted. This improves the flushing out of the eroded particles.

2.5 LAYERS IN EDMED SURFACE

Selection of the machining process is a very important task, particularly for manufacturing industries. Material removal rate and surface integrity of machined components are two major criteria Considered for selecting the EDM process.

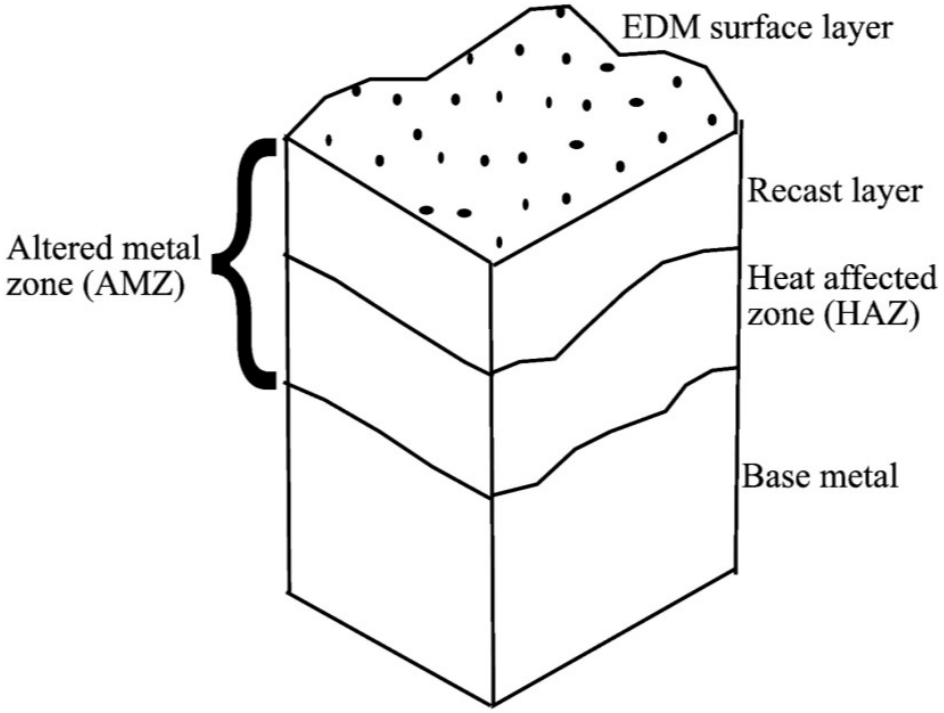

Figure 2.7 Different layers obtained after EDMed [35]

Surface integrity is basically divided into two parts such as surface topography and surface metallurgy. Surface integrity mainly deals with reliability, life, and performance of components. Different types of surface layer obtained after machining the component on EDM is shown in Figure 2.7. Metallurgical changes in surface and subsurface of work material are observed after machining. Three layers are created on the work material. The very thin top layer known as the spattered layer contains expelled molten material and

minor constituents of the electrode material. This spattered layer can be easily removed from the work surface.

The sparking action in EDM process produces a very high temperature (8000 to 12000 °C) in the electrode area. Temperature is enough to melt and vaporized the work material and hence molten metal pool is created in the sparking area. The molten metal is flush away in the form of debris with dielectric; the however rapid flow of dielectric recast the molten material. This re-solidified work material layer is known as recast or white layer which is very hard, brittle and contains micro-cracks due to quenching. It is quite to remove the recast layer from EDMed surface before it put into engineering applications otherwise it may fail due to the presence of micro-cracks. Recast layer is a thin layer with thickness ranges from 2.5 to 50 μm [37].

The third layer obtains below the recast layer is known as the heat-affected zone (HAZ). This layer is formed because of rapidly heating and cooling of work material. The high energy of spark is creating expansion and contraction of work material results in residual stress and deeper microcracks. Heat affected zone is also known as the annealed layer. There is no melting of work material but alterations in metallurgical structure due to heating. Quality of surface integrity of EDMed component mainly depends on the heat-affected zone (HAZ).

2.6 EFFECTS OF ALLOYING ELEMENTS IN DIE AND TOOL STEEL

Different types of steels and ferrous alloys are used as a tool and die materials. Plain carbon steel having a lack of properties such as hot strength and red hardness and hence properties can be improved by adding different alloying elements. Alloying elements such as aluminium, silicon, cobalt, copper, nickel, tungsten, chromium, manganese, molybdenum, titanium, and vanadium, etc. added in steel to enhance mechanical and physical properties. Effects of different alloying elements on steel properties are described below [38]:

Carbon: The percentage of carbon composition in steel is very important. Steel exhibits high hardness with a carbon percentage of more than 0.85%. Excellent wear resistance properties in steel can be observed with carbon percentage from 0.85 to 1.4%. Formation of undissolved carbide helps to increase resistance to wear. The optimum proportion of carbon in steel is helping to maintain tensile strength, machinability and melting point.

Chromium: Increase of chromium percentage in steel helps to improve abrasion resistance, wear-resistance, and hardenability. It works as carbide former between manganese and tungsten. Formed carbide has high hardness and wears resistance ability. With 10% addition of chromium in steel is exhibit excellent corrosion resistance.

Manganese: It helps to enhance strength and hardness in steel but less effective as compared to carbon. Presence of manganese in steel helps to reduce (counteracts) brittleness due to sulphur. A high percentage of manganese and carbon in steel helps to reduce ductility and weldability. Optimum proportions of manganese in high carbon steel help to improve hot working properties.

Silicon: It helps to improve the oxidation resistance of steel and alloys. Silicon strengthening low alloy steels and mainly act as deoxidizer. It helps to intensify the effects of molybdenum, chromium, and manganese in steel. When silicon combined with manganese, the toughness and strength of steels improved substantially. Their effect of carbide forming is less than that of ferrite.

Nickel: It is one of the fundamental alloying elements of steel. It helps to increases toughness and impact resistance of steel. Optimum proportions of nickel in steel helps to reduce distortion during quenching. It lowers the critical temperatures of steel and widens the range of successful heat treatments. It is also helpful to strengthen steel and its alloy. It renders high chromium iron alloys austenitic. It is highly soluble in both ferrite and gamma iron, thus it contributes to the strength and toughness of these phases. When alloyed in steels having high chromium content, it improves hardenability.

Tungsten: It uses to improve hardness and red hardness of steel. It produces fine grain structure with improvements in heat resistance. Tungsten promotes strength in steel at elevated temperatures. Excellent hardness and wear resistance in steel when proportions up to 4%. It enhances the carbide formation process in steel and hence improves abrasion and wear resistance in die steel.

Copper: Mainly addition of copper up to 0.5% in steel helps to increase resistance to atmospheric corrosion. Copper also acts as a strengthening agent. It used as a binder and no other adverse effects on steel.

Cobalt: It helps to improve mechanical properties such as tensile strength, fatigue strength, and hardness. It is contributing to improving red hardness by hardening of ferrite. Cobalt

helps to retard the transformation of austenite and thus increase hardenability and freedom from cracking and distortion. It is mind stabilizer of carbide and hence improves heat resistance.

Molybdenum: It promotes hardenability of steel and makes steel with fine-grained. Molybdenum makes steel unusually tough at various hardness levels. It counteracts the tendency towards temper brittleness. It raises tensile and creeps strength at high temperatures. It helps to improve corrosion resistance in steel.

Titanium: It prevents localized depletion of chromium in stainless steels during long heating. Titanium prevents the formation of austenite in high chromium steels. It reduces martensitic hardness and hardenability in medium chromium steels.

2.7 SURFACE MODIFICATION USING EDM

Electrical discharge machining (EDM) becomes one of the most material removal processes in tool and die making industries. The process is capable of machining different electrically conductive materials irrespective of hardness. However, the creation of the recast layer during machining is one of the major drawbacks of the process. Generated recast layer is hard, brittle and contains microcracks and hence it is required to remove before use of the component. Since last decade efforts have been made by researchers to modify the recast layer during machining rather than removing it. Which will helps to eliminate secondary surface treatments performed after machining work material on EDM. Cancellation of secondary surface treatment helps to reduce further cost and time of components. Various researchers have been carried out a feasibility study of surface modification using EDM. Improvements in carbon percentage of the machined surface have been observed by various researchers due to migration of dissociated carbon elements from hydrocarbon dielectric either in free form or carbide form, which will help to significantly improve the abrasion resistance of machined surface [39]. Surface modification using EDM performed using two methods – Surface modification using powder metallurgy (P/M) electrode and surface modification due to the mixing of conductive fine metallic powders in the dielectric. Here a summary of surface modification process performed by various researchers using EDM has been explained.

2.7.1 Surface modification using powder metallurgy (P/M) electrode

Tsai H. C. et al. (2003) tried to evaluate the performance of EDM using P/M composite electrode manufactured from Cu/Cr powders. The particle size of copper powder and chromium powders were considered 53 and 45 μm respectively. P/M electrodes were pressed at 20 Mpa and sintered at 200 °C temperature. The AISI 1045 steel was used as work material. Four responses such as MRR, EWR, Surface roughness and thickness of recast layers were investigated to evaluate the performance of P/M electrode. Migrations of Cu and Cr from P/M electrode have been observed during SEM and XRD analysis. Electrolytic copper electrode with positive polarity delivered highest MRR as compared to Cu/Cr electrode [40].

Shunmugam M. S. et al. (1994) reported improvements in wear resistance of work material machined on EDM operated by relaxation generator. Powder metallurgy electrodes made through tungsten carbide and the reverse polarity was selected for experimentation. Improvements in wear resistance of EDMed surface was observed using P/M electrode as compared to work surface machined with conventional EDM electrode [41].

Singh Balbir et al. (2015) Carried out experimental investigations on the surface alloying process of AA 6061/SiC_p using EDM with composite (Cu-W) powder metallurgy electrode. Effects of four input parameters such as gap voltage, peak current, pulse off time and pulse on time were investigated on three responses (MRR, EWR, and SR). Further SEM and EDS analysis have been carried out for the machined surface. Result of surface characterizations reveals improvements in microhardness due to migrations of P/M electrode elements on the machined surface. Thick recast layer was observed with a high value of peak current and pulse on time [42].

Cogun Can et al. (2015) carried out a comparative study of surface machined using three different electrodes. EDM electrodes such as Cu-B_4C composite electrode, solid electrolytic copper electrode, and pure copper powder P/M electrode were used for experimentation. Better microhardness and wear resistance of surface machined using Cu-B_4C composite electrode has been observed as compared to other electrodes. Presence of hardest constituents such as FeB, B_4C was observed on surface machined using Cu-B_4C composite electrode. Responses such as MRR, EWR, and SR were also evaluated for all three electrodes [43].

Patowari et al. (2010) performed experiments on EDM as per Taguchi's L8 orthogonal array to study the surface modification process of C-40. Effects of process parameters such as electrode compositions, compaction pressure, peak current, the polarity of electrode and pulse duration were considered for experimental work. The work material was machined using a green P/M composite electrode manufactured from mixtures of WC–Cu powders. Recast layer thickness 48.9 μm and an increase in microhardness up to 1632 VHN were obtained under optimum machining condition [44].

Ndaliman M. B. et al. (2013) investigated improvements in microhardness of Ti-6Al-4V machined on EDM with Cu–TaC powder metallurgy electrode. Distilled water was used as a dielectric with different concentrations of urea. Three input variables such as duty cycle, pulse duration, and peak current were considered for experimentation. Experiments were performed using Cu powder metallurgy electrode with distilled water as a dielectric. Maximum microhardness (1795 VH) was measured with Cu–TaC electrode at 10 g/l urea concentration [45].

Ndaliman M. B. et al. (2011) investigated different properties of EDM electrode manufactured through powder metallurgy process for finding optimum P/M electrode. Density, electrical conductivity and thermal conductivity of Cu-TaC composite electrode were measured for P/M electrode pressed at different compactions pressure. The green composite electrode was found optimum for EDM. Combinations of different properties such as electrical conductivity (94.96-189.92 $\Omega^{-1}m^{-1}$), thermal conductivity (29.70-33.20W/ m K), and density (6.13 -9.80 g/cm^3) were measured. Green compact electrodes found optimum with the best thermal and electrical conductivity as compared to sintered P/M electrode [46].

Jabbaripour B. et al. (2012) performed experiments to machine Ti–6Al–4V on EDM with the electrolytic copper electrode. The main aspect of experimentation was to investigate the effects of EDM parameters on surface integrity of Ti–6Al–4V steel. The result of responses such as MRR, TWR, surface crack density, and white layer thickness was measured at the end of experiments. ANOVA was carried out to find the significance of input variables on responses. The pulse duration and peak current were observed most effective variables for improve surface integrity. SEM and XRD analysis were carried out for EDMed surface and results indicate elements and compounds present on the surface. Maximum microhardness measured for recast surface was 1310 VHN. The SEM of the

machined surface shows micro-cracks, void, and micro-pits due to longer pulse duration [47].

Gangadhar et al. (1990) observed the migration of tool elements on to work surface under certain conditions. Surface alloying was observed during SEM and XRD analysis. Migrations of tool and dissociated elements from dielectric were found on EDMed surface with reverse polarity. Improvements in wear behavior and frictional resistance were observed [48].

Bhattacharya A. et al. (2013) performed experiments on EDM according to Taguchi's L18 orthogonal array. H11, HCHCr, and AISI 1045 were used as a work material and Graphite, W-Cu, and Brass were used as electrodes. Two different types of dielectric such as kerosene and EDM oil were used for experimentation. Silicon, graphite and tungsten powders were mixed separately in dielectrics with concentrations ranging from 0-10 g/l. Significance of individual parameters for SR and MH were obtained by ANOVA. Current, powder concentration and pulse on time were found most effective parameters for SR. SEM and EDS analysis were carried out for machined surface and results of surface characterization indicates migrations of significant amounts of materials from the electrode, decomposed carbon of dielectric and suspended powders particles. Improvements in micro-hardness were observed due to surface alloying [49].

Gill Amoljit Singh et al. (2015) performed experiments on EDM to investigate the surface conditions of H11 die and tool steel machined using P/M electrode. Set of 18 experiments were designed and performed according to Taguchi's L18 orthogonal array. Powder metallurgy electrodes were manufactured from combinations of copper and tungsten powders. The main aspect of work was to improve surface properties of the machined surface due to migrations of hardest constituents from P/M electrode. The variations in six input parameters such as compositions of P/M electrode, peak current, pulse durations, discharge voltage, and duty cycle were considered to evaluate SR and MH. Result of ANOVA indicates the significance of input parameters. Under favorable conditions transfer of Cu and W from the electrode was reported during the EDS analysis. Results of SEM, EDS, and XRD confirmed the transfer of significant amounts of P/M electrode constituents on the machined surface. Presence of hard constituents such as tungsten carbide and cementite was observed during XRD [50].

Chen Yuan-Feng et al. (2008) investigated the surface modification process of S15C type low carbon steel machined on EDM using semi sintered Cu-W powder metallurgy electrode. Effects of four process variables like peak current, discharge span, no-load voltage and machining time were considered to evaluate its effects on MRR, SDR, EWR, and MH. Corrosion resistance test of the machined area was carried out. The surface deposition was found rather than material removal when machining at low values of peak current and no-load voltage condition. Compositions of the machined area were controlled through changes of proportions of elements in P/M electrode. EDM was found economical and suitable for surface alloying [51].

Chen Hsin-Jen et al. (2014) performed experiments on AL 6061-T6 alloy using titanium (Ti) sintered EDM electrode manufactured using powder metallurgy. Four types of Ti electrodes with different sintering temperature were used for experiments. Wet EDC process performed using kerosene as a dielectric, while dry EDC process was performed using nitrogen gas. During wet EDC process, three variables such as peak current, pulse on time and TiN powder concentrations with two different Ti electrodes were used to study its effects on MRR and TWR. Dry EDC was performed with four different Ti electrodes and variations in peak current and pulse duration. Surface modifications were observed during SEM and XRD analysis. The polarity of Ti electrode and dielectric medium with peak current and pulse duration were observed most effective parameters. Improvements in wear resistance of EDMed surface were observed due to the formation of TiC layer [52].

Khanra A. K. et al. (2007) developed metal matrix composite electrode to reduce tool wear with optimum thermal and electrical conductivity. The electrodes were manufactured from mixtures of ZrB_2 (40 wt %) and Cu. Performance of electrodes was tested by machining mild steel on EDM. Comparative performance analysis of ZrB_2-Cu electrode and pure Cu electrode has been carried out. Dimensional accuracy and good surface finish were observed with Cu electrode as compared to ZrB_2-Cu electrode. SEM, EDS and XRD analysis of machined surface and tool surface were carried out. Better MRR with lower TWR was observed with ZrB_2-Cu electrodes. EDS and XRD analysis were confirmed migrations of electrode elements on the work material. Improvements in wear resistance of machined surface were confirmed formations of austenite [53].

Singh Harjot et al. (2016) studied the surface modification of AISI 1045 die steel machined on EDM using Cu- Cr powder metallurgy electrode. P/M composite electrodes were

manufactured using 10% Cu and 90% Cr (% of wt) powders. Four input parameters such as powder compaction pressure, peak current, discharge duration and pulse off time were selected to study its effects on surface characteristics. Surface deposition, surface roughness, and microhardness were considered as responses. Total of 30 numbers of experiments was performed according to second-order central composite design. SEM and XRD analysis of machined surface was carried out to study the surface characteristics. Improvements in corrosion and wear resistance of machined surface were observed due to deposition of Cr particle from the electrode to work surface. Pulse off time has been observed most effective parameters for surface deposition process [54].

Gill Amoljit Singh et al. (2016) investigated improvements in microhardness of surface machined using powder metallurgy electrode produce through compactions of Cu-Cr-Ni powders. Experiments were performed on H11 die steel. Comparative study of micro-hardness obtained with P/M electrode and conventional copper electrode have been carried out. Taguchi's L18 orthogonal array was used to design experiments. Four input variables such as percentage of alloying elements, peak current, pulse duration, and duty cycle were used to find its effects on microhardness. To evaluate surface characteristics of machined surface different tests like SEM, EDS and XRD were carried out. Result of experiments indicated 96.3% improvements in microhardness using P/M electrodes. The EDS analyses were confirmed migration of P/M electrode elements on the work material. Presence of Fe_3C, FeCrNi and Cr_7C_3 on the work surface during XRD analysis improves surface hardness [55].

Das Abhishek et al. (2012) carried out experiments on aluminium using EDM with P/M composite electrodes manufactured from TiC/Cu metallic powders. The main objective of work was to create hard and defects free recast layer of the machined surface. The effects of three variables such as compaction pressure, peak current, and pulse duration have been investigated to study its effects on microhardness, surface roughness and recast layer thickness. Total of 29 experiments was performed according to the Box – Behnken design of response surface methodology. Mathematical/regression model for surface roughness and microhardness were developed using RSM. Confirmation experiments were performed to validate the developed mathematical model. EDX analyses of EDMed surface confirmed migrations of P/M electrode constituents on the work surface [56].

Eswara Krishna M. et al (2014) carried out experimental work to obtain uniform recast layers on mild steel machined using EDM with P/M composite electrode. Powder metallurgy electrodes were manufactured from two different powders such as tungsten and copper (particle size 325 mesh). Compaction loads, pulse on time, pulse interval, and discharge current were varied to evaluate its effects on recast layer thickness (LT), material transfer rate (MTR), surface roughness (SR), and tool wear rate (TWR). P/M electrodes have been produced with combinations of W 75% and Cu 25% powders at different compactions load. Maximum recast layer thickness 1262.99 μm and a material transfer rate of 281 mg/min were obtained using P/M electrode. SEM indicates uniform recast layer thickness and improvements in microhardness of machined surface due to the transfer of P/M electrode elements. Four times improvements in microhardness were observed as compared to base materials [57].

Patowari P. K. et al. (2010) carried out experimentations to study surface modification phenomenon of C-40 steel on EDM. P/M electrodes were manufactured from a mixture of tungsten carbide (60% wt) and copper (40% wt) powders. A mixture of powders was pressed at compactions pressure ranging from 180 MPa to 360 MPa. Experimental works were divided into two parts; first parts (Experiments 1 to 16) were performed using single electrode produce at compaction pressure 180 MPa with different peak current and pulse duration while second parts (Experiments 17 to 28) were performed with three different P/M electrodes produced through compaction pressure ranging from 240 MPa to 360 MPa. The influences of different input variables were used to measure MTR, TWR, SR, and optical microscopy, SEM, EDS with XRD. Results of EDS and XRD confirm the deposition of tungsten carbide (WC) and copper on the machined surface helps to improve microhardness. Defects free work surface was observed during SEM [58].

Lung Hwang–Yu et al. (2010) performed electro-discharge coating (EDC) on nickel using EDM with a specially fabricated multi-layered electrode. Electrodes were manufactured by alternate stacking of same dimensions thin plates of graphite and titanium. Machining of work materials was carried out using multi-layer electrode and conventional electrode for comparative performance. Experiments were designed according to Taguchi's L9 orthogonal array. Effects of four parameters such as peak current (20-150 μs), pulse off time (20-150 μs), discharge currents (8-20 A) and capacitance (0-0.2 μF) were used to evaluate its effects on responses. Results of experiments indicate formations of the TiC layer on the work surface during machining. Deposition of TiC layer on work surface helps

to improve properties of the work surface. Significantly improvements in microhardness of machined surface were observed due to the formation of TiC layer [59].

Simao J. et al. (2003) studied the effects of input parameters on AISI H13 die steel machined on EDM using partially sintered WC/Co electrode. BP 180 hydrocarbon oil was used as a dielectric. Effects of open-circuit voltage (125-270), peak current (1-3 A), pulse on time (20-40 μs), electrode polarity (+ & -), and capacitance (0-0.1 μF) were considered to evaluate its effects on electrode wear and microhardness. Experiments were performed according to Taguchi's L8 orthogonal array. Fewer microcracks were observed on the machined surface using WC/Co electrode. The average thickness of the recast layer up to 30 μm was observed during optimum operating conditions and improvements in microhardness from 640 HK to 1319 HK [60].

Beri Naveen et al. (2014) performed XRD analysis and microhardness measurements of Inconel 718 surface machined on EDM using Cu-W electrode produced through powder metallurgy route. Machining was also performed using a conventional copper electrode to make a comparative analysis. Results of experiments indicate a weak bond between elements of P/M electrode help to transfer elements on the work surface and alloying the work surface. Due to the transfer of hardest constituents from the electrode to work surface, significantly Improvements in microhardness of EDMed work surface were observed. At optimum condition improvements in microhardness from 380.9 HV to 496.7 HV were observed. Formation of Fe_6W_6C phases was observed during XRD, which indicates dissociation of tungsten from P/M electrode and formation of tungsten carbide. Formations of Fe_6W_6C further helps to improve the microhardness of the machined surface. The thickness of the recast layer was measured at 30.14 μm [61].

Kumar Sanjeev et al. (2009) carried out an elaborative literature review for surface modifications of mold and die steels were performed using an electrical discharge machining process. Summary of reviews indicates two different ways such as (i) Machining of work surface was carried out using electrode produced through powder metallurgy process, and (ii) EDM operation was performed with mixing of various conductive powder in the dielectric. The following conclusions can be drawn from the review of different surface modification: 1). The process is still at an experimental stage and various difficulties yet to be resolved before the process was widely accepted in industries. 2). Surface modifications using EDM have been proven viable alternative

methods against costly and time-consuming secondary surface modification process. 3). Very fewer works were observed for surface modification of work materials using PMEDM, most of the work using PMEDM were carried out for study for effects of process parameters on responses like MRR, SR, etc. 4). No work found which indicate the comparative study of surface modifications using P/M electrode and PMEDM [62].

Mohri N. et al. (1993) reported surface modification of carbon steel and aluminium using EDM with the green composite electrode. EDM electrode was produced through the mixing of various metallic powders such as copper, aluminium, tungsten carbide, and titanium. During morphology study of the surface using SEM, EDS and XRD reported transfer/presence of electrode elements on the work surface. The modified surface has very high corrosion resistance, wear-resistance and fewer micro-cracks with uniform recast layer thickness. Formations of TiC and WC on material surface observed during EDS analysis helps to enhance the microhardness of EDMed surface [63].

Tyagi R. et al. (2018) performed various experiments on EDM to produce a solid lubricating surface on mild steel. Green electrodes produce from a homogeneous mixture of WS_2 and Cu powders were selected as EDM electrode. Effects of various process parameters like duty cycle, peak current, and the ratio of powder mixtures of WS_2 and Cu were studied to evaluate its effects on electric discharge coating process. Experiments were designed according to Taguchi's L32 orthogonal array. Wear behavior and surface integrity were investigated for machined samples. Result of experiments indicates a reduction in micro-hardness of coating surface from 180 to 44.11 VHN. Wear test of machined samples were carried out using a pin on disc tribometer. Improvements in wear resistance from 95.75 μm (base material) to 6.71 μm (coated surface) were reported. Formation of W, WS_2, Cu and Cu_2S phase were observed during XRD analysis. Significant improvements in coating properties were observed during surface machined with WS_2: Cu/60:40 (mixing ratio) type green compact [64].

Tsunekawa I. et al. (1994) carried out experiments to investigate the surface modification of aluminium using EDM with green P/M electrodes. P/M electrodes were manufactured from homogeneous mixtures of Ti (36% wt) and Al (64 % wt) powders. Variations in process parameters such as pulse width (2-1024 μs), discharge current (8-23 A), duty factor (0.1-0.8), machining time (30-1800 sec) and compaction pressure (98-539 Mpa) were selected to evaluate its effects on hardness and recast layer thickness. Result of

experiments shows the thickness of the modified recast layer up to 100 μm. Formations of TiC and TiAl were observed during XRD analysis. Transfer of hard constituents from the electrode to machine surface helps to increase hardness [65].

Soni J. S. et al. (1996) studied the variations in chemical compositions, the thickness of the recast layer and microhardness during machining of high carbon high chromium steel on EDM with the rotary electrode. EDM electrode was produced from mixtures of Cu-W (80% wt-20% wt) through powder metallurgy process and kerosene was used as the dielectric. The comparative analysis of surface machined using P/M electrode and conventional copper electrode have been carried out. Effects of input parameters like peak current (3-15 A) and electrode rotation (0-1000 rev/min) were studied on microhardness, the thickness of recast layer and changes in chemical compositions of the machined surface. Increases in surface hardness of machined samples were observed due to migrations of hardest constituents such as tungsten from P/M electrode [66].

Mussada E. K. et al. (2015) investigated influences of EDM parameters for electro-discharge surface coating process using W-Cu powder metallurgy electrode. Copper and tungsten powder with particle size 325 mesh was used to produce electrode. Experiments were performed as per Taguchi L32 orthogonal array. Influences of various parameters such as compaction load (5-20 tons), pulse on time (25-1010 μs), and discharge current (6-8 A) were considered to investigate material transfer rate (MTR), surface roughness (SR) and surface morphology. Result of experiments indicated the use of P/M electrode found suitable for EDC process. Material deposition rate 21.18 mg/min to 171.72 mg/min and surface roughness from 6.2 μm to 27.7 μm observed with P/M electrode. Peak current and pulse on time were found most effective parameters to improve recast layer thickness. An EDX analysis indicates the presence of W, Cu, Al and C. Formation of phases such as WC and W_2C were observed during XRD analysis, resulting in improvements in microhardness [67].

Murray J. W. et al. (2018) performed an electric discharge coating process (EDC) on 304 stainless steel using EDM. Attempts were made to produce single layer and multilayer coatings on 304 stainless steel substrate using different P/M electrodes. Different tool/ electrode such as TiC, WC, Zr, Si, and Cu was used for experimentations. Shell Paraol 250 oil was used as a dielectric with negative electrode polarity. Result of experiments proves the use of TiC electrode to develop coating without any micro cracks and porosity. Due to

the lower density of Si as compared to TiC able to reduce break down the strength of dielectric results in improved coating qualities. It was concluded that the migrations of electrodes materials on work surface mainly depend on the thermal properties of the electrode. [68].

Moro T. et al. (2004) performed an electric discharge coating (EDC) process on drill tool using EDM. The process was performed using TiC electrode manufactured through powder metallurgy process. The main aspect of EDC was to replace the CVD/PVD process used for coating hard layers on drilling, turning tool. CVD/PVD process was consumed larger time with high cost. Comparative study of TiC coated tool with the standard TiN tool was carried out. Result of experiments indicates TiC coated drill tools give better performance as compared to the TiN-coated drill tool. The process was not found proper for a flat end mill tool. At very high cutting speed performance of TiC coated tool deteriorate rapidly as compared to TiN tool. Finally, it is concluded that the EDC process can be effectively used in place of CVD /PVD process [69].

Mohan B. et al. (2002) developed Al-SiC metal matrix composite with 20% and 25% Silicon. Experiments were performed on EDM to evaluate effects of SiC percentage. Rotary electrodes of copper and brass with 12 mm diameter were used for experiments. Kerosene was used as dielectric with side flushing at pressure 3.5 kg/cm^2. Effects of various input process parameters such as electrode polarity, peak current, electrode material, pulse on time and rotations of the electrode were used to measure MRR, TWR, and SR. The main objective experimentation was to optimizing EDM performance. Improvement in the material removal rate is observed at high value of peak current with positive electrode polarity. High percentage SiC electrode with maximum rotational speed helps to improves MRR. Lower percentage SiC tool has smaller TWR [70].

Liew P. J. et al. (2018) developed CNF-Cu composite EDM electrode. Performance of the electrode and its effects on surface characteristic were measured by machining of RB-SiC ceramic. The variations in proportions of carbon nanofiber were used to evaluate MRR, EWR, SR, and surface morphology. ANOVA for MRR, EWR, and SR was carried out to obtain the percentage of contributions of process parameters. 65.08% improvements in material removal rate were observed with Cu–1.0 wt% CNF electrode as compared to Cu electrode. Higher electrode wear rate observed in electrode with a higher concentration of

CNF. The Cu–1.0 wt% CNF type electrode produce rough surface as compared to electrolytic copper electrode [71].

Li Li et al. (2001) studied the performance of sintered EDM electrode manufactured by rapid prototyping. Electrodes were produced in two phases through the mixing of four different powders such as copper, tungsten, titanium carbide, and nickel. In first phase Cu-(W/TiC) were mixed with composition Cu 25% wt (constant) and W/TiC 75% wt, further 75% wt W/TiC subdivided in six different proportions such as W 95%wt- Cu 5% wt, W 90%wt- Cu 10% wt, W 85%wt- Cu 15% wt, W 80%wt- Cu 20% wt, W 70%wt- Cu 30% wt, and W 40%wt- Cu 60% wt. Further mixtures of six different proportions were improved by adding a constant 3% wt Nickel (Ni) powder before fabricating electrode. Performances of electrodes were checked on EDM and studied its effects on MRR and TWR. Performances of TiC/Cu-W were improved with the addition of Ni powder. Improvements in surface finish observed with the composite electrode as compared to the conventional electrode [72].

Kumar Paras et al. (2016) carried out experiments on Al-B_4C metal matrix composite using EDM with different types of electrodes to optimize process parameters. Experiments were performed using EDM oil LL21and EN 19 electrode, graphite electrode, and copper electrode. Taguchi's L9 orthogonal array was used to design experiments. Levels of input process parameters such as current (2-6 A), pulse on time (6-10 μs), pulse off time (2-6 μs) and electrode materials were used to study its effects on MRR, EWR, and SR. Peak current and pulse on time were found most significant parameters for MRR during ANOVA. A linear relation was observed between the peak current and electrode wear rate. Maximum wear rate was observed in EN19 electrode. Surface roughness was greatly influenced by the discharge current and pulse on time. Graphite electrode was able to deliver finish surface [73].

Kanagarajan D. et al. (2008) performed experiments on WC-30 %Co cementite carbide using EDM. Copper electrode with kerosene as dielectric was used for experimentation. WC-Co alloy was produced through powder metallurgy process. Total of 31 experiments was performed according to the design matrix developed using response surface methodology. Variations in pulse on time, the rotational speed of electrode, peak current, and flushing pressure were used to investigate its effects on MRR and SR. Regression model for MRR and SR were developed using response surface methodology. Results of

experiments indicated peak current and electrode rotational speed found most significant for MRR. A linear relation between the percentage of cobalt and material removal rate was observed [74].

Chakraborty S. et al. (2018) experiments were performed to study the EDC process on Al 6351 alloy using EDM with the composite electrode. Electrodes were manufactured by mixing of Sic-Cu at different proportions using powder metallurgy. Kerosene was used as a dielectric. Experiments were designed as per Taguchi's L16 orthogonal array. Process parameters with their levels such as compaction load (5-20 ton), peak current (2-8 A), pulse duration (11-100 μs), and compositions of electrode (SiC 30%- Cu 70% and SiC 50%- Cu 50%) were used to study its effects on material deposition rate, tool wear rate, surface roughness, thickness of recast layer, and microhardness. Multi-response optimization techniques Fuzzy-TOPSIS was used to optimize process parameters for the EDC process. Compaction load was observed most significant parameters for the EDC process. Results obtained using FTOPSIS were confirmed by performing experiments on EDM. Finally, it is concluded that Fuzzy-TOPSIS multi-response optimization techniques were able to optimize the EDC process successfully [75].

Jeykrishnan. J et al. (2016) performed experiments on EN24 steel using EDM with Nickel-plated electrolytic copper electrode and EDM oil was used as the dielectric. Peak current (3-11 A), pulse on time (5-7 μs), pulse off time (4-6 μs) were used to find its effects on MRR and TWR. Taguchi's L9 orthogonal array was used to design the experiments. ANOVA of S/N ratio for MRR and TWR was carried out to find contributions of individual parameters. Result of experiments indicates the optimization of EDM parameters using the design of experiments [76].

Mathew Nibu et al. (2014) compared the performance of P/M electrode with the conventional copper electrode. Powder metallurgy electrode was manufactured from combinations of Cu 75% wt and W 25 % wt. Machining was performed on H11 die steel using EDM oil as the dielectric. Experiments were performed using combinations of various input process parameters according to Taguchi's L18 orthogonal array. Effects of types of tool electrode, peak current (4-14 A), gap voltage (40-60 V) and duty cycle (72-92 %) were used to measure the tool wear rate. Discharge current and gap voltage were observed most significant parameters for TWR. Low tool wear rate was observed with Cu-W electrode as compared to conventional copper electrode [77].

Goyal P. et al. (2017) investigate the changes occur in surface properties of EN-31 die and mould steel machined on EDM using powder metallurgy electrode. Experiments were performed using normal polarity and kerosene as the dielectric. Variations in microhardness and surface roughness were measured while machining performed with the copper electrode, copper-manganese (80:20 % of wt) electrode, and copper-manganese (70:30 % of wt) electrode. Discharge current, pulse on time, and types of the electrode were considered as variable parameters. Comparative analysis conventional copper electrode and powder metallurgy electrode were carried out. Maximum microhardness of machined surface was obtained using Cu-Mn (70:30 % of wt) type electrode. Migration of manganese powder from P/M electrode to work surface was observed during the EDS analysis. P/M composite electrode was produced better surface properties as compared to copper electrode [78].

Gill A. et al. (2015) performed the surface alloying process on EN 31 steel using EDM. Experiments were performed using powder metallurgy electrode manufactured through combinations of Cu-Cr-Ni powders and EDM oil as the dielectric. Total 18 experiments were performed as per combinations of various input process parameters derived using Taguchi's L18 orthogonal array. Effects of electrode polarity (+,-), % of Cr and Ni powders with copper (5-15%), peak current (5-15 A), pulse on time (100-200 μs), duty cycle (48-80 %), and discharge voltage (30-50 V) were used to measure variations in microhardness. EDS was carried out on selected samples, results of EDS shows 23% improvements in Cr, 38.7% improvements in Ni, and 23% improvements in Carbon. Formations of various phases such as Cr_3C_2, FeCrNi, and Fe_3C were observed on the EDMed surface. Uniform recast layer with no microcracks was observed during SEM analysis [79].

Gholipoor A. et al. (2014) carried out a comparative study of EDM performed with and without externally applied magnetic fields in near dry condition. Electrolytic copper rod with an eccentric hole was used as an electrode. Total nine experiments were performed according to Taguchi's L9 orthogonal array with magnetic conditions and another nine experiments without magnetic fields. MRR, TWR and SR were measured for both conditions. Maximum MRR was obtained during experiments performed with the magnetic field due to easy flushing of debris. Higher tool wear rate was observed during experiments performed with a magnetic field. An improved surface quality observed with magnetic field-assisted near dry EDM condition [80].

Bhanot V. et al. (2014) studied the performance of powder metallurgy electrode on superalloy Superni-800 as compared to conventional copper electrode. Both types of powder metallurgy electrodes were manufactured using homogeneous mixtures of copper-titanium (90 %wt Cu-10% wt Ti) and copper- titanium (80 %wt Cu-20% wt Ti). Taguchi's L18 orthogonal array was used to design experiments. The effects of electrode polarity (+,-), types of electrode, peak current (3-9 A), pulse on time (100-200 μs), and gap voltage (50 V) were investigated its effects on MRR and WR. ANOVA has been performed to find the contribution of individual parameters. Maximum MRR was obtained with copper- titanium (90 %wt Cu-10% wt Ti) P/M electrode. Peak current and electrode polarity were observed significant parameters for MRR [81].

2.7.2 Surface modification by mixing the metal powder in a dielectric (PMEDM)

Wong Y. S. et al. (1998) performed experiments on SKH-54 and AISI-O1 tool steels using EDM with square cross-sectional electrode manufactured from copper. The specially designed side flushing system was used to enhance optimum surface finish. Different conductive metallic powders such as graphite, silicon, and aluminium were mixed separately with dielectric. Metallic powders were injected at the inter-electrode gap through specially designed flushing system. During experimentation spark gap/ inter-electrode gap was varied in a range from 10 μm to 160 μm according to types of powders. Results of experiments indicate, due to mixing different conductive powders such as graphite, silicon helps to reduce break down the voltage at the high inter-electrode gap and hence mirror finish of work has been observed [82].

Sidhu Sarabjeet Singh et al. (2014) Studied surface modification phenomenon of different metal matrix composite such as 30vol%SiC/A359, 65vol%SiC/A356.2, and 10vol% SiC-5vol% quartz/Al machined on EDM with mixing Cu and Gr powders in a dielectric (EDM oil). Contributions of input parameters were evaluated through measurements of microhardness. Surface integrity was studied through SEM and XRD analysis. An improvement in microhardness was observed with high-density matrix composite. Results of SEM and XRD confirm the transfer of the hardest constituents of powders from dielectric to work surface [83].

Cogun Can et al. (2006) studied alterations in surface properties of prismatic steel machined using copper electrode on EDM. Graphite and boric acid powders at different concentration were mixed in kerosene. Variations in responses such as material removal

rate, tool wear rate, microhardness and surface roughness due to powder concentrations and EDM parameters were investigated. Two variables such as powder concentration and pulse durations were observed most responsible for obtaining the desired value of responses [84].

Kumar Harmesh et al. (2011) carried out experimental work to investigate the role of conductive powders (silicon) mixed with dielectric for machining Al10%S_iC_P work material on EDM. The role of process parameters and changes in silicon concentrations were investigated to improve EDM performance. The result of experiments concluded that the optimum levels of process parameters and concentration of silicon powder in a dielectric help to improve EDM performance such as high machining rate with minimum surface roughness. The concentration of silicon powder, discharge current, and duration of pulse was observed most significant process parameters [85].

Long et al. (2015) machined SKD 61 steel on EDM with two different electrodes. The copper and graphite electrode was used for machining the work material. Titanium powder with particle size 45 μm and concentration from 0 – 20 g/l were used for experimentation. Role of the electrode has been found important for enhancing machining characteristics like MRR, TWR and SR. Mixing of titanium powder in dielectric enhanced EDM performance. Powder mixed EDM process has been found as a viable alternative to improve productivity and accuracy over conventional EDM [86].

Molinetti Anderson et al. (2015) investigated EDM performance when metallic powders such as silicon or manganese mixed with different concentrations. AISI H13 die and tool steel was considered as work material and copper rod as EDM electrode. Effects of EDM parameters such as electrode polarity, pulse duration, pulse interval and discharge current were investigated on surface roughness and microhardness. SEM, EDS and XRD analysis was carried out for selective machined surfaces. Results indicate five times improvements in surface finish using copper electrode with mixing silicon powder in the dielectric. 40% of improvements in microhardness were observed with silicon and manganese powders in the dielectric. SEM analysis shows uniform and defects free recast layer [87].

Kumar Sanjeev et al. (2010) investigated variations in properties of OHNS tool and mould steel machined on EDM with additions of manganese powder in the dielectric. Discharge current, pulse on time and pulse off time were considered as variable parameters to performed experiments according to L9 orthogonal array. Experiments were carried out

with 15 g/l manganese powder concentrations with negative polarity. Improvements in microhardness were reported 73% as compared to conventional EDM process. Optical emission spectrometer results confirmed improvements in the percentage of manganese and carbon of machined surface as compared to the base material. Presence of manganese carbide was reported during XRD analysis. Formations of manganese carbide help to significantly improve the microhardness of EDMed surface [88].

Furutani et al. (2009) describe the effects of EDM parameters (pulse on time and discharge current) while machining AISI 1049 steel using copper electrode and mixing of Ti powder in the dielectric. Two different experimental conditions used to enhancing surface deposition and dressing process. The surface deposition process was performed using copper electrode on AISI 1049 steel while the dressing process was carried out on tungsten carbide. Results of experiments indicate the effects of selected parameters on the work surface. Maximum microhardness of machined surface reported up to 2000 VHN. XRD analysis of machined surface revealed formations of hard recast layer of TiC [89].

Pecas Paulo et al. (2008) investigated the effects on quality of EDMed surface due to variations in concentrations of silicon powder in dielectric and variations of flushing flow rate. Machined surfaces were analyzed under various surface characterizations techniques. Result of experimentation indicates a reduction in thickness of the white layer, crater diameter and shallow crater due to suspensions of silicon powder in kerosene. Desired surface qualities of the machined area obtained at a range of concentrations of silicon powder from 2 to 3 g/l. Lower flow rate causes abnormal discharge results in deteriorate surface [90].

Amorim Fred L. et al. (2016) performed powder mixed EDM process for AISI H13 steel. Molybdenum powders with particles size 5 to 15 μm were mixed in a dielectric with 3 g/l. Discharge current, pulse on time and pulse interval were considered as input process parameters to investigate its effects on surface characteristics. SEM and XRD analysis were confirmed surface modification using PMEDM. Due to the mixing of molybdenum powder in dielectric MoxC, Fe-Mo, and Mo were observed on the EDMed surface during XRD analysis. An improvement in microhardness has been observed due to modification in recast layers [91].

Long Banh Tien et al. (2016) analyzed the surface qualities of SKD61, SKT4, and SKD11 tool and die steel machined on EDM using Cu and Gr electrodes with mixing of titanium

powder in the dielectric. Taguchi's L27 orthogonal array was used to design and perform 27 numbers of experiments. Surface roughness and surface qualities were analyzed after performing EDM operations on the work material. ANOVA of S/N ratio of surface roughness was carried out to investigate contributions of input parameters. Pulse duration and peak currents were observed most effective parameters to increase in surface roughness. Mixing of Ti powder in dielectric helps to reduce SR and improve surface qualities [92].

Kuriachen B. et al. (2015) carried out experimental investigations to evaluate the effects of micro-size conductive powder (SiC) mixed in the dielectric to machined Ti-6Al- 4V on EDM. Tungsten carbide electrode was used for experimentations. The effects of parameters such as voltage, capacitance, and powder concentration were used to find its effects on MRR and TWR. Maximum MRR was obtained with powder concentrations 5 g/l. Minimum TWR was observed during lower powder concentration and higher levels of voltage and capacitance. During XRD analysis of the machined surface formation of tungsten carbide and silicon carbide were observed, which contribute to improvements in surface quality [93].

Patel Sagar et al. (2017) studied the effects of the rotary electrode on EDM performance while machining Inconel 718. Experiments were performed with the mixing of aluminium oxide (Al_2O_3) powder in kerosene and using copper-tungsten electrode. Experiments were designed according to Taguchi's L18 orthogonal array. Effects of different parameters such as peak current, pulse duration, sparking gap, duty cycle and powder concentrations were considered to measure its influences on MRR, TWR, SR and heat-affected zone. SEM analyses of machined samples were carried out to study surface morphology. Results of SEM indicates defect-free and multi-layer uniform recast layer. Peak current and duty cycles were observed most effective parameters to improve MRR [94].

Kumar S. et al. (2012) performed experiments on three different materials (OHNS die steel, D2 die steel and H13 die steel) using EDM with the electrolytic copper electrode. Tungsten powder with concentrations 15 gm/l was added in kerosene used as a dielectric. The main aspect of experimentations was to obtain the modified machined surface of die steel during EDM. Experiments were designed according to Taguchi's design of experimentation methodology. Effects of various input parameters on EDM performance as well as on different responses were investigated. The input variables such as peak

current (2-6 A), pulse on time (5-20 μs), and pulse off time (38-85 μs) were considered to study its effects on microhardness. Individual experiments were performed for 10 min durations. SEM and XRD analysis were carried out to confirm the transfer of tungsten from die electric to worksurface during machining. Results analyses of experiments were reported significant amounts of material depositions on work surface from suspended tungsten powder in the dielectric. Presence of tungsten carbide (WC) on the machined surface was observed during XRD analysis indicates reaction between tungsten particles and dissociated carbon elements from the dielectric, resulted in improvements in surface properties of all three die steel. Improvements in microhardness of EDMed surfaces were observed more than 100% as compared to base materials [95].

Min-Seop Han et al. (2007) investigate the surface integrity of Borosilicate glass machined using a new developed micro EDM process named electro-chemical discharge machining process. Tungsten carbide rod as a tool electrode with 200 μm diameters and NaOH solution as a dielectric was used. Fine graphite powder was mixed in the dielectric. Results of experiments indicate mixing of conductive graphite powders helps to enhanced surface integrity. Reduction in micro cracks and improvements in surface roughness from 4.86 μm to 1.44 μm were noticed due to the addition of graphite powder in dielectric [96].

Kansal H. K. Et al. (2007) carried out a detailed literature review of powder mixed electric discharge machining process. In PMEDM process various conductive metals powders such as Si, Cr, Gr, W, and Mg, etc added into the dielectric. The addition of conductive powders helps to reduce the insulating strength of dielectric and lead to an increase the inter-electrode gap. Due to increase gap between electrode and work material stabilized the process and hence improvements in MRR and SR. From the elaborative literature review, it is concluded that PMEDM process has promising future in the area of EDM [97].

Janmanee Pichai et al. (2012) performed a surface modification process of tungsten carbide on EDM with mixing of titanium powder in the dielectric. Machining process was performed using a rotary copper electrode. Individual experiments were performed with negative polarity and different machining time (15-60 min). Influences of discharge current (10-25 A) and duty cycle (20-80 %) were studied on microhardness and surface properties. SEM, EDS and XRD analysis was carried out to understand the effects of powder concentrations on surface morphology. The results of experiments indicated improvements in microhardness form 990 HV -1750 HV due to the addition of titanium powder in the

dielectric. Improvements in qualities of work surface with fewer microcracks were observed due to surface modification phenomenon of work surface [98].

Zain Z. M. et al (2014) investigate improvements in surface properties, microhardness and corrosion resistance of stainless steel machined on EDM with the addition of tantalum powder in the dielectric. Kerosene was used as a dielectric and copper rod as an EDM electrode. The concentration of tantalum powder was maintained constant (25 gm/l) during experimentations. Influences of various input parameters such as peak current, pulse on time, and pulse off time were considered to find its effects on microhardness. Corrosion test of achiness samples was carried out to studied improvements in corrosion resistance of the machined surface. Results of microhardness measurements indicate maximum microhardness was 1200 HV, which is 1.5 times as compared to the performance of experiments without the addition of Tantalum powder in the dielectric. Results of corrosion test indicate weigh loss of machined surface was 0.056 μg/min for sample machined with tantalum powder in the dielectric as compared to10.56 μg/min without the addition of powders [99].

Wu K. L. et al (2005) studied improvements in surface roughness of SKD 61steel machined on EDM with mixing of aluminium powder and surfactant (Polyoxyethylene-20-sorbitan monooleate) in the dielectric. Experiments were performed with (25 mm diameter) copper electrode and kerosene as a dielectric. Variations in concentrations of aluminium powder and surfactant were considered 0-5 gm/l during experimentation. Influences of various input parameters such as electrode polarity (+,-), peak current (0.3-2 A), pulse duration (1.5-25 μs), open voltage (90-240 V), and gap voltage (15-90 V) were considered to study its effects on surface roughness and surface characteristics. A result of experiments indicates 60% improvements in surface roughness as compared to results of SR measured under application of pure dielectric (no mixing of aluminium powder and surfactant). SEM analyses were carried out for morphology study of the machined surface. Image of SEM revealed defects free and smooth machined surface during machining were carried out with mixing of Aluminium powder and surfactant [100].

Talla G. et al. (2016) carried out a detailed literature review of various work performed on EDM with the mixing of various conductive powders in the dielectric. The main objective of the PMEDM process is to enhance the machining rate with good surface qualities. Recently, PMEDM process is also used as surface modification of various moulds and die

steels. Following conclusions can be drawn from the elaborative literature review: 1) properties of the metal powders such as thermal conductivity, electrical conductivity, and low density able to enhance higher MRR with good surface qualities. 2) Al, Si, and SiC powders were widely used during PMEDM because of low cost, easy availability and excellent results. 3) Kerosene has grater flashpoints and hence it was mostly used as EDM oil. 4) The process performed with positive polarity results in a better surface finish with a greater amount of powder depositions on the work surface. 5) Process parameters such as powder concentration, peak current, pulse-on time and duty cycle were observed most significant for PMEDM performance [101].

Singh Jagdeep et al. (2016) studied machining and environmental aspects of EDM operations performed on WC-Co with the copper electrode. Experiments were performed using different dielectrics such as kerosene, distilled water, and EDM oil the mixing of graphite powder. The concentration of graphite powder was considered 15 gm/l. Experiments were performed according to Taguchi's design of experiments L12 orthogonal array. Influences of various input process parameters a pulse-on time (15-100 μs), dielectric level (40-80 mm), peak current (3-9 A) and flushing pressure (0.2-0.6 kg/cm^2) were considered to find its effect on MRR, TWR, Aerosol concentration, and dielectric consumptions. It is concluded that types of dielectric have major effects on environments and the selection of appropriate dielectric is very important for performing EDM. Optimum dielectric properties and types further help in improving EDM performance for manufacturing concern (MRR, SR, and TWR) [102].

Singh Anoop Kumar et al. (2014) carried out experiments on super Co 605 steel on EDM. Experiments were conducted with graphite electrode (16 mm diameter) and the mixing of graphite powder in a dielectric (concentration 10 gm/l). Experiments were designed according to Taguchi's L18 orthogonal array. Combinations of various input parameters such as electrode polarity (+,-), peak current (3-9 A), pulse on time (20-100 μs), pulse off time (20-60 μs), discharge voltage (25-35 V), and flushing pressure (0.5-1.0 kg/cm^2) were considered to evaluate its effects on MRR, TWR and SR. SEM analysis of selective EDMed surface were carried out to study surface characteristics. Results of responses were deliberated improvement in MRR from 4.43 to 17.04 mm3/min (73.98 % improvements), TWR reduces from 0.5018 to 0.0323 mm3/min (93.56 % improvements) and SR decrease from 4.95 to 1.99 μm (148.99 % improvements). SEM was indicates defects free and uniform recast surface was obtained due to PMEDM [103].

Singh Anoop Kumar et al. (2014) studied influences on surface properties of Co 605 super alloy machined on EDM and the addition of conductive powder in the dielectric. EDM was operating with graphite electrode and mixing of graphite powder in the dielectric. The experimental design matrix was obtained according to Taguchi's L18 orthogonal array. Effects of variables input parameters such as polarity (+,-), peak current (3-9 A), pulse on time (20-100 μs), pulse off time (20-60 μs), discharge voltage (25-35 V), and flushing pressure (0.5-1.0 kg/cm2) were considered to find its effects on microhardness and surface roughness. ANOVA was performed for MH and SR to finding contributions of individual parameters. SEM analysis indicates smooth and defects free surface due to mixing graphite powder in the dielectric. Result of experiments indicates improvements in the microhardness from 320.82 to 1608.30 HV by conventional EDM and from 320.82 to 1315.2 HV by PMEDM. Improvements in carbon percentage of the machined surface were observed due to the transfer of carbon elements from the dielectric. Reductions in surface roughness (fine finish surface) were reported due to the mixing of graphite powder in dielectric [104].

Sahu S. K. et al. (2018) carried out experiments on Inconel 718 using die-sinking EDM with the electrolytic copper electrode. SiC powder was mixed with concentration 6 gm/l in kerosene. An effect of variations in peak current was measured on responses such as microhardness, surface roughness and morphology of the machined surface. Results of experimentations indicate mixing of SiC powder in dielectric enhanced MRR, reduce tool wear rate and surface roughness. Fewer micro-cracks, globules, and pockmarks were observed due to the mixing of SiC powder in the dielectric. Recast layer thickness was continuously increased due to PMEDM. Improvements in microhardness were recorded due to migrations of hardest constituents from dielectric to work surface. During XRD analysis formations of various phases like $AlNi_3C_{0.5}$, Ni_3, and NiC were observed [105].

Gunawan S. et al. (2014) experiments were performed on Inconel 718 using micro-EDM with a tungsten electrode. The MoS_2 powder was mixed in kerosene with concentrations 0-10 gm/l. Experiments were performed with variations in process parameters such as powder particle size (10 nm to 2 μm), voltage (70-110 V), and capacitance (3300-220 pF) to find its effects on surface qualities (size of micro-hole on the work surface) and MRR. Result of experiments indicates applications of various particle sizes MoS_2 were helps to improve qualities of the micro-hole. The small size of black traces was observed during experiments performed with powder particle size 50 nm and concentration 5 gm/l. The

maximum material removal rate was obtained during concentration of 10 gm/l. Effects of particle size on MRR also investigated, results indicated 50 nm particle size was able to deliver the highest MRR. Effects of various input parameters on surface roughness were also evaluated [106].

Prakash Chander et al. (2016) carried out experimentation on β-Ti alloy using EDM with Ti rod as an electrode. Silicon powder was mixed in hydrocarbon oil used as the dielectric. Variations in electrode polarity (+,-), pulse current (5-25 A), pulse duration (5-80 μs), and powder concentration (0-8 gm/l) were used to evaluate its effects on process capabilities and surface characteristics. Result of surface characteristics indicates a reduction in crack density, micro-cracks, pores, etc due to the mixing of Si powder in the dielectric. Amounts of powder concentrations in dielectric significantly affect on recast layer thickness. Increases in powder concentration from 4 gm/l to 8 gm/l were obtained improvements in recast layer thickness from 3 μm to 15 μm. PMEDM process was capable to the obtained biocompatible surface used in medical applications. The process was able to control the density of surface porosity. Improvements in MRR with a reduction in TWR and SR were observed due to the mixing of Si powder in the dielectric. Finally, it is concluded that PMEDM process was able to enhanced EDM performance with the required surface qualities [107].

Patel Sagar et al. (2017) performed experiments on Inconel 718 using EDM with a copper-tungsten rotary electrode. During experimentation, the EDM electrode was rotated at 300 rpm. Aluminium oxide (Al_2O_3) powder with different concentration was mixed in kerosene used as a dielectric. Experiments were designed as per Taguchi's L18 orthogonal array. Effects of powder concentrations (0.5-1.5 gm/l), voltage (50-62 V), peak current (9-28 A), pulse on time (50-150 μs), and duty cycle (0.4-0.6) were studied on MRR, TWR, SR, SEM, EDS, and XRD analysis. ANOVA for MRR, TWR, and SR were performed to find the significance of individual parameters on responses. Result of experiments indicates peak current and duty cycle were observed most significant to enhance material removal rate. Peak current and powder concentrations were found responsible for higher TWR. Very finish surface were obtained with lower Peak current, pulse on time and duty cycle. The EDS analysis of selected samples was revealed the transfer of aluminium oxide powder from dielectric to work surface. Defects free surface with uniform recast layer were reported during SEM analysis of machined surface [108].

Mohanty S. et al. (2018) studied the surface alloying process of Ti6Al4V carried out using μ-EDM. Experiments were performed using tungsten tool with de-ionized water as the dielectric. During experimentation tungsten disulphide (WS_2) powder with different concentrations was mixed in the dielectric. Experiments were performed according to combinations of process parameters derived using Taguchi's L9 orthogonal array. Variations in gap voltage (20-60 V), powder concentration (6-10 gm/l) and duty factor (40-60 %) were used to measure material removal rate, surface roughness, and microhardness. Surface morphology study was carried out using SEM and EDS analysis. Result of responses indicates the process was capable of alloying the surface of work material (Ti6Al4V). Improvement in material removal rate was observed during experimentation with high voltage and powder concentration. Improvement in the surface finish was observed at low voltage with high powder concentration [109].

Marashi H. et al. (2016) discussed previously performed powder mixed EDM work. Improvements in performance of EDM due to the mixing of various conductive powders were reported by various researched. Detailed literature review related to the use of different types of dielectric and its effects on EDM performance has been carried out. After elaborate the literature review following conclusions can be drawn: 1) recent past researchers were used various types of dielectric but still different hydrocarbon oils were observed most efficient. In some experimentation deionized water and gas have been used as a dielectric. Types of powder, properties of the powder, size of powder particle, the shapes of particles and levels of concentrations were greatly affected by the performance of EDM. Mixing of Al and Gr powders in dielectrics were mainly used to improve EDM performance (maximize MRR) while different powders such as Si, W, WC, Mg, SiC, Ti, and TiC were mainly used for surface modification process. Improvements in MRR, reduction in TWR and thick recast layer were observed during mixing small size powder particle in dielectric [110].

Kung et al. (2009) studied the effects of EDM parameters on EWR and MRR. Experiments were performed on WC-Co using EDM with the electrolytic copper electrode. EDM 44 oil was used as a dielectric. Experimental design matrix for 30 experiments was obtained as per central composite design (CCD) using response surface methodology. Effects of a particle of aluminium powder (1.5-2.5 μm), powder concentration (10-20 gm/l), discharge current (2-3 A), and pulse on time (100-200 μs) were used to find its effects on electrode wear ratio and material removal rate. Result of experiments indicates mixing of aluminium

powder with dielectric significantly improve EDM efficiency. Increase powder concentration up to some extent helps to improve MRR, but beyond a certain level reduction in MRR. Mixing of large particle size powder in dielectric helps to increase in MRR and TWR [111].

Kumar Amit et al. (2017) studied improvements in EDM performance due to the mixing of nanopowder of Al_2O_3 in the dielectric. Experiments were performed on Inconel 825 using copper electrode and deionized water as a dielectric. Total of 15 experiments was designed and performed according to response surface methodology. Effects of peak currents (2-8 A), pulse on time (4-10 μs), and gap voltage (10-50 V) were evaluated for material removal rate and peak current. ANOVA for MRR and SR were performed using Minitab 17 statistical software to find the significance of parameters. Performance of nanopowder mixed EDM compared with conventional EDM process. The high inter-electrode gap was maintained due to the mixing of nanopowder in the dielectric, which results in lesser arcing. Maximum MRR 47 mg/min and minimum SR 1.487 μm were observed during experiments. Improvements in surface qualities with fewer microcracks and void were observed due to the mixing of nanopowder in dielectric [112].

Kolli Murahari et al. (2015) studied variations in the behavior of dielectric, MRR, SR, the thickness of recast layer and surface topography of Ti-6Al-4V alloy machined on EDM with mixing of surfactant and graphite powder in the dielectric. Electrolytic copper electrode with spark erosion 450 EDM oil was used for experimentation. Experiments were designed according to Taguchi's L9 orthogonal array. Effects of discharge current (10-20 A), pulse on time (25-65 μs), pulse off time (24-48 μs), surfactant concentration (1-10 gm/l), and graphite powder concentration (1-20 gm/l) were investigated on material removal rate, surface roughness and recast layer thickness. Maximum MRR observed during surfactant concentration 6 gm/l and minimum SR during concentration of 0.25 gm/l. Small crater with few microcracks was observed with a surfactant concentration of 6.0 gm/l. Migration of copper and carbon elements were observed during EDX analysis. Improvement in material removal rate observed with surfactant up to 6 gm/l [113].

Janmanee et al. (2012) performed an electro-discharge coating process on tungsten carbide (WC) using EDM. EDM oil (Shell EDM fluid 2A) as a dielectric with the mixing of titanium powder and a copper rod was used as an electrode. Effects of machining time (15-60 min), peak current (10-25 A), and duty factor (20-80 %) were used to investigate its

effects on surface roughness, microhardness and chemical compositions of recast surface. Result of experiments indicates improvements of microhardness from 990 to 1750 VHN. Reduction in microcracks and improvements in microhardness were occurred because of migration of Ti powder from the dielectric. EDX spectrums confirm the presence of Ti on the machined surface [114].

Rathi M. G. et al. (2014) investigated improvements in EDM performance due to the mixing of different conductive powders in the dielectric. Experiments were performed on Inconel 718 with copper electrode and kerosene as a dielectric. Taguchi's L18 orthogonal array was used to design experiments. Effects of peak current (12-18 A), pulse on time (5-20 μs) and types of powders (SiC, Gr, Al_2O_3) were used to measure variations in MRR and TWR. ANOVA of S/N ratio for MRR and TWR was carried out using Minitab16 software. PMEDM process was observed as a successive method to enhance EDM performance. Highest MRR was observed at 18 A peak current, 5 μs pulse on time, 85% duty cycle and graphite powder mixed in the dielectric. Minimum TWR was observed at 12 A peak current, 20 μs pulse on time, 90% duty cycle and SiC powder mixed in dielectric [115].

Khundrakpam N. et al. (2018) carried out a comparative study of EDM performance during the wet condition, near dry EDM, and mixing of powder in near dry condition. Experiments were performed on EN-8 steel with the electrolytic copper electrode. Different dielectric such as deionized water for wet EDM, the mixture of deionized water and air for near dry EDM, a mixture of deionized water, air and graphite, a mixture of deionized water, air, and manganese, and a mixture of deionized water, air, and silicon carbide for powder mixed near dry EDM conditions. Responses such as MRR, TWR, and SR were measured with various dielectrics medium. Result of experiments indicates maximum MRR, TWR and SR observed with wet condition EDM. Minimum TWR was reported with powder mixed near dry EDM [116].

Ekmekci B. et al. (2016) performed experiments on Ti6Al4V using EDM with Aluminium 6082 electrode. SiC powder was mixed in deionized water at 20 gm/l concentration. Effects of peak current and pulse on time were used to study variations in surface qualities, surface roughness, and thickness of recast layer. Migration of SiC particles on the machined surface was observed during the EDS analysis. Finally, it is concluded that improvements in EDM performance were observed due to the mixing of SiC powder in dielectric [117].

Ekmekci N. et al. (2015) studied the effects of mixing of Hydroxyapatite in dielectric during EDM performance. Ti6Al4V was selected as work material and titanium rod as EDM electrode. Experiments were planned in three groups. In firs group variations in pulse on time (six levels), peak current (five levels) and polarity of tool electrode (+ve) were considered to measure its effects on EDM performance. In second phase experiments were performed with –ve tool electrode. Finally, in the third phase, hydroxyapatite powder concentration (5-20 gm/l) was used. Maximum migration of hydroxyapatite on work surface was reported during pulse on-time 50 μs. Reductions in microcracks were observed due to the mixing of hydroxyapatite powder in the dielectric. Reductions in crater size were observed with lower pulse-on time and discharge current [118].

Baseri H. et al. (2016) investigate improvements in EDM performance due to the mixing of TiO_2 nanoparticle conductive powder in the dielectric. Experiments were performed on H13 steel with a rotary electrode. Copper rod was used as an electrode and kerosene as the dielectric. Total of 30 experiments were performed as per the design of experiments. TiO_2 powder concentrations (0-3 gm/l), peak current (2-9A), pulse on time (35-100 μs), and rotational speed of electrode (0-600 rpm) were used to measure its effects on MRR, TWR, and SR. Improvements in MRR was observed with increasing rotational speed of electrode up to 200 rpm and rotational speed beyond 200 rpm adverse the MRR. TiO_2 powder concentrations 1gm/l deliver highest MRR. Finally, improvements in EDM performance was observed due to the mixing of TiO_2 powder in dielectric [119].

Bai X. et al. (2013) studied the effects of near dry EDM conditions on material removal rate using a rotational electrode. AISI 45 steel was used as work material with a tubular copper rod as EDM electrode and mineral oil as the dielectric. Experiments were performed on EDM according to Taguchi's L27 orthogonal array. Peak current (0.8-64 A), pulse on time (1.8-560 μs), pulse off time (2.4-750 μs), flow rate (1.502-0.066 ml/min), silicon powder concentration (0-15 gm/l), electrode rotational speed (2000-200 rpm) and air pressure (0.4-0.6 MPa) were varied to measure its effects on material removal rate. It is concluded that peak current, pulse on time and flow rate are the most significant parameters to maximize material removal rate [120].

Caydas U. et al. (2008) carried out experiments on Ti6Al4V for modeling and analyze the EDM process. Experiments were performed using a graphite electrode and kerosene as a dielectric. Experimental matrix was designed according to central composite second order

rotatable design (CCD) using response surface methodology. Total of 20 experiments was performed according to the design matrix to investigate its effects on electrode wear rate and thickness of the recast layer. The quadratic/ mathematical model was developed for EWR and WLT using response surface methodology. Good agreement between predicted R^2 and experimental value of R^2 has been observed. Peak current was found most significant for EWR and WLT. Finally, it is concluded response surface methodology successfully used for optimizing EDM parameters [121].

Velmurugan C. et al. (2011) carried out experiments on Al 6061 composite using EDM with a copper electrode and EDM oil as a dielectric. Total 31 experiments were performed as per central composite design using Minitab R14 software. Peak current (3-15 A), pulse on time (200-600 μs), voltage (30-70 V) and flushing pressure (1-5 psi) were considered to measure its effects on MRR, TWR, and SR. Regression model for MRR, TWR, and SR were developed using Minitab software. Adequacy of the regression model was checked using ANOVA. High MRR and SR were observed with the increase in peak current and pulse on time. SEM of machined surfaces was used to study surface morphology [122].

Hosni N. et al. (2018) concluded improvements in EDM performance due to the mixing of chromium powder in a dielectric. Experiments were performed on AISI D2 steel using EDM with a copper rod as electrode and kerosene as a dielectric. Total 20 experiments were designed according to central composite rotatable second-order (CCD) using response surface methodology. Discharge current (20-40 A), pulse on time (50-100 μs), and chromium powder concentration (0-4 gm/l) were used to study its effects on recast layer thickness. The regression equation for recast layer thickness was developed using Minitab software. Discharge current and pulse on time were found the most significant parameters for the recast layer thickness of AISI D2 steel. Predicted results were confirmed with experiments performed on EDM [123].

Ramesh S. et al. (2018) carried out experimental investigations on AISI P20 steel machined on EDM. Al, SiC, and Al_2O_3 powders were mixed in kerosene. Copper, brass, and tungsten rod were used as EDM electrode. Experiments were conducted according to Taguchi's L27 orthogonal array. Variations in types of conductive powders (Al, SiC, and Al2O3), powder concentration (0-6 gm/l), peak current (10-30 A), pulse on time (30-90 μs) and types of electrode materials (copper, brass, and tungsten) were used to investigates its influences on MRR, TWR, and radial over cut. It is concluded that combinations of Al

powder in dielectric and copper electrode were delivered maximum MRR. Types of electrode material and peak current were observed most significant to improve material removal rate [124].

Kumar S. et al. (2018) observed improvements in EDM performance while machining Inconel-800 with different types of electrodes and mixing of various powders in the dielectric. Cu, Cu-Cr, and Gr rods were used EDM electrode. Different powders such as tungsten carbide (WC), cobalt (Co) and boron carbide were mixed separately in kerosene. Total of 46 experiments was performed according to the Box-Behnken model of response surface methodology. Peak current (4-12 A), pulse on time (60-120 μs), pulse off time (30-60 μs), types of electrode and types of powder were used to measure its effects on surface roughness. Microcracks, debris, pockmarks, and large craters were observed during SEM due to high peak current. The EDS spectrum of selected machined samples confirmed the migration of electrode and powder particles on work material [125].

2.7.3 Multi-objective optimization of surface modification process using EDM

Beri Naveen et al. performed multi-objective optimizations of EDM parameters for D2 steel machined on EDM with P/M composite electrode. The Grey relational technique was used as a tool for multi-response optimization. The P/M electrodes were manufactured from mixtures of Cu and W powders with proportions of 25% Cu and 75% W. Experimentations were performed according to Taguchi's L18 orthogonal array. The four input variables like materials of electrode, flushing pressure, discharge current and duty cycle was selected for experimentations. Grey relational technique was successfully applied to solve multi-response characteristics of EDM process [126].

Assarzadeh S. et al. (2012) carried out experimental investigations to enhancing EDM efficiency while machining CK-45 die steel. The process was performed with the mixing of Al_2O_3 powder in kerosene. Particles size 45-50 μm of Al_2O_3 powder with concentration ranging from 2.5 – 2.8 g/l in kerosene. The experimental matrix was obtained according to second-order rotatable central composite design using response surface methodology. Multi- response optimization was carried out using composite desirability approach to model and analyze the responses. Three process variables such as source voltage, discharge current and pulse duration was considered to optimize MRR and SR. Appropriate regression model were developed for MRR and SR. Optimal set of input variables was derived using composite desirability to obtain maximum MRR with minimum SR.

Predicted results of responses were confirmed with experiments performed on EDM. A good agreement observed between the predicted and experimental result of responses with errors of less than 11% [127].

Padhee S. et al. (2012) conducted experiments on EN 31 steel using EDM. A 25 mm diameter copper rod was used as EDM electrode. Silicon powder was mixed in a dielectric with concentrations from 0-2 gm/l. Total of 30 experiments were performed according to the design matrix developed using response surface methodology. Variations in four process parameters such as powder concentrations, peak current, pulse on time and duty cycle were used to obtain its effects on MRR and SR. Results of responses have been analyzed to obtain a set of parameters deliver maximum MRR and minimum SR. To obtained an optimum solution for conflict nature responses, a multi-response optimization technique named non-sorted genetic algorithm (NSGA) was applied. An optimal set of process parameters were obtained using NSGA able to deliver maximum MRR and Minimum SR [128].

Taweel T. A. El et al. (2009) tried to study relations between EDM process parameters with Al–Cu–Si–TiC composite electrode produced through a rout of powder metallurgy process. CK–45 steel was machined on EDM as per setting levels of input parameters derived using response surface methodology. Central composite second order rotatable design (CCD) was used to develop an experimental matrix. MRR and TWR were recorded with variations of peak current, pulse durations, % of TiC in P/M electrode, and flushing pressure. The optimal set of input parameters derived for maximum MRR and minimum TWR using composite desirability approach. Predicted values of responses validate through performing experiments on EDM. Results of predicted values of responses and results obtained due to performance of experiments indicate good agreement with errors 7.2% and 7.4 % for MRR and TWR respectively [129].

Chittaranjan Das V. (2016) investigated the effects of silicon powder mixed in dielectric during machining of AISI 52100 steel on EDM. The process was performed using an electrolytic copper electrode with kerosene as a dielectric. Influences in variations of input parameters such as peak current (5–11 A), pulse on time (100-200 μs), duty cycle (0.7-0.9) and powder concentrations (0-4 g/l) were considered to measure MRR and SR. Experimental matrix was derived according to central composite second-order (CCD) rotatable design using response surface methodology. Objectives to maximize MRR and

minimize SR are conflicting in nature hence to obtain an optimal set of input parameters a multi-response optimization technique named composite desirability was used. Results of experiments indicate improvements in MRR and SR due to the addition of silicon powder in the dielectric. Peak current was the most significant parameters observed during ANOVA. Predicted results were confirmed with experimental results on EDM, good agreements between predicted and experimental results were observed with +5.2% and -4.65% errors for MRR and SR respectively [130].

Tripathy S. et al. (2016) performed multi-objective optimization of EDM process parameters using TOPSIS and Grey relational analysis techniques to improve process performance. Experiments were performed on H-11steel with the electrolytic copper electrode and mixing of chromium powder in the dielectric. Experiments were designed according to Taguchi's L27 orthogonal array. Effects of powder concentrations (0-6 gm/l), discharge current (3-9 A), pulse on time (100-200 μs) and duty cycle (7-9 %) were studied on electrode wear ratio, MRR, TWR, and SR. Analysis of variance was performed for all responses to investigate the significance of input parameters. TOPSIS and Grey relational analysis were used to obtain a single set of parameters which able to fulfil the objective of all responses. Results of experiments indicated values of surface roughness ranging from 3.8 μm to 9.2 μm without powder addition while adding Cr powder 3 gm/l reduce surface roughness 2.86 μm to 5.97 μm. TOPSIS and Grey relational analysis techniques were applied successfully to obtain the optimum set of input parameters [131].

Balasubramanian P. et al. (2014) performed experiments on EN8 and D3 steel using EDM. Machining was performed using sintered copper electrode produced through powder metallurgy process. Influence of various input process parameters such as peak current (9-34 A), pulse on time (100-1000 μs), dielectric flushing pressure (0.8-1.6 kg/cm^2), and electrode (tool) diameters (10-15mm) were considered to investigate its effects on MRR, TWR, and SR. Experiments were design according to response surface methodology (RSM) and 27 experiments were performed for each material. SEM of EDMed samples was carried out to investigate the effects of powder metallurgy electrode. Multi response optimization has been performed using Taguchi's Grey relational analysis. Results of experimental work were indicated good agreements between predicted R^2 and Adj R^2, which confirm developed models quite significant and used for further analysis. Defects free machined surface were observed during SEM analysis [132].

Singh Jagdeep et al. (2017) investigate environmental and manufacturing aspects of powder mixed EDM process performed on tungsten carbide with the electrolytic copper electrode. Graphite powder with concentration 15 gm/l was mixed in EDM oil. Efforts have been made to investigate the role of various parameters in the generation of aerosols and fumes during EDM operations, which is very harmful to human life and environments. Effects of various input parameters like a pulse on time, dielectric level, current intensity, and flushing pressure were considered to investigate MRR and TWR. Experiments were performed as per Taguchi's L27 orthogonal array. Multi-objective optimizations were performed using three different evolutionary algorithms such as grey relational analysis, combinations of grey-fuzzy and grey adaptive neuro-fuzzy analysis. Grey relational grades calculated based on three algorithms were considered to find the effectiveness of the algorithm for optimization. Predicted results of three algorithms were confirmed with conducting experiments on EDM. Lower flushing pressure was observed most significant for generating larger fumes [133].

Singh S. et al. (2012) used grey relational analysis to optimize EDM parameters for machining 6061Al/Al_2O_{3p}/20p type metal matrix composite using electrolytic copper electrode. SiC powder was mixed in a dielectric with concentration 8-12 gm/l. Experiments were performed according to the design matrix of Taguchi's L18 orthogonal array. Variations in aspect ratio (0.6-1), pulse currents (10-20 A), pulse on time (50-200 μs), duty cycle (0.4-0.7 %), gap voltage (40-50 V), and abrasive particle size (74-37 μm) were used to evaluate its effects on MRR, TWR, and SR. Following conclusions can be drawn: 1) A Grey relational technique successfully applied to optimize multi-response problems. 2) Pulse on time was found most significant parameters to enhance EDM performance [134].

Sharma R. K. et al. (2014) optimized powder mixed EDM process using grey relational analysis. Experimentations were performed as per Taguchi's L27 orthogonal array using die-sinking EDM to machine WC-Co alloy. Two different powders graphite and aluminium oxide were mixed separately in Kerosene with concentration 15 gm/l. Effects of four parameters like a pulse on time (15-100 μs), pulse off time (10-75 μs), current (3-9 A), and types of powder (graphite and aluminium oxide) were used to investigate variations in microhardness and surface roughness. Grey relational grades were calculated based on the mean value of the grey relational coefficient of both responses. Set of the parameter has the highest value of GRG indicates an optimum multi-response solution. Predicted values of responses based on grey relational grades were confirmed with running experiments on

EDM with setting input parameters predicted by the grey relational analysis. Pulse on time was found the most significant parameter [135].

Reddy V. V. et al. (2014) investigate the effects of various process parameters of die-sinking EDM on performance characteristics such as MRR, TWR and SR. Experiments were performed on PH17-4 steel using electrolytic copper electrode. SAE 450 EDM oil was used as a dielectric. Experiments were performed as per combinations of various process parameters obtained using Taguchi's L9 orthogonal array. Levels of different parameters like peak current (10-20 A), surfactant concentrations (4-8 gm/l), graphite powder concentrations (4.5-13.5 gm/l) were used for experimentations. Multi-objective optimization carried out using Taguchi- DEAR method. The optimal set of input parameters were derived from maximizing MRR and minimize SR and TWR [136].

Ramprabhu T. et al. (2018) validate a new meta-heuristic algorithm named passing vehicle search algorithm using previously performed experiments on EDM. As compared to other optimization techniques better results obtained using a passing vehicle search algorithm. Localized optimum results can be obtained using the Pareto front because of the regression model and the PVS algorithm based on populations [137].

Parsana Sohil et al. (2018) carried out multi-response optimization of EDM parameters using metaheuristic algorithm named passing vehicles search algorithm. Experiments were performed on Mg–RE–Zn–Zr alloy using EDM with the copper electrode. Kerosene was used as EDM dielectric. Experiments were design based on Box–Behnken design using response surface methodology. EDM process parameters such as discharge current (1-50A), pulse on time (1-10 μs), and pulse off time (1-10 μs) were used to study its effects on MRR, TWR, and roundness of hole. A mathematical model based on response surface methodology (regression analysis) were developed for MRR, TWR, and roundness of hole. Priori articulation was used to identify the weight of individual parameters for multi-objective optimization. An optimal set of input parameters were identified based on the Pareto front for Maximum MRR and minimum TWR and roundness [138].

Nguyen H. et al. (2018) performed experiments on different steel SKD61, SKD11, and SKT4 using EDM. Copper and graphite rod were used as EDM electrode. HD-1 oil was selected as dielectric and titanium powder mixed at different concentration. Experiments were performed as per Taguchi's L27 orthogonal array. Influence of types of the electrode (Cu, Gr), electrode polarity (+,-), pulse on time (5-20 μs), peak current (4-8 A), pulse off

time (38-85 μs), and powder concentration (0-20 gm/l) were evaluated on MRR, SR, and MH. EDM parameters were optimized using TOPSIS- Taguchi methods. Results of experiments were concluded that improvement in EDM efficiency due to mixing Ti powder. Increased in MRR and MH with a reduction in SR were observed due to the mixing of Ti powder. SEM images indicate a reduction in microcracks, porosity, and crater. [139].

Kumar Anil et al. (2010) carried out the multi-response optimization of abrasive PMEDM parameters using grey relational analysis. Experiments were performed on EN-24 steel using EDM with 8 mm diameter copper electrode and kerosene as a dielectric. Silicon powder with different concentrations was mixed in kerosene. Experiments were designed using Taguchi's L8 orthogonal array. Both the objective (maximize MRR and minimize SR) are in conflict nature and hence multi-response optimization technique named grey relational analysis was used to obtained an optimal set of input parameters. Grey relational grade (GRD) was calculated for all experiments using gray relational coefficient. Grey relational analysis was successfully used to optimize PMEDM process parameter [140].

Kumar Satish et al. (2017) performed experiments on Inconel-800 using EDM with different types of electrode. Experiments were performed using SEA 450 EDM oil with the mixing of tungsten carbide, cobalt and boron carbide powders at 6 gm/l concentrations. Experiments were designed as per the Box-Behnken model of response surface methodology. Total of 46 experiments was performed as per combinations of process parameters. Effects of peak current (4-12 A), pulse on time (60-120 μs), pulse off time (30-60 μs), material of tool electrode (tungsten- carbide, cobalt, and boron-carbide) and types of powders were investigated on responses material removal rate (MRR) and tool wear rate (TWR). The mathematical model was developed using regression analysis. Multi-objective optimization has been performed using composite desirability approach to an obtained single set of process parameters which maximize MRR and Minimize TWR. Results of experiments indicated peak currents, pulse on time and material of the electrode have been found most significant parameters for MRR. Pulse on time and tool materials were the most significant parameters for TWR. Predicted results of responses were confirmed with the experimental result by performing experiments on EDM. EDS/XRD analysis indicates migration of powder particles from dielectric to work surface [141].

Khullar Ved Raj et al. (2017) carried out a comparative study of various flushing methods of EDM performance. Experiments were performed on AISI 5160 steel using electrolytic copper electrode. Process parameters such as pulse-on time (100-500 μs), pulse off time (30-390 μs), peak current (1-12 A) and flushing mode (1-5) were used to study its effects on MRR and SR. Total 30 experiments were performed as per second-order central composite rotatable design using response surface methodology. Regression/mathematical model for MRR and SR were obtained using response surface methodology. Multi-objective optimization technique NSGA-II was used for obtaining a single set of input parameters. T_{on} (31.1%) and T_{off} (30.49%) was observed most significant parameters to enhance MRR while T_{on}: 28.46%; T_{off}: 25.27%; I: 16.69% were observed most significant for surface roughness. Predicted results of responses were confirmed by performing experiments on EDM. Good agreements between predicted results and experimental results of responses were observed with tolerable errors [142].

Kanagarajan D. et al. (2007) studied the effects of levels of parameters on machining WC-Co alloy. Experiments were performed using a copper electrode with kerosene as a dielectric. Total of 27 experiments was performed using combinations of various parameters as per Taguchi's L27 orthogonal array. The effects of rotational speed (250-1000 rpm), pulse current (5-15 A), pulse on time (200-1000 μs), and flushing pressure (0.5-1.5 kg/cm^2) were used to find its effects on MRR and SR. Mathematical/regression model for MRR and SR have been developed using Minitab statistical software. Multi-objective optimization has been performed to the obtained optimal (single) set of process parameters for maximum MRR and minimum SR using NSGA-II. Results of experiments indicate a total of 26 solutions have been obtained using NSGA-II, and solutions can be selected according to the objective of responses [143].

Singh Jagdeep et al. (2016) performed experiments on tungsten carbide (WC) using EDM with a copper rod as the electrode. During experimentation, two conductive powders graphite and Al_2O_3 were mixed separately in the dielectric with concentrations 15gm/l. Experimental matrix was derived as per Taguchi's L27 orthogonal array. Pulse on time (15-100 μs), pulse off time (10-75 μs), peak current (3-9 A), and types of powders were selected to study its effects on microhardness and surface roughness. SEM, EDS, and XRD analysis were performed to study the surface morphology of the machined surface. The EDS spectrum indicates migration of powder elements from dielectric to work surface. Both the objective (maximize MH and minimize SR) are opposite in nature, hence multi-

objective optimization has been performed using grey relational analysis. Maximum grey relational grade indicates the optimum solution. Results of experiments indicate MH and SR improved by 12.31% and 5.61% respectively. Formation of various phases such as F6W6Cal, FeC, Fe6W6CWCC, and Fe6W6CC was observed during XRD analysis. SEM analysis indicates defects free and uniform recast surface [144].

Dr. Xuan et al. (2017) performed multi-response optimization of EDM parameters using particle swarm and kriging model algorithm. Experiments were performed on AISI P20 steel and copper rod used as an electrode. Experiment matrix was obtained as per Taguchi's L27 orthogonal array. Variations in peak current (4-13 A), discharge voltage (50-70 V), pulse on time (2-8 μs), and pulse off time (4-12 μs) were used to investigate its effects on MRR, TWR, and SR. Main objective of experimental work was to maximize MRR, minimize TWR and SR. Multi-objective optimization was carried out using combinations of kriging model and particle swarm optimization algorithm to obtained single set of parameters able to fulfil objectives of work [145].

Baraskar S. et al. (2013) performed multi-objective optimizations of EDM parameters using NSGA-II algorithm. Experiments were performed on EN-8 steel with the rectangular copper electrode and EDM oil as a dielectric. Total of 20 experiments was performed according to combinations of various input parameters obtained using response surface methodology. Regression/quadratic model has been developed for MRR and SR using Design Experts 8.0 software. According to ANOVA result, discharge current was observed most significant parameters. The optimal set of input parameters has been obtained according to the Pareto optimal chart using NSGA-II algorithm [146].

P. Mathan Kumar et al. (2017) performed experiments on Monel 400 alloy using EDM with powder metallurgy electrode. Powder metallurgy electrode manufactured from combinations of copper-titanium diboride powders. Experiments were designed as per central composite rotatable design (CCD) using response surface methodology. Total of 30 experiments was performed as per combinations of various input process parameters. Percentage of TiB_2 (4-20 %of wt), pulse current (2-10 A), flushing pressure (0.4-1.2 MPa), pulse on time (10-50 μs), were used to measure variations in MRR and TWR. Quadratic equations for MRR and TWR were developed using design expert software. TiB_2 proportions with copper helped to reduce TWR. Good agreements were observed between the predicted and experimental value obtained by performing experiments on EDM [147].

Kolahan Farhad et al. (2008) performed experiments on cobalt bonded tungsten carbide using powder mixing EDM. Aluminium powder was mixed in kerosene and the copper rod was used as EDM electrode. Experimental matrix for 30 experiments designed according to second-order central composite rotatable design (CCD) using response surface methodology. The particle size of aluminium powder (1.5-2.5 μm), powder concentration (10-20 gm/l), peak current (2-3 A), and pulse on time (100-200 μs) were used to study variations in MRR and EWR. ANOVA for MRR and EWR were carried out to find the contribution of input parameters. Multi-objective optimization has been performed using the genetic algorithm. Finally, it is concluded that the genetic algorithm is successfully applied to optimize EDM parameters [148].

Singh B. et al. (2015) performed experiments on H13 steel using EDM, while chromium powder mixed with kerosene. Electrolytic copper rod was used as EDM electrode. Total of 31 experiments was performed as per Taguchi's L31 orthogonal array. Regression equations for MRR and TWR were developed using Minitab13 software. Both the objectives are conflicting nature and hence multi-objective optimization using desirability functions was carried out to find the optimal solution of parameters which satisfy both the objectives (maximum MRR and minimum TWR). Peak current and duty cycle were observed the most significant parameters for MRR. Lower tool wear rate was observed with high chromium powder concentration [149].

Singh K. et al. (2018) carried out multi-objective optimization of powder mixed EDM parameters using grey relational analysis. AISI D2 steel was selected as work material and kerosene was used as a dielectric. Experiments were designed/performed according to Taguchi's L16 orthogonal array derived using Minitab7 statistical software. The effects of variations in pulse on time (20-30 μs), discharge current (10-20 A), types of electrode material (Cu-Cr, and Cu), and grit size of powder particles (280-600) were considered to measure MRR, TWR, and SR. Grey relational grades were obtained from the values of grey relational co-efficient of MRR, TWR, and SR. Highest value of grey relational grade indicate an optimal set of input parameters. The optimum value of MRR was obtained 28.089 mm^3/min with Cu-Cr electrode at peak current = 20A, pulse on-time = 30 μs, and grit size = 280. Highest TWR was obtained in Cu-Cr electrode [150].

2.8 GAPS IN LITERATURE

From the elaborative study of literature related to surface modification using EDM, it has been observed that the process is still at an experimental stage. Experiments were performed on the different tool and die steel to reveal that the transfer of electrode elements on the work surface under optimum machining conditions. Variations in the microstructure of EDMed surface was observed due to the addition of carbon in free form or carbide form through pyrolysis of hydrocarbon dielectric. Although the surface modification process using EDM is governed by a large number of process parameters, experimentation by researchers carried out using limited numbers of process parameters using the Taguchi method. After rigorous studies of published literature related to surface modification of die and tool steel using EDM, the following important gaps have been identified.

- No surface modification work using EDM has been reported with P20+Ni steel as work material, the steel is very popular and widely used for manufacturing die and tool for composite plastic products.
- No surface modification work has been reported related to use of EDM electrode manufactured from metallic powders such as copper (75% of wt), tungsten (23% of wt) and silicon (2% of wt).
- Numbers of research work have been reported with limited numbers of process parameters; however, it is necessary to consider combinations of powder metallurgy electrode parameters and EDM parameters to obtained optimum machining conditions.
- The literature review indicates that the researchers have performed most of the experimental work related to development, control and monitoring EDM process, however limited work available regarding optimization of surface modification process variables.
- The effect of machining parameters on P20+Ni die steel has not been fully explored using powder metallurgy electrode manufactured a homogeneous mixture of three conductive powders such as copper, tungsten, and silicon.
- Very less work available was related to surface qualities and surface morphology of EDMed surface using SEM, EDS and XRD analysis.
- Very less attention has been given to perform multi-response optimization of EDM process used for surface modification with P/M electrode.

CHAPTER – 3

EXPERIMENTAL PLANNING AND PROCEDURE

3.1 INTRODUCTION

Transfer of either electrode material or powder particles from dielectric to work surface have been observed under specific machining conditions only. Therefore, it is very mportant to select the proper levels of process parameters for surface modification. Quality and topography of surface obtained is mainly depends on the level of process parameter and P/M electrode parameter. List of machining and electrode parameters, which greatly affect on surface modification process are listed in Table 3.1.

Table 3.1 List of process governing parameters

Machining Parameters	**Electrode Parameters**
Peak current	The average particle size of the powder
Pulse on time and off time	Composition of powders
Pulse waveform	The shape of powder particles
Duty cycle	Compaction load
Discharge voltage	Sintering temperature
Polarity	
Electrode gap	
Types of dielectric	
Flushing pressure	
Pulse frequency	

Each parameter has a specific role to contribute the surface modification process. Number of parameters with specific objectives have been considered by researchers during experimentation and their outcomes have been summarised as the literature review. In the present experimental work three machining parameters and one P/M electrode parameter have been considered for surface modification. Four parameter have been selected with

five levels. Experimental setup (EDM machine) has facility to set selected levels of individual parameters conveniently.

It is an important task to select process parameters and their levels for final experiments. Number of preliminary experiments were performed to decide the desire range of effective parameters for pilot experiments. Level of parameters for final experiments were decided based on the result of pilot experiments. Varying one parameter at time approach was used to finalise the levels of process parameters for pilot experiments. Experiments were performed using straight polarity (electrode negative) on EDM.

3.2 MACHINE TOOL SPECIFICATIONS

Experiments were performed on die sinker EDM model M25-6040 (Make: Maruti machine tools, Baroda, India) shown in Figure 3.1. The EDM was installed at the workshop of Government Engineering College, Bhavnagar, Gujarat, India. The die sinker EDM has the following specifications listed in Table 3.2.

Table 3.2 Specifications of EDM machine

Machine Element		**Specification**
Size of Oil Container	:	650 X 400 X 300 mm
Table Size	:	400 X 250 mm
X-Axis travel	:	250 mm
Y-Axis travel	:	150 mm
Z-Axis travel	:	150 mm
Maximum job height	:	165 mm
Maximum job weight	:	150 kg
Maximum current	:	25 Amp
Best MMR	:	140 mm^3
Connected load	:	2 KVA
die electric tank capacity	:	200 ltr
Supply Volts	:	415 V, 3 Ø, 50 Hz
Maximum Table-Quill distance	:	340 mm
Minimum Table-Quill distance	:	190 mm

Figure 3.1 Pictorial view of EDM machine used for experimentation

3.3 WORK MATERIAL

For the present experimental work, one of the most popular and widely accepted die steel P20+Ni is used as work material. Generally, injection moulding die and die frame used for the composite plastic product is manufactured from P20+Ni steel. The steel is also used to manufacture large size plastic product mould, home appliances, car accessories, electronic equipment, boaster plates of presses, shoe block for drop hammers etc. The chemical composition of P20+Ni steel is given in Table 3.3.

Table 3.3 Composition of P20+Ni steel

Element	C	Si	Mn	P	S	Cr	Mo	Ni	Cu	V	Fe
Wt %	0.36	0.27	1.25	0.01	0.006	1.86	0.17	0.95	0.071	0.065	Balance

P20+Ni steel exposed very high strength and toughness and hence machining of such steel using conventional technique is found most difficult and hence, The P20+Ni steel categorized under difficult to machine material. The various physical and mechanical properties of P20+Ni steel are given in Table 3.4.

Table 3.4 Physical and Mechanical properties of P20+Ni steel

Physical/Mechanical Properties	Value
Density	7861 Kg/m^3
Specific Gravity	7.86
Modulus of Elasticity	190- 207 GPa
Poisson's Ratio	0.27-0.30
Thermal Conductivity	41.5 w/m/°k
Tensile Strength (Ultimate)	965-1030 MPa
Tensile Strength (Yield)	827-862 MPa
Compressive Strength	862 MPa

The individual experiments were performed on P20+Ni steel specimens. The specimens were cut into size 25 mm x 25 mm x 10 mm and finished using surface grinder. The pictorial views of machined samples of P20+Ni steel are shown in Figure 3.2.

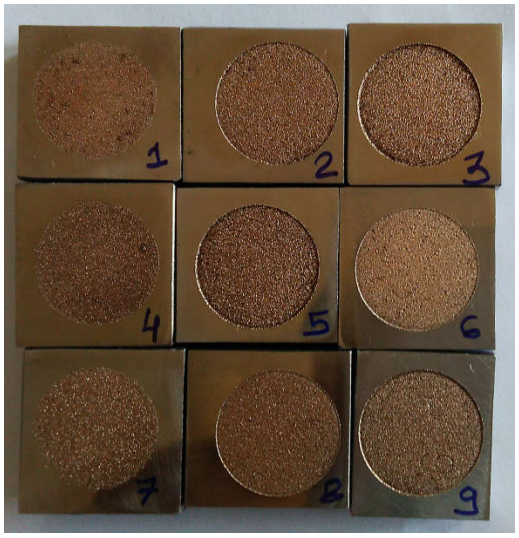

Figure 3.2 Work material specimens used for experimentation

3.4 PROPERTIES OF POWDERS USED FOR PREPARING ELECTRODE

For present experimental work, three different powders such as copper, tungsten and silicon are used to manufacture EDM electrode. The powders were mixed in proportions

such as copper (75 % of wt), tungsten (23 % of wt) and silicon (2 % of wt). The pictorial view of three powders and their properties are given in Figure 3.3 and Table 3.5 respectively.

Copper Powder (Cu) Tungsten Powder (W) Silicon Powder (Si)

Figure 3.3 Pictorial views of copper, tungsten and silicon powders

Table 3.5 Properties of metal powders

Material	Density (gm/cm^3)	Melting Point (k)	Specific heat (J/Kg K)	Thermal conductivity (W/mK)	Coefficient of thermal expansion *(10^{-6}/K)	Particle size (micron)	Electrical Conductivity (S/m) at 20 °C
Cu Powder	8.97	1355	385	393	16.5	44	5.96×10^7
W Powder	19.29	3683	138	166	4.5	10	1.79×10^7
Si Powder	2.33	1687	680	149	2.6	44	1.00×10^3

3.5 PREPARATION OF POWDER METALLURGY ELECTRODE

Physical and mechanical properties of powder metallurgy electrodes play significant role in the surface modification process to be performed using P/M electrode. It is desired to obtain the density of powder metallurgy electrode lower than conventional EDM electrode, results in easily separation of hard constituents from P/M electrode. Following steps are followed to manufacture powder metallurgy electrodes:

Step 1: P/M electrodes were produced from a mixture of three fine metallic powders such as copper (75 % wt), tungsten (23 % wt) and silicon (2 % wt). The powder materials were weighted separately using laboratory precision balance has weight accuracy 0.001 gm. Precision balance used is shown in Figure 3.4(a).

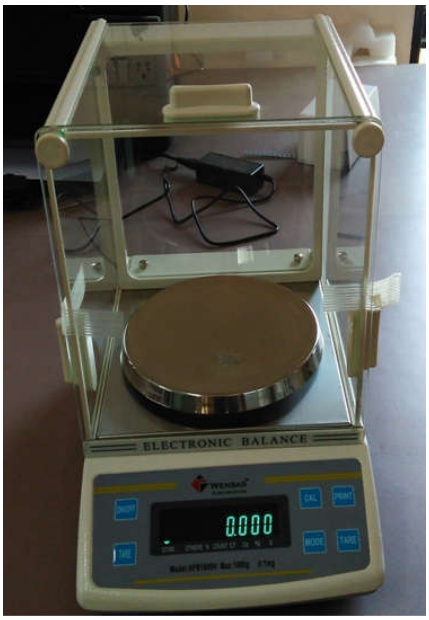

Figure 3.4(a) Precision electronic balance used for weighing metal powder

Step 2: After weighing three powders separately as per the required quantity, the next step is to obtained proper mixtures of it. A specially fabricated stirer was used for mixing the powders. Powder blending device was fabricated from galvanised sheet strips, which fitted with lead of jar shown in Figure 3.4(b). After pouring three powders into jar stirrer was fitted with the jar and finally the device was clamped with lathe chuck shown in Figure 3.4(c). Lathe chuck was operated at different rpm for total 1 hrs duration.

Figure 3.4(b) Stirrer used for mixing metal powders

It is desired that the three metal powders mixed properly prier to compacting and hence SEM of powder mixture was carried out. The distribution of tungsten (white) and silicon (black) in copper matrix have been observed during SEM shown in Figure 3.4(d). Further EDS of powder mixture was also carried out to evaluate the elements present in powder

mixture. No presence of any foreign material/impurity other than powders were observed during EDS analysis. The EDS picks are shown in Figure 3.4(e).

Figure 3.4(c) The stirrer clamped on lathe chuck

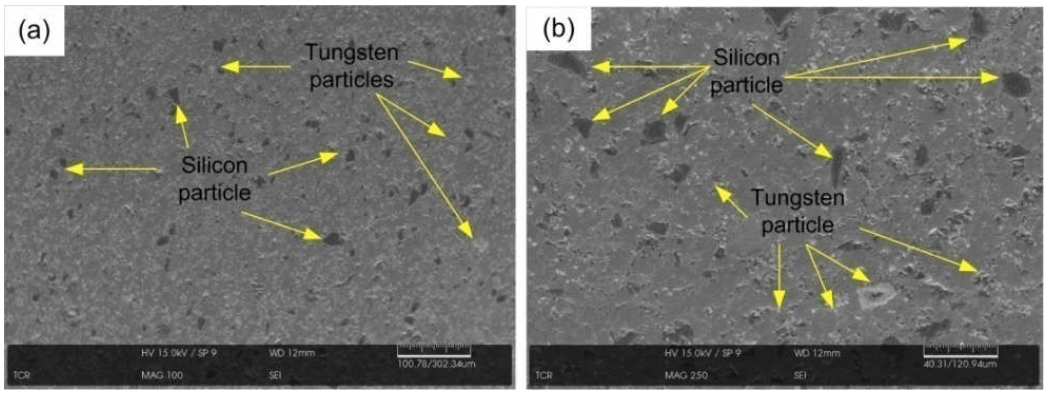

Figure 3.4(d) SEM images of powder mixture

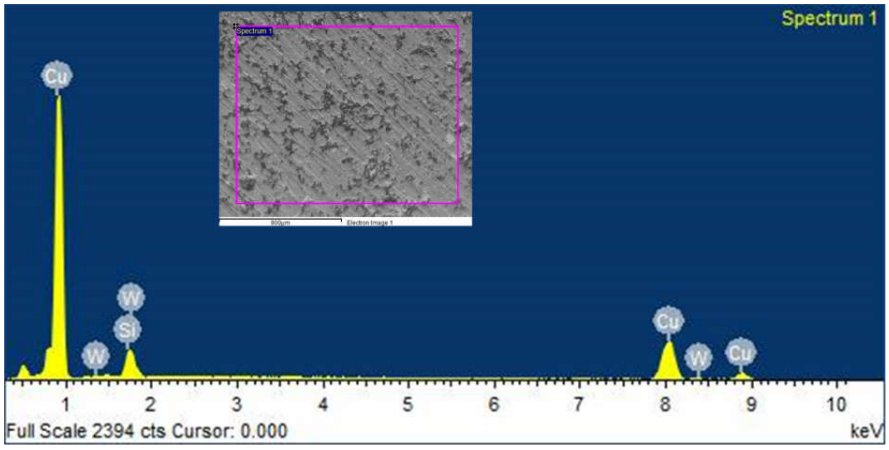

Figure 3.4(e) EDS spectrum of powder mixture

Step 3: After confirmed a proper mixture of Cu, W and Si powders, the mixture was pressed using die assembly (Bore dia. = 19mm) fabricated from tool steel shown in Figure 3.4(f). Die, punch and die cap were manufactured using in-house workshop facilities and then chrome plated to maintain the required surface finish, hardening and wear properties.

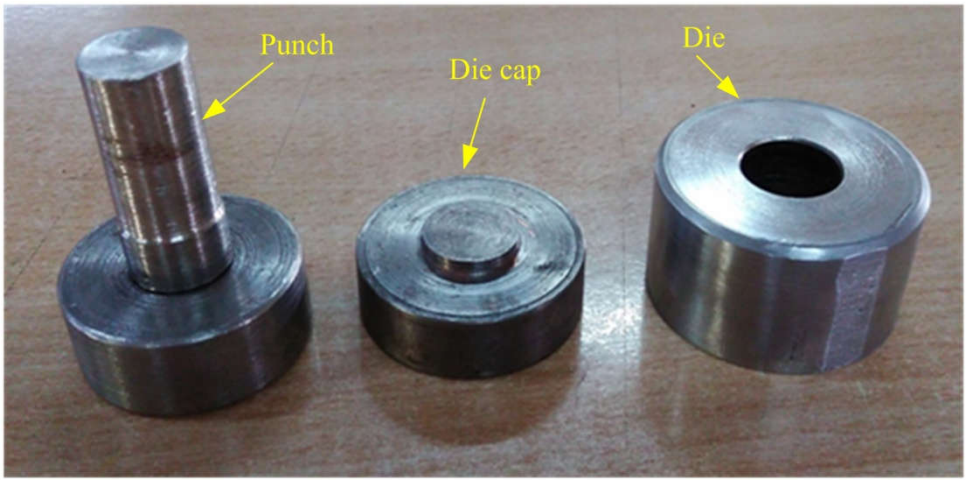

Figure 3.4(f) Die elements used to produce P/M compact

Step 4: Powder mixture was poured in to die and pressed it using a hydraulic press at different compaction pressure. The hand-operated hydraulic press was used to press the mixture of powder. Compaction pressure can be easily controlled using hand-operated the hydraulic press. The pictorial view of hand operated hydraulic press is shown in Figure 3.5(g).

Figure 3.4(g) Hand operated hydraulic press

Step 5: Electrode is ejected after pressing the powder mixture to die at a specific load. The applied load was held for a few minutes and then released. After realising load, the compact is ejected from die. The ejected compacts are shown in Figure 3.4(h).

Figure 3.4(h) Ejected P/M compact from die

Step 6: The P/M electrodes are small in length (10 mm) and hence cannot clamp directly on EDM. Specially fabricated aluminium fixture was used to clamp the P/M electrode. Electrolytic copper rod was fitted at one end and P/M compact at other end using an adjustable clamp. Proper care was taken, while clamping different P/M compact for individual experiment. The fabricated aluminium fixture is shown in Figure 3.4(i).

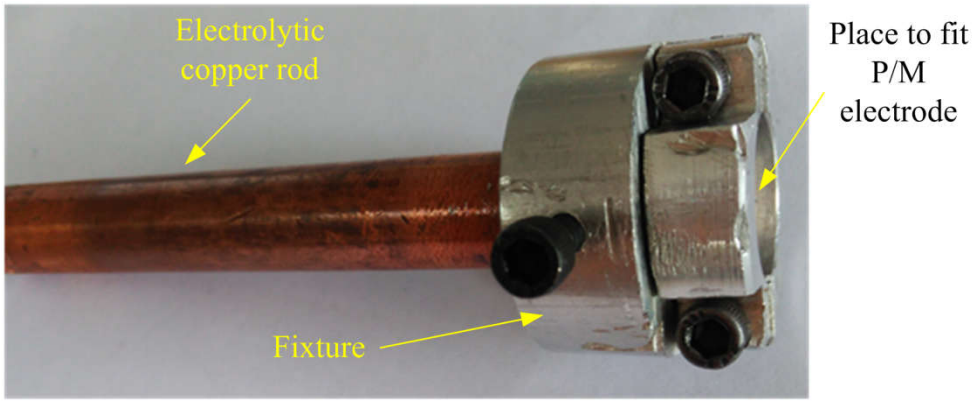

Figure 3.4(i) Fixture used for clamping P/M compact

3.6 MEASUREMENT OF RESPONSES

Experimental work was carried out as an aspects of surface modification of P20+Ni die steel using P/M electrode. Elements from P/M electrode were transferred under specific machining conditions only. Hence, it is necessary to measure the performance of EDM while machining is performed using P/M electrode. Attempts have been made to study the role of P/M electrode on surface morphology and surface topography. Various responses such as material removal rate (MRR), tool wear rate (TWR), surface roughness (SR) and

microhardness (MH) were evaluate and analysed during experimental work. Further SEM, EDS and XRD were also carried out for selected machined samples to confirm the migration of P/M electrode materials and to investigate the surface condition. The methodologies used for the measurement of responses are described below:

3.6.1 Material removal rate (MRR)

Powder metallurgy electrode must be capable to machining the work material. If the electrode is not capable to erode the work material, then no molten pool created, results in no transfer of electrode material. Amount of work material removed within the unit time is calculated by measuring the weight of the workpiece before and after machining. Steel specimens were cleaned using acetone before and after machining to maintain desired accuracies. Weight of work material was measured using laboratory precision balance. The material removal rate is calculated using equation 3.1.

$$MRR = \frac{W_{bm} - W_{am}}{T_m} \ gm/min \quad \text{------} \quad \textbf{(3.1)}$$

Where,

MRR = material removal rate gm/min

W_{bm} = weight of workpiece before machining in gm

W_{am} = weight of workpiece after machining in gm

T_m = total machining time in minutes

3.6.2 Tool wear rate (TWR)

Tool wear rate is very important parameters for EDM operation performed as an aspects of surface modification. Dimensional accuracy and surface quality of the EDMed product is mainly depends on electrode wear. Very high electrode wear is deteriorate the EDM performance because of arcing. Optimum tool wear rate is desirable for surface modification. The electrode is cleaned using acetone before and after machining. The TWR is calculated using formula 3.2.

$$TWR = \frac{W_{tb} - W_{ta}}{T_m} \ gm/min \quad \text{--------} \quad \textbf{(3.2)}$$

Where,

TWR = tool wear rate gm/min

W_{tb} = weight of tool before machining in gm

W_{ta} = weight of tool after machining in gm

T_m = total machining time in minutes

3.6.3 Surface roughness (SR)

The rough surface of engineering component is always work as stress raiser, which results in development of crack and corrosion, will lead to early failure of component. Irregularities in surface obtained during machining are considered as rough surface. In other words, surface roughness is defined as the deviation of a surface from its geometrical mean. If the deviation is higher than it is considered as rough surface and surface with lower deviation is finish surface. Ra value of machined sample was measured using "ITI surf test RS 232" (make: ITI, India) surface roughness tester shown in Figure 3.5. The cut-off length was 10 mm for measurement of average deviations. Mean value of three measurements in different directions is considered as the final results for further analysis.

Figure 3.5 Surface roughness tester

3.6.4 Microhardness (MH)

Increase in microhardness of work surface during machining are desired as compared to the base material. Microhardness of work material was measured prior and after the experiment. Three reading of microhardness were taken at different locations and the mean value of it was considered as final microhardness. The microhardness of the work surface was measured using digital microhardness tester (Model No. 7005 – B, Vaisesika).

Microhardness is measured under 300 gf load condition with 15 second dwell time. Sample machined using P/M electrodes indicates high microhardness as compared to electrolytic copper electrode. Vickers microhardness tester was used for measuring microhardness is shown in Figure 3.6.

Figure 3.6 Vickers microhardness tester

3.6.5 Surface morphology

Scanning electron microscope (SEM) is an important metallurgical device used to study the surface morphology of machined samples. SEM uses focused beam of electrons to produce an image of the machined samples. Interaction between electrons produces various signals that can be detected and studied to derived information about surface topography. The electron beam is generally scanned in a raster scan pattern, and the beam's position is combined with the detected signal to produce an image. SEM can achieve a resolution better than 1 nanometre. The EDS analysis of selected machined samples were carried out to confirm the migration of P/M electrode elements on the work surface during machining. TRACOR NORTHERN, TN-5500 attachment with SEM was used for the EDS. SEM images with different magnification were obtained using a microscope (Make: JOEL, Japan, Model: JSM- 6010 LA) shown in Figure 3.7.

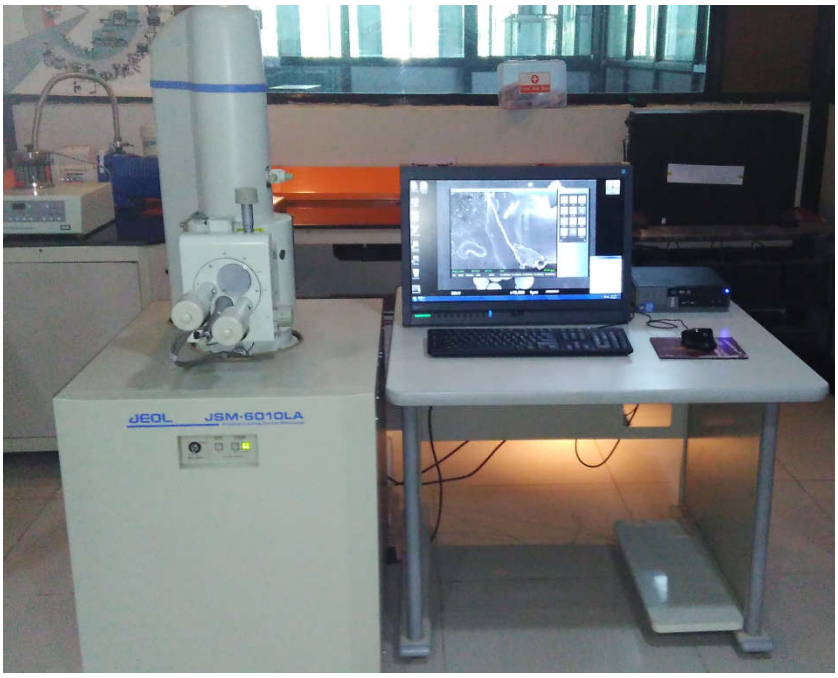

Figure 3.7 Scanning electron microscope setup

3.6.6 Identification of various phases

The various phases formed during machining were confirmed using X-ray diffractometer. Presence of tungsten, silicon and copper were observed during the EDS analysis. Hardness and abrasion resistance of EDMed surface depended on phases formed during machining. Selected EDMed samples were analysed using X-ray diffractometer (Make: BRUKER, USA, Model: D2 PHASER) shown in Figure 3.8(b).

X-ray diffraction is working on the principle of Bragge's law. During the interaction of X-ray with electron atom, some photons of them deflect its directions and scattering pattern of photons was generated. These scattered X-rays were carried information about the distribution of electron in the material. Diffracted waves from different atoms can interfere with each other and the resultant intensity distribution is strongly modulated by this interaction. If the atoms are arranged in a periodic fashion, as in crystals, the diffracted waves will consist of sharp interference maxima (peaks) with the same symmetry as in the distribution of atoms. Measuring the diffraction pattern, therefore, allows us to deduce the distribution of atoms in a material.

The peaks in an x-ray diffraction pattern are directly related to the atomic distances. Let us consider an incident x-ray beam interacting with the atoms arranged in a periodic manner

as shown in two dimensions in the following illustrations. For a given set of lattice plane with an inter-plane distance of d, the condition for diffraction (peak) to occur can be simply written as:

$$\mathbf{2d\sin\theta = n\,\lambda \quad ------ \quad (Bragge's\ law) \quad (3.3)}$$

This is known as the Bragg's law. In the equation, **λ** = wavelength of the x-ray, **θ** = the scattering angle, and **n** = an integer representing the order of the diffraction peak. Bragg's Law is used for interpreting x-ray diffraction data. It's principle is shown in Figure 3.8(a).

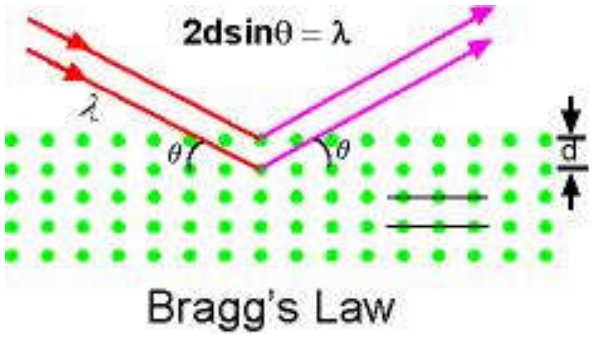

Figure 3.8(a) Principle of Bragg's law

Figure 3.8(b) X-Ray diffractometer

3.7 EXPERIMENTAL DESIGN STRATEGY FOR PILOT EXPERIMENTS

In this experimental works, an attempts have been made to obtain a surface modification of the P20+Ni die steel using electrode manufactured through powder metallurgy process. The migration of elements from P/M electrode has been observed under specific machining conditions only, therefore variation in input process parameters during pilot experiments were considered as follow:

a) Three levels of compaction pressure (C_p): The main reason to vary compaction pressure is to find an optimum density level of P/M electrode. If the density of P/M electrode is lower, resulting high tool wear rate. High wear rate transfers a large amount of electrode material towards the inter-electrode gap and hence unstable sparking action with arcing.
b) Three levels of peak current (I_p): More than two levels of process parameter are desired to study non-linear behaviour of the process. Peak current was one of the important parameter observed during a literature survey.
c) Three levels of pulse on time (T_{on}): Pulse on time is indicate time of discharge during a cycle. If experiments were performed with a longer pulse on time, high energy available for longer duration and hence improvement in EDM performance.

Experiments were designed using Taguchi's design of experiments technique. Three parameters and each has three levels were considered to study its effects on responses such as MRR, TWR, SR and MH. Experiments were performed as per Taguchi's L9 orthogonal array. Effects of process parameters on material removal rate were considered to evaluate the machining capability of EDM using P/M electrode. Efficient and economical machining is desired using the P/M electrode. Tool wear rate (TWR) was considered as second responses. Optimum tool wear is an ideal condition for surface modification using EDM. Excess TWR is leads to high machining cost and unstable machining operation. Surface roughness was considered as a third response. Reduction in lubrication condition and initiation of microcracks will lead to early failure of components due to the rough surface. Therefore the significance of process parameters was evaluated to obtained finish surface. Microhardness was considered as a fourth response. Improvement in microhardness of machined surface was desired as an aspect of surface modification.

Effects of process parameters on MRR, TWR, SR and MH were studied using Taguchi technique. Experimental results were analyzed using Minitab17 statistical software to

obtain optimum machining condition with contribution of individual parameters for surface modification. Experiments were performed on EDM with auto flush mode and quill moved periodically up and down to flush away the debris. An individual experiment was performed for 10 minutes duration. The parameters kept constant during experimentation are shown in Table 3.6.

Table 3.6 Fixed input process parameters

Sr. No.	Working Conditions	Description
1	Work piece material	P20+Ni die steel
2	Electrode composition	75 % Cu+ 23% W+2%Si (% of weight)
3	Electrode diameter	Φ = 19 mm
4	Polarity	Negative Electrode
5	Dielectric fluid	EDM Oil (Pacific oil 300)
6	Flushing type	Side flushing
7	Flushing pressure	0.75 kg/cm^2
8	Processing time	10 minutes
9	Duty cycle	50 %
10	Gap voltage	60 Volt

3.7.1 Selection of orthogonal array for pilot experiments

In this experimental work, the effects of three process parameters such as compaction pressure, peak current and pulse on time were considered to derive the optimum machining condition, which transfers the hardest constituents of the electrode on the work surface. Each parameter has been selected with three levels. According to Taguchi technique, total numbers of experiments should be higher than total numbers of degrees of freedom. Degree of freedom is defined as a number of levels (n) minus one for a individual parameter. In this case, each parameter has three levels, therefore two degree of freedom for each parameters. Total degrees of freedom for three parameters are six. Standard orthogonal array, which has higher than six degrees of freedom is L9 orthogonal array. Therefore pilot experiments were decided to perform using standard L9 orthogonal array. The combinations of different levels in L9 orthogonal array is shown in Table 3.7 [151].

Table 3.7 L9 Orthogonal array of Taguchi design of experiment

Exp. No	Column for Factors		
	A	B	C
1	1	1	1
2	1	2	2
3	1	3	3
4	2	1	2
5	2	2	3
6	2	3	1
7	3	1	3
8	3	2	1
9	3	3	2

The individual experiments were performed by setting levels of parameters given in the row of the orthogonal array. Experiments were performed randomly to avoid the effects of noise. The individual experiment was performed thrice to minimize the effect of uncontrollable factors. The final result of the response is the mean value of the three results, which used for further analysis.

3.7.2 Signal to noise (S/N) ratio for responses

The result of responses mainly depends on controllable and uncontrollable parameters. Controllable parameters are those whose value can be easily set or controlled. Some of the parameters like tool wear, temperature, humidity etc. are not under control during experimentation. These uncontrollable parameters are known as noise. Experiments must be performing with a high signal-to-noise ratio to avoid the effect of uncontrollable parameters. The optimum levels of selected parameters are determined using the design of experiment technique [152]. The deviation of response from its target value is known as quality loss. Uncontrollable parameters are mainly responsible for the deviation of responses from its target values. Taguchi method is helpful to develop a robust design of experiment with the minimum effect of noise.

The main purpose of performing experiments is to obtain the highest signal-to-noise ratio of the responses. The maximum value of signal-to-noise ratio indicates that the effects of signals (controllable parameters) are higher than noise (uncontrollable parameters). According to objectives of responses, following three types of signal-to-noise ratios are considered for experimental works.

1) Larger the better:

$$\frac{S}{N} = -10 \log_{10}[\frac{1}{n} \Sigma\, 1/y_i^2] \quad \text{---------- (3.4)}$$

Where n is a number of results in a row, here, in this case, n = 1, and y = value of i^{th} experiment in a row.

2) Smaller the better:

$$\frac{S}{N} = -10 \log_{10}[\frac{1}{n} \Sigma\, y_i^2] \quad \text{-------- (3.5)}$$

Where n is a number of results in a row, here, in this case, n = 1, and y = value of i^{th} experiment in a row.

3) Nominal the best:

$$\frac{S}{N} = 10 \log_{10}[\frac{1}{n} \Sigma\, (y_i - y_0)^2] \quad \text{--------- (3.6)}$$

Where, y_i = value of i^{th} experiment in a row

y_o = Nominal value of the responses

n = Number of results in a row

For present experimental work following targets have been set for responses.

(1)	Response Name	:	Material removal rate (MRR)
	Response Type	:	Larger the better
	Units	:	gm/min
(2)	Response Name	:	Tool wear rate (TWR)
	Response Type	:	Smaller the better
	Units	:	gm/min

(3) Response Name : Surface roughness
Response Type : Smaller the better
Units : Ra value in microns

(4) Response Name : Microhardness
Response Type : Larger the better
Units : Vickers hardness number (VHN)

Results of responses were analyzed using S/N ratio and best combinations of input parameters were obtained using Taguchi technique. Signal to noise ratio for MRR and MH were calculated using equation 3.4. Subsequently, the S/N ratio for TWR and SR were calculated using equation 3.5. ANOVA was performed for MRR, TWR, SR and MH to derive the contribution of the individual parameter to achieve the desired objective [153].

3.8 SELECTED INPUT PARAMETERS FOR PILOT EXPERIMENTATION

After elaborating numbers of previous work, it has been observed that the peak current and pulse on-time play significant role to establish the surface modification phenomenon. Further, selection of compaction load for powder metallurgy electrode is also important. Effect of these parameters on MRR, TWR, SR and MH were evaluated during pilot experimentation. Amount of material transfer from the electrode body to work surface is mainly depends on electrode wear. However high electrode wear is also responsible for arcing due to discharge of excess powder particles at the inter-electrode gap. Weight of work material and electrode are measured before and after the experiments to obtain MRR and TWR. Microhardness of work material before the machning is measured 322 VHN using vickers microhardness tester.

Table 3.8 Selected input parameters and their levels

Symbol	Parameters	Unit	Levels		
			L1	L2	L3
A	Compaction pressure (C_p)	(kg/cm^2)	125	225	325
B	Peak Current (I_p)	(Amp.)	6	12	18
C	Pulse on time (T_{on})	(μs)	50	90	130

The level of input process parameters for pilot experiments were decided based on cause and effect analysis, combining the reference available in EDM operation manual, manufacturer's catalogue and material handbook. Further number of trail runs performed prior to pilot experimentation. Finally, pilot experiments were performed using variables and levels shown in Table 3.8.

3.9 RESULT ANALYSIS OF MATERIAL REMOVAL RATE (MRR)

The effect of compaction pressure, peak current and pulse-on time on MRR were studied using analysis of variance (ANOVA). Taguchi's L9 orthogonal array is used for designing the experiments. Each experiment was performed thrice to minimize the effect of noise. All the experiments were performed randomly. The mean value of three results of MRR was used to calculate the signal-to-noise ratio. ANOVA was performed using the S/N ratio to obtain the contribution of the individual parameter. Experimental matrix with MRR and its S/N ratio is shown in Table 3.9.

Table 3.9 Observed average value for MRR and their S/N ratio

Exp. No	Cp (Kg/cm^2)	Ip (A)	Ton (µs)	Material Removal Rate (MRR) gm/min			Mean MRR (gm/min)	S/N Ratio (dB)
				I	II	III		
1	125	6	50	0.1177	0.1031	0.1167	0.1125	-18.9769
2	125	12	90	0.1983	0.2048	0.1894	0.1975	-14.0887
3	125	18	130	0.2986	0.2964	0.3032	0.2994	-10.4750
4	225	6	90	0.1465	0.1375	0.1456	0.1432	-16.8811
5	225	12	130	0.2149	0.2624	0.2382	0.2385	-12.4502
6	225	18	50	0.1826	0.1782	0.1534	0.1714	-15.3198
7	325	6	130	0.1532	0.1468	0.1569	0.1523	-16.3460
8	325	12	50	0.1534	0.1662	0.1766	0.1654	-15.6293
9	325	18	90	0.2743	0.2828	0.2712	0.2761	-11.1787

3.9.1 Analysis of variance (ANOVA) for MRR

Table 3.10 ANOVA using S/N ratio data for MRR

Factor	DOF	SS	V	F	P	% of contribution
Compaction pressure	2	0.4027	0.2014	0.20	0.830	0.64
Peak Current	2	39.9643	19.9821	20.29	0.047	63.84
Pulse on time	2	20.2549	10.1275	10.28	0.089	32.36
Error	2	1.9695	0.9847			
Total	8	62.5914				
S = 1.80958 R-Sq = 99.03% R-Sq(adj) = 96.11%						

Table 3.11 MRR response table for S/N ratio (Larger is better)

Level	Compaction pressure	Peak current	Pulse on time
1	-14.51	-17.40	-16.64
2	-14.88	-14.06	-14.05
3	-14.38	-12.32	-13.09
Delta	0.50	5.08	3.55
Rank	**3**	**1**	**2**

The signal-to-noise ratio for MRR is calculated using equation 3.4 with "Larger the better" criteria. Calculated S/N ratio is used to perform Analysis of variance. ANOVA is used to obtained the contribution of the individual parameter for maximum MRR. ANOVA for MRR with a 99% confidence level is shown in Table 3.10. ANOVA of MRR represents the sum of the square, variance, F value and P-value. The F- test is helpful to decide the contribution of individual parameter. A parameter with high F-value indicates the largest contribution to maximize MRR. ANOVA indicates compaction pressure (F value 0.20), peak current (F value 20.29) and pulse on time (F value 10.28) are significantly contributing to maximize MRR. The rank of individual parameter relative to its contribution to maximize MRR is shown in Table 3.11. Peak current was observed most significant parameters with 63.84 % contribution. Pulse on time (32.36 % contribution) and compaction pressure (0.64 % contribution) were also play significant role up to a considerable extent.

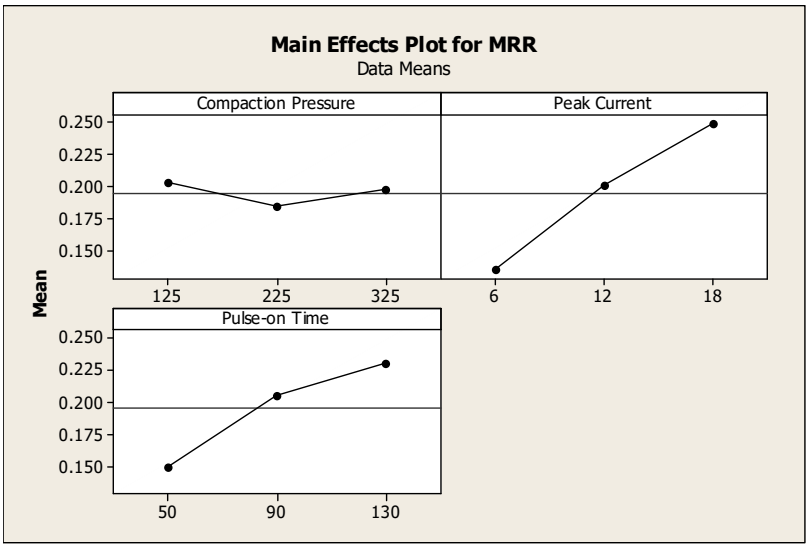

Figure 3.9(a) Main effect plot for MRR

The main effects plots for MRR using S/N ratio is shown in Figure 3.9(a). Improvements in MRR is observed while increase in peak current from 6 to 18 ampere. Pulse on time is

also plays important role to enhance MRR. Pulse duration is high than the same amount of heat energy is available for longer duration resulting in to more melting and vaporization of work material.

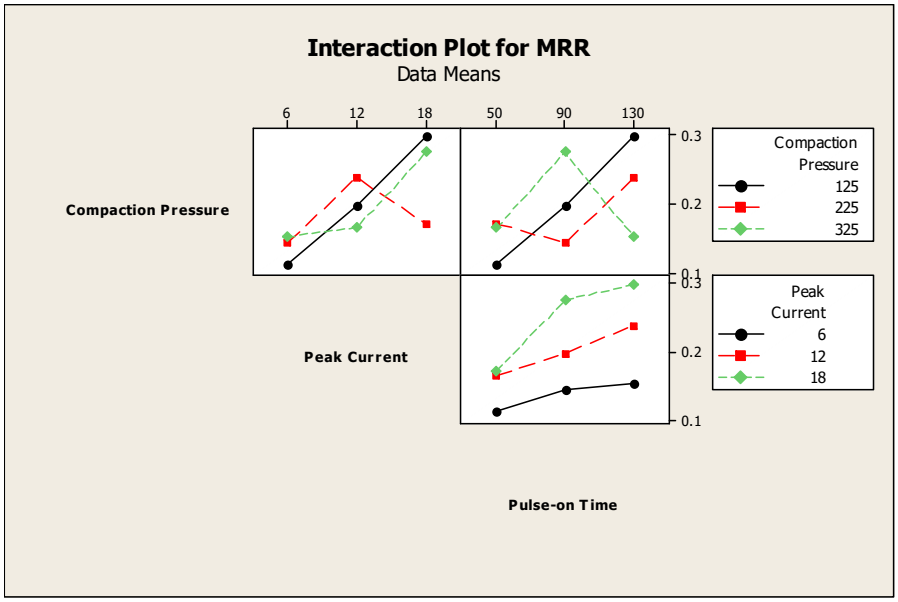

Figure 3.9(b) Interaction plots for MRR

The interaction plots of MRR is shown in Figure 3.9(b). Interaction of peak current with a pulse on time is observed most significant for MRR. Interactions of compaction pressure with a pulse on time and compaction pressure with peak current are found less significant for MRR [154].

3.10 RESULT ANALYSIS OF TOOL WEAR RATE (TWR)

Maintain optimum tool wear is important for the operational economy and stability. Weight of P/M electrode was measured before and after experiments using the electronic precision balance. Tool wear rate is calculated using the following relations.

$$TWR = \frac{W_{tb} - W_{ta}}{T_m} \; gm/min$$

Where, TWR = tool wear rate gm/min

W_{tb} = weight of tool before machining in gm

W_{ta} = weight of tool after machining in gm

T_m = total machining time in minutes

The effects of compaction pressure, peak current and pulse-on time on TWR was analysed using analysis of variance (ANOVA). Experiments were performed as per Taguchi's L9 orthogonal array. Each experiment was run thrice to minimize the effects of noise. The sequence of experiments was decided using a random number. The mean value of three results of TWR was used to calculate the signal-to-noise ratio. ANOVA was performed using the S/N ratio to the obtained contribution of individual parameters. Experiment matrix with the results of TWR and its S/N ratio is shown in Table 3.12.

Table 3.12 Observed average value for TWR and their S/N ratio

Exp. No	Cp (Kg/cm^2)	Ip (A)	Ton (µs)	Tool Wear Rate (TWR) gm/min			Mean TWR (gm/min)	S/N Ratio (dB)
				I	II	III		
1	125	6	50	0.0110	0.0120	0.0124	0.0118	38.5624
2	125	12	90	0.0492	0.0503	0.0496	0.0497	26.0729
3	125	18	130	0.0621	0.0617	0.0607	0.0615	24.2225
4	225	6	90	0.0102	0.0093	0.0099	0.0098	40.1755
5	225	12	130	0.0438	0.0444	0.0432	0.0438	27.1705
6	225	18	50	0.0438	0.0427	0.0431	0.0432	27.2903
7	325	6	130	0.0055	0.0059	0.0072	0.0062	44.1522
8	325	12	50	0.0200	0.0207	0.0202	0.0203	33.8501
9	325	18	90	0.0366	0.0369	0.0363	0.0366	28.7304

3.10.1 Analysis of variance (ANOVA) for TWR

The signal-to-noise ratio for TWR was calculated using equation 3.5 with "Smaller the better" criteria. Calculated S/N ratio is used to perform analysis of variance (ANOVA). The main purpose to perform ANOVA was to obtain the contribution of individual parameters to minimize TWR. ANOVA with a 99% confidence level for TWR is shown in Table 3.13.

Table 3.13 ANOVA using S/N ratio data for TWR

Factor	DOF	SS	V	F	P	% of contribution
Compaction pressure	2	55.469	27.735	20.65	0.046	13.45
Peak Current	2	349.674	174.837	130.17	0.008	84.82
Pulse on time	2	4.436	2.218	1.65	0.377	1.08
Error	2	2.686	1.343			
Total	8	412.266				
S = 1.15895 R-Sq = 99.35% R-Sq(adj) = 97.39%						

Sum of the square (SS), variance (V), F-value and P-value for TWR are shown in ANOVA. The F- test is helpful to decide the contribution of individual parameters. Parameter with maximum F-vales is considered the most significant parameter to minimize TWR.

Table 3.14 TWR response table for S/N ratio (Smaller is better)

Level	Compaction pressure	Peak current	Pulse on time
1	29.62	40.96	33.23
2	31.55	29.03	31.66
3	35.58	26.75	31.85
Delta	5.96	14.22	1.57
Rank	**2**	**1**	**3**

In ANOVA compaction pressure (F value 20.65), peak current (F value 130.17) and pulse on time (F value 1.65) are contributing to minimize the TWR. The rank of parameter considering its contribution to minimizing TWR are shown in table 3.14. The combination of levels A3B1C1 is able to deliver a lower tool wear rate. Peak current was observed most significant parameters with 84.82 % contribution [155]. Pulse on time (1.08 % contribution) and compaction pressure (13.45 % contribution) also observe significant up to a considerable extent.

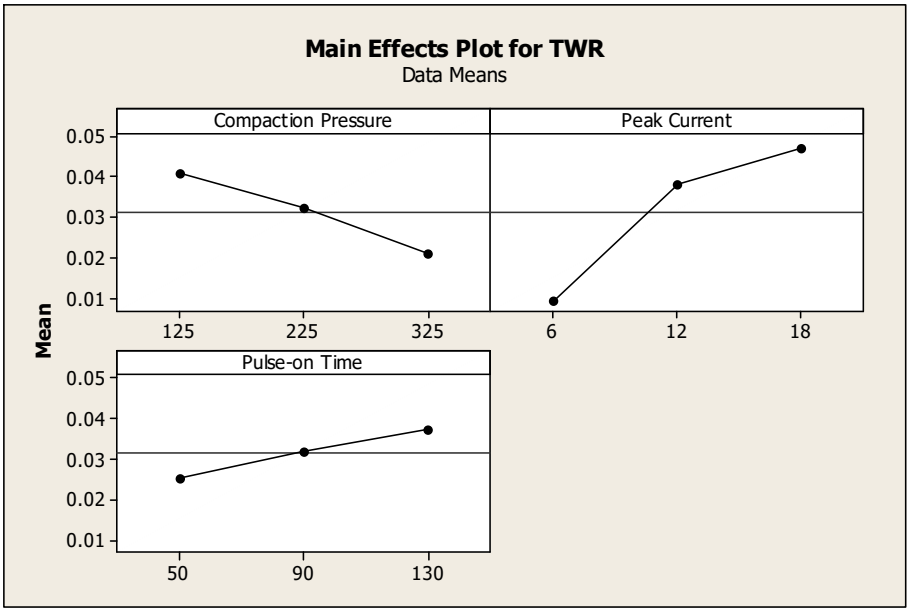

Figure 3.10(a) Main effect plot for TWR

The main effects plot for the tool wear rate using S/N ratio are shown in Figure 3.10(a). Increase in TWR has been observed with the increase in peak current from 6 to 18 ampere.

The level of pulse on time is also important to increase the TWR. If pulse duration is higher than heat energy available for longer duration, hence high melting and vaporization of tool material. The interaction plot for TWR with parameters is shown in Figure 3.10(b).

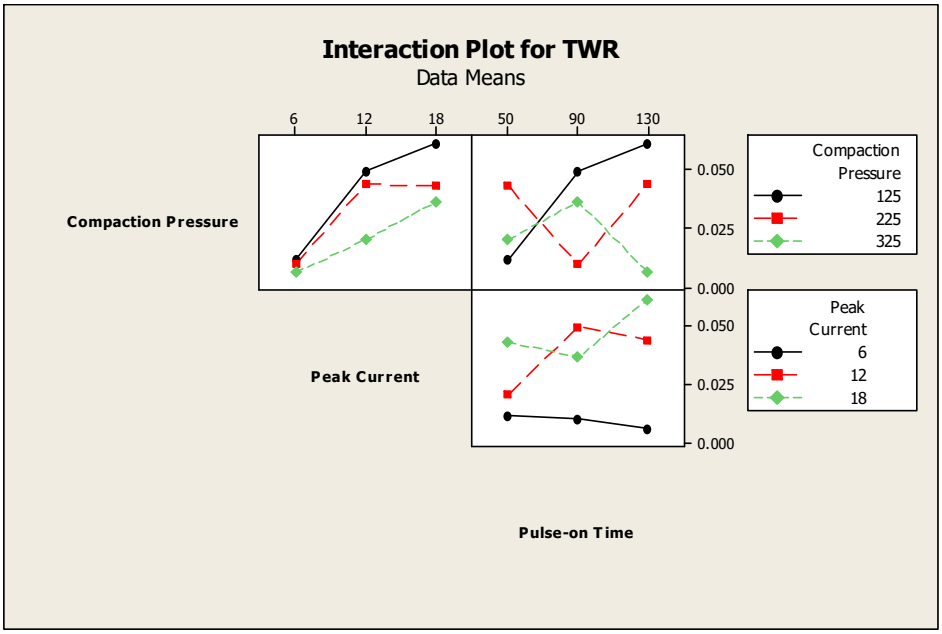

Figure 3.10(b) Interaction plots for TWR

Interaction of compaction pressure with peak current is observed most significant for lower the TWR. Compaction pressure with a pulse on time and pulse on time with peak current are non-significant for TWR. The experiment should be performed at a lower value of peak current and pulse on time to reduce TWR.

3.11 RESULT ANALYSIS OF SURFACE ROUGHNESS (SR)

Surface quality of engineering goods and component obtained through machining is very important to decide the life of the component. Rough surface is increase the stress and hence the initiation of crack and corrosion will leads to failure a component. Further rough surface is also responsible for the initiation of residual tensile stress. Hence, attempts shall be made to obtain finish surface during machining the work using P/M electrode.

The effect of selected parameters such as compaction pressure, peak current and pulse on time on surface roughness is analyzed using analysis of variance (ANOVA). Taguchi's L9 orthogonal array is used for designing the experiments. Each experiment was performed thrice to minimize the effect of noise. Sequence of experiment was decided on random

basis. The mean value of three results of SR was used to calculate the signal-to-noise ratio. The S/N ratio was calculated using "smaller the better" criteria and the following relation.

$$\frac{S}{N} = -10 \log_{10}[\frac{1}{n} \Sigma y_i^2]$$

Where n is a number of results in a row, here, in this case, n = 1, and y = value of i^{th} experiment in a row. ANOVA was performed using the S/N ratio to obtained contribution of individual parameters for minimize the SR. Experiment matrix with the results of SR and its S/N ratio is shown in Table 3.15.

Table 3.15 Observed average value for SR and their S/N ratio

Exp. No	Cp (Kg/cm^2)	Ip (A)	Ton (µs)	Surface Roughness (SR)			Mean SR (µm)	S/N Ratio (dB)
				I	II	III		
1	125	6	50	6.26	5.78	8.25	6.43	-16.1642
2	125	12	90	8.07	8.12	6.94	7.71	-17.7411
3	125	18	130	8.45	11.57	9.38	9.80	-19.8245
4	225	6	90	5.44	8.23	7.78	7.15	-17.0861
5	225	12	130	8.83	8.31	7.22	8.12	-18.1911
6	225	18	50	7.65	8.61	9.87	8.71	-18.8004
7	325	6	130	7.28	9.15	6.91	7.78	-17.8196
8	325	12	50	6.60	7.55	8.08	7.41	-17.3964
9	325	18	90	9.48	9.44	8.92	9.28	-19.3510

3.11.1 Analysis of variance (ANOVA) for SR

The signal-to-noise ratio for surface roughness was calculated using equation 3.5 with "Smaller the better" criteria. Calculated S/N ratio was used to perform analysis of variance (ANOVA). The main purpose of ANOVA is to obtain the contribution of individual parameters to minimize surface roughness. ANOVA for SR with a 99% confidence level is shown in Table 3.16.

Table 3.16 ANOVA using S/N ratio data for SR

Factor	DOF	SS	V	F	P	% of contribution
Compaction pressure	2	0.1179	0.0589	1.34	0.428	1.12
Peak Current	2	8.2656	4.1327	93.87	0.011	78.83
Pulse on time	2	2.0132	1.0066	22.86	0.042	19.20
Error	2	0.0881	0.0440			
Total	8	10.4847				
S = 0.250207 R-Sq = 99.09% R-Sq(adj) = 96.35%						

Table 3.16 indicates the sum of the square, variance, F value and P-value for SR. The F-test is helpful to decide the significance of the individual parameter. High values of F-test indicate the significant contribution of the parameter to minimize the SR.

Table 3.17 SR response table for S/N ratio (Smaller is better)

Level	Compaction pressure	Peak current	Pulse on time
1	-17.19	-17.02	-17.45
2	-18.03	-17.78	-18.06
3	-18.19	-19.33	-18.61
Delta	0.28	2.30	1.16
Rank	**3**	**1**	**2**

ANOVA table for SR indicates compaction pressure (F value 1.34), peak current (F value 93.87) and pulse on time (F value 22.86) are significantly contributed to minimize the SR. The rank of individual parameter relative to its contribution is shown in Table 3.17. The combination of parameter levels A1B1C1 is deliver lower surface roughness. Peak current observed most significant parameters with 78.83 % of the contribution. Pulse on time (19.20 % contribution) and compaction pressure (1.12 % contribution) are also significants up to a considerable extent [156].

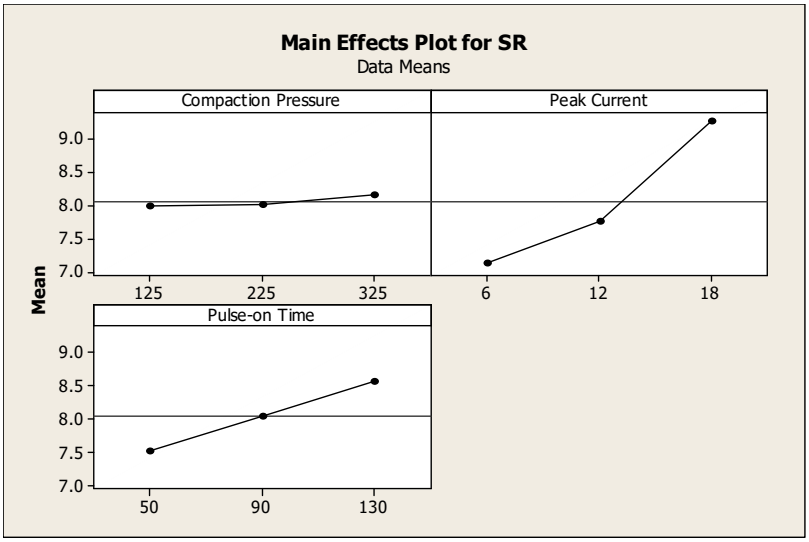

Figure 3.11(a) Main effect plot for SR

Effects of parameters on surface roughness are shown in figure 3.11(a). SR is increased with the increase in peak current from 6 to 18 ampere. Pulse on time also plays an important role to increase SR. If pulse duration is higher than heat energy available for longer duration responsible for detoriates the surface quality.

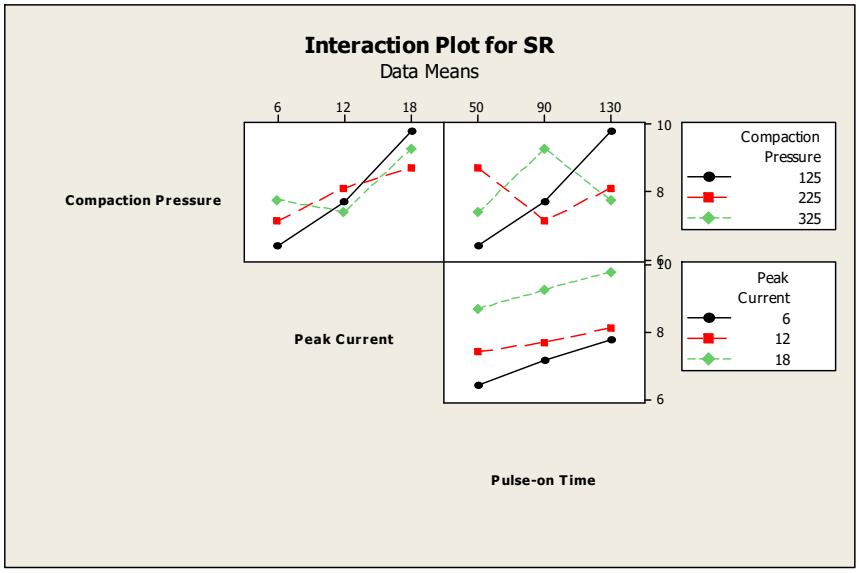

Figure 3.11(b) Interaction plots for SR

The interaction plot for SR is also shown in Figure 3.11(b). Interaction of peak current with a pulse on time is observe significant for SR. Compaction pressure with peak current and pulse on time with compaction pressure are non effective for SR. Lower value of peak current with smaller pulse duration is helpful to minimize the surface roughness.

3.12 RESULT ANALYSIS OF MICROHARDNESS (MH)

Die is exposed to very sever abrasion, wear, corrosion and high temperature and hence it is necessary to improve its surface properties. Migration of hardest constituents from electrode to die surface was observed under specific machining condition. Attempts have been made to obtain optimum machining conditions, which enable to transfer the hardest constituents from P/M electrode to work surface. Microhardness of work material was measured before and after machining using vickers microhardness tester shown in Table 3.18.

Table 3.18 Microhardness of work material before machining

Material	P20+Ni die steel
Micro-hardness (Vickers hardness number)	322

Microhardness was measured at three different locations on work surface and the mean value of it was considered for further analysis.The effect of selected parameters such as

compaction pressure, peak current and pulse on time on microhardness were analyzed using analysis of variance (ANOVA). Taguchi's L9 orthogonal array is used for designing experiments. Each experiment was performed thrice to minimize effects of noise. All the experiments were performed randomly. The mean value of three results of MH was used to calculate the signal-to-noise ratio. The S/N ratio is calculated with "larger the better" criteria using the following relation.

$$\frac{S}{N} = -10\log_{10}[\frac{1}{n}\Sigma\, 1/y_i^2]$$

Where n is a number of results in a row, here, in this case, n = 1, and y = value of i^{th} experiment in a row. ANOVA was performed using the S/N ratio to the obtained contribution of individual parameters. Experiment matrix with the results of MH and its S/N ratio is shown in Table 3.19.

Table 3.19 Observed average value for MH and their S/N ratio

Exp. No	Cp (kg/cm^2)	Ip (A)	Ton (µs)	Micro Hardness (MH)			Mean MH (HVN)	S/N Ratio (dB)
				I	II	III		
1	125	6	50	578	659	701	646	56.2047
2	125	12	90	939	878	727	848	58.5679
3	125	18	130	1072	967	991	1010	60.0864
4	225	6	90	708	662	592	654	56.3116
5	225	12	130	856	872	942	890	58.9878
6	225	18	50	773	839	902	838	58.4649
7	325	6	130	637	693	737	689	56.7644
8	325	12	50	831	815	688	778	57.8196
9	325	18	90	851	816	946	871	58.8004

3.12.1 Analysis of variance (ANOVA) for MH

The signal-to-noise ratio for microhardness is calculated using equation 3.4 with "larger the better" criteria. Calculated S/N ratio was used to perform analysis of variance (ANOVA). The main purpose to perform ANOVA is to obtain the contribution of individual parameters to maximize the microhardness. ANOVA with a 99% confidence level for MH is shown in table 3.20. ANOVA table of MH indicates the sum of the square, variance, F value and P-value. The F- test is helpful to decide the contribution of individual parameters. Higher values of F-test indicate the maximum contribution of the parameter to maximize the microhardness.

Table 3.20 ANOVA using S/N ratio data for MH

Factor	DOF	SS	V	F	P	% of contribution
Compaction pressure	2	0.3908	0.1954	13.25	0.070	2.76
Peak Current	2	11.7993	5.8997	399.95	0.002	83.43
Pulse on time	2	1.9219	0.9609	65.14	0.015	13.59
Error	2	0.0295	0.0147			
Total	8	14.1416				
S = 1.80958 R-Sq = 99.03% R-Sq(adj) = 96.11%						

Table 3.21 Microhardness response table for S/N ratio (Larger is better)

Level	Compaction pressure	Peak current	Pulse on time
1	58.29	56.43	57.50
2	57.92	58.46	57.89
3	57.79	59.12	58.61
Delta	0.49	2.69	1.12
Rank	**3**	**1**	**2**

ANOVA indicates compaction pressure (F value 13.25), peak current (F value 399.95) and pulse on time (F value 65.14) are the parameters significantly contribute to maximize the MH. The rank of the individual parameter for maximizing MH are shown in Table 3.21. The combinations of parameter levels A1B3C3 is able to deliver maximum microhardness. Peak current was observed most significant parameters with 83.43 % of the contribution. Pulse on time (13.59 % contribution) and compaction pressure (2.76 % contribution) are also observed significant up to a considerable extent [157].

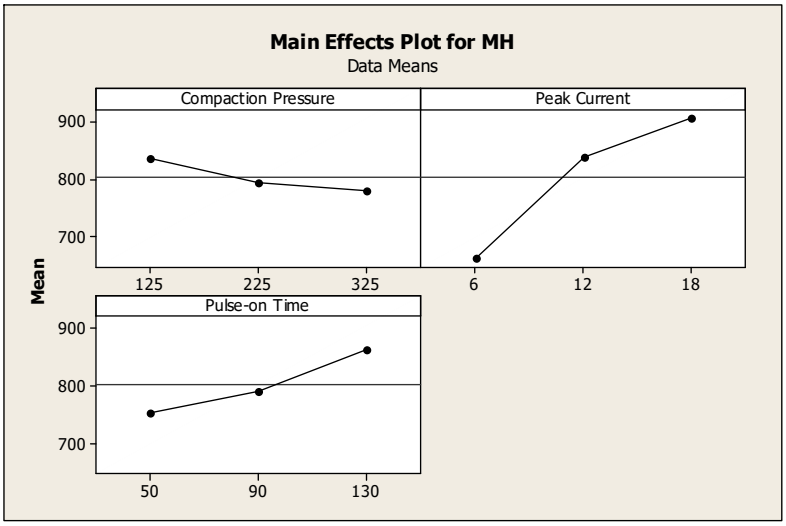

Figure 3.12(a) Main effect plot for MH

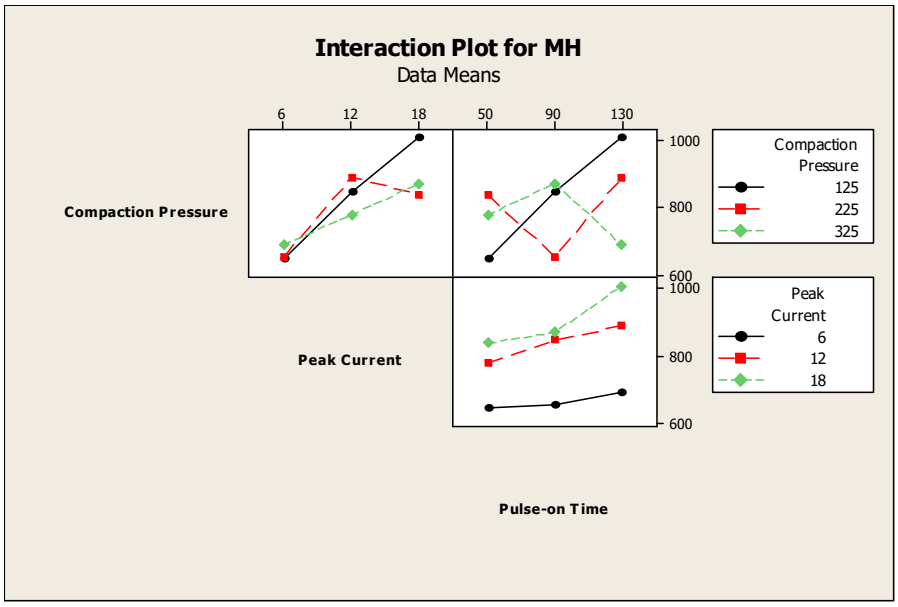

Figure 3.12(b) Interaction plots for MH

Effect of parameters on microhardness is shown in Figure 3.12(a). Increase in MH is observed with the increase in peak current from 6 to 18 ampere. Pulse on time also plays an important role to increase MH. Heat energy is available for a longer duration at high value of pulse on time, which will increase rate of melting and vaporization of work material, leads to alloying the surface of work material. The interaction plot for MH is shown in Figure 3.12(b). Interaction of peak current with a pulse on time is found most significant for MH. Compaction pressure with peak current and pulse on time with compaction pressure are observed non-significant for MH. It is concluded that the high value of peak current and pulse duration should be selected to maximize microhardness.

3.13 SCANNING ELECTRON MICROSCOPY (SEM)

Scanning Electron Microscope (SEM) is an electron microscope working on a focused beam of electrons to produce an image of surface. The interaction between electrons on the sample produces various signals that can be detected and studied to get information about the sample's surface topography. The electron beam is generally scanned in a raster scan pattern, and the beam's position is combined with the detected signal to produce an image. SEM can achieve a resolution better than 1 nanometre.

Two machined samples (Trial No. 3 and 8) were taken for SEM and EDS analysis. SEM image with different magnification for work material machined at 18 A peak current, 130

μs pulse- on time and powder metallurgy electrode of compaction pressure 125 kg/cm^2 shown in Figure 3.13(a-b).

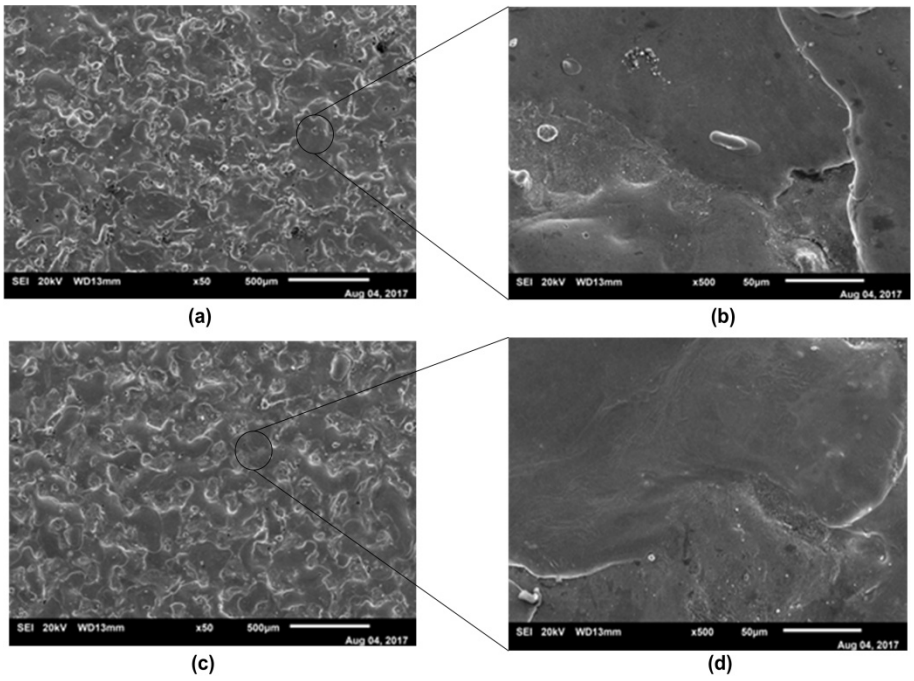

Figure 3.13(a-d) SEM images of EDMed samples

The SEM image confirmed the formation of layer by layer and defects free recast surface. No any major surface defects such as micro-cracks and microvoids are observed. SEM image of Trial No.8 taken with two different magnifications after work material machined at 12 A peak current, 50 μs pulse on time and powder metallurgy electrode with compaction pressure 325 kg/cm^2 are shown in Figure 3.13(c-d). Reduction in thickness of recast layer with less amount of waviness is observed due to lower peak current as compared to Trial No. 3. In both cases, a significant amount of presence of copper was observed on the work surface during EDS, which indicates migration of copper particles from powder metallurgy electrode.

3.14 ENERGY DISPERSIVE SPECTROMETRY (EDS) ANALYSIS

The EDS analysis of selected EDMed samples is carried out to confirm the migrations of P/M electrode elements on work surface. The result of EDS indicates significant amounts of P/M electrode elements are migrated while machining the work using P/M electrode.

The compositions of work material for trial 3 & 8 after EDS analysis are shown in Figure 3.14(a-b). EDS spectrum of trial 3 is shown in Figure 3.14(a).

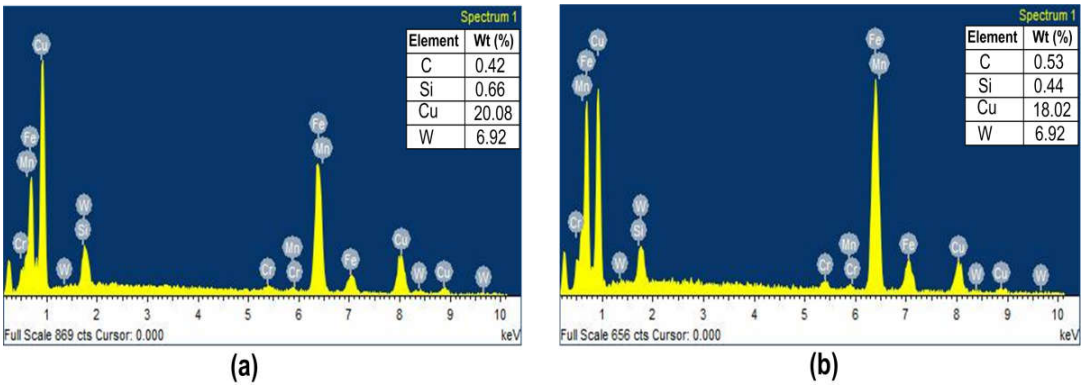

Figure 3.14(a-b) EDS Spectrum of trial 3 and 8

The result of EDS for trial 3 is 0.66% Si, 0.62% Cr, 0.66% Mn, 0.42% C, 20.08% Cu and 6.92 % W. EDS spectrum of trial 8 is shown in Figure 3.14(b). The result of EDS for Exp. no. 8 is found to be 0.44% Si, 1.06% Cr, 0.92% Cr, 0.53% C, 18.02% Cu and 5.46% W. The EDS confirm the transfer of material from powder metallurgy electrode to work surface. Increase in carbon percentage of EDMed surface as compared to the base material is due to broken down hydrocarbon from dielectric and migrate on the work material. Presence of tungsten (W) on work surface (previously not part of compositions of work material) strongly confirm the migration of material from powder metallurgy electrode [158]. The elements identified during the EDS analysis are shown in Figure 3.14(a-b).

3.15 X-RAY DIFFRACTION (XRD) ANALYSIS

X-ray diffraction (XRD) is a versatile, non-destructive analytical technique that is usually used to study crystalline materials. It determined the detailed information about the chemical composition and type of molecular bond of the crystalline phase. When a focused X-ray beam interacts with these planes of atoms, part of the beam is transmitted, the part is absorbed by the sample, the part is refracted and scattered, and part is diffracted. XRD is an efficient technique to expose the crystallographic structure of natural and manufactured materials. The X-ray source was operated at a voltage of 40 kV and a current of 35 mA. The diffraction angle was varied in the range of 0-90 degrees while the scanning rate was 5degree/s.

X-ray diffraction of a selected sample of the pilot experiment (Trial 8) was carried out using X-ray diffractometer. Improvements in Si, W and Cu percentage of the machined surface as compared to base material clearly indicates migration of electrode elements on

the work surface during machining. X-ray diffraction pattern of trial 8 is shown in Figure 3.15.

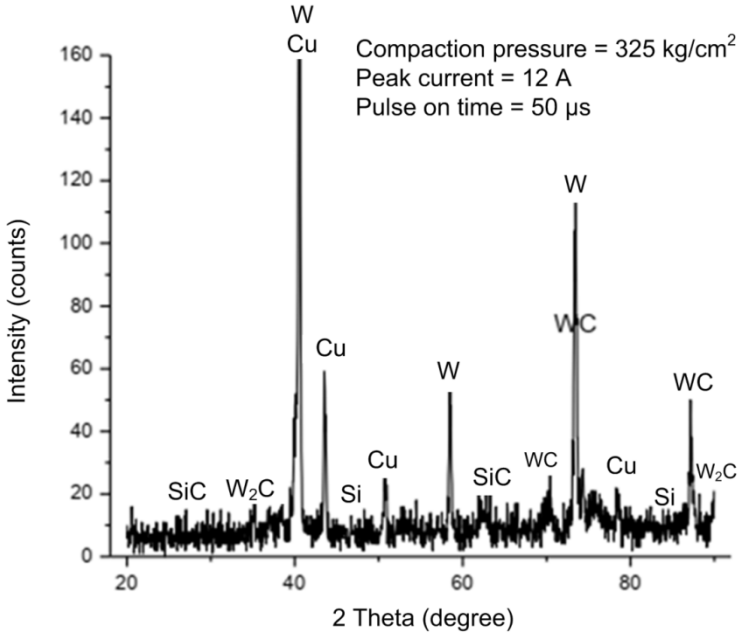

Figure 3.15 X-ray diffraction pattern of trial 8

Presence of tungsten carbide (WC & W_2C) and silicon carbide (SiC) was observed due to bonding between electrode elements and carbon element dissociated from hydrocarbon oil at high temperature. Formation of carbide leads to significant improvements in microhardness.

3.16 SELECTION OF PROCESS PARAMETERS FOR FINAL EXPERIMENTS

Process parameters for final experiments were selected based on the results obtained during pilot experiments shown in Table 3.22. Flow chart of experimental work/ research methodology is shown in Figure 3.16.

Table 3.22 Input parameters and their levels for final experiments

Symbol	Parameters	Unit	Levels				
			-2	-1	0	1	2
A	Compaction pressure	(kg/cm^2)	125	175	225	275	325
B	Peak Current	(Ampere)	6	9	12	15	18
C	Pulse on time	(µs)	50	70	90	110	130
D	Duty cycle	(%)	75	80	85	90	95

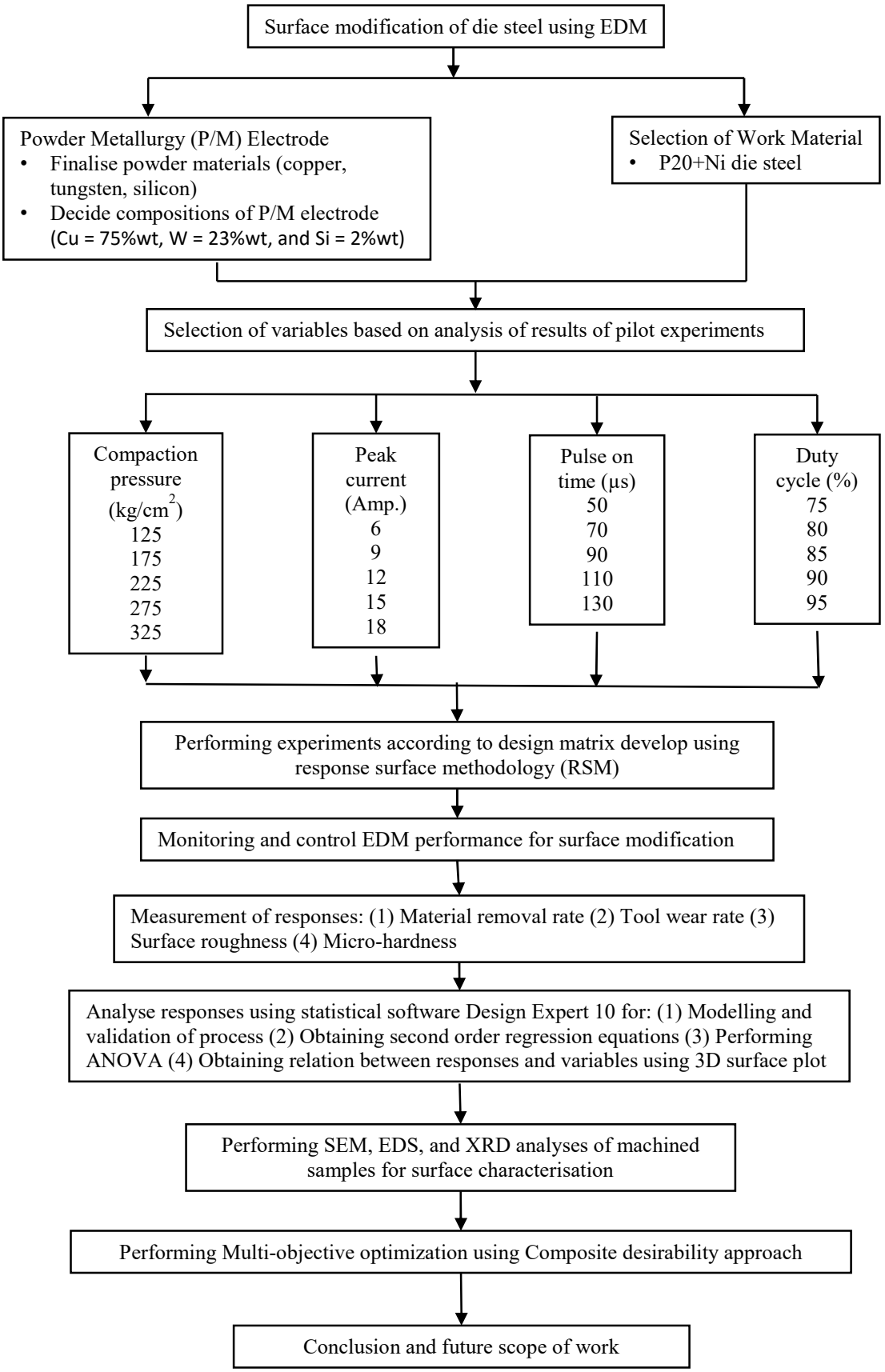

Figure 3.16 Flow Chart of Research Methodology

Favourable machining conditions for surface modification during pilot experiments were used to identify the range of compaction pressure, peak current and pulse on time. The influence of changes in pulse off-time as an independent parameter (it has been used as part of duty cycle along with pulse on-time) was missing in the available literature and this aspect needed further exploration [39]. Hence, duty cycle was included as the fourth parameter during final experimentation. Five levels of compaction pressure, peak current, pulse on time and duty cycle were considered for final experiments.

Parameters maintain constant during final experimentation are summarise in Table 3.23.

Table 3.23 Working condition of experimentation

Working Conditions	**Description**
Workpiece material	P20+Ni die steel
Electrode Composition	75 % Cu+ 23% W+2%Si (% of weight)
Electrode diameter	Φ = 19 mm
Polarity	Negative Electrode
Dielectric fluid	EDM Oil (Pacific oil 300)
Flushing type	Side flushing
Flushing pressure	0.75 kg/cm^2
Processing time	10 minutes

CHAPTER – 4

EXPERIMENTAL RESULTS AND ANALYSIS

4.1 INTRODUCTION

Response surface methodology (RSM) is a statistical tools mainly used to solve multi-response industrial problems. In the present chapter, response surface methodology is used to analyze the results of responses. Experiments were planned based on central composite second order rotatable design. Total 30 experiments were performed according to design matrix developed using RSM. Four input process parameters such as compaction pressure (C_p), peak current (I_p), pulse-on time (T_{on}) and duty cycle (τ) were considered with five levels for experimentation. Individual experiments were performed thrice by setting levels of parameters shown in the design matrix. Second-order regression equations (statistical models) for material removal rate (MRR), tool wear rate (TWR), surface roughness (SR) and microhardness (MH) were developed using response surface methodology. Results of responses were analysed using the latest and widely accepted statistical software "Design Experts 10" (DX 10). The process parameters and their levels are shown in Table 4.1.

Table 4.1 Selected input process parameters with their levels

Symbol	Parameters	Unit	Levels				
			-2	-1	0	1	2
A	Compaction pressure (C_p)	(kg/cm^2)	125	175	225	275	325
B	Peak Current (I_p)	(Ampere)	6	9	12	15	18
C	Pulse on time (T_{on})	(μs)	50	70	90	110	130
D	Duty cycle (τ)	(%)	75	80	85	90	95

4.2 RESPONSE SURFACE METHODOLOGY (RSM)

Response surface methodology (RSM) is combinations of mathematical and statistical techniques, widely used to develop, analyse, improve and optimize the industrial process. Nowadays, RSM became one of the most acceptable and robust tools for solving or modeling the industrial process in which several input variables affect the quality

characteristics of output products. Most real-world applications of RSM will involve during more than one response govern the output. In present experimental work, response surface methodology is used for developing and modelling electrical discharge machining responses such as material removal rate (MRR), tool wear rate (TWR), surface roughness (SR) and microhardness (MH). All response prediction models were obtained by regression processes in which several independent input variables affect the results of outputs [42].

Design of experiments (DOE) technique was used to formulate and conduct the experiments for results of responses. In response surface methodology technique, if all variables are assumed measurable, then the mathematical model can be represented according to the equation:

$$\mathbf{Y_i = f\,(C_p, I_p, T_{on}, \tau) + \varepsilon} \quad \text{--------} \quad \mathbf{(4.1)}$$

Where, Y_i = Response of EDM such as MRR, TWR, SR, and MH

C_p = coded value of machining input parameters compaction pressure

I_p = coded value of machining input parameters peak current

T_{on} = coded value of machining input parameters pulse on time

τ = coded value of machining input parameters duty cycle, and

ε = fitting error for i^{th} observation.

The first important step in RSM is to predict the true functional relationship between the output responses and individual independent input parameters. When large numbers of input variables affect the response, then a quadric model for any responses can be represented as follows:

$$Y = \alpha_0 + \alpha_1 C_p + \alpha_2 I_p + \alpha_3 T_{on} + \alpha_4 \tau + \alpha_5 C_p I_p + \alpha_6 C_p T_{on} + \alpha_7 C_p \tau + \alpha_8 I_p T_{on} + \alpha_9 I_p \tau + \alpha_{10} T_{on} \tau + \alpha_{11} C_p^2 + \alpha_{12} I_p^2 + \alpha_{13} T_{on}^2 + \alpha_{14} \tau^2 + \varepsilon \qquad \mathbf{(4.2)}$$

Where C_p, I_p, T_{on} and τ are the input variables which influence on response Y. The set of regression coefficient α are known parameters and estimated by least square, and "ε" is a random error, which is normally distributed with mean as per observed response. The coefficients of the regression model were estimated by using data obtained from the

experimental results. Design Experts 10 statistical software programming is used for the analysis of data. Statistical tests such as F- test (lack of fit test), and normal probability plot of residuals versus predicted response are used to test the validity of the models before applying them to solve the optimization problem.

4.2.1 Experimental design based on CCD

In this experimental work, the levels of compaction pressure, peak current, pulse on time and duty cycle were selected through rigours study of past work and by performing numbers of pilot experiments (trial runs). EDM and powder metallurgy handbook are also referred to decide the governing factors and its general contributions in process [45]. Each input parameters with their levels used for experimental work are listed in Table 4.1. Parameters maintained constant during the main experiments are shown in Table 4.2 with their level.

Table 4.2 Constant machining parameters during final experimentation

Sr. No.	Working Conditions	Description
1	Work piece material	P20+Ni die steel
2	Electrode Composition	75 % Cu+ 23% W+2%Si (% of weight) & ϕ = 19 mm
3	Polarity	Negative Electrode
4	Dielectric fluid	EDM Oil (Pacific oil 300)
5	Flushing type	Side flushing
6	Flushing pressure	0.75 kg/cm^2
7	Processing time	10 minutes
8	Duty cycle	50 %
9	Gap voltage	60 Volt

In this work, Experiments were designed using the design of experiments (DOE) techniques. A second-order rotatable central composite design composed for a total of 30 experiments. It further consisted of 2β fractional runs with sixteen corner points, six centre points and eight axial runs located at 2α levels. Experiment matrix with coded and actual values of input variables are shown in Table 4.3. The regression equations for the selected model are obtained for the response characteristics, viz., material removal rate, tool wear rate, surface roughness and microhardness [46]. These regression equations are developed using the experimental data (Table 4.3) and plotted to investigate the effect of process

variables on various response characteristics. The analysis of variance (ANOVA) is performed to statistically analyze the results.

Table 4.3 Experimental design matrix

Exp. No	Input process parameters							
	C_p		I_p		T_{on}		τ	
	Actual	Coded	Actual	Coded	Actual	Coded	Actual	Coded
1	175	-1	9	-1	70	-1	80	-1
2	275	1	9	-1	70	-1	80	-1
3	175	-1	15	1	70	-1	80	-1
4	275	1	15	1	70	-1	80	-1
5	175	-1	9	-1	110	1	80	-1
6	275	1	9	-1	110	1	80	-1
7	175	-1	15	1	110	1	80	-1
8	275	1	15	1	110	1	80	-1
9	175	-1	9	-1	70	-1	90	1
10	275	1	9	-1	70	-1	90	1
11	175	-1	15	1	70	-1	90	1
12	275	1	15	1	70	-1	90	1
13	175	-1	9	-1	110	1	90	1
14	275	1	9	-1	110	1	90	1
15	175	-1	15	1	110	1	90	1
16	275	1	15	1	110	1	90	1
17	125	-2	12	0	90	0	85	0
18	325	2	12	0	90	0	85	0
19	225	0	6	-2	90	0	85	0
20	225	0	18	2	90	0	85	0
21	225	0	12	0	50	-2	85	0
22	225	0	12	0	130	2	85	0
23	225	0	12	0	90	0	75	-2
24	225	0	12	0	90	0	95	2
25	225	0	12	0	90	0	85	0
26	225	0	12	0	90	0	85	0
27	225	0	12	0	90	0	85	0
28	225	0	12	0	90	0	85	0
29	225	0	12	0	90	0	85	0
30	225	0	12	0	90	0	85	0

4.3 EXPERIMENTAL RESULTS

Experiments were performed by combining the levels of individual parameters shown in Table 4.3. Each experiment was performed thrice to minimize the effect of uncontrollable factors and mean of three results of responses are shown in Table 4.4.

Table 4.4 Observed mean value of responses

Exp. No.	Run Order	Input process parameters								Mean Values of Responses			
		C_p		I_p		T_{on}		τ		MRR (gm/min)	TWR (gm/min)	SR (μm)	MH (HVN)
		Actual	Coded	Actual	Coded	Actual	Coded	Actual	Coded				
1	12	175	-1	9	-1	70	-1	80	-1	0.1623	0.0283	5.635	886
2	6	275	1	9	-1	70	-1	80	-1	0.1334	0.0252	4.755	831
3	9	175	-1	15	1	70	-1	80	-1	0.2344	0.0326	8.192	1026
4	28	275	1	15	1	70	-1	80	-1	0.2082	0.0293	7.481	936
5	4	175	-1	9	-1	110	1	80	-1	0.1843	0.0266	6.443	852
6	27	275	1	9	-1	110	1	80	-1	0.1511	0.0249	5.387	791
7	14	175	-1	15	1	110	1	80	-1	0.2486	0.0271	8.684	908
8	20	275	1	15	1	110	1	80	-1	0.2323	0.0304	8.126	883
9	11	175	-1	9	-1	70	-1	90	1	0.1855	0.0352	6.477	1103
10	16	275	1	9	-1	70	-1	90	1	0.1462	0.0271	5.119	868
11	2	175	-1	15	1	70	-1	90	1	0.2816	0.0385	9.831	1189
12	22	275	1	15	1	70	-1	90	1	0.2461	0.0339	8.614	1092
13	5	175	-1	9	-1	110	1	90	1	0.2113	0.0324	7.387	1021
14	19	275	1	9	-1	110	1	90	1	0.1684	0.0251	5.882	793
15	29	175	-1	15	1	110	1	90	1	0.3032	0.0331	10.605	1056
16	15	275	1	15	1	110	1	90	1	0.2683	0.0292	9.481	924
17	10	125	-2	12	0	90	0	85	0	0.2361	0.0331	8.263	1059
18	25	325	2	12	0	90	0	85	0	0.1712	0.0269	5.985	861
19	18	225	0	6	-2	90	0	85	0	0.1211	0.0238	4.235	821
20	7	225	0	18	2	90	0	85	0	0.2924	0.0347	10.323	1094

Exp. No.	Run Order	Input process parameters								Mean Values of Responses			
		C_p		I_p		T_{on}		τ		MRR (gm/min)	TWR (gm/min)	SR (µm)	MH (HVN)
		Actual	Coded	Actual	Coded	Actual	Coded	Actual	Coded				
21	30	225	0	12	0	50	-2	85	0	0.1982	0.0333	6.934	974
22	21	225	0	12	0	130	2	85	0	0.2463	0.0258	8.617	822
23	13	225	0	12	0	90	0	75	-2	0.1681	0.0271	5.882	869
24	23	225	0	12	0	90	0	95	2	0.2363	0.0335	8.266	1071
25	26	225	0	12	0	90	0	85	0	0.2186	0.0267	7.628	846
26	3	225	0	12	0	90	0	85	0	0.2192	0.0264	7.573	837
27	1	225	0	12	0	90	0	85	0	0.2154	0.0266	7.591	843
28	8	225	0	12	0	90	0	85	0	0.2231	0.0268	7.683	849
29	24	225	0	12	0	90	0	85	0	0.2185	0.0261	7.671	831
30	17	225	0	12	0	90	0	85	0	0.2172	0.0265	7.622	841

4.4 ANALYSIS AND DISCUSSION OF MATERIAL REMOVAL RATE RESULTS

Machining cost is contribute the major part in the total production cost of dies and tools. One of the major drawback of EDM is, it has a very poor material removal rate. Therefore attempts have been made to obtain higher MRR using P/M electrode. Care has been taken that the P/M electrode is capable to machine the material during the surface modification. Weight of work material is measured before and after the experiments using the electronic precision balance. Work material shown in Figure 4.0, is cleaned before and after the experiment using acetone. Following equation is used to calculate material removal rate.

$$MRR = \frac{W_{bm} - W_{am}}{T_m} \; gm/min \text{ ------} \quad \textbf{(4.3)}$$

Where, MRR = material removal rate gm/min, W_{bm} = weight of workpiece before machining in gm, W_{am} = weight of workpiece after machining in gm, and T_m = total machining time in minutes

The individual experiments were performed thrice by setting levels of process parameters shown in Table 4.3. Mean value of the three results of MRR is used for further analysis. The regression model for MRR was developed using statistical software Design Expert 10 (DX 10). Adequacy of the developed model was checked using the sum of squares, lack of fit test and model summary statistics. Analysis of variance (ANOVA) was also performed to find the contribution of the individual parameter into enhancing the MRR. Three-dimensional surface plots were developed to find the effects of process parameters on MRR [48]. The results of MRR for three sets and its mean values are given in Table 4.5.

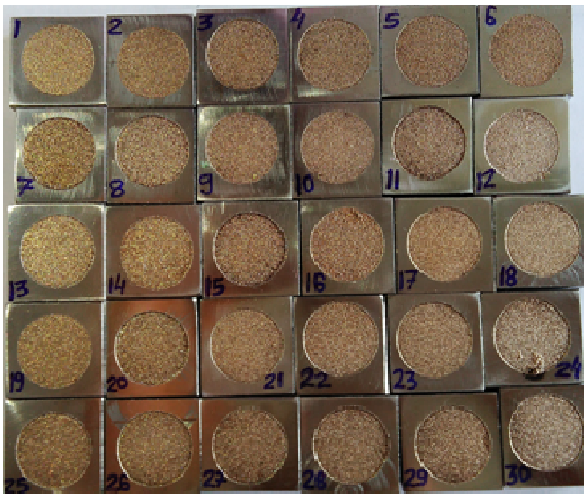

Figure 4.0 Pictorial view of work material P20+Ni die steel

Table 4.5 Design of experiment matrix and the observed value of MRR

Exp. No.	Run Order	Input process parameters								Response			Mean MRR (gm/min)
		C_p		I_p		T_{on}		τ		MRR-1 (gm/min)	MRR-2 (gm/min)	MRR-3 (gm/min)	
		Actual	Coded	Actual	Coded	Actual	Coded	Actual	Coded				
1	12	175	-1	9	-1	70	-1	80	-1	0.1616	0.1645	0.1608	0.1623
2	6	275	1	9	-1	70	-1	80	-1	0.1339	0.1332	0.1331	0.1334
3	9	175	-1	15	1	70	-1	80	-1	0.2341	0.2362	0.2329	0.2344
4	28	275	1	15	1	70	-1	80	-1	0.2076	0.2103	0.2067	0.2082
5	4	175	-1	9	-1	110	1	80	-1	0.1831	0.1863	0.1835	0.1843
6	27	275	1	9	-1	110	1	80	-1	0.1515	0.1501	0.1517	0.1511
7	14	175	-1	15	1	110	1	80	-1	0.2473	0.2524	0.2461	0.2486
8	20	275	1	15	1	110	1	80	-1	0.2327	0.2324	0.2318	0.2323
9	11	175	-1	9	-1	70	-1	90	1	0.1854	0.1868	0.1843	0.1855
10	16	275	1	9	-1	70	-1	90	1	0.1456	0.1463	0.1467	0.1462
11	2	175	-1	15	1	70	-1	90	1	0.2805	0.2830	0.2813	0.2816
12	22	275	1	15	1	70	-1	90	1	0.2466	0.2461	0.2456	0.2461
13	5	175	-1	9	-1	110	1	90	1	0.2121	0.2094	0.2124	0.2113
14	19	275	1	9	-1	110	1	90	1	0.1668	0.1727	0.1657	0.1684
15	29	175	-1	15	1	110	1	90	1	0.3024	0.3047	0.3025	0.3032
16	15	275	1	15	1	110	1	90	1	0.2692	0.2681	0.2676	0.2683
17	10	125	-2	12	0	90	0	85	0	0.2373	0.2329	0.2381	0.2361
18	25	325	2	12	0	90	0	85	0	0.1697	0.1755	0.1684	0.1712
19	18	225	0	6	-2	90	0	85	0	0.1202	0.1239	0.1192	0.1211
20	7	225	0	18	2	90	0	85	0	0.2924	0.2919	0.2929	0.2924

Exp. No.	Run Order	Input process parameters								Responses			Mean MRR (gm/min)
		C_p		I_p		T_{on}		τ		MRR-1 (gm/min)	MRR-2 (gm/min)	MRR-3 (gm/min)	
		Actual	Coded	Actual	Coded	Actual	Coded	Actual	Coded				
21	30	225	0	12	0	50	-2	85	0	0.1984	0.1995	0.1967	0.1982
22	21	225	0	12	0	130	2	85	0	0.2452	0.2476	0.2461	0.2463
23	13	225	0	12	0	90	0	75	-2	0.1673	0.1708	0.1662	0.1681
24	23	225	0	12	0	90	0	95	2	0.2376	0.2335	0.2378	0.2363
25	26	225	0	12	0	90	0	85	0	0.2173	0.2199	0.2186	0.2186
26	3	225	0	12	0	90	0	85	0	0.2186	0.2218	0.2172	0.2192
27	1	225	0	12	0	90	0	85	0	0.2183	0.2092	0.2187	0.2154
28	8	225	0	12	0	90	0	85	0	0.2174	0.2357	0.2162	0.2231
29	24	225	0	12	0	90	0	85	0	0.2169	0.2208	0.2178	0.2185
30	17	225	0	12	0	90	0	85	0	0.2183	0.2144	0.2189	0.2172

4.4.1 Selection of adequate model for MRR

The adequacy of the developed model of MRR was checked by performing various statistical tests such as a sequential model sum of squares, lack of fit tests and model summary statistics. The results obtained by three statistical tests are shown in Table 4.6 to 4.8. The quadratic model has been found optimum as per sequential model sum of the square test. The result of the sequential model sum of squares test is given in Table 4.6. It shows how the terms of increasing complexity contribute to the model. The lack of fit test is helpful to compare pure error and residual error from replicated design points. The quadratic model was observed most significant during lack of fit tests because, it does not show a significant lack of fit. Further quadratic model is found significant during model summary statistics test. Hence, results of three statistical tests were confirmed quadratic model as significant and it can be used for further analysis. Low standard deviation, high R-squared and smaller PRESS values of model summary statistics are strongly confirmed quadratic model for MRR.

Table 4.6 Sequential Model Sum of Squares for MRR

Sequential Model Sum of Squares (Type I)						
Source	**Sum of Squares**	**df**	**Mean Square**	**F value**	**p-value Prob>F**	
Mean vs. Total	1.34	1	1.34			
Linear vs. Mean	0.059	4	0.015	208.12	< 0.0001	
2FI vs. Linear	7.887E-004	6	1.315E-004	2.53	0.0572	
Quadratic vs. 2FI	8.887E-004	4	2.222E-004	33.28	< 0.0001	Suggested
Cubic vs. Quadratic	4.724E-005	8	5.905E-006	0.78	0.6343	Aliased
Residual	5.291E-005	7	7.559E-006			
Total	1.40	30	0.047			

Table 4.7 Lack of fit tests for MRR

Lack of Fit Tests						
Source	**Sum of Squares**	**df**	**Mean Square**	**F value**	**p-value Prob>F**	
Linear	1.745E-003	20	8.724E-005	13.30	0.0047	
2FI	9.561E-004	14	6.829E-005	10.41	0.0087	
Quadratic	6.735E-005	10	6.735E-006	1.03	0.5217	Suggested
Cubic	2.012E-005	2	1.006E-005	1.53	0.3024	Aliased
Pure Error	3.279E-005	5	6.559E-006			

Table 4.8 Model summary statistics for MRR

Model Summary Statistics						
Source	**Std. Dev.**	**R - Squared**	**Adjusted R - Squared**	**Predicted R - Squared**	**PRESS**	
Linear	8.432E-003	0.9708	0.9662	0.9572	2.612E-003	
2FI	7.214E-003	0.9838	0.9752	0.9730	1.645E-003	
Quadratic	2.584E-003	0.9984	0.9968	0.9929	4.352E-004	Suggested
Cubic	2.749E-003	0.9991	0.9964	0.9517	2.944E-003	Aliased

4.4.2 Analysis of variance (ANOVA) for MRR

Analysis of variance (ANOVA) has been carried out to check the adequacies of the developed model and to find the significance of individual parameters for material removal rate (MRR). The result of ANOVA for MRR model is shown in Table 4.9. The calculated F-value of predicted MRR model is 651.22, indicates the model is significant. There is only 0.01% possibility of larger F-value occurs due to noise. In this case, C_p, I_p, T_{on}, τ, C_pI_p, $C_p\tau$, $I_p\tau$, C_p^2, I_p^2, T_{on}^2, and τ^2 are observed significant terms (P-value less than 0.05). The "lack of fit" for F-value is 1.03 which indicates lack of fit is not significant relative to the pure error.

Table 4.9 ANOVA for MRR

Source	**Sum of Squares**	**df**	**Mean Square**	**F Value**	**P- value Prob>F**	
Model	0.061	14	4.348E-003	651.22	< 0.0001	significant
C_p	6.240E-003	1	6.240E-003	934.68	< 0.0001	
I_p	0.044	1	0.044	6528.62	< 0.0001	
T_{on}	2.948E-003	1	2.948E-003	441.57	< 0.0001	
τ	6.416E-003	1	6.416E-003	960.94	< 0.0001	
C_pI_p	6.162E-005	1	6.162E-005	9.23	0.0083	
C_pT_{on}	4.225E-007	1	4.225E-007	0.063	0.8048	
$C_p\tau$	1.440E-004	1	1.440E-004	21.57	0.0003	
I_pT_{on}	1.960E-006	1	1.960E-006	0.29	0.5959	
$I_p\tau$	5.688E-004	1	5.688E-004	85.20	< 0.0001	
$T_{on}\tau$	1.190E-005	1	1.190E-005	1.78	0.2017	
C_p^2	3.332E-004	1	3.332E-004	49.91	< 0.0001	
I_p^2	2.015E-004	1	2.015E-004	30.18	< 0.0001	
T_{on}^2	3.720E-005	1	3.720E-005	5.57	0.0322	
τ^2	4.061E-004	1	4.061E-004	60.83	< 0.0001	
Residual	1.001E-004	15	6.677E-006			
Lack of Fit	6.735E-005	10	6.735E-006	1.03	0.5217	Not Significant
Pure Error	3.279E-005	5	6.559E-006			
Cor Total	0.061	29				
R-Squared = 0.9984					Adj R-Squared= 0.9968	
Pred R-Squared = 0.9929					Adeq Precision= 98.912	

There is a good agreement between “Pred-R-squared” (0.9929) and “Adj- R- squared” (0.9968) with the difference value of less than 0.2. It is desirable for “Adeq precision” ratio greater than 4. In this case “Adeq precision” ratio is 98.912 indicates an adequate signal.

Statistical inferences:

1. The Model F-value of 651.22 implies that the model is significant. There is only a 0.01% chance that an F-value this large could occur due to noise.
2. Values of "Prob > F" less than 0.0500 indicate model terms are significant. In this case, C_p, I_p, T_{on}, τ, C_pI_p, $C_p\tau$, $I_p\tau$, C_p^2, I_p^2, T_{on}^2, τ^2 are significant model terms.
3. The "Lack of Fit F-value" of 1.03 implies the Lack of Fit is not significant relative to the pure error. There is a 52.17% chance that a "Lack of Fit F-value" this large could occur due to noise. Non-significant lack of fit is good for predicted model.
4. The "Pred R-Squared" of 0.9929 is in reasonable agreement with the "Adj R-Squared" of 0.9968; i.e. the difference is less than 0.2.
5. "Adeq Precision" measures the signal to noise ratio. A ratio greater than 4 is desirable. Your ratio of 98.912 indicates an adequate signal. This model can be used to navigate the design space.

The regression analysis is used to develop a regression model for the material removal rate (MRR). The non-significant terms (P-value greater than 0.05) are not considered during regression analysis [50]. The second order regression eqation of MRR in coded terms and actual terms are given in equations 4.4 and 4.5.

Second order regression equation of MRR (Coded terms):

$$MRR = 0.22 - 0.032 * A + 0.085 * B + 0.022 * C + 0.033 * D + 7.850\ E\text{-}003 * AB - 0.012 * AD + 0.024 * BD - 0.014 * A^2 - 0.011 * B^2 + 4.658\ E\text{-}003 * C^2 - 0.015 * D^2 \quad \textbf{(4.4)}$$

Second order regression equation of MRR (Actual terms):

$$MRR = 0.22 - 0.032 * C_p + 0.085 * I_p + 0.022 * T_{on} + 0.033 * \tau + 7.850\ E\text{-}003 * C_pI_p - 0.012 * C_p\tau + 0.024 * I_p\tau - 0.014 * C_p^2 - 0.011 * I_p^2 + 4.658\ E\text{-}003 * T_{on}^2 - 0.015 * \tau^2 \quad \textbf{(4.5)}$$

The adequacy of developed regression model of material removal rate (MRR) has been examined using residual analysis. Figure 4.1(a) and (b) indicate the plot of normal

probability v/s internally studentized residuals and actual v/s predicted MRR respectively. The result of the plot indicates that the actual MRR v/s predicted MRR data spread approximately linear which indicates a good agreement between predicted and actual values of MRR. Hence, the proposed MRR model is significant.

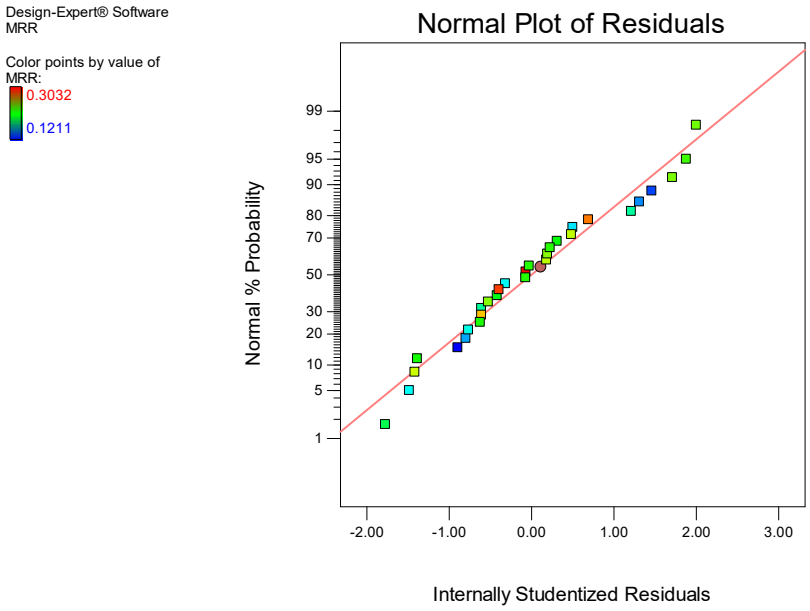

Figure 4.1(a) Normal vs. internally studentized residuals

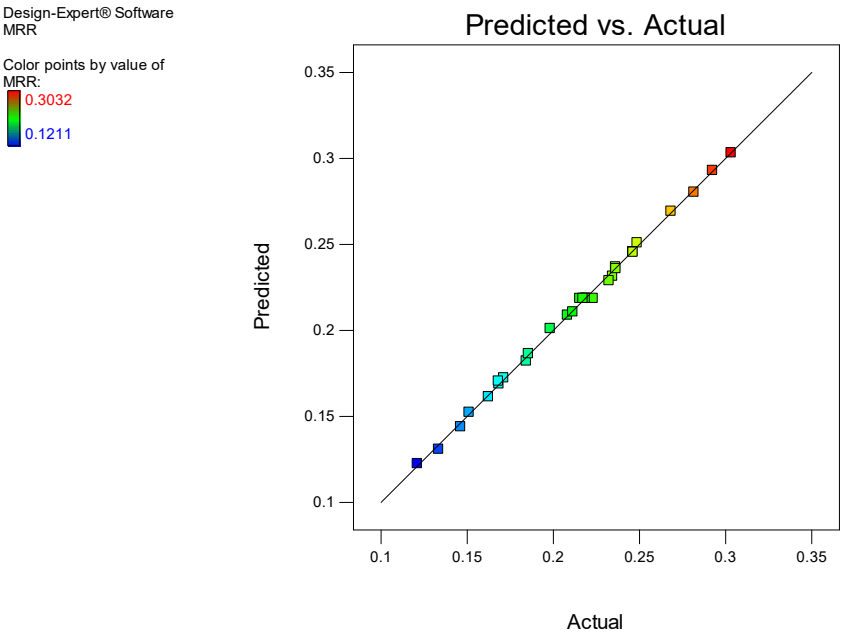

Figure 4.1 (b) Predicted vs. Actual MRR

4.4.3 Effects of machining parameters on MRR

The parametric analysis has been carried out to study the influence of various process parameters such as compaction pressure (C_p), peak current (I_p), pulse on time (T_{on}) and duty cycle (τ) on material removal rate (MRR) during surface modification of P20+Ni steel using EDM. Design Expert 10 (DX 10) statistical software is used to develop three dimensional (3D) surface plots for MRR. Three-dimensional response surface plots are able to deliver insight knowledge regarding the relation between input process parameters with MRR.

Based on response surface methodology (RSM) second-order model, the effects of peak current and compaction pressure on MRR, while keeping the levels of other two parameters; T_{on} = 90 μs and τ = 85% constant is shown in Figure 4.2(a) 3D surface plot. Non-linear variation in MRR with peak current has been obtained and it is concluded that with an increase in peak current from 6 to 18 Ampere, there is a continuous increase in MRR from 0.1211 gm/min to 0.3032 gm/min. Improvement in MRR with an increase in peak current is due to the availability of high discharge energy in the sparking area, that facilitate the melting and vaporizing of work material. The amount of discharge energy produced during the EDM operation mainly depends on the value of peak current. Therefore maximum discharge energy is available in the sparking area with a high value of peak current. Transfer of maximum amount of heat energy due to high peak current able to improve disintegration of work material resulting in maximum material removal rate [51].

Further increase in peak current is from 6 to 18 ampere (keeping compaction pressure at 125 kg/cm^2 and peak current 12 amperes) leads to an increase in MRR from 0.1211 to 0.2373 gm/min. This increase in MRR (while maintaining constant C_p = 125 kg/cm^2) can be attributed to the fact that an increase in the rate of heat energy generated, which further improve in melting and vaporization of work material.

The influence of pulse on time (T_{on}) and compaction pressure (C_p) on MRR, while keeping the levels of other two parameters; Ip = 12 Ampere and τ = 85% constant are shown in Figure 4.2(b) as a 3D surface plot. The non-linear variation of MRR with a pulse on time has been observed and concluded that for an increase in pulse on time from 50 to 130 μs, there is a continuous increase in MRR from 0.1211 gm/min to 0.3032 gm/min. Improvement in MRR with the increase in pulse on time is due to the availability of the

same heating temperature for a longer period. Hence, improvement in MRR is observed with a high pulse on time at the same machining duration [54].

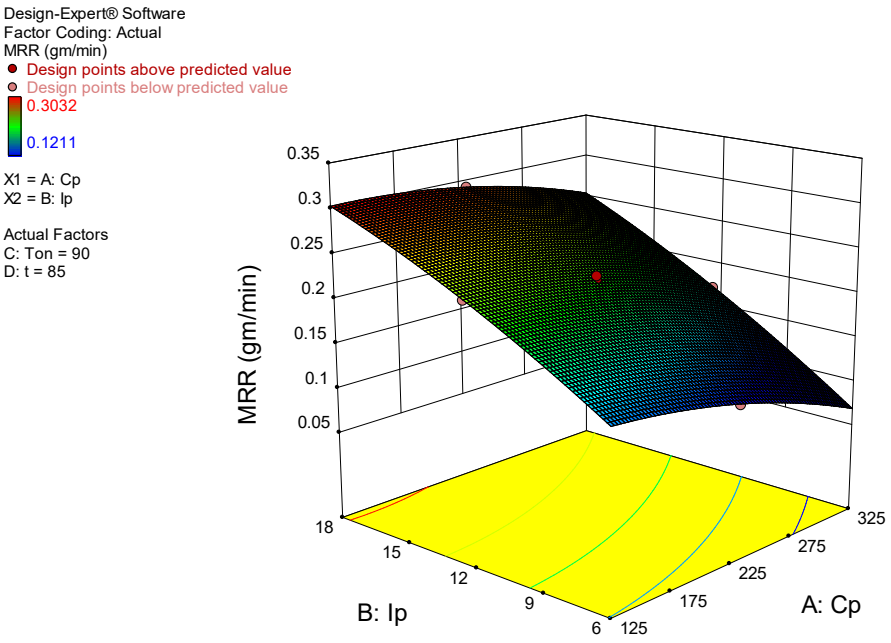

Figure 4.2 (a) Surface plot of MRR vs. Peak current and Compaction pressure

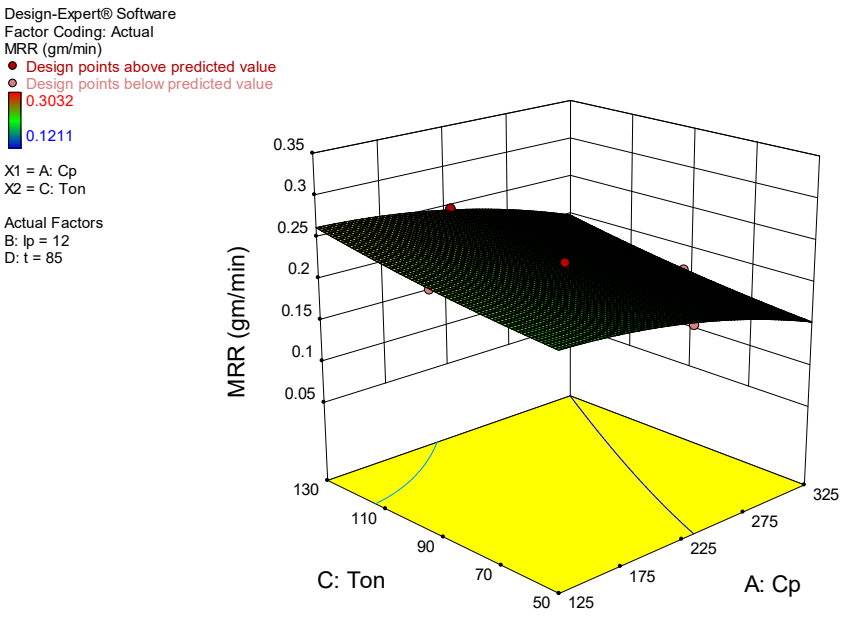

Figure 4.2 (b) Surface plot of MRR vs. Pulse on time and Compaction pressure

The influence of duty cycle (τ) and compaction pressure (C_p) on MRR, while keeping the levels of other parameters; I_p = 12 ampere and T_{on} = 90 µs constant are shown in Figure 4.2(c) as a 3D surface plot. The non-linear variation in MRR with duty cycle has been observed and it is concluded that for an increase in duty cycle from 75 to 95 %, there is a continuous increase in MRR from 0.1211 gm/min to 0.3032 gm/min. This improvement in MRR with the increase in the duty cycle is due to large pulse duration at the upper value of the duty cycle. Duty cycle is defined as the percentage of pulse on time with reference to total cycle time. Hence, a higher level of duty cycle means longer pulse duration. Therefore the same amount of heat energy available for longer duration in the machining area during experiments results in improved MRR [55].

Similarly, the effects of pulse on time (T_{on}) and peak current (I_p) on MRR, while keeping the levels of other two parameters; C_p = 225 kg/cm^2 and τ = 85% constant are shown in Figure 4.2(d) as a 3D surface plot. The non-linear variation of MRR with a pulse on time and peak current have been observed and it is concluded that for an increase in pulse on time from 50 to 130 µs, with peak current 6 to 18 Ampere, there is continuous increase in MRR from 0.1211 gm/min to 0.3032 gm/min. This improvement in MRR with the increase in pulse on time is due to the availability of the same heating temperature for a longer period of time. Hence, improvement in MRR is observed for the same machining duration with a longer pulse on time.

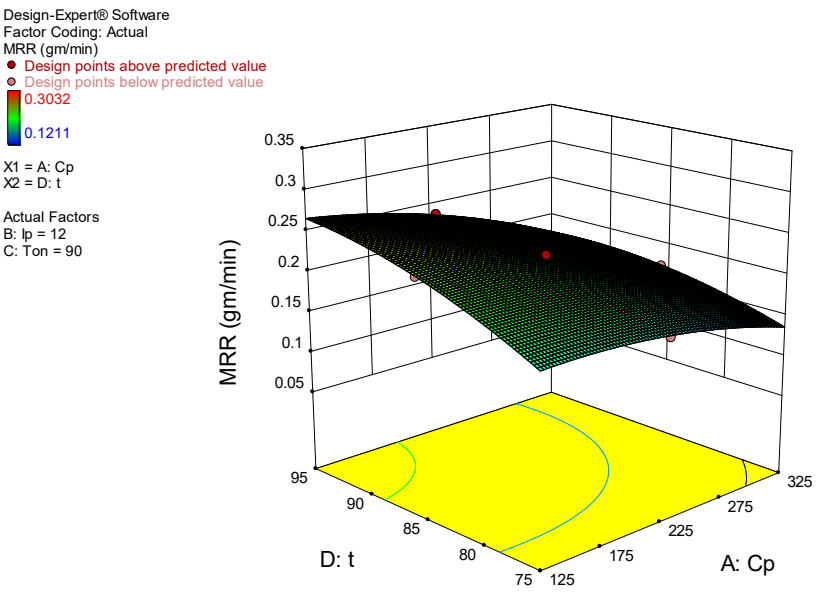

Figure 4.2 (c) Surface plot of MRR vs. Duty cycle and Compaction pressure

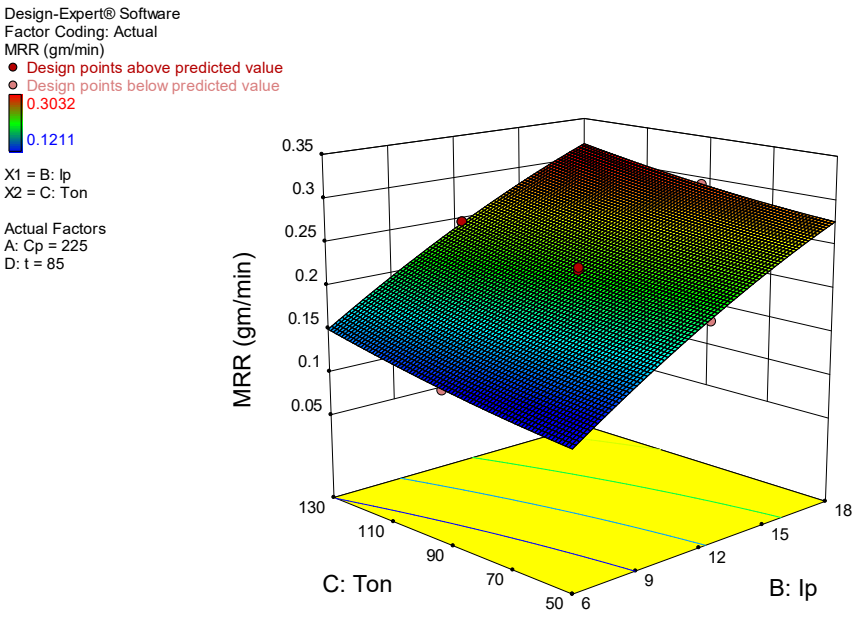

Figure 4.2 (d) Surface plot of MRR vs. Pulse on time and Peak current

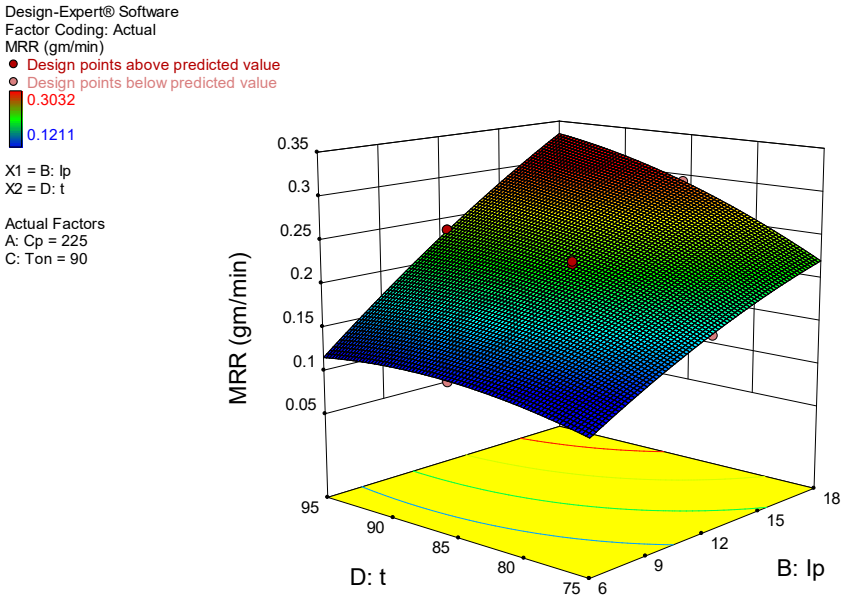

Figure 4.2 (e) Surface plot of MRR vs. Duty cycle and Peak current

The influence of duty cycle (τ) and peak current (I_p) on MRR, while keeping the levels of other two parameters; C_p = 225 kg/cm^2 and T_{on} = 90 µs constant are shown in Figure 4.2

(e) as a 3D surface plot. The non-linear variation of MRR with duty cycle has been obtained and it is concluded that for an increase in duty cycle from 75 to 95 %, there is a continuous increase in MRR from 0.1211 gm/min to 0.3032 gm/min. Further improvement in MRR is also observed with increase in peak current (Ip), while maintaining a constant duty cycle. This improvement in MRR with the increase in the duty cycle is due to longer pulse duration. Therefore the same amount of heat energy is available for longer duration able to disintegrate large amount of material resulting improvements in MRR.

Similarly, The influence of duty cycle (τ) and pulse on time (T_{on}) with MRR, while keeping the levels of other two parameters; C_p = 225 kg/cm^2 and I_p = 12 ampere constant are shown in Figure 4.2(f) as a 3D surface plot. The non-linear variation of MRR with duty cycle has been obtained and it is concluded that for an increase in duty cycle from 75 to 95 %, there is a continuous increase in MRR from 0.1211 gm/min to 0.3032 gm/min. Further improvements in MRR were also observed with an increase in pulse on time (T_{on}) while maintaining duty cycle at the same level [55].

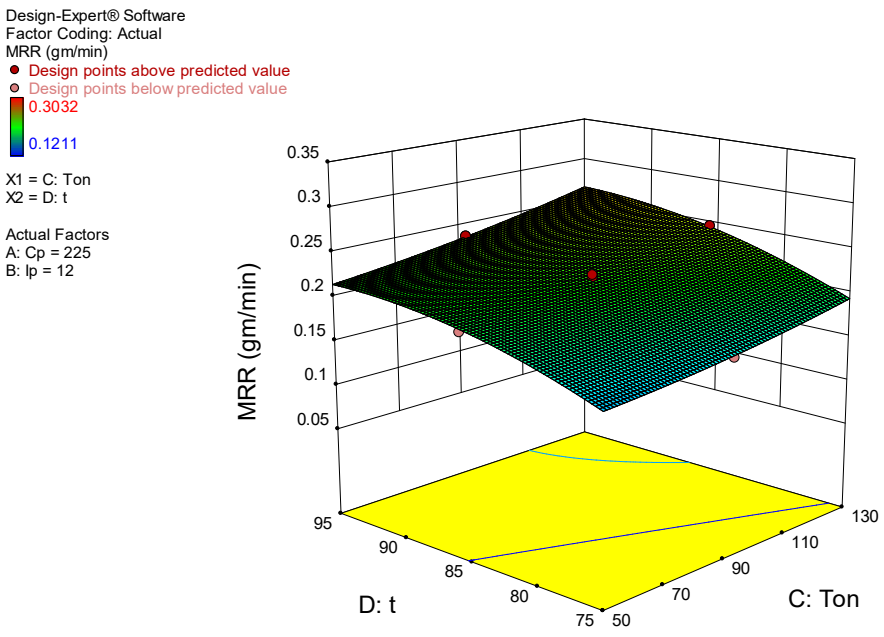

Figure 4.2 (f) Surface plot of MRR vs. Duty cycle and Pulse on time

4.5 ANALYSIS AND DISCUSSION OF TOOL WEAR RATE RESULTS

Optimum tool wear rate (TWR) is a desired condition for surface modification process performed using EDM. High tool wear rate is responsible for introducing large numbers of

powder particles at the inter-electrode gap (IEG). Presence of excess powder particles at IEG will deteriorate machining performance due to arcing. Besides of this, very low tool wear could not able to transfer the hardest elements from the electrode to work material. Attempts have been made to design/manufacture P/M electrode able to deliver optimum tool wear rate and also capable to modify the work material with adequate machining performance. Tool wear rate (TWR) is calculated using the following relation.

$$TWR = \frac{W_{tb} - W_{ta}}{T_m} \; gm/min \qquad \text{------- (4.6)}$$

Where,

TWR = tool wear rate gm/min

W_{tb} = weight of tool before machining in gm

W_{ta} = weight of tool after machining in gm

T_m = total machining time in minutes

Experiments were planned and performed using response surface methodology. The individual experiment was performed thrice by setting levels of process parameters shown in Table 4.3. Mean value of the three results of TWR is used for further analysis. The regression model of tool wear rate (TWR) is developed using statistical software Design Expert 10 (DX 10). Adequacy of the developed model was checked using the sum of squares, lack of fit test and model summary statistics. Analysis of variance (ANOVA) is also performed to find the contribution of the individual parameter to minimize TWR. Three-dimensional surface plots were developed to study the effects of process parameters on TWR. The results of the tool wear rate with its mean values are given in Table 4.10.

Figure 4.3 Powder metallurgy electrodes

Table 4.10 Design of experiment matrix and the observed value of TWR

Exp. No.	Run Order	Input process parameters								Response			Mean TWR (gm/min)
		C_p		I_p		T_{on}		τ		TWR-1 (gm/min)	TWR-2 (gm/min)	TWR-3 (gm/min)	
		Actual	Coded	Actual	Coded	Actual	Coded	Actual	Coded				
1	12	175	-1	9	-1	70	-1	80	-1	0.0274	0.0278	0.0297	0.0283
2	6	275	1	9	-1	70	-1	80	-1	0.0267	0.0261	0.0228	0.0252
3	9	175	-1	15	1	70	-1	80	-1	0.0318	0.0319	0.0341	0.0326
4	28	275	1	15	1	70	-1	80	-1	0.0278	0.0284	0.0317	0.0293
5	4	175	-1	9	-1	110	1	80	-1	0.0274	0.0262	0.0262	0.0266
6	27	275	1	9	-1	110	1	80	-1	0.0258	0.0257	0.0232	0.0249
7	14	175	-1	15	1	110	1	80	-1	0.0257	0.0288	0.0268	0.0271
8	20	275	1	15	1	110	1	80	-1	0.0318	0.0305	0.0289	0.0304
9	11	175	-1	9	-1	70	-1	90	1	0.0353	0.0363	0.0340	0.0352
10	16	275	1	9	-1	70	-1	90	1	0.0278	0.0257	0.0278	0.0271
11	2	175	-1	15	1	70	-1	90	1	0.0367	0.0377	0.0411	0.0385
12	22	275	1	15	1	70	-1	90	1	0.0348	0.0346	0.0323	0.0339
13	5	175	-1	9	-1	110	1	90	1	0.0335	0.0324	0.0313	0.0324
14	19	275	1	9	-1	110	1	90	1	0.0242	0.0255	0.0256	0.0251
15	29	175	-1	15	1	110	1	90	1	0.0336	0.0319	0.0338	0.0331
16	15	275	1	15	1	110	1	90	1	0.0276	0.0281	0.0319	0.0292
17	10	125	-2	12	0	90	0	85	0	0.0324	0.0338	0.0331	0.0331
18	25	325	2	12	0	90	0	85	0	0.0272	0.0282	0.0253	0.0269
19	18	225	0	6	-2	90	0	85	0	0.0264	0.0259	0.0191	0.0238
20	7	225	0	18	2	90	0	85	0	0.0336	0.0334	0.0371	0.0347

Exp. No.	Run Order	Input process parameters								Response			Mean TWR (gm/min)
		C_p		I_p		T_{on}		τ		TWR-1 (gm/min)	TWR-2 (gm/min)	TWR-3 (gm/min)	
		Actual	Coded	Actual	Coded	Actual	Coded	Actual	Coded				
21	30	225	0	12	0	50	-2	85	0	0.0321	0.0335	0.0343	0.0333
22	21	225	0	12	0	130	2	85	0	0.0271	0.0271	0.0232	0.0258
23	13	225	0	12	0	90	0	75	-2	0.0258	0.0276	0.0279	0.0271
24	23	225	0	12	0	90	0	95	2	0.0336	0.0326	0.0343	0.0335
25	26	225	0	12	0	90	0	85	0	0.0255	0.0248	0.0298	0.0267
26	3	225	0	12	0	90	0	85	0	0.0267	0.0266	0.0259	0.0264
27	1	225	0	12	0	90	0	85	0	0.0248	0.0279	0.0271	0.0266
28	8	225	0	12	0	90	0	85	0	0.0271	0.0261	0.0272	0.0268
29	24	225	0	12	0	90	0	85	0	0.0252	0.0258	0.0273	0.0261
30	17	225	0	12	0	90	0	85	0	0.0257	0.0267	0.0271	0.0265

4.5.1 Selection of adequate model for TWR

The adequacy of the developed mathematical model of TWR is checked by performing various statistical tests such as a sequential model sum of squares, lack of fit tests and model summary statistics. The results of statistical tests are given in Table 4.11 to 4.13. Quadratic model is found most appropriate according to the sequential model sum of the square testfor TWR. The sequential model sum of squares test shows how the terms of increasing complexity contribute to the model. The lack of fit tests is helpful to compare pure error with residual error from replicated design points. The quadratic model is found the best choice during lack of fit tests because of not showing a significant lack of fit. Model summary statistics also confirm the quadratic model. Hence, based on the result of three statistical tests, the quadratic model is selected and used for further analysis. Low standard deviation, high R-squared and smaller PRESS values of model summary statistics also strongly confirm the quadratic model [56].

Table 4.11 Sequential model sum of squares for TWR

Sequential Model Sum of Squares (Type I)						
Source	**Sum of Squares**	**df**	**Mean Square**	**F value**	**p-value Prob>F**	
Mean vs Total	0.026	1	0.026			
Linear vs Mean	3.115E-004	4	7.786E-005	16.96	< 0.0001	
2FI vs Linear	4.523E-005	6	7.539E-006	2.06	0.1069	
Quadratic vs 2FI	5.576E-005	4	1.394E-005	15.20	< 0.0001	Suggested
Cubic vs Quadratic	1.158E-005	8	1.448E-006	4.66	0.0285	Aliased
Residual	2.174E-006	7	3.106E-007			
Total	0.026	30	8.674E-004			

Table 4.12 Lack of fit tests for TWR

Lack of Fit Tests						
Source	**Sum of Squares**	**df**	**Mean Square**	**F value**	**p-value Prob>F**	
Linear	1.144E-004	20	5.722E-006	92.79	< 0.0001	
2FI	6.921E-005	14	4.943E-006	80.16	< 0.0001	
Quadratic	1.345E-005	10	1.345E-006	21.81	0.0017	Suggested
Cubic	1.866E-006	2	9.329E-007	15.13	0.0076	Aliased
Pure Error	3.083E-007	5	6.167E-008			

Table 4.13 Model summary statistics for TWR

Model Summary Statistics						
Source	**Std. Dev.**	**R - Squared**	**Adjusted R - Squared**	**Predicted R - Squared**	**PRESS**	
Linear	2.142E-003	0.7308	0.6877	0.6300	1.577E-004	
2FI	1.913E-003	0.8369	0.7511	0.6343	1.559E-004	
Quadratic	9.576E-004	0.9677	0.9376	0.8172	7.790E-005	Suggested
Cubic	5.573E-004	0.9949	0.9789	0.3686	2.691E-004	Aliased

4.5.2 Analysis of variance (ANOVA) for TWR

Analysis of variance (ANOVA) is carried out to check the adequacies of the developed model and to find the contribution of individual parameters for the tool wear rate (TWR). The result of ANOVA for TWR is shown in Table 4.14. The calculated F-value for predicted TWR model is 32.13 which indicate significant model. There is a 0.01% possibility of larger F-value could occur due to noise. In this case, C_p, I_p, T_{on}, τ, C_pI_p, C_pT_{on}, $C_p\tau$, $T_{on}\tau$, C_p^2, I_p^2, T_{on}^2 and τ^2 are significant terms (P-value less than 0.05). The "lack of fit" for F-value is 21.81 which show lack of fit is significant relative to the pure error.

Table 4.14 ANOVA for TWR

Source	**Sum of Squares**	**df**	**Mean Square**	**F Value**	**P-value Prob>F**	
Model	4.125E-004	14	2.946E-005	32.13	< 0.0001	significant
C_p	7.107E-005	1	7.107E-005	77.50	< 0.0001	
I_p	1.088E-004	1	1.088E-004	118.64	< 0.0001	
T_{on}	5.490E-005	1	5.490E-005	59.87	< 0.0001	
τ	7.668E-005	1	7.668E-005	83.62	< 0.0001	
C_pI_p	8.556E-006	1	8.556E-006	9.33	0.0080	
C_pT_{on}	5.641E-006	1	5.641E-006	6.15	0.0255	
$C_p\tau$	2.280E-005	1	2.280E-005	24.86	0.0002	
I_pT_{on}	3.706E-006	1	3.706E-006	4.04	0.0628	
$I_p\tau$	1.563E-008	1	1.563E-008	0.017	0.8979	
$T_{on}\tau$	4.516E-006	1	4.516E-006	4.92	0.0423	
C_p^2	2.258E-005	1	2.258E-005	24.62	0.0002	
I_p^2	1.372E-005	1	1.372E-005	14.96	0.0015	
T_{on}^2	1.679E-005	1	1.679E-005	18.30	0.0007	
τ^2	2.580E-005	1	2.580E-005	28.13	< 0.0001	
Residual	1.376E-005	15	9.171E-007			
Lack of Fit	1.345E-005	10	1.345E-006	21.81	0.0017	
Pure Error	3.083E-007	5	6.167E-008			
Cor Total	4.262E-004	29				
R-Squared = 0.9677					Adj R-Squared= 0.9376	
Pred R-Squared = 0.8172					Adeq Precision= 21.395	

There is a good agreement between “Pred-R-squared” (0.8172) and “Adj- R- squared” (0.9376) with the difference less than 0.2. It is desirable for “Adeq precision” ratio greater than 4. In this case “Adeq precision” ratio is 21.395, indicates an adequate signal.

Statistical inferences:

1. The Model F-value of 32.13 implies the model is significant. There is only a 0.01% chance that an F-value this large could occur due to noise.
2. Values of "Prob > F" less than 0.0500 indicate model terms are significant. In this case, C_p, I_p, T_{on}, τ, C_pI_p, C_pT_{on}, $C_p\tau$, $T_{on}\tau$, C_p^2, I_p^2, T_{on}^2, τ^2 are significant model terms.
3. The "Lack of Fit F-value" of 21.81 implies the Lack of Fit is significant. There is only a 0.17% chance that a "Lack of Fit F-value" this large could occur due to noise. Significant lack of fit is bad for predicted model.
4. The "Pred R-Squared" of 0.8172 is in reasonable agreement with the "Adj R-Squared" of 0.9376; i.e. the difference is less than 0.2.
5. "Adeq Precision" measures the signal to noise ratio. A ratio greater than 4 is desirable. Your ratio of 21.395 indicates an adequate signal. This model can be used to navigate the design space.

The regression analysis is used to develop a statistical model for the tool wear rate (TWR). The non-significant terms (P-value greater than 0.05) were removed during regression analysis. The regression model for TWR with coded terms and actual terms are given in equation 4.7 and 4.8.

Second order regression equation of TWR (Coded terms):

$$TWR = 0.027 - 3.425\text{ E-}003 * A + 4.258\text{ E-}003 * B - 3.025\text{ E-}003 * C + 3.575\text{ E-}003 * D + 2.925\text{ E-}003 * AB + 2.375\text{ E-}003 * AC - 4.775\text{ E-}003 * AD - 2.125\text{ E–}003 * CD + 3.588\text{ E–}003 * A^2 + 2.838\text{ E-}003 * B^2 + 3.138\text{ E-}003 * C^2 + 3.888\text{ E-}003 * D^2 \text{ ------ } \mathbf{(4.7)}$$

Second order regression equation of TWR (Actual terms):

$$TWR = 0.027 - 3.425\text{ E-}003 * C_p + 4.258\text{ E-}003 * I_p - 3.025\text{ E-}003 * T_{on} + 3.575\text{ E-}003 * \tau + 2.925\text{ E-}003 * C_pI_p + 2.375\text{ E-}003 * C_pT_{on} - 4.775\text{ E-}003 * C_p\tau - 2.125\text{ E–}003 * T_{on}\tau + 3.588\text{ E–}003 * C_p^2 + 2.838\text{ E-}003 * I_p^2 + 3.138\text{ E-}003 * T_{on}^2 + 3.888\text{ E-}003 * \tau^2 \text{ ------- } \mathbf{(4.8)}$$

The adequacy of the developed statistical model based on regression using RSM for tool wear rate has been examined using residual analysis. Figures 4.4(a) & (b) indicates a plot of normal probability v/s internally studentized residuals and actual v/s predicted TWR respectively. The results of the plot indicate that the actual TWR v/s predicted TWR data spread approximately linear which indicates a good agreement between predicted and actual values of TWR. Hence, the proposed TWR model is significant [58].

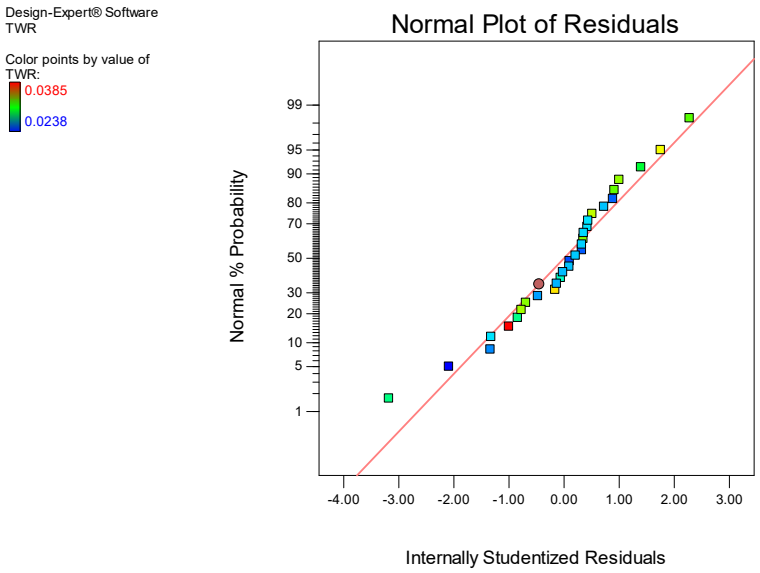

Figure 4.4 (a) Normal vs. Internally studentized residuals

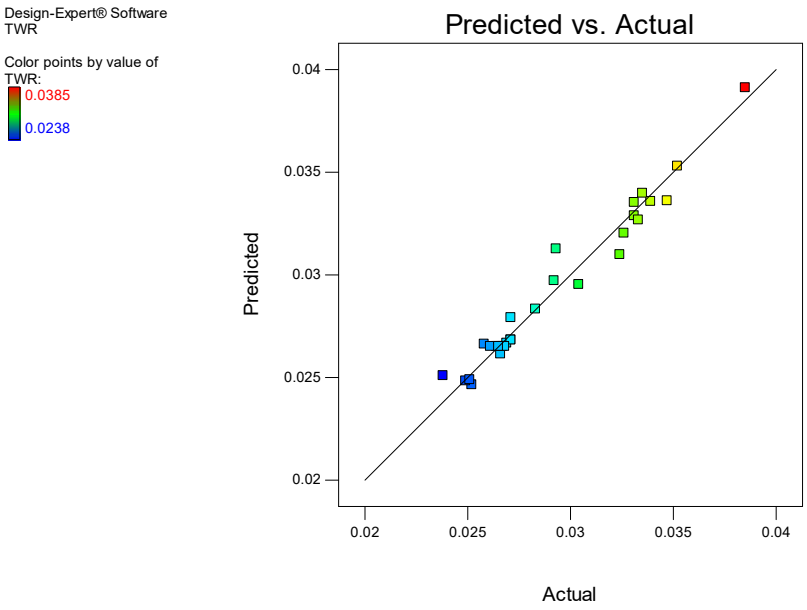

Figure 4.4 (b) Predicted vs. Actual TWR

4.5.3 Effects of machining parameters on TWR

Tool wear greatly affects the dimensional accuracy of the EDMed component because of process based on projection manufacturing. The tool wear rate (TWR) mainly depends on the mechanical and thermophysical properties of the electrode. Electrode wear plays a significant role in the surface modification process. Migrations of hardest constituents from the electrode is desired during machining work material on EDM for surface modification. Excess tool wears greatly influence the dimensional accuracy and operation stability, while lower TWR could not transfer hardest electrode constituents on the work surface. Optimum tool wear rate is the desired conditions to modify the work surface using EDM.

The parametric analysis has been carried out to study the effects of various process parameters such as compaction pressure (C_p), peak current (I_p), pulse on time (T_{on}) and duty cycle (τ) on tool wear rate (TWR) during surface modification of P20+Ni steel using EDM. The statistical software Design Expert 10 (DX 10) was used to develop the three dimensional (3D) surface plots for TWR. Three-dimensional response surface plots are able to deliver insight knowledge regarding the relation between input process parameters and the TWR[60].

Based on response surface methodology (RSM) second-order model the effects of peak current and compaction pressure on TWR, while keeping the levels of other two parameters; T_{on} = 90 μs and τ = 85% constant is shown in Figure 4.5 (a) as a 3D surface plot. The non-linear variation of TWR with peak current has been observed and it is concluded that for an increase in peak current from 6 to 18 ampere, there is a continuous increase in TWR from 0.0238 gm/min to 0.0385 gm/min. This increase in TWR at the high peak current is due to the availability of large discharge energy, that facilitates the melting and vaporizing of work and tool material in the sparking area. The amount of discharge energy obtained during EDM operation mainly depends on the peak current. Therefore maximum discharge energy is available in the sparking area with a high value of peak current. Transfer of maximum amount of heat energy at high peak current able to enhance the disintegration of tool material.

High tool wear rate from 0.0238 to 0.0331 gm/min has been observed with an increase in peak current from 6 to 18 ampere (keeping compaction pressure at 125 kg/cm^2 and peak current 12 amperes). This high TWR value (while maintaining constant C_p = 125 kg/cm^2) can be attributed to the fact that an increase in the rate of heat energy generated, which

further improve the rate of melting and vaporization of tool material. Hence the lower value of peak current should be desired to maintain lower TWR [62].

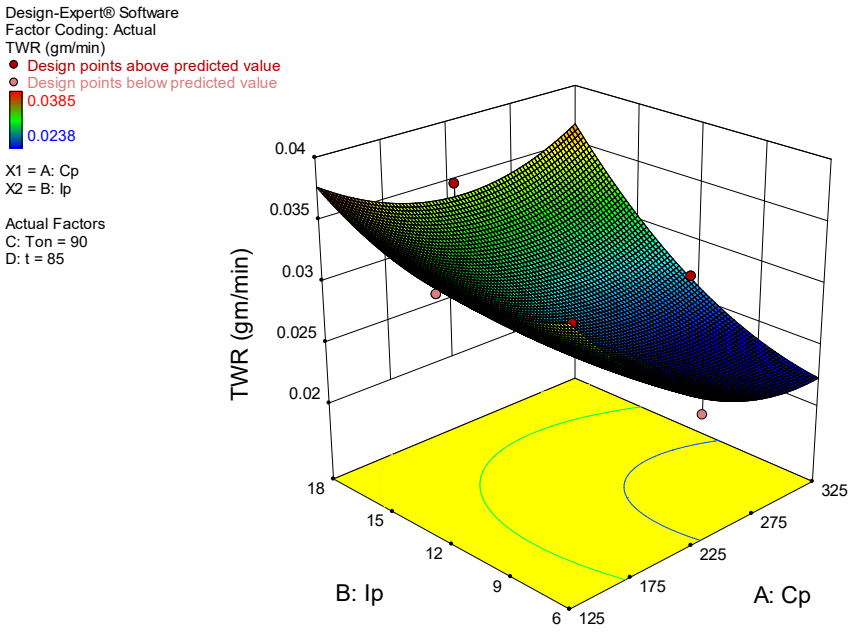

Figure 4.5 (a) Surface plot of TWR vs. Peak current and Compaction pressure

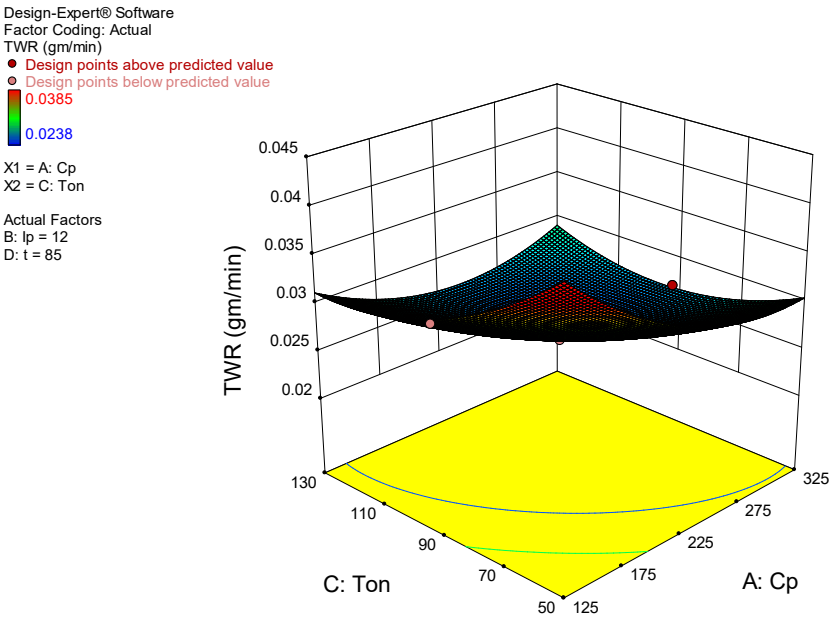

Figure 4.5 (b) Surface plot of TWR vs. Pulse on time and Compaction pressure

The influence of pulse on time (T_{on}) and compaction pressure (C_p) on TWR, while keeping the levels of other two parameters; I_p = 12 ampere and τ = 85% constant are shown in Figure 4.5(b) as a 3D surface plot. The non-linear variation of TWR with a pulse on time has been observed. Reduction in TWR has been observed with higher levels of compaction pressure while maintaining a constant pulse on time. Compaction pressure of P/M electrode from 125 to 325 kg/cm^2 leads to reduce the tool wear rate from 0.0385 to 0.0238 gm/min while maintaining a pulse on-time 50 µs. This reduction in tool wear rate may be attributed to the lower bonding strength between individual elements of the P/M electrode. Further the effects of duty cycle (τ) and compaction pressure (C_p) on TWR, while keeping the levels of other two parameters; I_p = 12 ampere and T_{on} = 90 µs constant are shown in Figure 4.5(c) as a 3D surface plot. The non-linear variation of TWR with duty cycle has been observed and it can be concluded that for an increase in duty cycle from 75 to 95 %, there is an increase in TWR from 0.0238 gm/min to 0.0385 gm/min. This increase in TWR at higher levels of duty cycle is due to longer pulse duration. Duty cycle is defined as the percentage of pulse on time with reference to total cycle time [61]. Hence, the selection of a higher level of duty cycle results in a longer pulse duration. Therefore the same amount of heat energy available for longer duration in the machined area which further increases TWR.

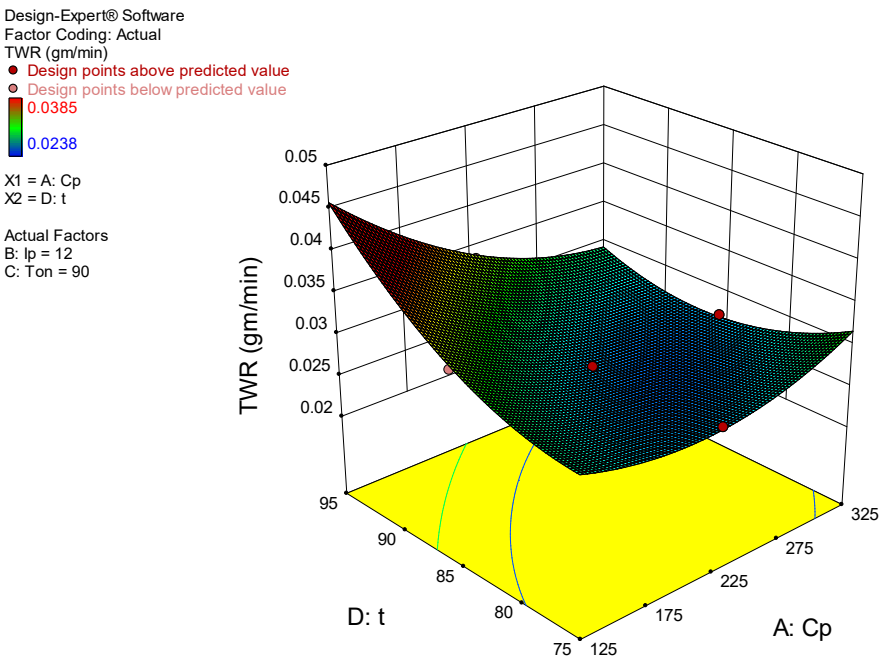

Figure 4.5 (c) Surface plot of TWR vs. Duty cycle and Compaction pressure

Moreover, the influence of pulse on time (T_{on}) and peak current (I_p) on TWR, while keeping the levels of other two parameters; C_p = 225 kg/cm^2 and τ = 85% constant is shown in Figure 4.5(d) as a 3D surface plot. The non-linear variation of TWR with a pulse on time and peak current have been observed and it is concluded that for an increase in pulse on time from 50 to 130 µs, with peak current 6 to 18 ampere, there is a continuous increase in TWR from 0.0238 gm/min to 0.0385 gm/min. This increase in TWR with a high value of pulse on time is due to the availability of the same heating temperature for a longer period of time. Hence, the increase in TWR has been observed with a high pulse on time. Further increase in TWR observed at high-level peak current due to intense discharge energy. Hence care should be taken while selecting levels of T_{on} and I_p for obtaining optimum TWR.

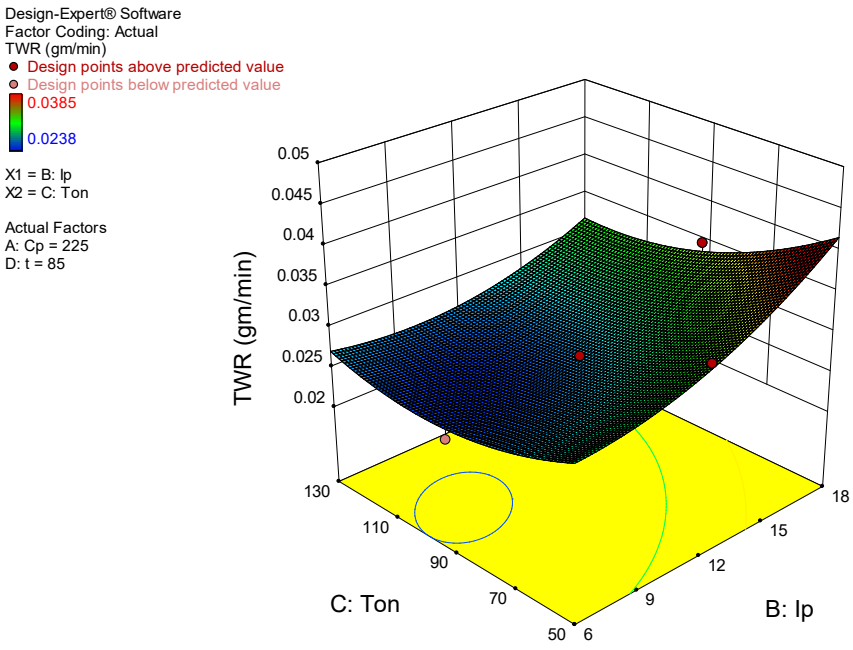

Figure 4.5 (d) Surface plot of TWR vs. Pulse on time and Peak current

Similarly, the influence of duty cycle (τ) and peak current (I_p) on TWR, while keeping the levels of other two parameters; C_p = 225 kg/cm^2 and T_{on} = 90 µs constant is shown in Figure 4.5(e) as a 3D surface plot. The non-linear variation of TWR with duty cycle has been observed and it is concluded that for an increase in duty cycle from 75 to 95 %, there is a continuous increase in TWR from 0.0238 gm/min to 0.0385 gm/min. Further increase in TWR is also observed with increase in peak current (I_p) while maintaining a constant

duty cycle. This increase in TWR at a higher level of duty cycle is due to the longer pulse duration.

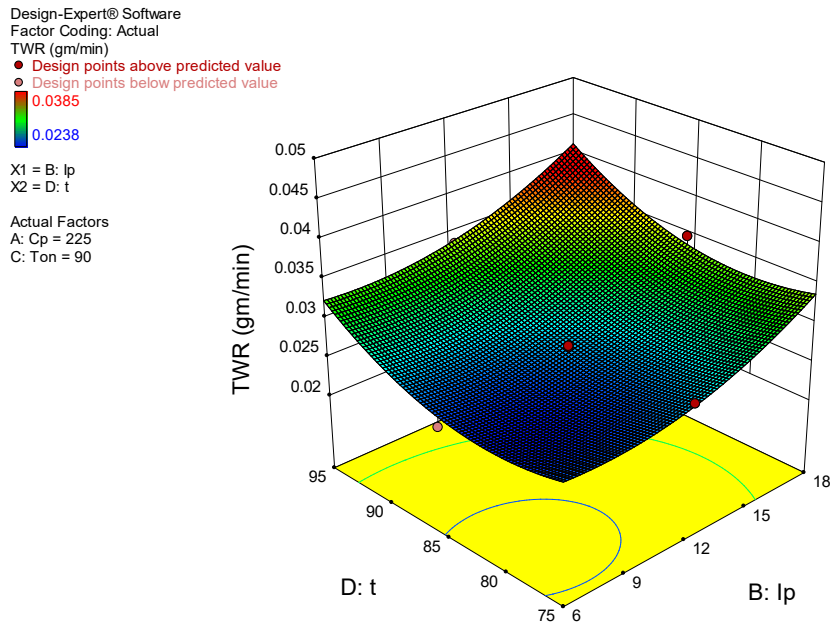

Figure 4.5 (e) Surface plot of TWR vs. Duty cycle and Peak current

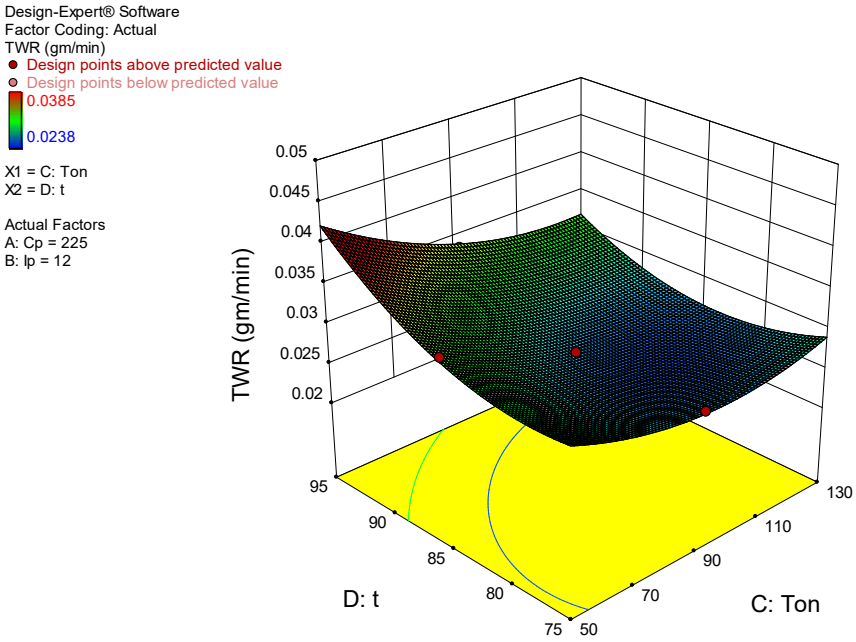

Figure 4.5 (f) Surface plot of TWR vs. Duty cycle and Pulse on time

Similarly, The influence of duty cycle (τ) and pulse on time (T_{on}) on TWR, while keeping the levels of other two parameters; C_p = 225 kg/cm^2 and I_p = 12 Ampere constant are shown in Figure 4.5(f) as a 3D surface plot. The non-linear variation of TWR with duty cycle has been observed and it is concluded that for an increase in duty cycle from 75 to 95 %, there is a continuous increase in TWR. Further, the increase in TWR from 0.0238 to 0.0335 gm/min was also observed with an increase in duty cycle from 75 to 95 % while maintaining constant peak current (I_p) at 12 amperes. It can be concluded that the high value of Ip and τ would be able to generate more discharge energy, which disintegrates the tool elements during machining. Maintain appropriate tool wear is desired conditions for surface modification; hence the selection of peak current and duty cycle level is attributed to maintaining stable machining condition [66].

4.6 ANALYSIS AND DISCUSSION OF SURFACE ROUGHNESS RESULTS

Surface finish and dimensional accuracy of the component mainly depend on the material of die and tool used to produce it. Functional performance of engineering components mainly depends on surface quality and dimensional accuracies. In this experimental work, care has been taken to obtained optimum surface quality during surface modification of P20+Ni steel using EDM. Experiments were planned and performed using response surface methodology. Individual experiments performed thrice by setting levels of process parameters shown in Table 4.3. Mean value of three results of surface roughness (SR) was used for further analysis. The regression model for surface roughness (SR) was developed using statistical software Design Expert 10 (DX 10). Adequacy of the developed model was checked using the sum of squares, lack of fit test and model summary statistics. Analysis of variance (ANOVA) is carried out to obtain the contribution of the individual parameter to maintain minimum SR. Three-dimensional surface plots were developed to investigate the effect of process parameters on SR. The experimental results of surface roughness and its mean values are given in Table 4.15.

Table 4.15 Design of experiment matrix and the observed value of SR

Exp. No.	Run Order	Input process parameters								Response			Mean SR (µm)
		C_p		I_p		T_{on}		τ		SR-1 (µm)	SR-2 (µm)	SR-3 (µm)	
		Actual	Coded	Actual	Coded	Actual	Coded	Actual	Coded				
1	12	175	-1	9	-1	70	-1	80	-1	5.298	5.742	5.865	5.635
2	6	275	1	9	-1	70	-1	80	-1	5.153	4.671	4.441	4.755
3	9	175	-1	15	1	70	-1	80	-1	7.891	8.217	8.468	8.192
4	28	275	1	15	1	70	-1	80	-1	7.531	7.147	7.765	7.481
5	4	175	-1	9	-1	110	1	80	-1	6.303	6.465	6.561	6.443
6	27	275	1	9	-1	110	1	80	-1	4.904	5.278	5.979	5.387
7	14	175	-1	15	1	110	1	80	-1	8.677	8.224	9.151	8.684
8	20	275	1	15	1	110	1	80	-1	8.164	7.872	8.342	8.126
9	11	175	-1	9	-1	70	-1	90	1	6.418	6.732	6.281	6.477
10	16	275	1	9	-1	70	-1	90	1	5.407	4.771	5.179	5.119
11	2	175	-1	15	1	70	-1	90	1	10.108	9.644	9.741	9.831
12	22	275	1	15	1	70	-1	90	1	8.618	8.584	8.640	8.614
13	5	175	-1	9	-1	110	1	90	1	7.211	7.623	7.327	7.387
14	19	275	1	9	-1	110	1	90	1	6.228	5.701	5.717	5.882
15	29	175	-1	15	1	110	1	90	1	10.824	10.329	10.662	10.605
16	15	275	1	15	1	110	1	90	1	9.553	9.619	9.271	9.481
17	10	125	-2	12	0	90	0	85	0	7.962	8.512	8.315	8.263
18	25	325	2	12	0	90	0	85	0	5.988	5.644	6.323	5.985
19	18	225	0	6	-2	90	0	85	0	4.146	4.358	4.201	4.235
20	7	225	0	18	2	90	0	85	0	9.818	10.369	10.782	10.323

Exp. No.	Run Order	Input process parameters								Response			Mean SR (µm)
		C_p		I_p		T_{on}		τ		SR-1 (µm)	SR-2 (µm)	SR-3 (µm)	
		Actual	Coded	Actual	Coded	Actual	Coded	Actual	Coded				
21	30	225	0	12	0	50	-2	85	0	7.273	6.883	6.646	6.934
22	21	225	0	12	0	130	2	85	0	8.345	8.529	8.977	8.617
23	13	225	0	12	0	90	0	75	-2	5.811	6.152	5.683	5.882
24	23	225	0	12	0	90	0	95	2	8.362	7.888	8.548	8.266
25	26	225	0	12	0	90	0	85	0	7.757	7.836	7.291	7.628
26	3	225	0	12	0	90	0	85	0	7.926	6.782	8.011	7.573
27	1	225	0	12	0	90	0	85	0	8.114	6.904	7.755	7.591
28	8	225	0	12	0	90	0	85	0	7.821	7.661	7.567	7.683
29	24	225	0	12	0	90	0	85	0	6.793	7.868	8.352	7.671
30	17	225	0	12	0	90	0	85	0	7.454	7.638	7.774	7.622

4.6.1 Selection of adequate model for SR

The adequacy of the developed model for SR checked by performing various statistical tests such as a sequential model sum of squares, lack of fit tests and model summary statistics. The suggested results of three statistical tests are given in Table 4.16 to 4.18. Quadratic model is found optimum as per sequential model sum of the square test. The sequential model sum of squares test (Table 4.16) shows how the terms of increasing complexity contribute to the model. The lack of fit tests helps to compare pure error and residual error from replicated design points. The quadratic model is found appropriate during lack of fit tests because it does not show a significant lack of fit. Model summary statistics test further confirm the quadratic model. Hence, based on the results of three statistical tests it can be concluded that the quadratic model is significant and used for further analysis. Low standard deviation, high R-squared and smaller PRESS values of model summary statistics strongly suggest the quadratic model.

Table 4.16 Sequential Model Sum of Squares for SR

Sequential Model Sum of Squares (Type I)						
Source	**Sum of Squares**	**df**	**Mean Square**	**F value**	**p-value Prob>F**	
Mean vs. Total	1648.31	1	1648.31			
Linear vs. Mean	72.44	4	18.11	208.46	< 0.0001	
2FI vs. Linear	1.10	6	0.18	3.27	0.0222	
Quadratic vs. 2FI	0.96	4	0.24	34.69	< 0.0001	Suggested
Cubic vs. Quadratic	0.070	8	8.720E-003	1.77	0.2333	Aliased
Residual	0.035	7	4.929E-003			
Total	1722.92	30	57.43			

Table 4.17 Lack of Fit Tests for SR

Lack of Fit Tests						
Source	**Sum of Squares**	**df**	**Mean Square**	**F value**	**p-value Prob>F**	
Linear	2.16	20	0.11	58.11	0.0001	
2FI	1.06	14	0.076	40.67	0.0003	
Quadratic	0.095	10	9.496E-003	5.10	0.0430	Suggested
Cubic	0.025	2	0.013	6.77	0.0378	Aliased
Pure Error	9.304E-003	5	1.861E-003			

Table 4.18 Model Summary Statistics for SR

Model Summary Statistics						
Source	**Std. Dev.**	**R - Squared**	**Adjusted R - Squared**	**Predicted R - Squared**	**PRESS**	
Linear	0.29	0.9709	0.9662	0.9564	3.25	
2FI	0.24	0.9857	0.9781	0.9765	1.75	
Quadratic	0.083	0.9986	0.9973	0.9925	0.56	Suggested
Cubic	0.070	0.9995	0.9981	0.9512	3.64	Aliased

4.6.2 Analysis of variance (ANOVA) for SR

Analysis of variance is performed to check the adequacies of the developed model. The result of ANOVA for developed SR model is shown in Table 4.19. The calculated F-value for predicted SR model is 765.61 that indicate the model is significant. There is only a 0.01% possibility of larger F-value occurs due to noise. In this case, C_p, I_p, T_{on}, τ, C_pI_p, $C_p\tau$, $I_p\tau$, $T_{on}\tau$, C_p^2, I_p^2, T_{on}^2 and τ^2 are found significant terms (P-value less than 0.05). The "lack of fit" for F-value is 5.10 which indicate lack of fit is significant relative to the pure error. There is a good agreement between "Pred-R-squared" (0.9925) and "Adj- R- squared" (0.9973) with the difference less than 0.2. It is desirable for "Adeq precision" ratio greater than 4. In this case "Adeq precision" ratio is 107.325 indicates an adequate signal.

Table 4.19 ANOVA for SR

Source	**Sum of Squares**	**df**	**Mean Square**	**F Value**	**P- value Prob>F**	
Model	74.51	14	5.32	765.61	< 0.0001	significant
C_p	7.00	1	7.00	1007.56	< 0.0001	
I_p	54.32	1	54.32	7813.76	< 0.0001	
T_{on}	3.57	1	3.57	513.65	< 0.0001	
τ	7.55	1	7.55	1086.12	< 0.0001	
C_pI_p	0.088	1	0.088	12.71	0.0028	
C_pT_{on}	3.706E-004	1	3.706E-004	0.053	0.8205	
$C_p\tau$	0.25	1	0.25	35.93	< 0.0001	
I_pT_{on}	7.014E-003	1	7.014E-003	1.01	0.3311	
$I_p\tau$	0.72	1	0.72	104.12	< 0.0001	
$T_{on}\tau$	0.034	1	0.034	4.88	0.0431	
C_p^2	0.36	1	0.36	51.87	< 0.0001	
I_p^2	0.16	1	0.16	22.73	0.0002	
T_{on}^2	0.064	1	0.064	9.17	0.0085	
τ^2	0.44	1	0.44	63.80	< 0.0001	
Residual	0.10	15	6.951E-003			
Lack of Fit	0.095	10	9.496E-003	5.10	0.0430	
Pure Error	9.304E-003	5	1.861E-003			
Cor Total	74.61	29				
R-Squared = 0.9986				Adj R-Squared= 0.9973		
Pred R-Squared = 0.9925				Adeq Precision= 107.325		

Statistical inferences:

1. The Model F-value of 765.61 implies the model is significant. There is only a 0.01% chance that an F-value this large could occur due to noise.
2. Values of "Prob > F" less than 0.0500 indicate model terms are significant. In this case, C_p, I_p, T_{on}, τ, C_pI_p, $C_p\tau$, $I_p\tau$, $T_{on}\tau$, C_p^2, I_p^2, T_{on}^2, τ^2 are significant model terms.
3. The "Lack of Fit F-value" of 5.10 implies the Lack of Fit is significant. There is only a 4.30% chance that a "Lack of Fit F-value" this large could occur due to noise. Significant lack of fit is bad for predicted model.
4. The "Pred R-Squared" of 0.9925 is in reasonable agreement with the "Adj R-Squared" of 0.9973; i.e. the difference is less than 0.2.
5. "Adeq Precision" measures the signal to noise ratio. A ratio greater than 4 is desirable. Your ratio of 107.325 indicates an adequate signal. This model can be used to navigate the design space.

The regression analysis was used to develop a statistical model for surface roughness (SR). The non-significant terms (P-value greater than 0.05) were removed during regression analysis. The second order regression model of SR in coded terms and actual terms are given in equations 4.9 and 4.10 respectively.

Second order regression equation of SR (Coded terms):

$$SR = 7.63 - 1.08 * A + 3.01 * B + 0.77 * C + 1.12 * D + 0.30 * AB - 0.50 * AD + 0.85 * BD + 0.18 * CD - 0.46 * A^2 - 0.30 * B^2 + 0.19 * C^2 - 0.51 * D^2 \quad \text{-------} \quad \textbf{(4.9)}$$

Second order regression equation of SR (Actual terms):

$$SR = 7.63 - 1.08 * C_p + 3.01 * I_p + 0.77 * T_{on} + 1.12 * \tau + 0.30 * C_pI_p - 0.50 * C_p\tau + 0.85 * I_p\tau + 0.18 * T_{on}\tau - 0.46 * C_p^2 - 0.30 * I_p^2 + 0.19 * T_{on}^2 - 0.51 * \tau^2 \quad \text{--------} \quad \textbf{(4.10)}$$

The adequacy of the developed regression model using RSM for surface roughness (SR) has been examined through residual analysis. The figures 4.6(a) & (b) indicates the plot of normal probability v/s internally studentized residuals and actual v/s predicted surface roughness (SR) respectively. The result of the plot indicates that the actual SR v/s predicted SR data spread approximately linear results a good agreement between predicted and actual values of SR. Hence, the proposed surface roughness model is significant [68].

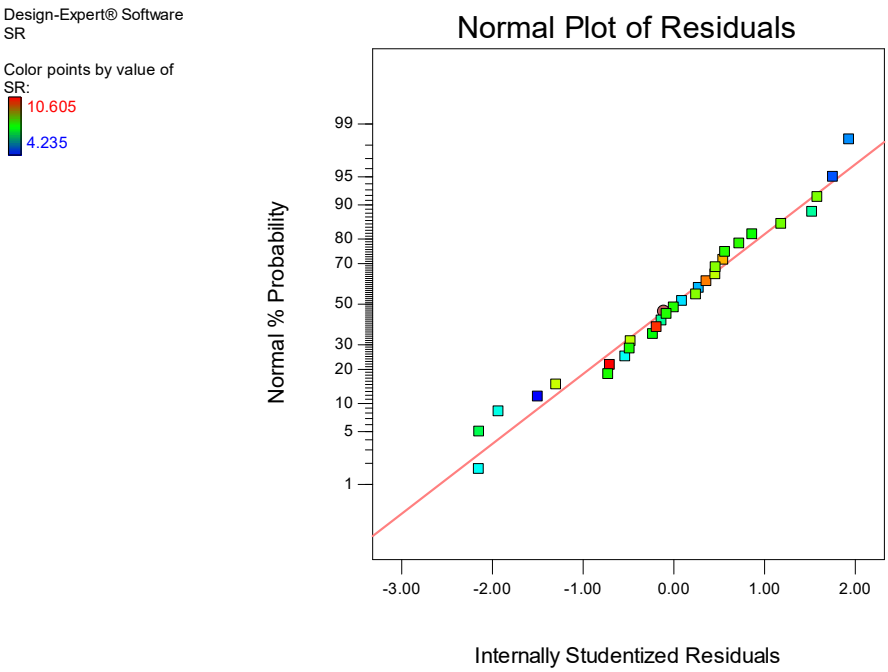

Figure 4.6 (a) Normal vs. Internally studentized residuals

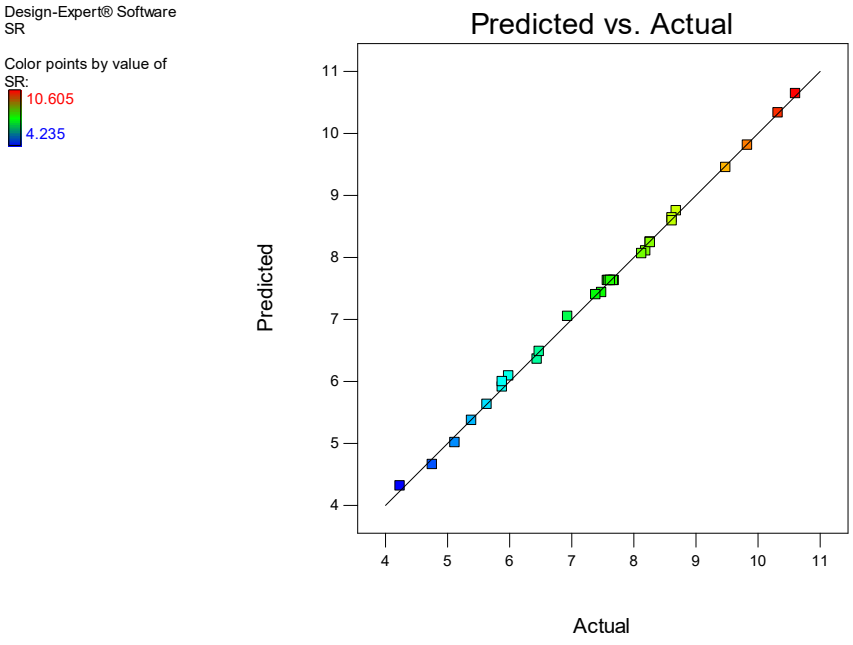

Figure 4.6 (b) Predicted vs. Actual Surface roughness

4.6.3 Effects of machining parameters on SR

Reliability of the engineering component also depends on surface quality obtained during machining. Rough surface works as a stress raiser and hence micro-cracks lead to early failure of a component. Further tribological behaviour of component greatly influenced by the rough surface. Efforts have been made to maintain finish surface during surface modification of P20+Ni die steel using EDM. The parametric analysis carried out to study the effects of various parameters such as compaction pressure (C_p), peak current (I_p), pulse on time (T_{on}) and duty cycle (τ) on surface roughness. The Design Expert 10 (DX 10) is used to develop the three dimensional (3D) surface plots for SR based on quadratic (second-order) model based on response surface methodology. Three-dimensional response surface plots are able to deliver insight knowledge regarding the relation between input process parameters and surface roughness.

Based on response surface methodology (RSM) second-order model the effects of peak current and compaction pressure on SR, while keeping the levels of remaining two parameters; T_{on} = 90 μs and τ = 85% constant are shown in Figure 4.7 (a) as a 3D surface plot. The non-linear variation of SR with peak current has been observed and it is concluded that for an increase in peak current from 6 to 18 ampere, there is a continuous increase in SR from 4.235 μm to 10.605 μm. This increase in SR with peak current is due to the availability of high discharge energy in the sparking area, that facilitate the melting and vaporizing of work material. The amount of discharge energy obtained during the EDM operation depends on the peak current value. Therefore maximum discharge energy is available with a high value of peak current. Transfer of maximum amount of heat energy disintegrates the work material severly which resulting rough surface during machining.

Further increase in peak current is from 6 to 18 ampere (keeping compaction pressure at 125 kg/cm^2) leads to an increase the SR from 4.235 to 8.263 μm. This increase in surface roughness value (while maintaining constant C_p = 125 kg/cm^2) can be attributed to the fact that increase in the rate of heat energy generated, which further increase the rate of melting and vaporization of work material resulting rough surface. So from the above result, it can be concluded that lower value of peak current with smaller pulse duration deliver very finish surface [70].

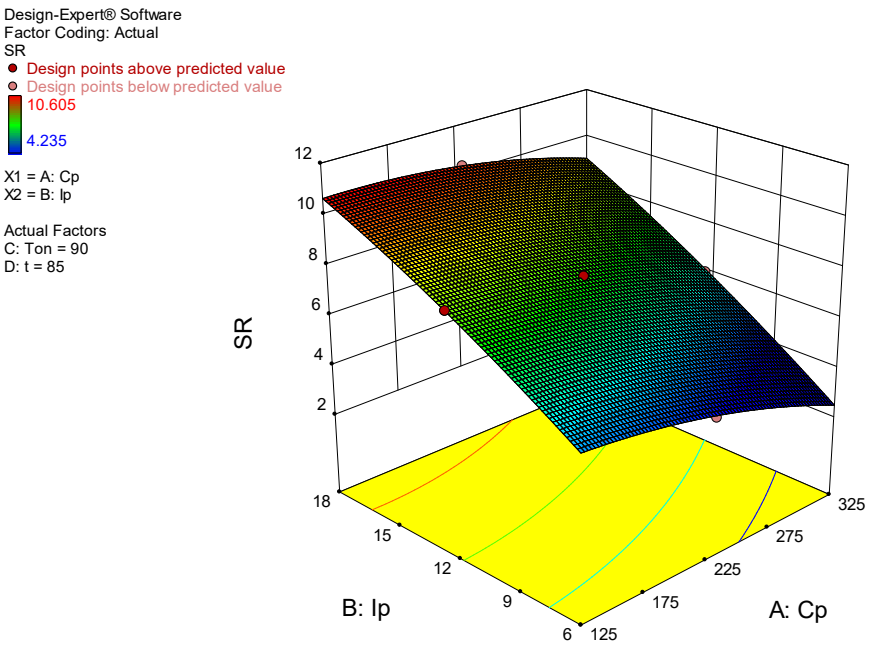

Figure 4.7 (a) Surface plot of SR vs. Peak current and Compaction pressure

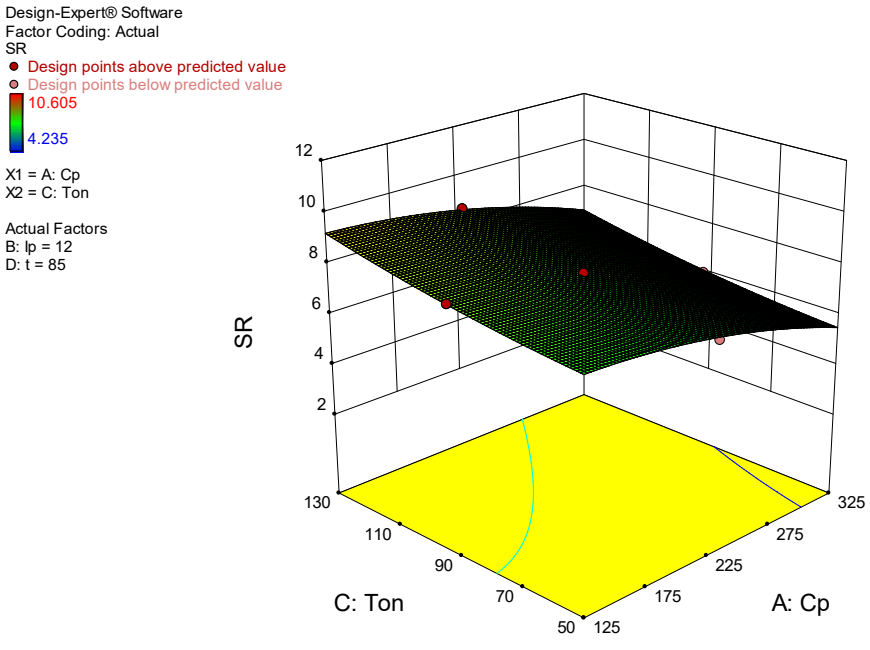

Figure 4.7 (b) Surface plot of SR vs. Pulse on time and Compaction pressure

The effects of pulse on time (T_{on}) and compaction pressure (C_p) on SR, while keeping the levels of other two parameters; I_p = 12 ampere and τ = 85% constant are shown in Figure 4.7(b) as a 3D surface plot. The non-linear variation of SR with a pulse on time has been obtained and it is concluded that for an increase in pulse on time from 50 to 130 µs, there is a continuous increase in SR from 4.235 µm to 10.605 µm. This increase in SR with the pulse on time is due to the availability of the same heating temperature for a longer period of time. Hence, the rough surface was observed during machining performed with a high pulse on time. Finish surface was observed, while machining performed with high compaction P/M electrode because of lower disintegration of electrode materials.

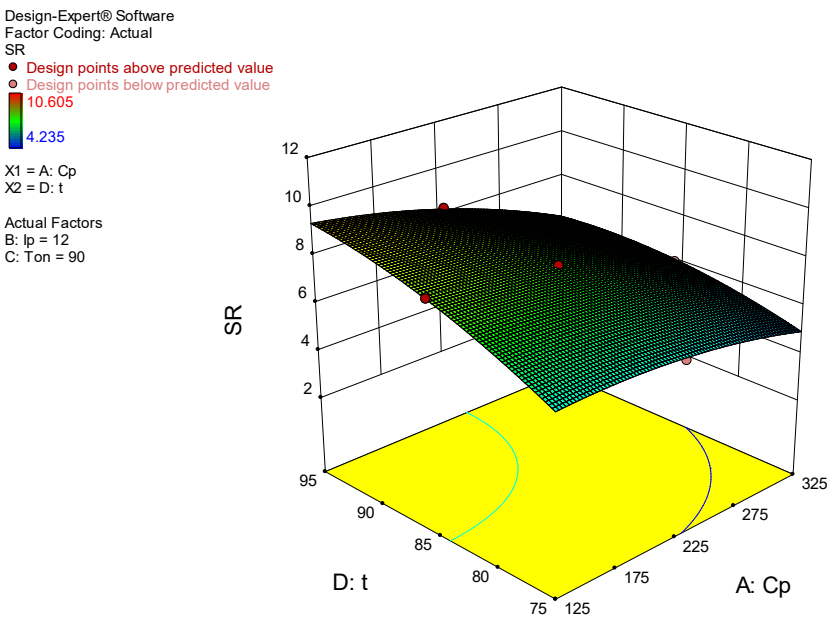

Figure 4.7 (c) Surface plot of SR vs. Duty cycle and Compaction pressure

The influence of duty cycle (τ) and compaction pressure (C_p) on SR, while keeping the levels of other two parameters; Ip = 12 Ampere and T_{on} = 90 µs constant are shown in Figure 4.7(c). The non-linear variation of SR with the duty cycle has been observed. It is concluded that for an increase in duty cycle from 75 to 95 %, there is a continuous increase in SR from 4.235 to 10.605 µm. This increase in roughness of surface at higher duty cycle is due to the longer pulse duration. In this case heat energy available for longer duration in the machining area, which deteriorates the qualities of the surface. Moreover, the influence of pulse on time (T_{on}) and peak current (I_p) on SR, while keeping the levels of other two parameters; Cp = 225 kg/cm^2 and τ = 85% constant is shown in Figure 4.7(d) as a 3D

surface plot. The non-linear variation of SR with a pulse on time and peak current has been observed and it is concluded that for an increase in pulse on time from 50 to 130 µs, with peak current 6 to 18 ampere, there is a continuous increase in surface roughness from 4.235 to 10.605 µm. Increase in surface roughness with a pulse on time is due to the availability of high heat for a longer period of time. Hence, an increase in surface roughness was observed while machining with a high pulse on time.

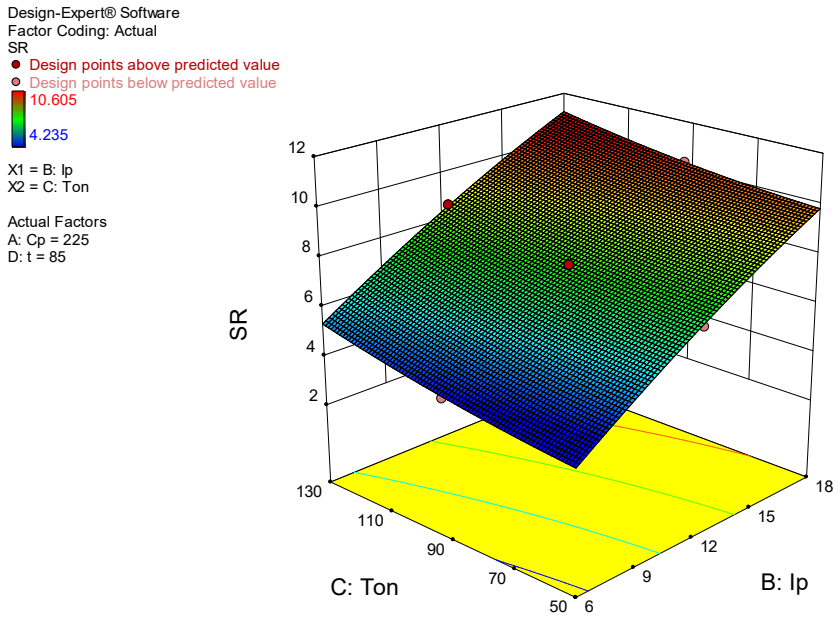

Figure 4.7 (d) Surface plot of SR vs. Pulse on time and Peak current

The influence of duty cycle (τ) and peak current (I_p) on SR, while keeping the levels of other two parameters; C_p = 225 kg/cm^2 and T_{on} = 90 µs constant are shown in Figure 4.7(e). The non-linear variation of SR with the duty cycle has been observed and it is concluded that for an increase in duty cycle from 75 to 95 %, there is a continuous increase in surface roughness. Further increase in SR was also observed with high peak current (Ip) while maintaining a constant duty cycle. This increase in roughness at a higher level of duty cycle is due to the longer pulse duration. Therefore the amount of heat energy applied for longer duration is responsible for deteriorating the surface quality.

Similarly, The influence of duty cycle (τ) and pulse on time (T_{on}) on SR, while keeping the levels of other two parameters; C_p = 225 kg/cm^2 and I_p = 12 ampere constant are shown in Figure 4.2(f) as a 3D surface plot.

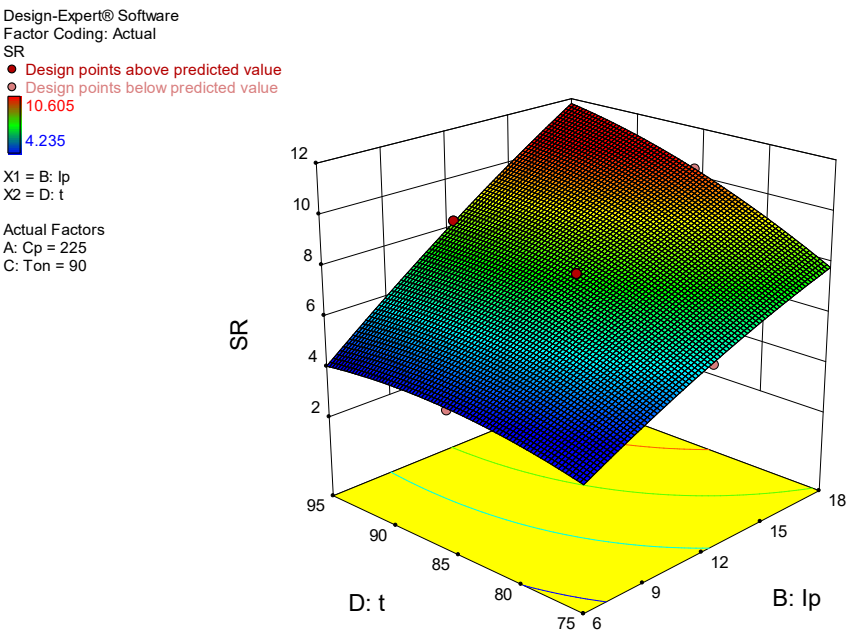

Figure 4.7 (e) Surface plot of SR vs. Duty cycle and Peak current

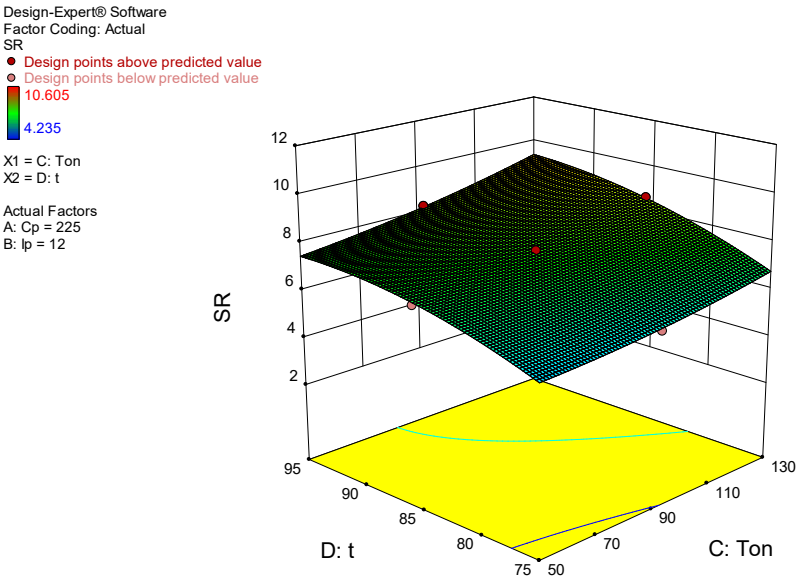

Figure 4.7 (f) Surface plot of SR vs. Duty cycle and Pulse on time

The non-linear variation of SR with duty cycle has been observed and it is concluded that for an increase in duty cycle from 75 to 95 %, there is a continuous increase in SR from 4.235 µm to 10.605 µm. Further increase in SR is also observed while the increase in pulse on time (T_{on}) from 50 to 130 µs while maintaining duty cycle constant.

4.7 ANALYSIS AND DISCUSSION OF MICROHARDNESS RESULTS

It is intended to improve the microhardness of die and tool surface to resist abrasion and wear. In this experimental work, attempts have been made to improve the microhardness of work material using P/M electrode. P/M electrodes were manufactured using tungsten, copper and silicon powders. Migrations of hardest constituents such as tungsten, silicon and copper were observed during EDMed of P20+Ni steel using P/M electrode. Modified recast layer due to migration of electrode constituents exhibits excellent abrasion and wear resistance. Microhardness of work material is measured before and after using vickers microhardness tester. In this experimental work, attempts have been made to obtain maximum microhardness on the work surface during surface modification of P20+Ni steel using EDM.

Experiments were planned and performed using response surface methodology. Individual experiments were performed thrice by setting levels of parameters given in Table 4.3. Mean value of three microhardness readings is considered as the final result and used for further analysis. The regression model of microhardness (MH) is developed using statistical software Design Expert 10 (DX 10). Adequacy of developed model checked using the sum of squares, lack of fit test and model summary statistics. Analysis of variance (ANOVA) also performed to find the contribution of the individual parameter to maximize MH. Three-dimensional surface plots were developed to study the effects of parameters on microhardness (MH) [76]. The results of microhardness measured for three sets and its mean values are given in Table 4.20.

Table 4.20 Design of experiment matrix and the observed value of MH

Exp. No.	Run Order	Input process parameters								Response			Mean MH (VHN)
		Cp		Ip		Ton		τ		MH-1 (VHN)	MH-2 (VHN)	MH-3 (VHN)	
		Actual	Coded	Actual	Coded	Actual	Coded	Actual	Coded				
1	12	175	-1	9	-1	70	-1	80	-1	878	854	926	886
2	6	275	1	9	-1	70	-1	80	-1	844	847	802	831
3	9	175	-1	15	1	70	-1	80	-1	986	1035	1057	1026
4	28	275	1	15	1	70	-1	80	-1	932	982	894	936
5	4	175	-1	9	-1	110	1	80	-1	873	786	897	852
6	27	275	1	9	-1	110	1	80	-1	821	791	761	791
7	14	175	-1	15	1	110	1	80	-1	967	909	848	908
8	20	275	1	15	1	110	1	80	-1	834	881	934	883
9	11	175	-1	9	-1	70	-1	90	1	1137	1074	1098	1103
10	16	275	1	9	-1	70	-1	90	1	838	881	885	868
11	2	175	-1	15	1	70	-1	90	1	1172	1121	1274	1189
12	22	275	1	15	1	70	-1	90	1	1122	1021	1133	1092
13	5	175	-1	9	-1	110	1	90	1	1044	993	1026	1021
14	19	275	1	9	-1	110	1	90	1	782	824	773	793
15	29	175	-1	15	1	110	1	90	1	1048	1062	1058	1056
16	15	275	1	15	1	110	1	90	1	955	901	916	924
17	10	125	-2	12	0	90	0	85	0	1064	1064	1049	1059
18	25	325	2	12	0	90	0	85	0	902	798	883	861
19	18	225	0	6	-2	90	0	85	0	785	868	810	821
20	7	225	0	18	2	90	0	85	0	1136	1011	1135	1094

Exp. No.	Run Order	Input process parameters								Response			Mean MH (VHN)
		Cp		Ip		Ton		τ		MH-1 (VHN)	MH-2 (VHN)	MH-3 (VHN)	
		Actual	Coded	Actual	Coded	Actual	Coded	Actual	Coded				
21	30	225	0	12	0	50	-2	85	0	977	956	989	974
22	21	225	0	12	0	130	2	85	0	813	903	750	822
23	13	225	0	12	0	90	0	75	-2	911	869	824	868
24	23	225	0	12	0	90	0	95	2	1052	1054	1107	1071
25	26	225	0	12	0	90	0	85	0	873	835	830	846
26	3	225	0	12	0	90	0	85	0	840	794	877	837
27	1	225	0	12	0	90	0	85	0	806	858	865	843
28	8	225	0	12	0	90	0	85	0	852	841	854	849
29	24	225	0	12	0	90	0	85	0	861	871	761	831
30	17	225	0	12	0	90	0	85	0	827	867	829	841

4.7.1 Selection of adequate model for MH

The adequacy of the developed microhardness model was checked by performing various statistical tests such as a sequential model sum of squares, lack of fit tests and model summary statistics. The results of the three statistical tests are given in Table 4.21 to 4.23. Quadratic model is found most appropriate as per sequential model sum of the square test. The sequential model sum of squares test shows, how the terms of increasing complexity contribute to the model. The lack of fit tests helps to compare pure error and residual error from replicated design points. The quadratic model was observed appropriate during lack of fit tests because the quadratic model does not show a significant lack of fit. Model summary statistics also confirm the quadratic model for MH. Hence, according to three statistical tests, the quadratic model can be the best choice and used for further analysis. Low standard deviation, high R-squared and smaller PRESS values of model summary statistics also strongly confirmed the quadratic model for MH.

Table 4.21 Sequential Model Sum of Squares for MH

Sequential Model Sum of Squares (Type I)						
Source	**Sum of Squares**	**df**	**Mean Square**	**F value**	**p-value Prob>F**	
Mean vs. Total	2.572E+007	1	2.572E+007			
Linear vs. Mean	2.737E+005	4	68420.46	18.75	< 0.0001	
2FI vs. Linear	23944.38	6	3990.73	1.13	0.3842	
Quadratic vs. 2FI	60174.17	4	15043.54	31.79	< 0.0001	Suggested
Cubic vs. Quadratic	6084.67	8	760.58	5.25	0.0208	Aliased
Residual	1014.42	7	144.92			
Total	2.608E+007	30	8.694E+005			

Table 4.22 Lack of Fit Tests for MH

Lack of Fit Tests						
Source	**Sum of Squares**	**df**	**Mean Square**	**F value**	**p-value Prob>F**	
Linear	91008.80	20	4550.44	108.95	< 0.0001	
2FI	67064.42	14	4790.32	114.69	< 0.0001	
Quadratic	6890.25	10	689.02	16.50	0.0032	Suggested
Cubic	805.58	2	402.79	9.64	0.0192	Aliased
Pure Error	208.83	5	41.77			

Table 4.23 Model Summary Statistics for MH

Model Summary Statistics						
Source	**Std. Dev.**	**R - Squared**	**Adjusted R - Squared**	**Predicted R - Squared**	**PRESS**	
Linear	60.40	0.7500	0.7100	0.6678	1.212E+005	
2FI	59.50	0.8156	0.7186	0.6278	1.358E+005	
Quadratic	21.75	0.9805	0.9624	0.8904	39988.56	Suggested
Cubic	12.04	0.9972	0.9885	0.6813	1.163E+005	Aliased

4.7.2 Analysis of variance (ANOVA) for MH

Analysis of variance (ANOVA) is carried out to check the adequacy of develop a model and investigate the significance of individual parameters on microhardness (MH). The result of ANOVA for developed MH model is shown in Table 4.24. The calculated F-value for predicted SR model is 54.00 that entails that the selected MH model is significant. There is a 0.01% possibility of larger F-value occurs due to noise. In this case, C_p, I_p, T_{on}, τ, C_pI_p, $C_p\tau$, I_pT_{on}, $T_{on}\tau$, C_p^2, I_p^2, $T_{on}^2$and τ^2 are significant terms (P-value less than 0.05). The "lack of fit" for F-value is 16.50 which indicate lack of fit is significant relative to the pure error.

Table 4.24 ANOVA for MH

Source	**Sum of Squares**	**df**	**Mean Square**	**F Value**	**P-value Prob>F**	
Model	3.578E+005	14	25557.17	54.00	< 0.0001	significant
C_p	72490.04	1	72490.04	153.17	< 0.0001	
I_p	83898.38	1	83898.38	177.27	< 0.0001	
T_{on}	42588.38	1	42588.38	89.99	< 0.0001	
τ	74705.04	1	74705.04	157.85	< 0.0001	
C_pI_p	3570.06	1	3570.06	7.54	0.0150	
C_pT_{on}	45.56	1	45.56	0.096	0.7606	
$C_p\tau$	13282.56	1	13282.56	28.07	< 0.0001	
I_pT_{on}	3630.06	1	3630.06	7.67	0.0143	
$I_p\tau$	473.06	1	473.06	1.00	0.3333	
$T_{on}\tau$	2943.06	1	2943.06	6.22	0.0248	
C_p^2	24531.67	1	24531.67	51.83	< 0.0001	
I_p^2	23517.03	1	23517.03	49.69	< 0.0001	
T_{on}^2	5692.53	1	5692.53	12.03	0.0034	
τ^2	28582.74	1	28582.74	60.39	< 0.0001	
Residual	7099.08	15	473.27			
Lack of Fit	6890.25	10	689.02	16.50	0.0032	
Pure Error	208.83	5	41.77			
Cor Total	3.649E+005	29				
R-Squared = 0.9805				Adj R-Squared= 0.9624		
Pred R-Squared = 0.8904				Adeq Precision= 27.563		

There is a good agreement between “Pred-R-squared” (0.8904) and “Adj- R- squared” (0.9624) with the difference less than 0.2. It is desirable to have “Adeq precision” ratio greater than 4. In this case “Adeq precision” ratio is 27.563 indicating an adequate signal.

Statistical inferences:

1. The Model F-value of 54.00 implies the model is significant. There is only a 0.01% chance that an F-value this large could occur due to noise.
2. Values of "Prob > F" less than 0.0500 indicate model terms are significant. In this case, C_p, I_p, T_{on}, τ, C_pI_p, $C_p\tau$, I_pT_{on}, $T_{on}\tau$, C_p^2, I_p^2, T_{on}^2, τ^2 are significant model terms.
3. The "Lack of Fit F-value" of 16.50 implies the Lack of Fit is significant. There is only a 0.32% chance that a "Lack of Fit F-value" this large could occur due to noise. Significant lack of fit is bad for predicted model.
4. The "Pred R-Squared" of 0.8904 is in reasonable agreement with the "Adj R-Squared" of 0.9624; i.e. the difference is less than 0.2.
5. "Adeq Precision" measures the signal to noise ratio. A ratio greater than 4 is desirable. Your ratio of 27.563 indicates an adequate signal. This model can be used to navigate the design space.

The regression analysis was used to develop the statistical model for microhardness (MH). The non-significant terms (P-value greater than 0.05) are removed during regression analysis. The regression model for MH in coded terms and actual terms are given in equations 4.11 and 4.12.

Second order regression equation of MH (Coded terms):

$$MH = 841.17 - 109.92 * A + 117.92 * B - 83.92 * C + 111.42 * D + 58.75 * AB - 115.25 * AD - 60.25 * BC - 53.25 * CD + 119.54 * A^2 + 117.04 * B^2 + 57.54 * C^2 + 129.54 * D^2 \quad \textbf{(4.11)}$$

Second order regression equation of MH (Actual terms):

$$MH = 841.17 - 109.92 * C_p + 117.92 * I_p - 83.92 * T_{on} + 111.42 * \tau + 58.75 * C_pI_p - 115.25 * C_p\tau - 60.25 * I_pT_{on} - 53.25 * T_{on}\tau + 119.54 * C_p^2 + 117.04 * I_p^2 + 57.54 * T_{on}^2 + 129.54 * \tau^2 \quad \textbf{(4.12)}$$

The adequacy of the developed statistical model based on regression analysis for microhardness has been examined using residual analysis. Figures 4.8 (a) and (b) indicates a plot of normal probability v/s internally studentized residuals and actual v/s predicted microhardness respectively. The results of the plot indicate that the actual MH v/s predicted MH data spread approximately linear, which shows a good agreement between predicted and actual values of MH [48]. Hence, the proposed microhardness (MH) model is significant and could be considered for further analysis.

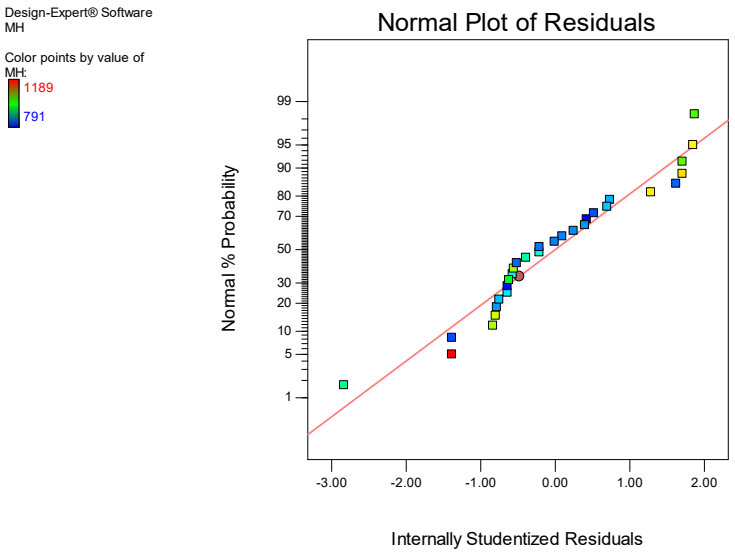

Figure 4.8 (a) Normal vs. Internally studentized residuals

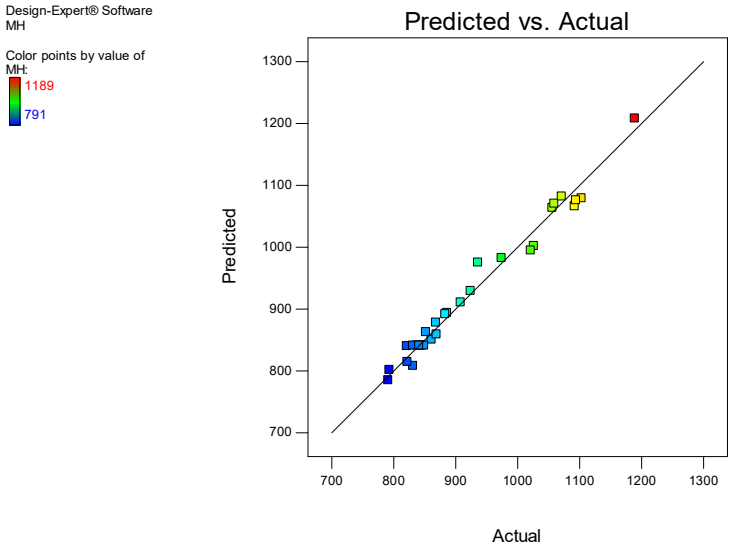

Figure 4.8 (b) Predicted vs. Actual Microhardness

4.7.3 Effects of machining parameters on MH

Die and tools used to manufacture products from composite plastics are always subject abrasions, wear, high pressure and temperature. Therefore it is desirable to have good wear resistance ability in steels used to manufacture die and tools. In this experimental works, attempts have been made to enhance the microhardness of P20+Ni steel during machining on EDM using P/M electrode. Under specific machining condition migrations of hardest constituents of P/M electrode on work, the surface has been observed. Therefore efforts have been made to investigate machining condition, which able to modify the work surface [78]. Deposition of hard elements of P/M electrode either in free or carbide form on work surface could able to improve wear resistance of work material and hence improvements in die and tool life.

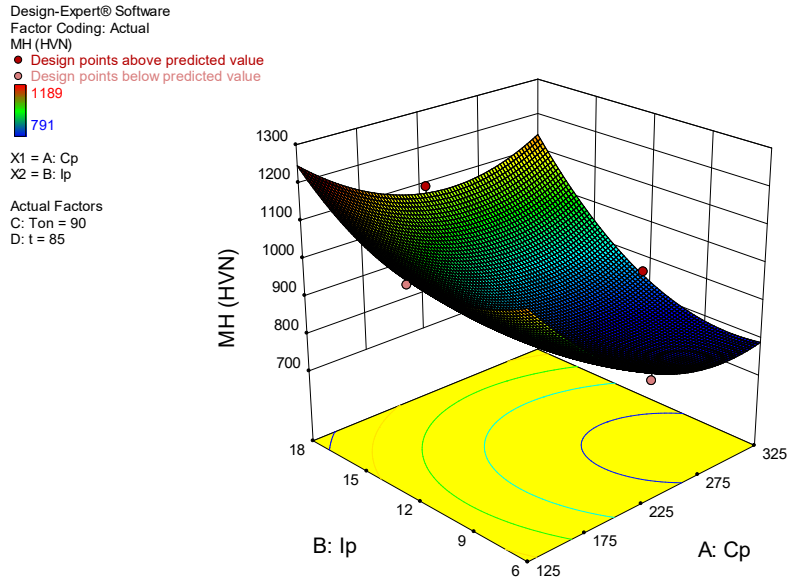

Figure 4.9 (a) Surface plot of MH vs. Peak current and Compaction pressure

Based on response surface methodology second-order model the effect of peak current and compaction pressure on microhardness, while maintaining the levels of other two parameters; T_{on} = 90 µs and τ = 85% constant is shown in Figure 4.9(a). The non-linear variation of MH with peak current has been observed. It is concluded that for an increase in peak current from 6 to 18 ampere, there is a continuous increase in MH from 791 to 1189 VHN. This improvement in MH with peak current is due to the Improvements in discharge energy available in the sparking area, which facilitates the melting and vaporizing of work material. The amount of discharge energy produced during the EDM

operation mainly depends on the level of peak current. Therefore the highest discharge energy available in the sparking area during the high value of peak current. Presence of maximum heat energy due to high peak current able to disintegrate tool and work material conclude allying of the work surface. Presence of hardest elements of the electrode on work surface either in free form or carbide forms able to improve the microhardness significantly.

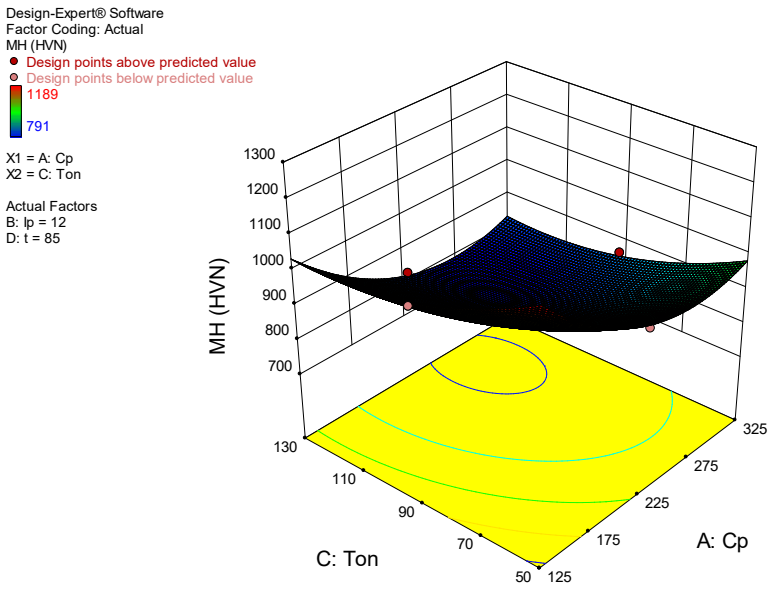

Figure 4.9 (b) Surface plot of MH vs. Pulse on time and Compaction pressure

The influence of pulse on time (T_{on}) and compaction pressure (C_p) on MH, while keeping the levels of other two parameters; I_p = 12 Ampere and τ = 85% constant is shown in Figure 4.9(b). The non-linear variation of MH with a pulse on time has been observed due to variation in electrical and physical properties of P/M electrode.

Moreover, the influence of duty cycle (τ) and compaction pressure (C_p) on MH, while keeping the levels of other two parameters; I_p = 12 ampere and T_{on} = 90 µs constant is shown in Figure 4.9(c). The non-linear relation of MH with duty cycle has been observed and it is concluded that for an increase in duty cycle from 75 to 95 %, there is an increase in microhardness from 791 to 1189 VHN. This improvement in MH with the increase in the duty cycle is due to a longer pulse duration. Duty cycle is defined as the percentage of pulse on time to total cycle time. Hence, a pulse remains on for longer duration during the high level of the duty cycle. Therefore heat energy available for longer duration in the machining area, which results in improved microhardness [79].

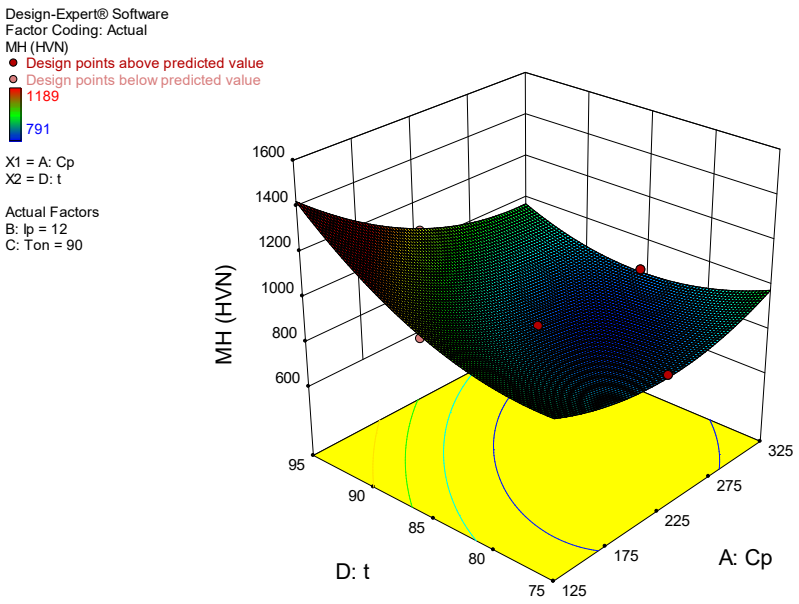

Figure 4.9 (c) Surface plot of MH vs. Duty cycle and Compaction pressure

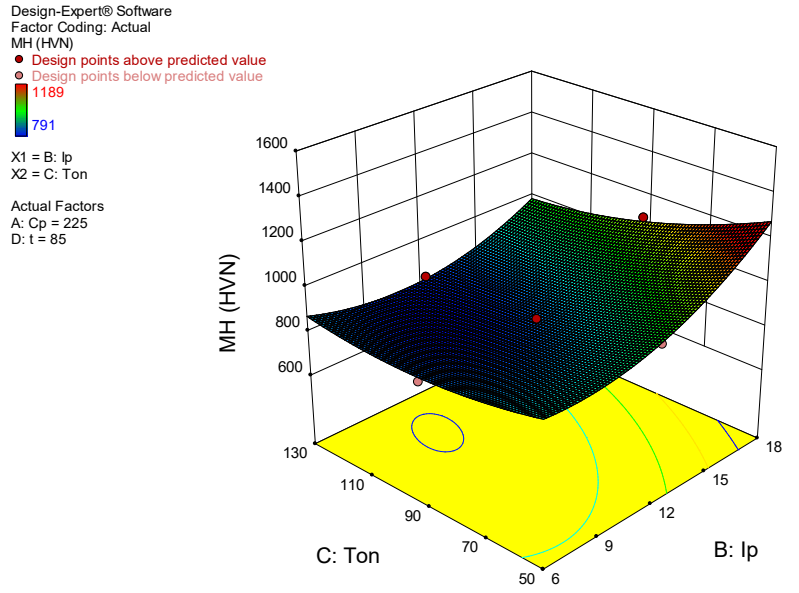

Figure 4.9 (d) Surface plot of MH vs. Pulse on time and Peak current

Similarly, the influence of pulse on time (T_{on}) and peak current (I_p) on MH, while keeping the levels of other two parameters; C_p = 225 kg/cm^2 and τ = 85% constant shown in Figure 4.9(d). The non-linear variation of MH with a pulse on time and peak current has been observed and it is concluded that for an increase in pulse on time from 50 to 130 µs, and peak current 6 to 18 ampere, there is a continuous increase in MH. This improvement in

MH with the increase in pulse on time and the peak current is due to the high heating temperature for a longer period of time. A sharp improvement in microhardness has been observed while an increase in peak current from 15 to 18 ampere. Hence, higher levels of Ip and T_{on} should be selected to improve microhardness.

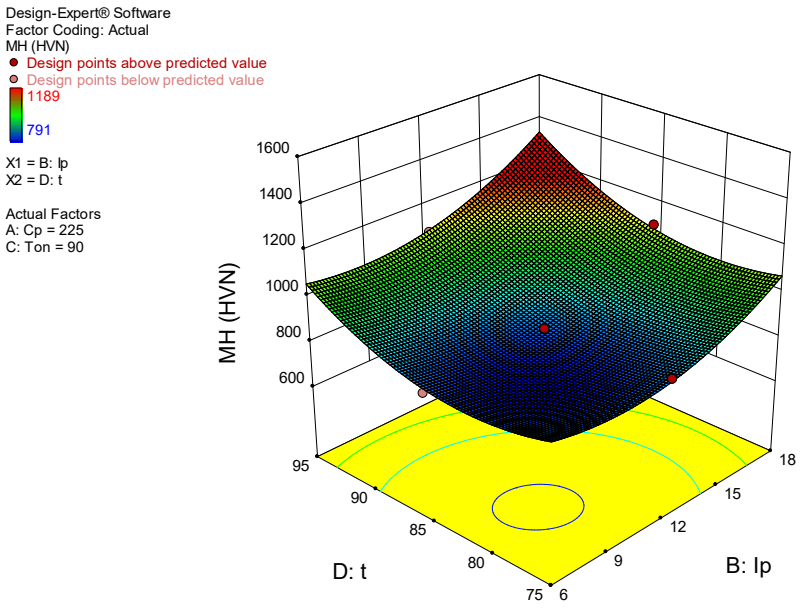

Figure 4.9 (e) Surface plot of MH vs. Duty cycle and Peak current

The effects of duty cycle (τ) and peak current (I_p) on MH, while keeping the levels of other two parameters; C_p = 225 kg/cm^2 and T_{on} = 90 µs constant shown in Figure 4.9 (e). The non-linear relation of MH with duty cycle has been observed and it is concluded that while an increase in duty cycle from 75 to 95 %, there is continuously increased in MH. Further improvements in MH were also observed while an increase in peak current. This improvement in MH with the increase in the duty cycle is due to a longer pulse on time. Hence, the upper level of duty cycle delivers a longer pulse duration. Therefore a high amount of heat energy applied for a long time, in the machining area, which will deliver high MH. Similarly, the effects of duty cycle (τ) and pulse on time (T_{on}) on MH, while keeping the levels of other two parameters; C_p = 225 kg/cm^2 and I_p = 12 amperes are shown in Figure 4.9 (f) [79]. The microhardness is varying non-linearly with duty cycle. It is concluded that for an increase in duty cycle from 75 to 95 %, there is a continuous increase in MH from 791 to 1189 VHN.

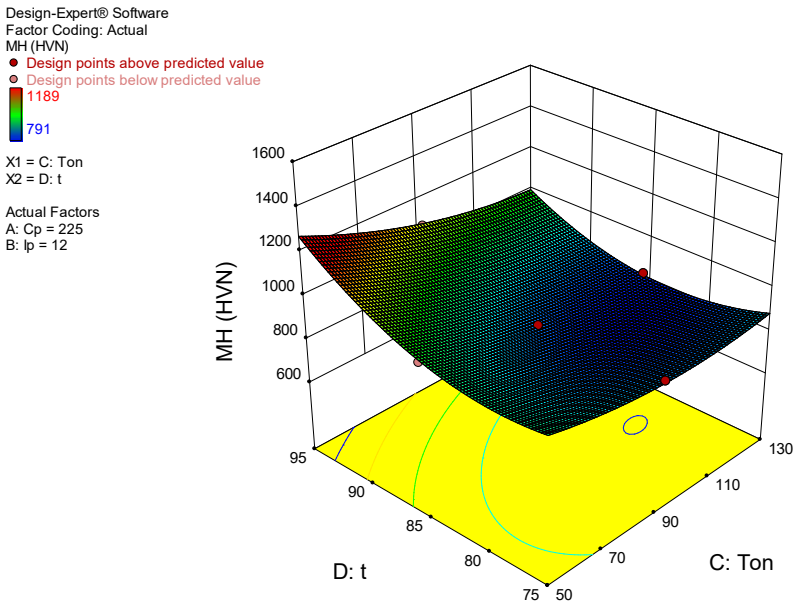

Figure 4.9 (f) Surface plot of MH vs. Duty cycle and Pulse on time

4.8 MICROSTRUCTURE ANALYSIS

Surface integrity of EDMed component plays a vital role to evaluate the process performance. Surface integrity is comprised of two parts such as surface morphology and surface topography. Surface morphology includes various surface irregularities such as surface crater, globule, spherical deposition, melted material deposition, pockmarks and white layer. Surface topography includes measuring thickness and depth of white layer, surface crack density, residual stress and microhardness. It also deals with the metallurgy of EDMed surface includes material migration from P/M electrode, phase change, strain effect and grain refinement etc. Hence, the elaborative study of surface integrity is one of the vital parameters to assess the quality of the machined surface.

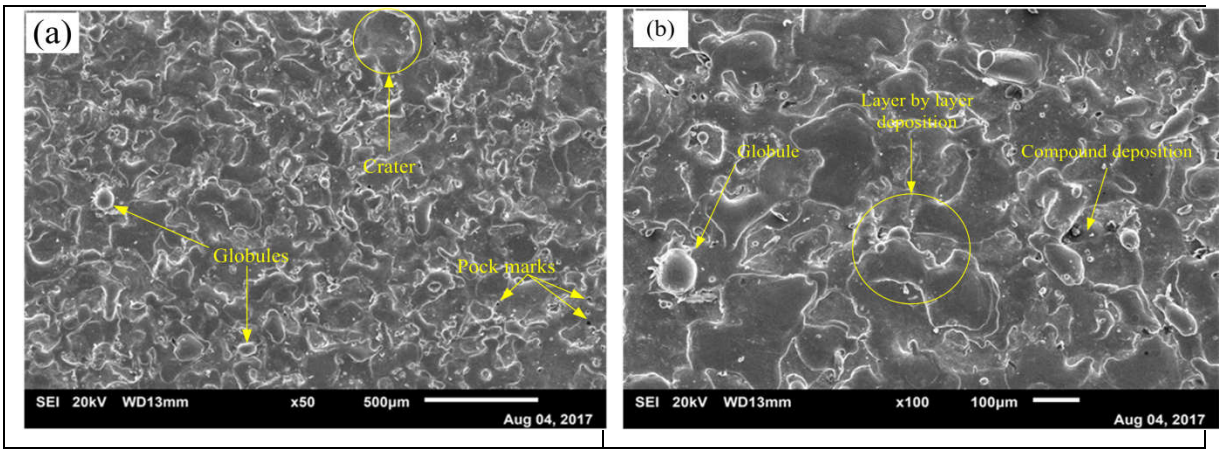

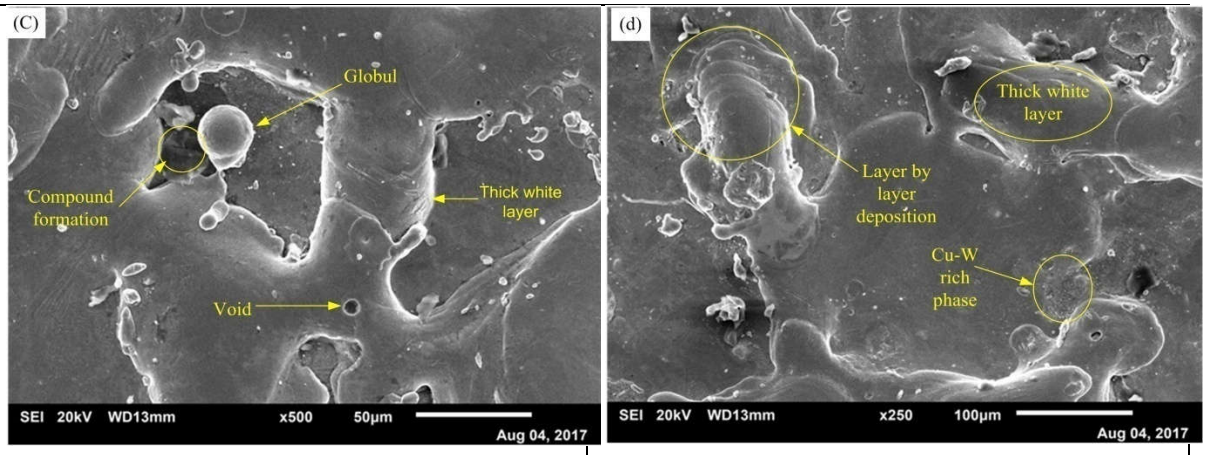

Figure 4.10 (a - d) SEM micrograph of surface machined at compaction pressure 175 kg/cm^2, peak current 9 Ampere, pulse on-time 70 µs and duty cycle 80 % (Trial 1)

In this context, the selected EDMed samples were analysed using a scanning electron microscope (SEM) to study the surface topography. From studies of SEM images taken at different magnification, it is concluded that uniformity in surface topography while machining using P/M electrode. This may be attributed to the distribution of spark energy over the entire surface covered by the electrode. SEM analysis is performed on SEM model JSM 6010 LA manufactured by JEOL, Japan at TCR Advanced engineering testing lab, Vadodara, Gujarat, India.

Figure 4.10 (a-d) indicates the SEM images taken at different magnification (50X, 100X, 500X and 250X) for trail 1. No micro-cracks were observed due to performing experiments with lower peak current. Migrations of copper (Cu) and tungsten (W) from P/M electrode has been shown by Cu-W rich phase encircle at different locations in SEM images.

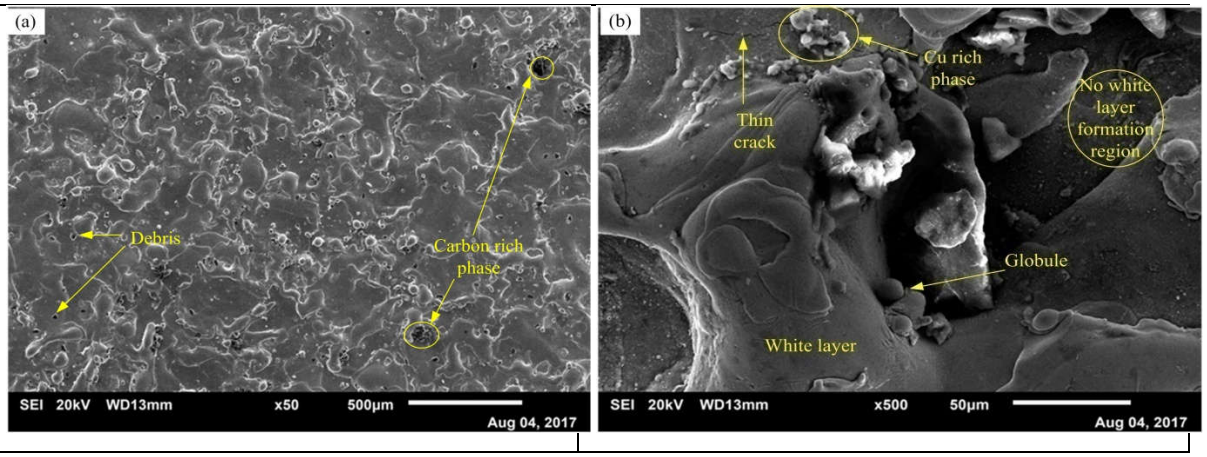

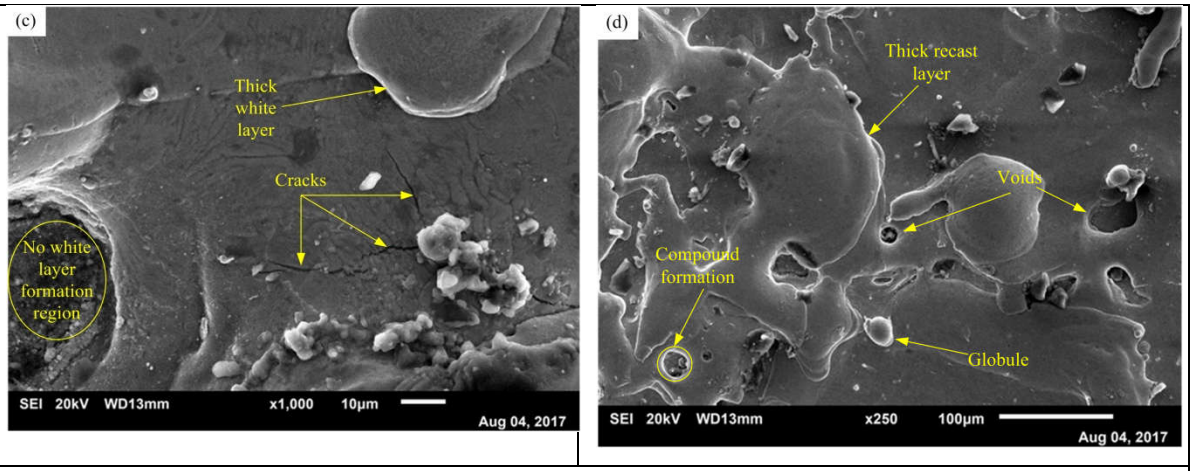

Figure 4.11 (a - d) SEM micrograph of surface machined at compaction pressure 275 kg/cm^2, peak current 15 Ampere, pulse on-time 70 µs and duty cycle 80 % (Trial 4)

Layer by layer deposition is observed at different locations in the surface due to the different melting temperature of electrode elements. Traces of copper are clearly visible on the surface due to the largest proportions and low melting temperature. The high rate of coagulate deposition is responsible for the rough surface. However, at lower current minimum coagulations are observed. The compound formation is clearly visible on the surface which attributes to enhance microhardness of machined surface [83].

The SEM images with magnifications 50X, 500X, 1000X and 250X of work surface machined with P/M electrode (compaction pressure 275 kg/cm^2, peak current 15 amperes, pulse on-time 70 µs and duty cycle 80 %) are shown in Figure 4.11(a-d). The presence of micro-cracks and globules are observed due to the very high peak current. Further formation of carbide phase is noticed due to breaking down of hydrocarbon type dielectric (EDM oil). Larger crater size is noticed with high peak current and pulse on time. Layer by layer deposition observed due to subsequent sparking action and also the different melting temperature of various elements. Voids are noticed due to the formation and collapse of vapour bubbles during high frequencies machining.

The peak current is the most vital parameter that is responsible for deterioration of the surface texture. This is due to the reason that with the hike of current high discharge energy is transferred to the machining area, so that melting and evaporation take place, resulting in the formation of a small crater [45]. Also, deep craters were formed by the successive electrical discharge and vaporized the work specimen [25]. The results of this study agree with [34].

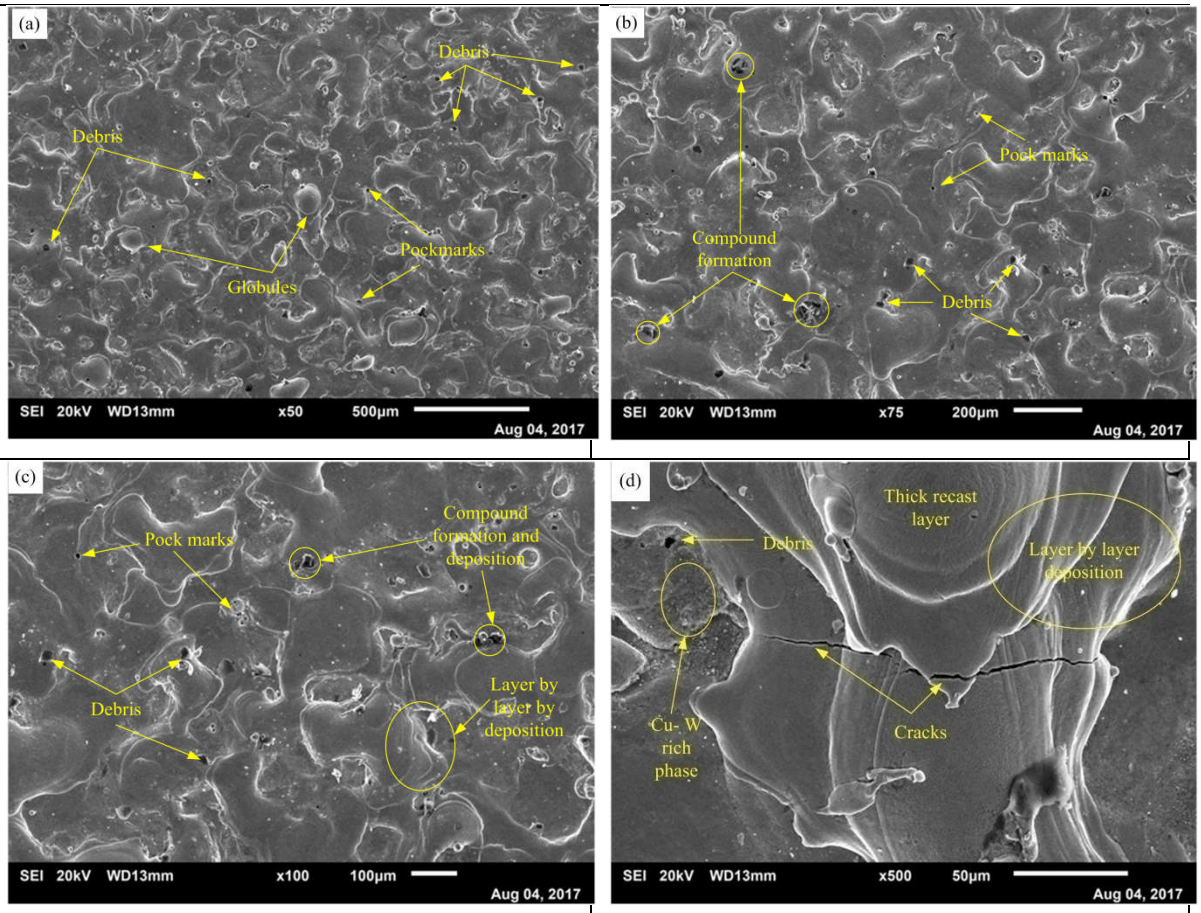

Figure 4.12 (a - d) SEM micrograph of surface machined at compaction pressure 275 kg/cm^2, peak current 9 Ampere, pulse on-time 110 µs and duty cycle 90 % (Trial 14)

The SEM micrographs at 50X, 75X, 100X and 500X of work material machined with P/M electrode (compaction pressure 275 kg/cm^2, peak current 9 amperes, pulse on-time 110 µs and duty cycle 90 %) are shown in Figure 4.12 (a-d). Pockmarks were observed due to the impulse of peak current. Micro-cracks are formed due to uneven expansion and contraction of the thick recast layer. Compound formation and deposition are reported due to the generation of high heat energy at a higher level of pulse on time. Deposition of debris on top of the surface is responsible for a rough surface. Cu-W rich phase was clearly visible in microstructure with traces of copper at different locations indicates migrations of P/M electrode elements on the work material.

Similarly, the SEM micrographs with 50X, 100X, 500X and 500X of work material machined with P/M electrode (compaction pressure 325 kg/cm^2, peak current 12 amperes, pulse on-time 90 µs and duty cycle 85 %) are shown in Figure 4.13 (a-d). The different surface topography observed during SEM analysis encircled in SEM images.

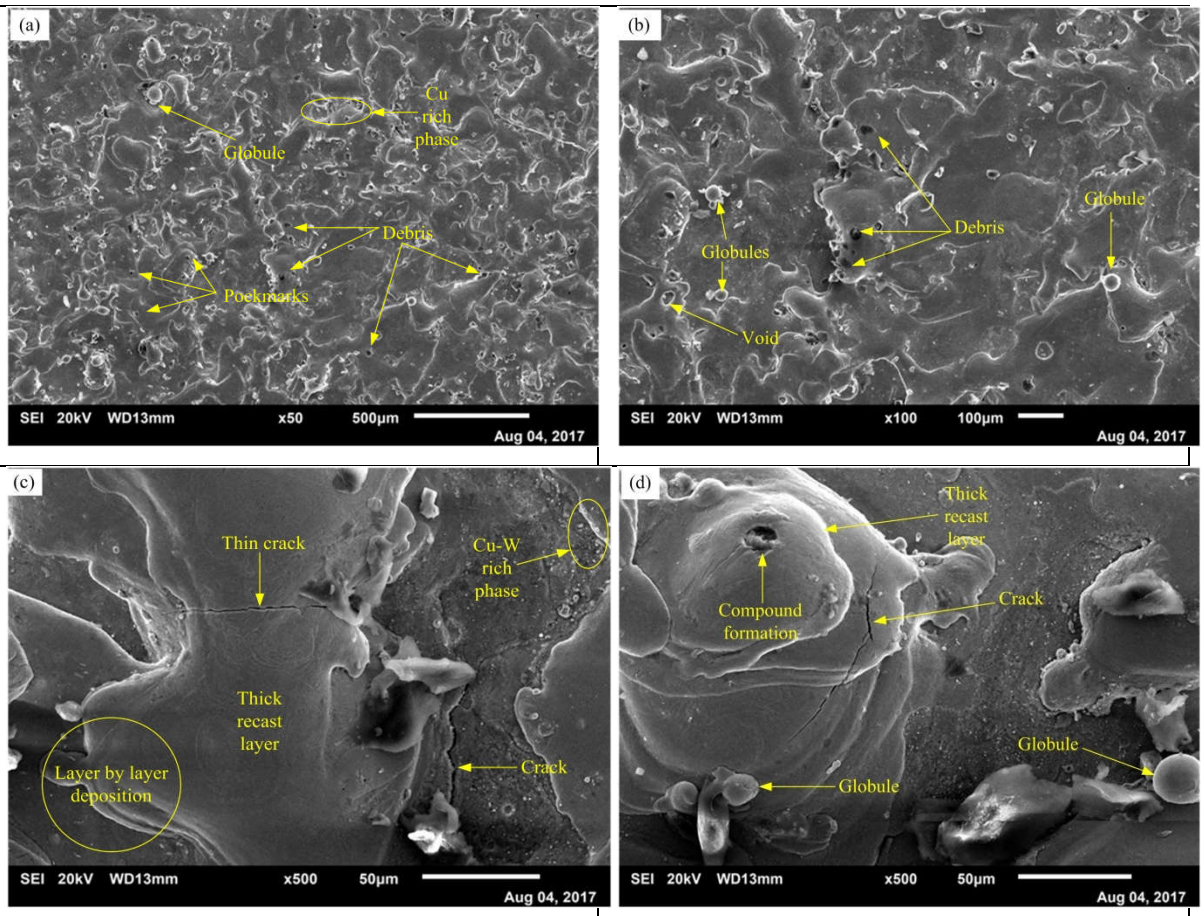

Figure 4.13 (a - d) SEM micrograph of surface machined at compaction pressure 325 kg/cm^2, peak current 12 Ampere, pulse on-time 90 µs and duty cycle 85 % (Trial 18)

The SEM micrographs at 50X, 75X, 250X and 500X of work material machined with P/M electrode (compaction pressure 225 kg/cm^2, peak current 6 amperes, pulse on-time 90 µs and duty cycle 85 %) are shown in Figure 4.14 (a-d). The different surface topographies observed during SEM analysis are shown in SEM images.

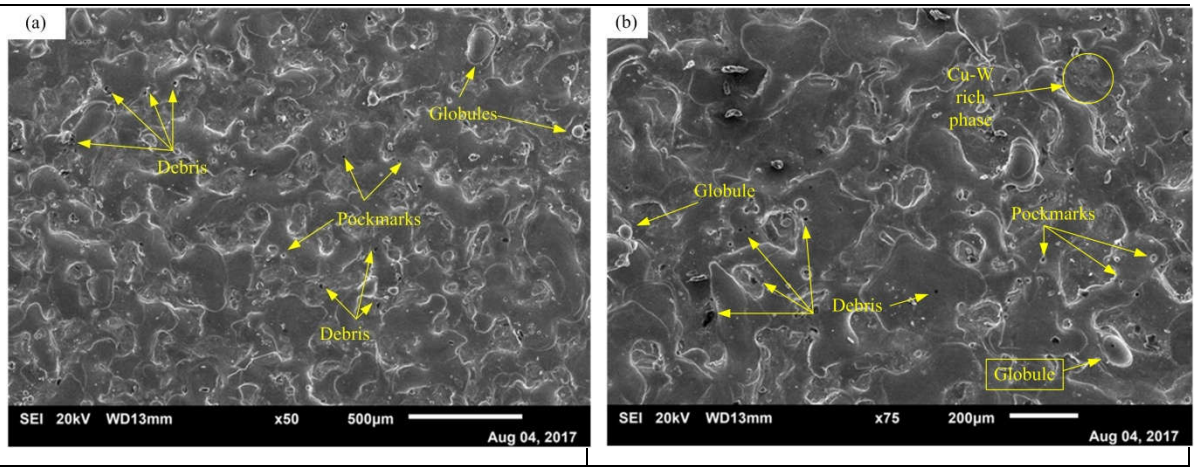

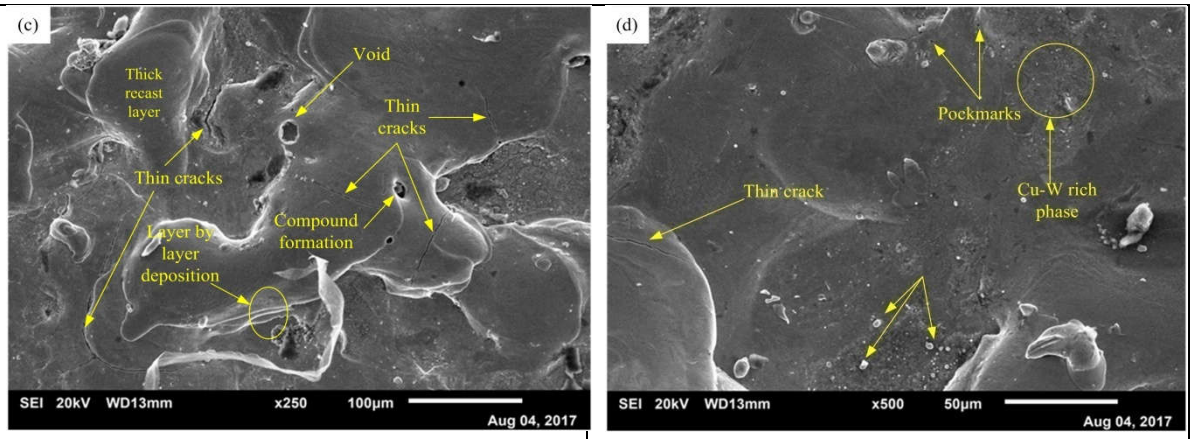

Figure 4.14 (a - d) SEM micrograph of surface machined at compaction pressure 225 kg/cm^2, peak current 6 Ampere, pulse on-time 90 µs and duty cycle 85 % (Trial 19)

The machined surface exhibited a Cu-W rich phase region as encircled on SEM micrograph. The SEM images show relatively very less thick white layers due to a lower setting of peak current. Further very few voids are observed because of the lower amount of heat energy. Copper enriched white boundaries are observed due to the uniform distribution of small debris. Very small globules are formed at lower peak current. Cu-W rich phase and copper enriched white layers strongly confirm the migration of P/M electrode elements on the work surface during machining. Increase in the carbon percentage observed due to breaking down of hydrocarbon from a dielectric (EDM Oil). Dissociated carbon elements from hydrocarbon oil combined as an intermetallic bond with tungsten and silicon and surface was alloyed in carbide forms. Proper dispersion of hard elements is observed in the microstructures. Hard particles dispersion and compound formation in the form of carbides (cementite formation) significantly increase microhardness of EDMed surface.

Moreover, The SEM micrographs at 50X, 75X, 250X and 1000X of work material machined with P/M electrode (compaction pressure 225 kg/cm^2, peak current 18 amperes, pulse on-time 90 µs and duty cycle 85 %) are shown in Figure 4.15(a-d). Different surface irregularities such as coagulation, void, pockmarks and globules are observed on the machined surface due to very high peak current. Layer by layer deposition observed at various locations due to the different melting temperature of elements presence in P/M electrode. Cu-W rich phase due to migration of copper (Cu) and tungsten (W) from P/M electrode encircled at different locations in SEM images. Deposition of debris on the machined surface resulting rough surface [88].

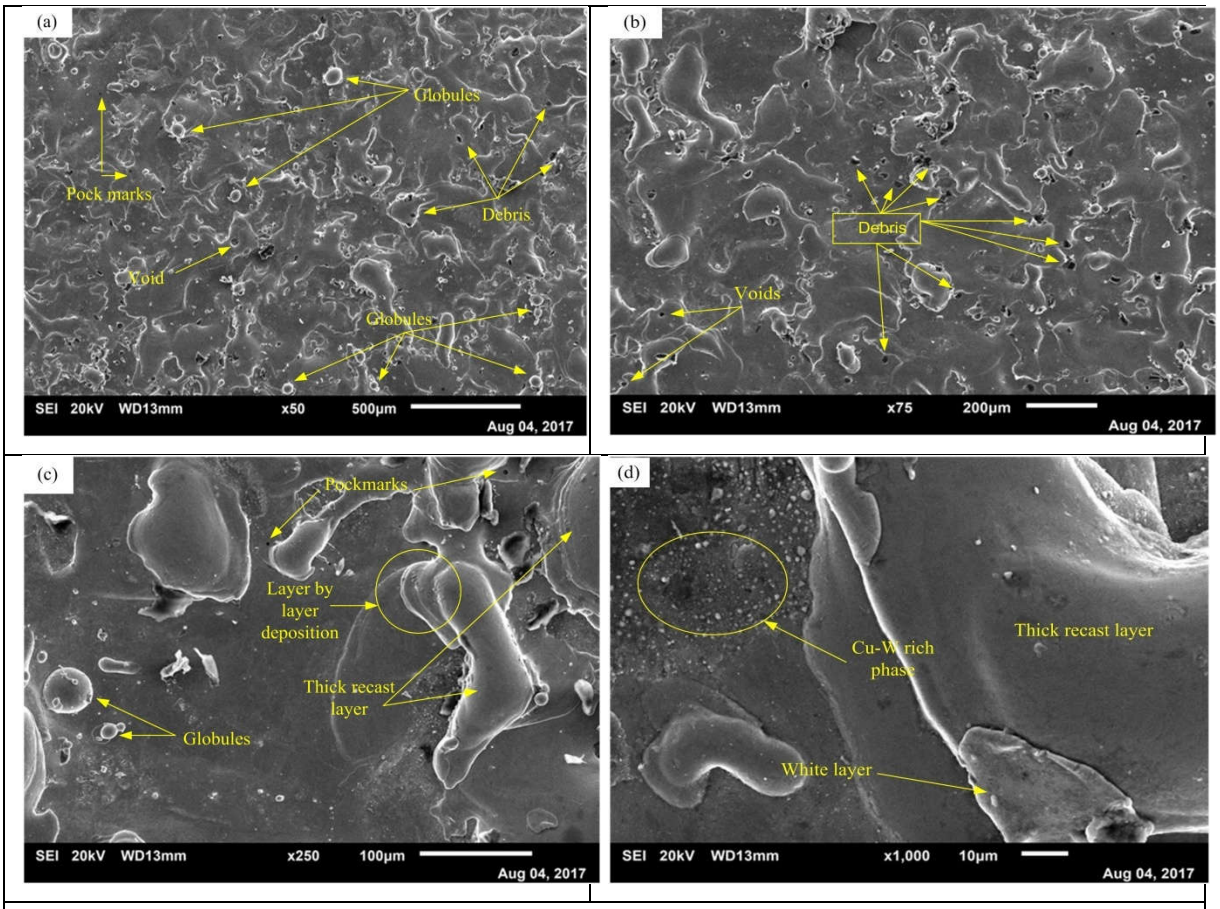

Figure 4.15 (a - d) SEM micrograph of surface machined at compaction pressure 225 kg/cm^2, peak current 18 Ampere, pulse on-time 90 µs and duty cycle 85 % (Trial 20)

Formations of cracks are observed due to variation of contraction stresses, generation of high discharge energy resulting in frequent cracking. The debris particles are also noticed on the machined surface. The presence of the debris particles on the machined surface is due to the disintegration of work material and P/M electrode at high discharge energy. It can be noted that an increase in the discharge current, surface irregularities also increase, results in deeper and large craters. This is imputable to the fact that as the electric current increases with a pulse on time, machined material will melt with the most amount of high temperature transferred to the machined surface (Kumar et al; 2013).

4.9 ENERGY DISPERSIVE SPECTROMETRY (EDS) ANALYSIS

Energy dispersive spectrometry is used to decide the weight percentage of compositions of the base material. Similarly, it is helpful to detect the presence of foreign elements transferred during machining. The EDS analysis of machined samples has been carried out using EDS attachment with a scanning electron microscope (Make: JEOL- Japan, Model:

JSM-6010 LA), to decide the compositions of EDMed surface. The spectrometry result of base material is C = 0.36, Si = 0.27, Mn = 1.25, P = 0.01, S = 0.006, Cr = 1.86, Mo = 0.17, Ni = 0.95, Cu = 0.071 and V = 0.065. The EDS spectrum for trial 1 is shown in Figure 4.16.

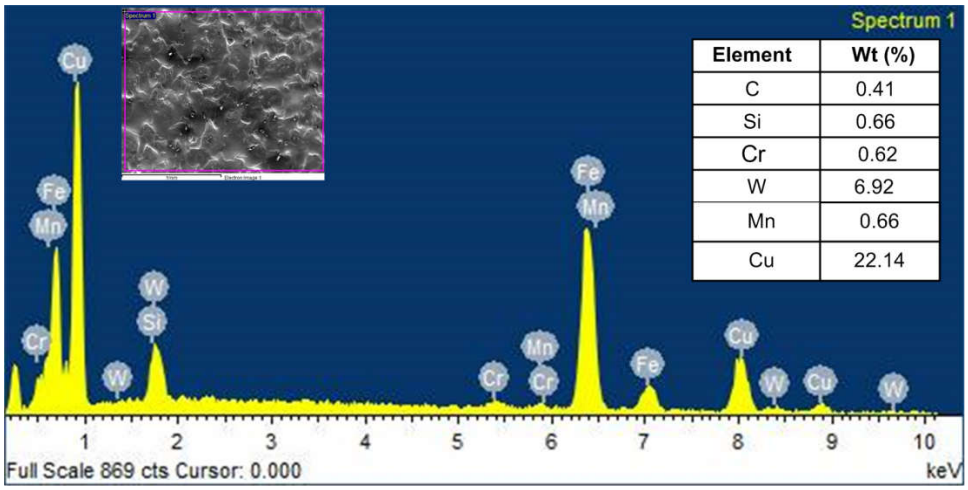

Figure 4.16 EDS spectrum of trial 1

The EDS result of machined sample (trial 1) shows the changes in compositions of surface as compared to base material is C = 0.36 to 0.41, Si = 0.27 to 0.66, Cr = 1.86 to 0.62, W = 0 to 6.92, Mn = 1.25 to 0.66 and Cu = 0.071 to 22.14. The EDS spectrum for trial 8 is shown in Figure 4.17.

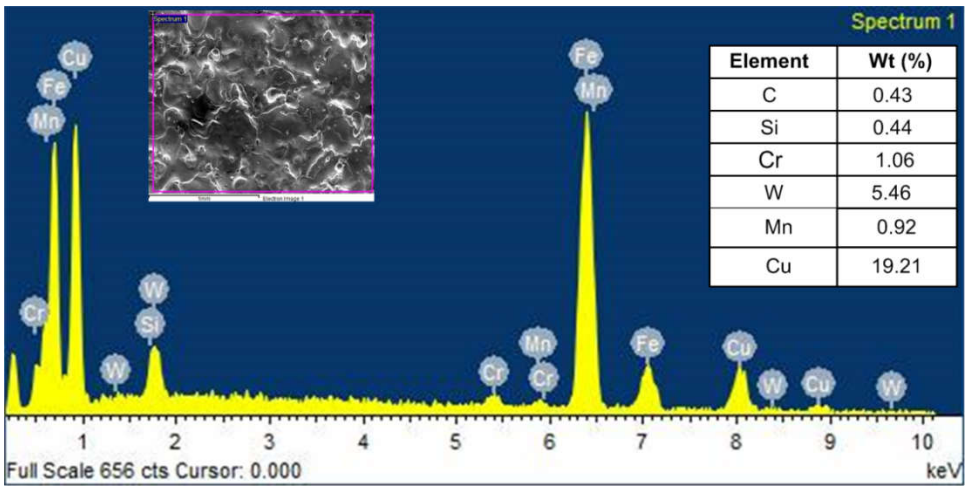

Figure 4.17 EDS spectrum of trial 8

The EDS result of trial 8 indicates changes in compositions of machined surface is C = 0.36 to 0.43, Si = 0.27 to 0.44, Cr = 1.86 to 1.06, W = 0 to 5.46, Mn = 1.25 to 0.92 and Cu = 0.071 to 19.21. The EDS spectrum for trial 19 is shown in Figure 4.18.

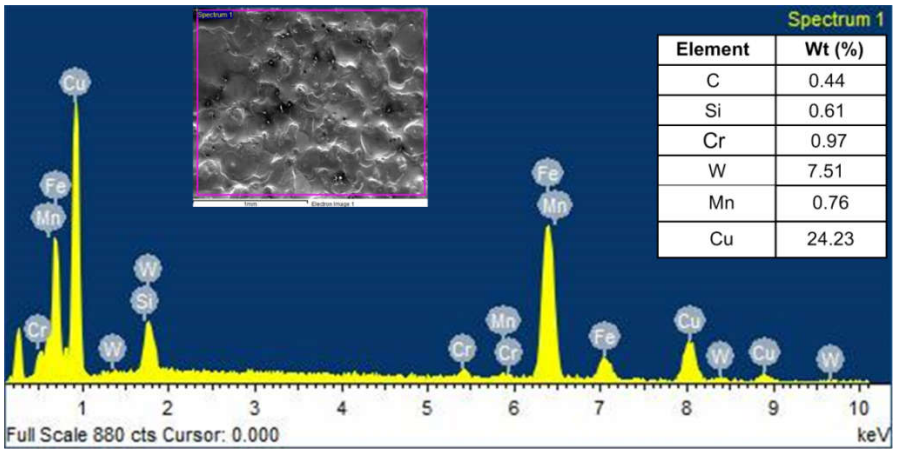

Figure 4.18 EDS spectrum for trial 19

The EDS result of trial 19 indicates changes in compositions of machined surface is C = 0.36 to 0.44, Si = 0.27 to 0.61, Cr = 1.86 to 0.97, W = 0 to 7.51, Mn = 1.25 to 0.76 and Cu = 0.071 to 24.23. The EDS spectrum for trial 20 is shown in Figure 4.19.

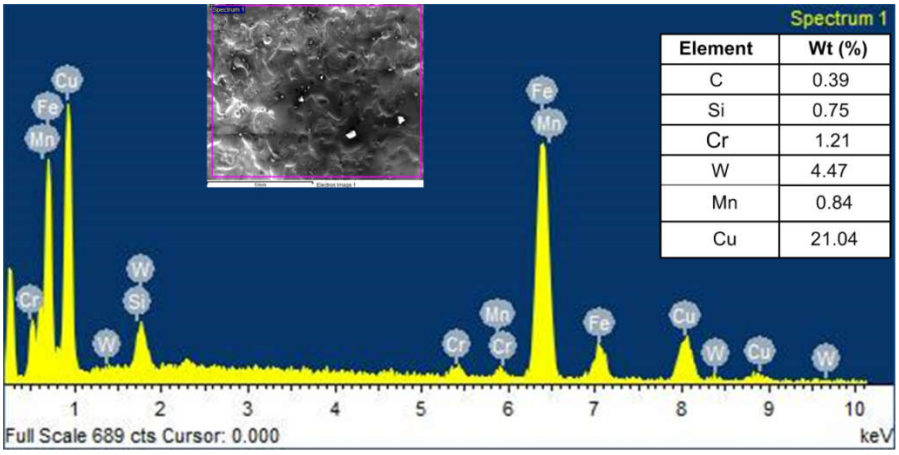

Figure 4.19 EDS spectrum for trial 20

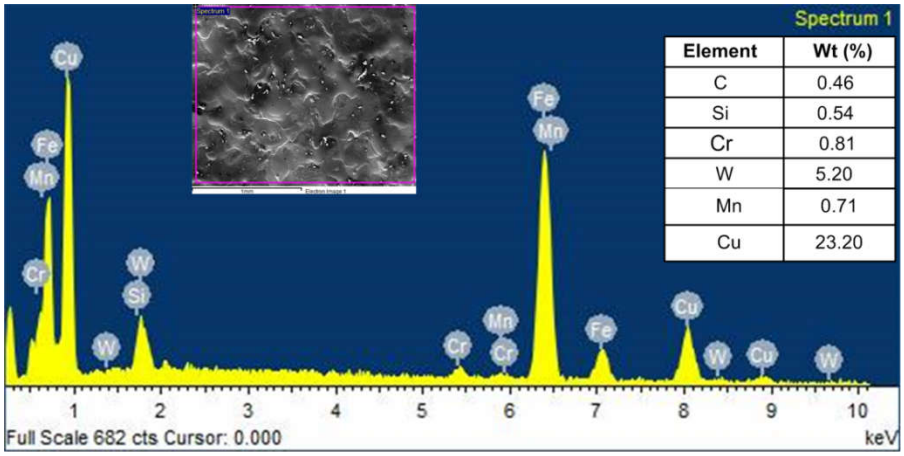

Figure 4.20 EDS spectrum for trial 22

The EDS result of trial 20 indicates variation in compositions of machined surface is C = 0.36 to 0.39, Si = 0.27 to 0.75, Cr = 1.86 to 1.21, W = 0 to 4.47, Mn = 1.25 to 0.84 and Cu = 0.071 to 21.04. The EDS spectrum for trial 22 is shown in Figure 4.20.

The EDS result of trial 22 indicates variation in compositions of machined surface is C = 0.36 to 0.46, Si = 0.27 to 0.54, Cr = 1.86 to 0.81, W = 0 to 5.20, Mn = 1.25 to 0.71 and Cu = 0.071 to 23.20. The results of EDS spectrum of five machined samples are confirmed migration/transfer of significant amounts of Cu, W and Si from P/M electrode. Further improvements in carbon percentage of EDMed surface attributed to the dissociation of carbon element from hydrocarbon oil. The migration hardest constituents of P/M electrode on work material is contributing to improvements of the microhardness [92].

4.10 X-RAY DIFFRACTION (XRD) ANALYSIS

Improvements in the microhardness of the EDMed surface is observed due to the migration of P/M electrode elements on the work surface. The X-ray diffraction analysis is carried out using XRD analyser (Make: BRUKER, Model: D2 PHASER), to study the phases present on the machined surface. The presence of wider peaks in a smaller region indicates an amorphous structure.

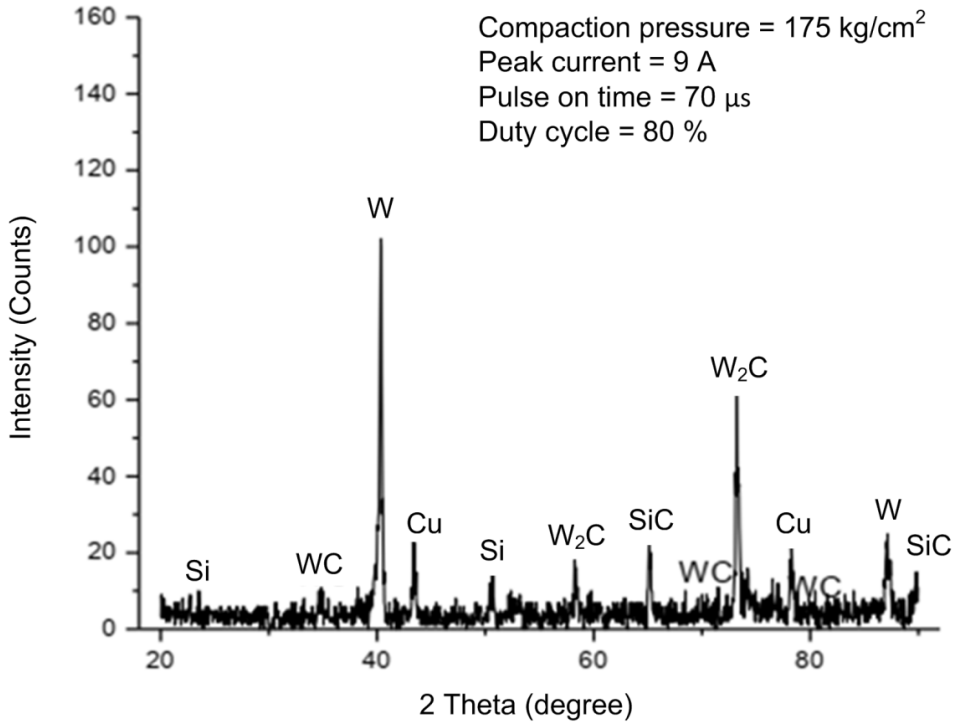

Figure 4.21 XRD peaks of trial 1

Amorphous structure is generated due to rapid quenching of the work surface by EDM oil. Which is able to deliver very high microhardness. Further increase in carbon percentage help to impart high microhardness, strength and wear resistance. The improvement in thermal properties and corrosion resistance were contributed by the increase of copper percentage [95]. The XRD peaks of P20+Ni steel surface EDMed with Cu-W-Si green P/M composite electrode are shown in Figures 4.21to 4.26. The peaks of different phase presence on a surface such as silicon carbide (SiC) and tungsten carbide (WC and W_2C) with Silicon, Copper and tungsten are shown in Figure. The formation of silicon carbide and tungsten carbide were observed at very high temperature due to dissociation of carbon element from hydrocarbon oil. The formation of carbide is attributed high microhardness [96].

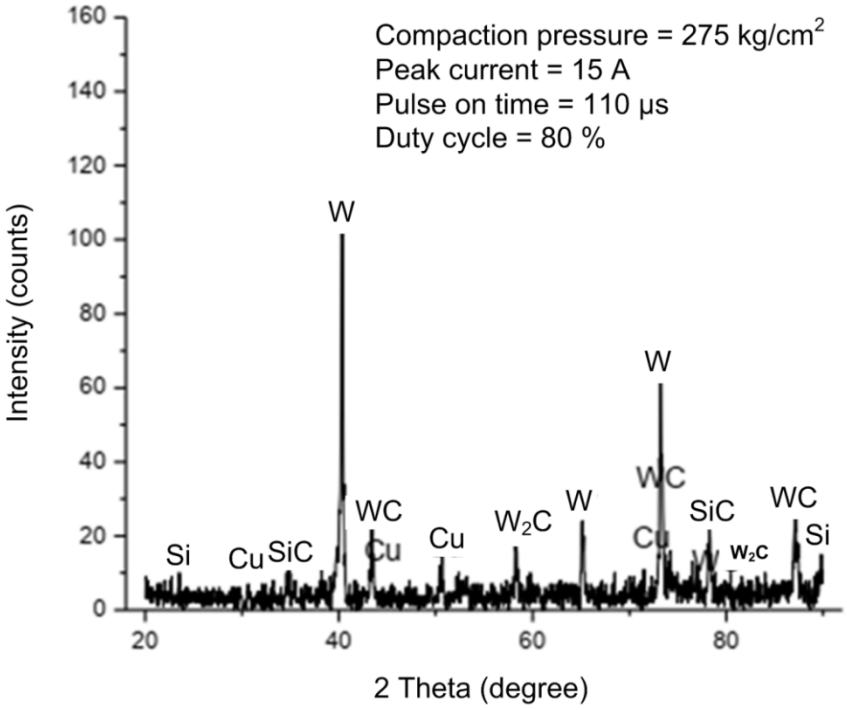

Figure 4.22 XRD peaks of trial 8

The various phases and compounds discussed above were formed on the machined surface due to interaction with the parent metal elements of workpiece and dissociated carbon element from hydrocarbon dielectric fluid. Further interactios were also observed between P/M electrode elements and dissociated carbon from dielectric, which results in formation of tungsten carbide and siicon carbide. Presence of carbides helps significantly to enhance microhardness results in improvements of abrasion and wear resistance.

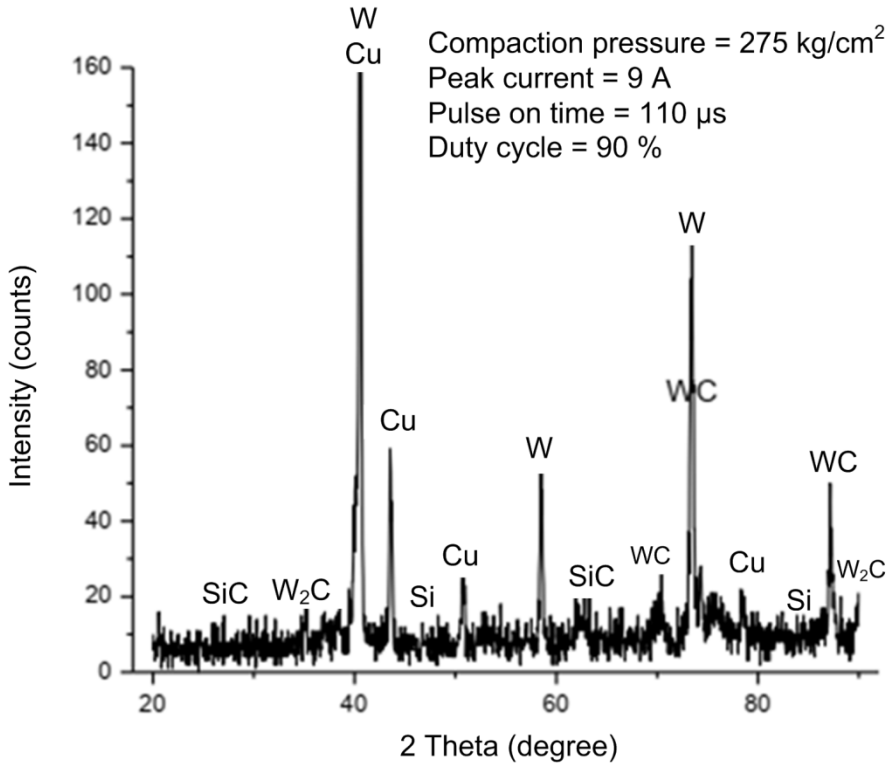

Figure 4.23 XRD peaks of trial 14

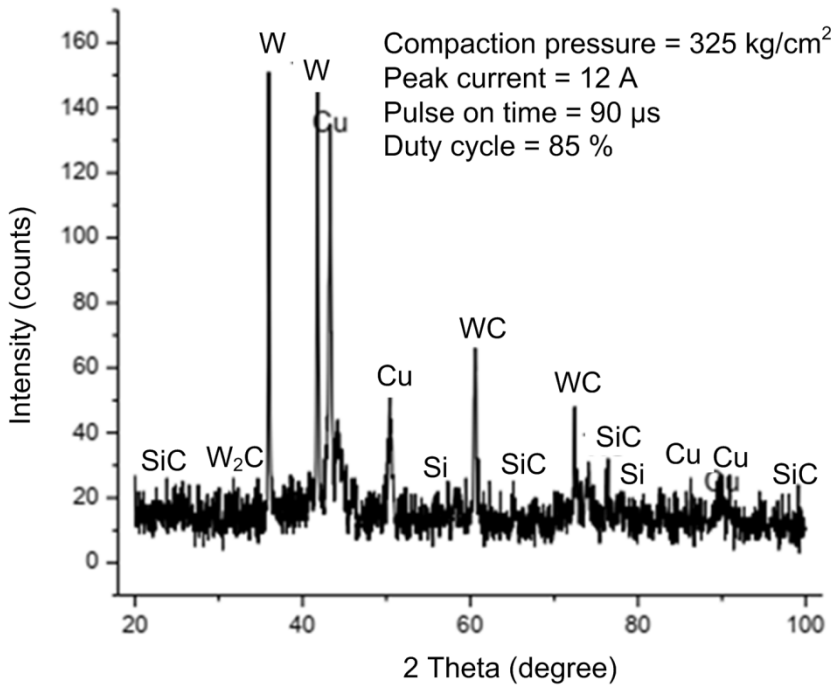

Figure 4.24 XRD peaks of trial 18

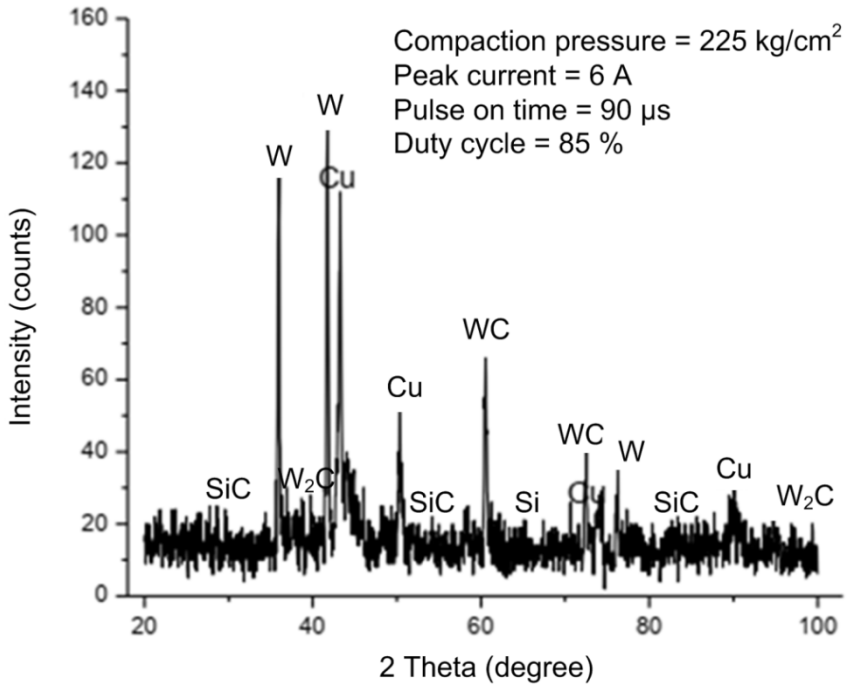

Figure 4.25 XRD peaks of trial 19

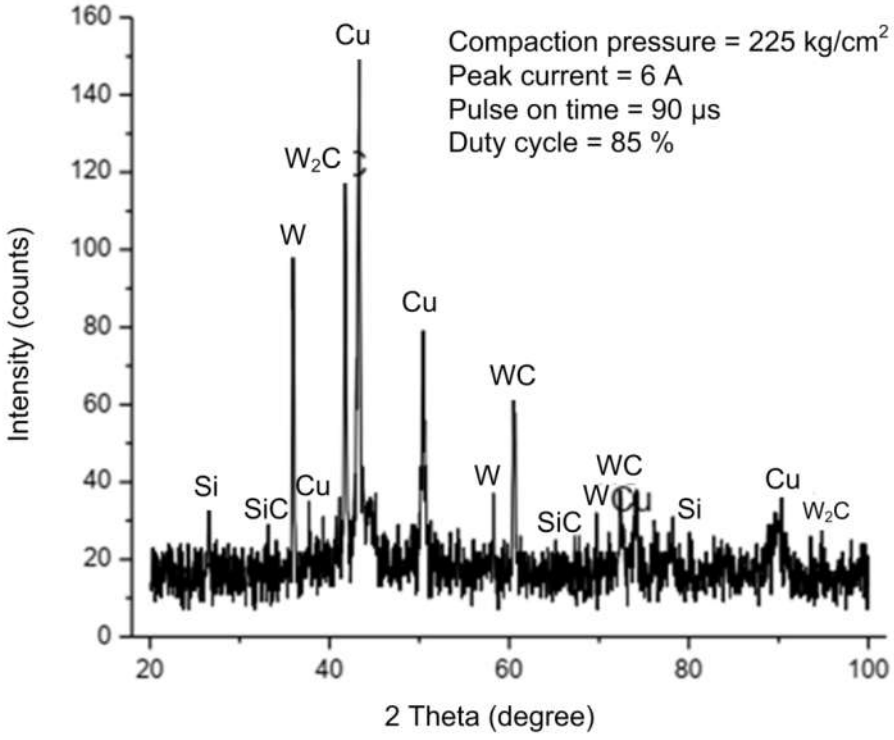

Figure 4.26 XRD peaks of trial 20

CHAPTER – 5

MULTI-RESPONSE OPTIMIZATION USING COMPOSITE DESIRABILITY

5.1 INTRODUCTION TO COMPOSITE DESIRABILITY APPROACH

If industrial problem dealing with only a single response, it is quite simple to provide an optimal solution using a single response optimization technique. However, most of the industrial process is concerned with multi-response and hence need to derive a set of parameters able to satisfy all objectives instead of a single response. In the present experimental work, four responses such as material removal rate (MRR), tool wear rate (TWR), surface roughness (SR) and microhardness (MH) have been considered for optimization. For the production purpose, the combination of process parameters should produce maximum MRR, minimum TWR, Minimum SR, and maximum MH has been investigated. The said objectives are conflicting in nature and hence single objective optimization technique will not fulfil our objectives. Hence, to solve the multi-response problem an appropriate multi-objective optimization technique need to be selected. Here, in present experimental work "Composite Desirability" approach has been selected to optimize the EDM process [102].

Desirability function approach was described by Derringer and Suich in 1980. This technique has been widely used by different industries to solve the multi-response problem. The technique is based on the concept that "the quality of a product that has multiple quality characteristics is completely unacceptable when one of the characteristics does not meet the desired limits". The method obtains a set of best-operating conditions that deliver the "most desirable" response value. For individual response X_i , a desirability function d_i assign numbers between 0 and 1 to the possible value of X_i, with $d_i = 0$ indicate a completely undesirable value of input parameters and if $d_i = 1$, indicates most idle response value. The individual desirability is then combined using an aggregation criterion such as a geometric mean, which gives the overall desirability (D) [127]. The arrangement

of parameters with the highest total desirability is considered to be the optimal parameter condition [129]. The general procedure to be followed to achieve optimal solutions is:

- Use response surface methodology to fit a polynomial to each response.
- Obtain the individual desirability (d_i) for each response.
- Obtain overall desirability (D) by taking the geometric mean of individual desirability function.
- Maximize the composite desirability and identify the optimal input variable setting.

If individual response desirable to maximize the individual desirability is defined as,

$$\begin{aligned} d_i &= 0, && X_i < L_i \\ d_i &= \{(X_i - L_i) / (H_i - L_i)\}^{wi} && L_i \le X_i \le T_i \\ d_i &= 1, && X_i > H_i \end{aligned} \qquad \textbf{(5.1)}$$

If the response X_i is to minimize, then the individual desirability (d_i) is defined as,

$$\begin{aligned} d_i &= 0, && X_i > H_i \\ d_i &= \{(H_i - X_i) / (H_i - L_i)\}^{wi} && L_i \le X_i \le H_i \\ d_i &= 1 && X_i < L_i \end{aligned} \qquad \textbf{(5.2)}$$

Similarly, the desirability (di) can be calculated as, when the response X_i, is at target (T_i),

$$\begin{aligned} di &= 0, && X_i < L_i \\ d_i &= \{(X_i - L_i) / (T_i - L_i)\}^{wi} && L_i \le X_i \le T_i \\ d_i &= \{(H_i - X_i) / (H_i - T_i)\}^{wi} && T_i \le X_i \le H_i \\ di &= 0, && X_i > H_i \end{aligned} \qquad \textbf{(5.3)}$$

Where,

X_i = Predicted value of i^{th} response,

T_i = Target value for i^{th} response,

L_i = Lowest acceptable value for i^{th} response,

H_i = Highest acceptable value for i^{th} response,

d_i = Desirability for i^{th} response,

D = Composite desirability, and

w_i = Weight of desirability function of i^{th} response.

The next step is to obtain the single composite desirability (D) by combining individual response desirability (d_i). The composite desirability (D) is weighted geometric mean of the individual desirability for each response. The composite desirability is expressed as,

$$D = \left[d_1^{w1} \times d_2^{w2} \times d_3^{w3} \times \ldots\ldots\ldots\ldots d_n^{wn}\right]^{1/n} \quad \textbf{OR}$$

$$D = \left[\prod (di)^{wi}\right]^{1/w} \qquad \text{------- (5.4)}$$

Where n = number of response and value of w_i lying between 0 to 1 and $w = \Sigma w_i$, sum of $w_1, w_2, w_3, \ldots\ldots\ldots w_n$ equals to one.

In this experimental work total, four responses such as MRR, TWR, SR, and MH have been considered for multi-objective optimization. Analysis has been carried out to identify the optimal set of input parameters able to deliver maximum material removal rate (MRR), minimum tool wear rate (TWR), minimum surface roughness (SR) and maximum micro-hardness (MH). The four responses are expressed in form of mathematical functions are:

$$MRR = f_1 \{C_p, I_p, T_{on}, \tau\}$$

$$TWR = f_2 \{C_p, I_p, T_{on}, \tau\}$$

$$SR = f_3 \{C_p, I_p, T_{on}, \tau\} \qquad \text{------- (5.5)}$$

$$MH = f_4 \{C_p, I_p, T_{on}, \tau\}$$

The above objectives are depends on the following conditions for maximize MRR, minimize TWR, minimize SR and maximize MH.

$$(125 \leq C_p \leq 325)$$

$$(6 \leq I_p \leq 18)$$

$$(50 \leq T_{on} \leq 130)$$

$$(75 \leq \tau \leq 95)$$

The criteria considered for multi-objective optimization with all given constraints of responses, goal and weight (w) given to individual responses are shown in the individual section [128].

5.2 MULTI-RESPONSE OPTIMIZATION USING COMPOSITE DESIRABILITY

The effects of process parameters on the selected responses such as MRR, TWR, SR, and MH are studied during surface modification of P20+Ni die steel using EDM. However, all the responses are conflicts in nature and hence single objective optimization technique would not able to solve the problem. Attempts have been made to optimize the set of responses using a multi-response tool known as a "composite desirability" approach based on response surface methodology (RSM). Different multi characteristic response models have been developed. Limits and goals were established for responses in order to precisely determine their impact on overall desirability. A maximum or minimum level is provided for all response characteristics which are to be optimized. Weights are assigned in order to give added emphasis to upper or lower bounds or to emphasize a target value. The importance varies from 1(least important) to 5 (most important) is assigned to each response compared to the other responses.

5.2.1 Optimization of MRR and TWR

The goals and ranges of different input variables such as compaction pressure (C_p), peak current (I_p), pulse on time (T_{on}) and duty cycle (τ) with the response characteristics MRR and TWR are given in Table 5.1. Both the responses (MRR and TWR) have been assigned equal important levels of 3.

Table 5.1 Constraints of input parameters and responses (MRR and TWR)

Name	Goal	Lower Limit	Upper Limit	Lower Weight	Upper Weight	Importance
A:Compaction Pressure	is in range	125	325	1	1	3
B:Peak Current	is in range	6	18	1	1	3
C:Pulse on Time	is in range	50	130	1	1	3
D:Duty Cycle	is in range	75	95	1	1	3
MRR	maximize	0.1211	0.3032	1	1	3
TWR	minimize	0.0238	0.0385	1	1	3

The main objective of the problem is to obtain an optimal set of process parameters which able to deliver the desired goal. The value of desirability for individual responses varies from 0 to 1, and the result of the desirability of individual responses mainly depends on how closely the limits (upper and lower) are set compare to the actual optimum. A set of different four optimal results are obtained within the given constraints of design space to optimizing MRR and TWR using statistical software Design Expert 10. Out of different four results, the set of process parameters possessing maximum desirability is considered as an optimal condition for the desired objective. Table 5.2 indicates the optimal set of input process parameters with desirability required for obtaining an optimum combination of responses under given constraints.

Table 5.2 Set of optimum solutions for MRR and TWR

Sr. No	C_p	I_p	T_{on}	τ	MRR	TWR	Desirability	
1	205.183	14.758	129.999	85.510	0.289	0.029	0.792	Selected
2	204.925	14.755	129.971	85.437	0.289	0.028	0.792	
3	206.428	14.710	129.999	85.550	0.289	0.028	0.792	
4	205.226	14.769	129.140	85.478	0.289	0.028	0.792	

The optimum level of individual process parameters and responses with composite desirability are represented in the form of the dot in the ramp function graph shown in Figure 5.1. The level of the dot in ramp function indicates how much desirable the levels of selected input parameters. The lower and upper weight for the individual parameter is selected level 1 and equal important level 3 for all four process parameters. The bar graph shown in Figure 5.2 indicates the individual desirability and composite desirability of responses MRR and TWR. The composite desirability varies from 0 to 1 and its value mainly depend on how the closeness of individual responses (MRR and TWR) towards the target.

Table 5.3 indicates the levels of individual parameters, which is considered as an optimal set for optimization of MRR and TWR with highest composite desirability. Further, the predicted value of individual responses at 95% of the confidence interval is given in Table 5.4. The predicted value of responses is confirmed through performing an experiment on EDM by setting the level of parameters shown in Table 5.3. Good agreement between the predicted value and the experimental value of responses are observed, which strongly validate the predicted model of responses.

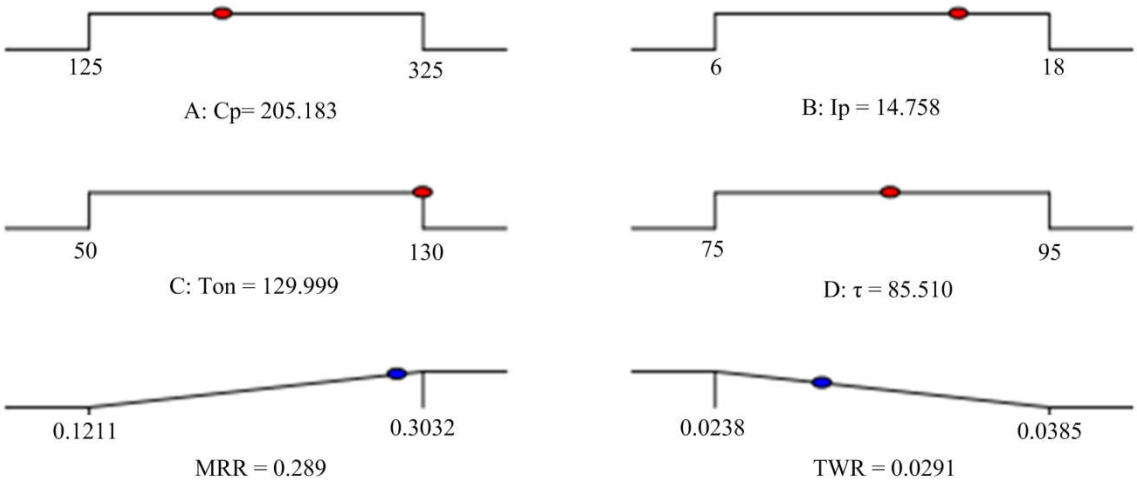

Figure 5.1 Ramp function graph of desirability for MRR and TWR

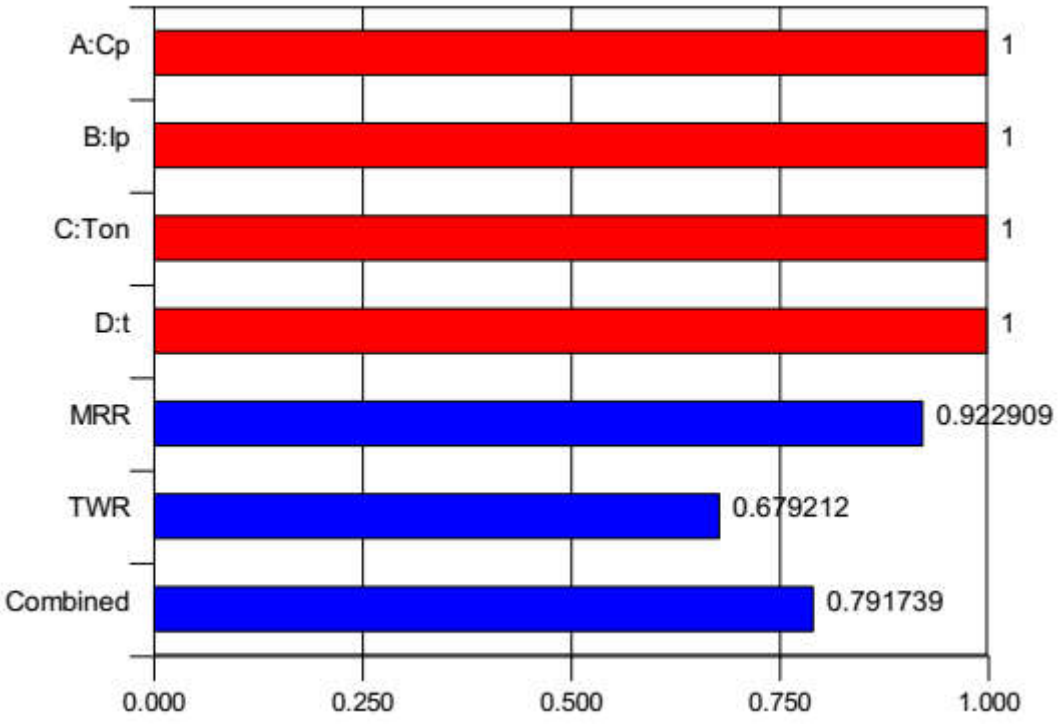

Figure 5.2 Bar graph of desirability for MRR and TWR

Table 5.3 Optimal set of parameters for MRR and TWR

Factor coding	Name of Factor	Optimum level
A	Compaction Pressure (C_p)	205.183
B	Peak Current (I_p)	14.758
C	Pulse on Time (T_{on})	129.999
D	Duty Cycle (τ)	85.510

Table 5.4 Experimental validations of predicted responses (MRR & TWR)

Responses	Desirability	Predicted value	Experimental value	Prediction Error (%)
MRR (gm/min)	0.9229	0.289	0.281	2.76
TWR (gm/min)	0.6792	0.029	0.030	3.33
Overall composite desirability: 0.7917				

The 3D surface plots for desirability are developed with keeping parameters in range for maximum MRR and minimum TWR using Design Expert 10. Figure 5.3(a) shows the distribution of desirability for P20+Ni steel according to peak current and compaction pressure. It is concluded that the value of composite desirability is lower in the region of smaller peak current with high compaction pressure. The overall composite desirability is observed higher than 0.79 and it reduces continuously while moving either side. Similarly, Figure 5.3 (b) indicates the distribution of desirability for duty cycle and pulse on time. It is concluded that composite desirability value is lower in the region of high duty cycle with a lower pulse on time.

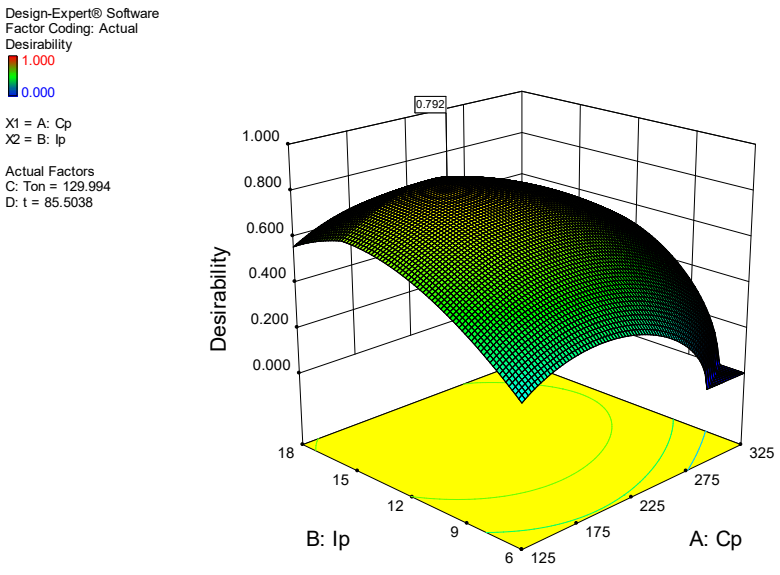

Figure 5.3 (a) 3D surface graph of desirability for MRR and TWR (I_p & C_p)

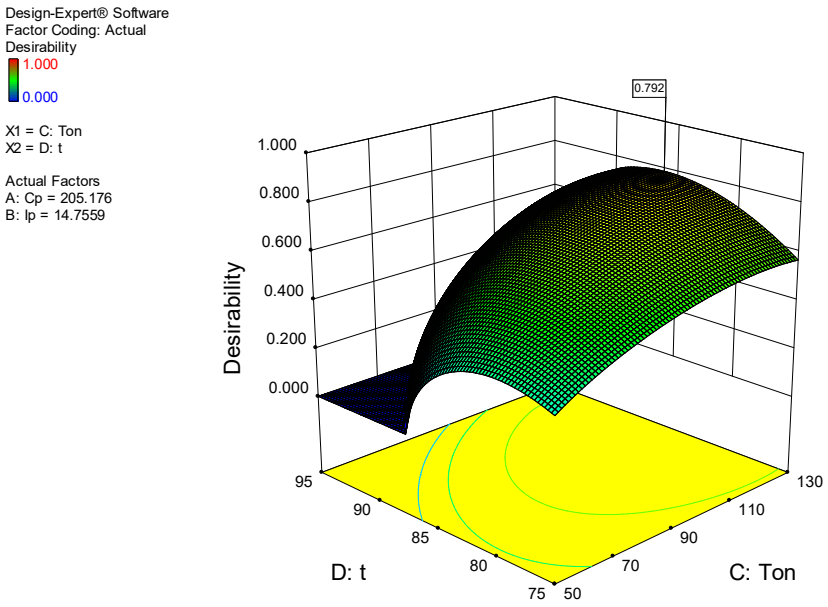

Figure 5.3 (b) 3D surface graph of desirability for MRR and TWR (τ & T_{on})

5.2.2 Optimization of SR and MH

The goal and range of different input variables such as compaction pressure (C_p), peak current (I_p), pulse on time (T_{on}) and duty cycle (τ) with the response characteristics SR and MH are given in Table 5.5. Both the responses (SR and MH) have been assigned equal importance levels of 3.

Table 5.5 Constraints of input parameters and responses (SR and MH)

Name	Goal	Lower Limit	Upper Limit	Lower Weight	Upper Weight	Importance
A:Compaction Pressure	is in range	125	325	1	1	3
B:Peak Current	is in range	6	18	1	1	3
C:Pulse on Time	is in range	50	130	1	1	3
D:Duty Cycle	is in range	75	95	1	1	3
SR	minimize	4.235	10.605	1	1	3
MH	maximize	791	1189	1	1	3

The main objective of the optimization is to obtain an optimal set of process parameters that able to deliver the desired goal of responses. The value of desirability for individual responses varies from 0 to 1, and the result of desirability for individual response mainly depends on how closely the limits (upper and lower) are set compare to the actual optimum. Set of a total of 67 optimal results are obtained for the specified constraints of

design space for SR and MH using statistical software Design Expert 10. Out of different 67 results, the set of process parameters possessing maximum desirability is considered as an optimal condition for the desired responses. Table 5.6 indicates the optimal set of input process parameters with desirability required for obtaining an optimum combination of responses under given constraints.

Table 5.6 Set of optimum solutions for SR and MH

Sr. No	Cp	Ip	Ton	τ	SR	MH	Desirability	
1	183.151	6.243	50.755	94.952	4.123	1329.844	1.000	**Selected**
2	163.477	6.006	50.478	94.839	4.223	1409.641	1.000	
3	214.302	6.923	54.195	94.690	4.204	1190.689	1.000	
4	195.907	6.010	74.914	94.990	4.227	1190.699	1.000	
5	198.889	6.476	56.779	94.026	4.218	1203.717	1.000	
6	214.259	6.746	51.340	94.948	4.008	1215.523	1.000	
7	185.759	6.029	64.484	94.413	4.213	1239.615	1.000	
8	163.106	6.009	50.757	94.924	4.230	1413.879	1.000	
9	209.910	6.077	60.325	94.934	3.746	1192.223	1.000	
10	219.378	7.106	53.454	94.945	4.221	1189.225	1.000	
11	196.245	6.064	59.139	94.084	3.999	1208.868	1.000	
12	223.021	7.205	50.648	94.869	4.188	1189.568	1.000	
13	197.024	6.121	64.466	94.918	4.074	1218.402	1.000	
14	178.691	6.011	50.453	92.494	4.152	1247.247	1.000	
15	209.255	6.855	51.138	94.533	4.199	1214.729	1.000	
16	178.198	6.038	57.803	94.234	4.212	1287.761	1.000	
17	173.450	6.150	51.001	94.596	4.220	1352.182	1.000	
18	222.469	6.052	50.341	94.902	3.332	1196.517	1.000	
19	194.431	6.206	64.919	94.284	4.227	1198.990	1.000	
20	221.221	7.091	50.019	94.657	4.142	1189.192	1.000	
21	174.365	6.112	54.538	94.788	4.228	1340.900	1.000	
22	165.635	6.009	52.350	94.989	4.220	1398.252	1.000	
23	214.587	6.358	53.327	94.952	3.748	1206.656	1.000	
24	224.029	7.282	50.897	94.998	4.222	1190.868	1.000	
25	172.474	6.061	56.172	94.984	4.233	1350.767	1.000	
26	190.950	6.306	52.819	93.621	4.171	1233.813	1.000	
27	195.577	6.002	75.925	95.000	4.248	1189.344	0.999	
28	167.629	6.000	50.000	89.692	4.345	1189.133	0.991	
29	162.892	6.000	50.169	89.174	4.400	1189.007	0.987	
30	191.949	6.000	80.689	95.000	4.415	1189.001	0.986	
31	191.262	6.016	81.545	95.000	4.459	1189.001	0.982	
32	155.124	6.000	50.012	88.235	4.467	1189.266	0.982	
33	190.732	6.000	82.400	94.999	4.476	1189.002	0.981	
34	171.450	6.000	70.065	95.000	4.477	1301.508	0.981	
35	126.131	6.000	50.064	84.041	4.488	1188.999	0.980	
36	152.124	6.006	50.001	87.852	4.491	1189.004	0.980	
37	138.731	6.003	50.001	95.000	4.495	1535.492	0.979	
38	151.333	6.001	50.000	90.029	4.506	1264.175	0.979	
39	148.808	6.000	50.000	88.044	4.517	1207.849	0.978	
40	145.550	6.000	50.000	86.986	4.519	1189.002	0.977	
41	144.589	6.000	50.002	86.856	4.522	1189.021	0.977	

Sr. No	Cp	Ip	Ton	τ	SR	MH	Desirability	
42	133.198	6.008	50.001	85.209	4.530	1189.325	0.977	
43	144.018	6.000	50.000	92.524	4.534	1394.584	0.976	
44	189.457	6.000	84.299	94.999	4.542	1189.003	0.976	
45	125.821	6.031	51.991	84.299	4.548	1189.006	0.975	
46	188.418	6.000	85.960	95.000	4.600	1189.000	0.971	
47	125.000	6.000	50.000	82.934	4.410	1169.431	0.962	
48	239.241	6.000	50.000	94.995	2.958	1155.635	0.957	
49	240.604	7.736	50.000	95.000	4.235	1154.633	0.956	
50	125.000	6.000	60.300	93.708	4.858	1495.525	0.950	
51	130.227	6.000	69.765	95.000	4.960	1494.295	0.941	
52	181.530	6.000	99.332	94.951	5.065	1189.002	0.933	
53	125.000	6.000	50.000	81.170	4.254	1137.199	0.931	
54	125.002	6.000	78.098	94.984	5.199	1493.488	0.921	
55	125.000	6.001	50.000	80.521	4.189	1127.356	0.919	
56	256.487	8.161	50.024	94.999	4.235	1123.983	0.915	
57	251.679	6.000	50.000	94.890	2.715	1121.569	0.911	
58	179.615	6.011	108.216	95.000	5.361	1189.003	0.907	
59	178.871	6.000	115.348	95.000	5.588	1189.001	0.887	
60	125.000	6.010	50.167	78.003	3.900	1098.870	0.880	
61	324.998	10.885	50.000	95.000	4.660	1119.609	0.878	
62	324.999	10.948	50.000	95.000	4.706	1121.878	0.877	
63	325.000	11.096	50.000	95.000	4.813	1127.288	0.877	
64	324.999	11.235	50.000	95.000	4.913	1132.521	0.876	
65	320.628	10.150	50.065	95.000	4.235	1095.526	0.875	
66	125.002	6.002	98.943	95.000	5.744	1447.842	0.874	
67	323.071	14.857	50.004	75.000	5.749	1189.002	0.873	

The optimum level of individual process parameters and responses with composite desirability are represented in the form of the dot in the ramp function graph shown in figure 5.4. The level of the dot in ramp function indicates how much desirable individual parameter. The lower and upper weight for the individual parameter is considered 1and important level 3 for all four process parameters. The bar graph shown in Figure 5.5 indicates the individual desirability of responses SR and MH with composite desirability. The composite desirability varies between 0 to 1 and its value mainly depending on how the closeness of individual responses (SR and MH) towards the target.

Table 5.7 indicates the levels of individual parameters, which is considered as an optimal set for optimization of SR and MH with the highest composite desirability. Further, the predicted value of individual responses at 95% of the confidence interval is given in Table 5.8. Predicted values of responses are confirmed by performing an experiment on EDM with setting levels of parameters shown in Table 5.7. A good agreement between the predicted value and the experimental value of responses are observed, which strongly validate the predicted model of responses.

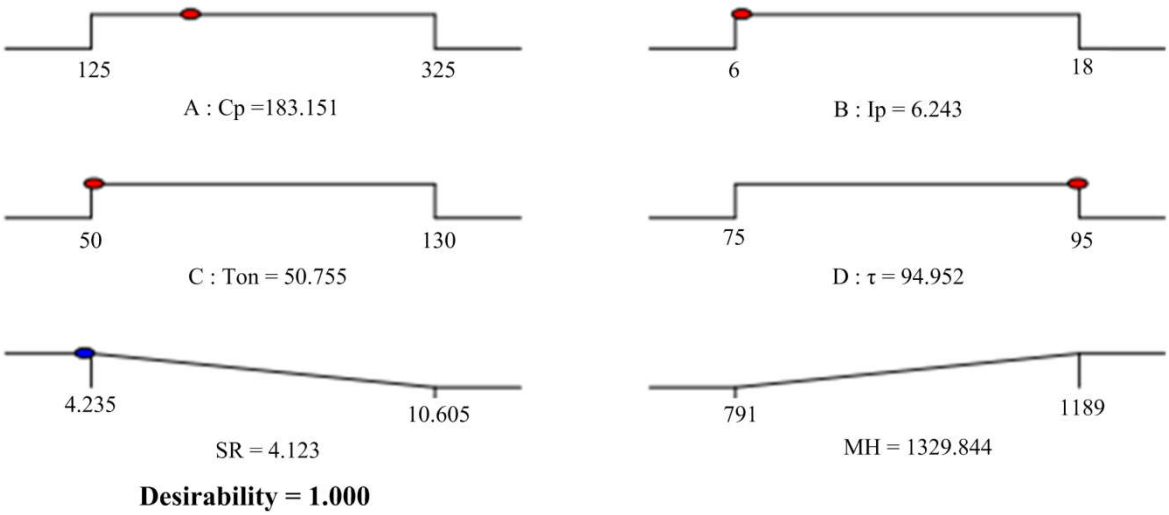

Figure 5.4 Ramp function graph of desirability for SR and MH

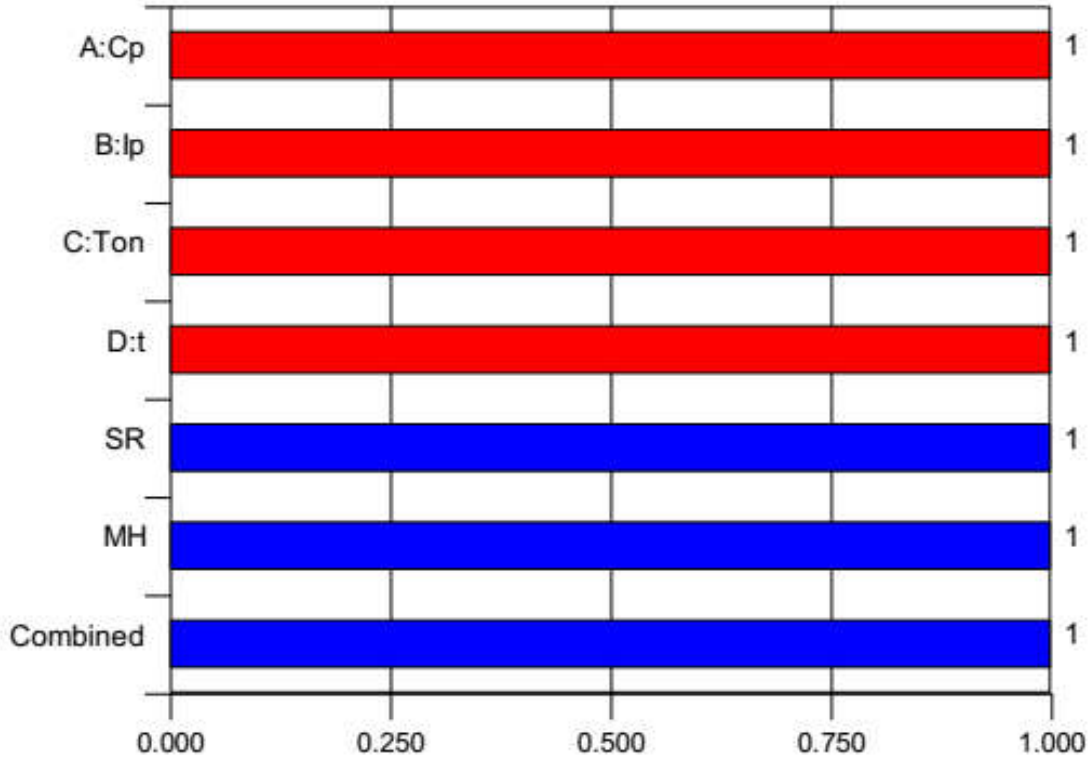

Figure 5.5 Bar graph of desirability for SR and MH

Table 5.7 Optimal set of parameters for SR and MH

Factor coding	Name of Factor	Optimum level
A	Compaction Pressure (C_p)	183.151
B	Peak Current (I_p)	6.243
C	Pulse on Time (T_{on})	50.755
D	Duty Cycle (τ)	94.952

Table 5.8 Experimental validations of predicted responses (SR & MH)

Responses	Desirability	Predicted value	Experimental value	Prediction Error (%)
SR (μm)	1.000	4.123	4.403	6.35
MH (HVN)	1.000	1329.844	1267.257	4.71
Overall composite desirability: 1.000				

The 3D surface plots for desirability are developed with keeping the parameters in range for maximum MH and minimum SR using Design Expert 10. Figure 5.6(a) indicates the distribution of desirability for P20+Ni steel according to peak current and compaction pressure. It is concluded that composite desirability value is lower in the region of high peak current with lower compaction pressure. The overall composite desirability was observed at 1.00. Similarly, Figure 5.6 (b) indicates the distribution of desirability for duty cycle and pulse on time.

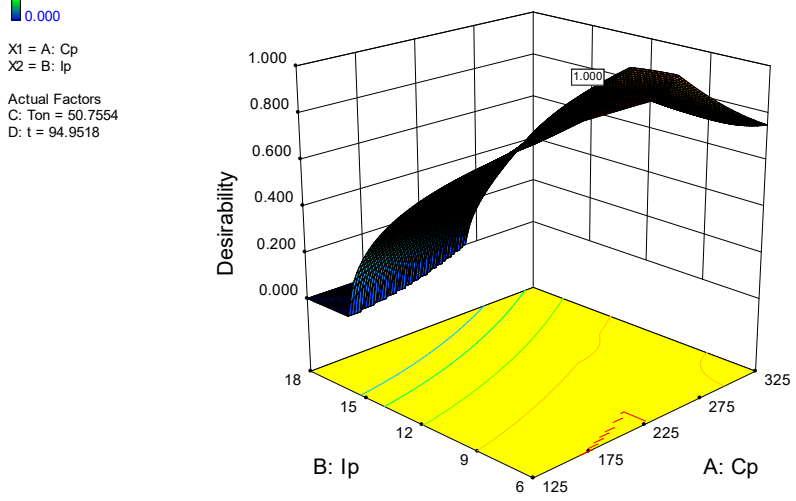

Figure 5.6 (a) 3D surface graph of desirability for SR and MH (I_p & C_p)

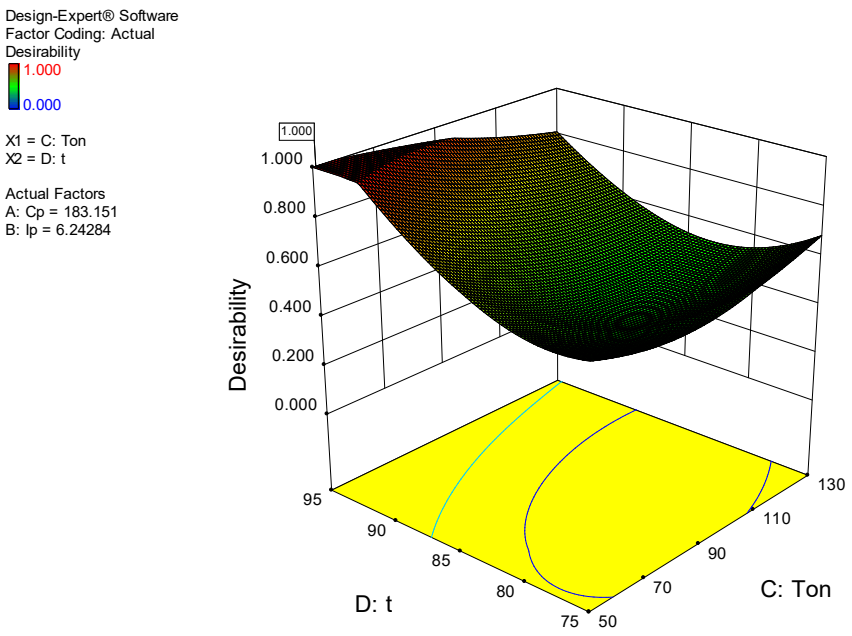

Figure 5.6 (b) 3D surface graph of desirability for SR and MH (τ & T_{on})

5.2.3 Optimization of MRR, TWR, and SR

The goals and ranges of different input parameters such as compaction pressure (C_p), peak current (I_p), pulse on time (T_{on}) and duty cycle (τ) with the response characteristics MRR, TWR and SR are given in Table 5.9. All the responses (MRR, TWR, and SR) have been assigned equal important index levels 3.

Table 5.9 Constraints of input parameters and responses (MRR, TWR, and SR)

Name	Goal	Lower Limit	Upper Limit	Lower Weight	Upper Weight	Importance
A:Compaction Pressure	is in range	125	325	1	1	3
B:Peak Current	is in range	6	18	1	1	3
C:Pulse on Time	is in range	50	130	1	1	3
D:Duty Cycle	is in range	75	95	1	1	3
MRR	maximize	0.1211	0.3032	1	1	3
TWR	minimize	0.0238	0.0385	1	1	3
SR	minimize	4.235	10.605	1	1	3

The main objective of the optimization is to obtain an optimal set of process parameters that will able to deliver the desired goal of responses. The value of desirability for individual responses varies from 0 to 1, and the result of the desirability of individual responses mainly depends on how closely the limits (upper and lower) are set compare to

the actual optimum. A set of one optimal result is obtained for the specified constraints of design space for MRR, TWR, and SR using statistical software Design Expert 10. The set of process parameters possessing maximum desirability is considered as an optimal condition for the desired responses. Table 5.10 indicates the optimal set of input process parameters with desirability required for obtaining an optimum combination of responses under given constraints.

Table 5.10 Set of optimum solutions for MRR, TWR, and SR

Sr. No	Cp	Ip	Ton	τ	MRR	TWR	SR	Desirability	
1	241.088	10.809	107.650	83.910	0.203	0.025	7.098	0.616	Selected

The optimum level of individual process parameters and responses with composite desirability are represented in the form of the dot in the ramp function graph shown in Figure 5.7. The level of the dot in ramp function indicates how much desirable individual parameter. The lower and upper weight for the individual parameter is considered 1and importance level 3 assigned for all four process parameters. The bar graph shown in Figure 5.8 indicates the desirability of individual responses MRR, TWR and SR with composite desirability. The composite desirability varies between 0 to 1 and its value mainly depending on how the closeness of individual responses (MRR, TWR, and SR) towards the target.

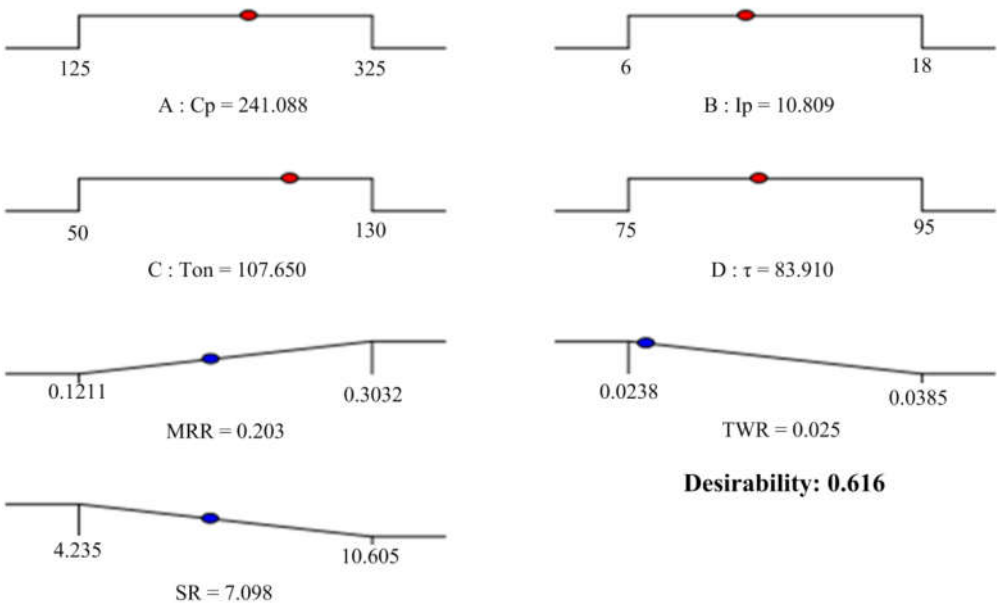

Figure 5.7 Ramp function graph of desirability for MRR, TWR & SR

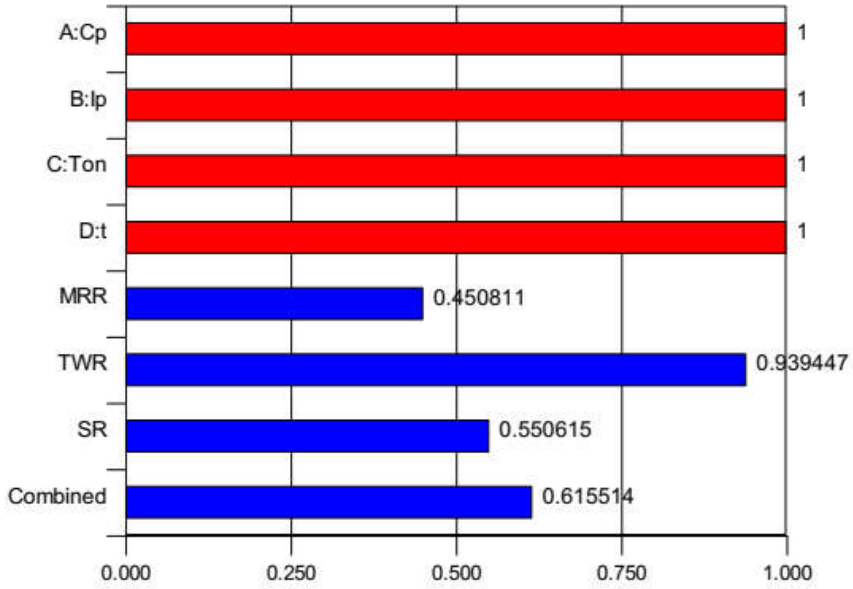

Figure 5.8 Bar graph of desirability for MRR, TWR & SR

Table 5.11 indicates the levels of individual parameters, which is considered as an optimal set for optimization of MRR, TWR, and SR with the highest composite desirability. Further, the predicted the value of individual responses at 95% of confidence interval given in table 5.12. The predicted value of responses is confirmed by performing an experiment on EDM with a setting the level of parameters shown in Table 5.11. A good agreement between the predicted value and the experimental value of responses are observed, which strongly validate the predicted model of responses.

Table 5.11 Optimal set of parameters for MRR, TWR, and SR

Factor coding	Name of Factor	Optimum level
A	Compaction Pressure (C_p)	241.088
B	Peak Current (I_p)	10.809
C	Pulse on Time (T_{on})	107.650
D	Duty Cycle (τ)	83.910

Table 5.12 Experimental validations of predicted responses (MRR, TWR & SR)

Responses	Desirability	Predicted value	Experimental value	Prediction Error (%)
MRR (gm/min)	0.4508	0.203	0.192	5.41
TWR (gm/min)	0.9394	0.025	0.026	3.84
SR (μm)	0.5506	7.098	6.792	4.31
Overall composite desirability: 0.616				

The 3D surface plots for desirability were developed with keeping the selected parameters in range for maximum MRR and minimum TWR & SR using Design Expert 10. Figure 5.9

(a) indicates the distribution of desirability for P20+Ni steel according to peak current and compaction pressure.

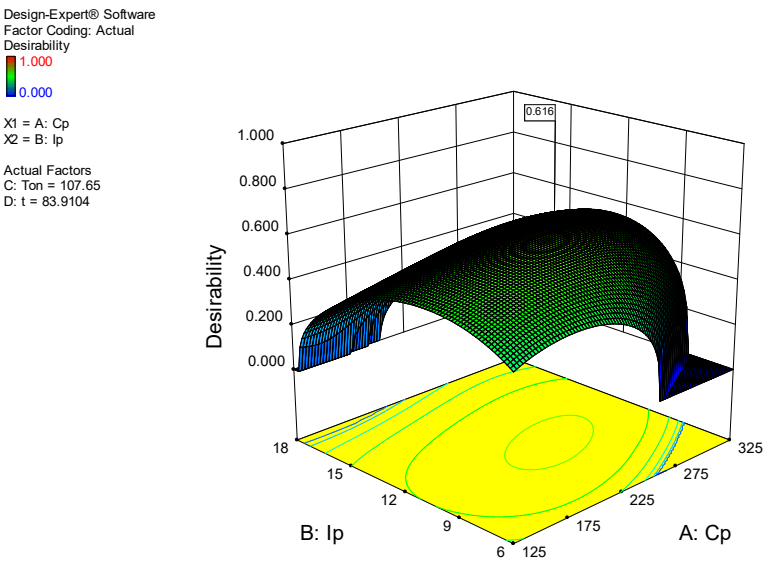

Figure 5.9 (a) 3D surface graph of desirability for MRR, TWR & SR (I_p & C_p)

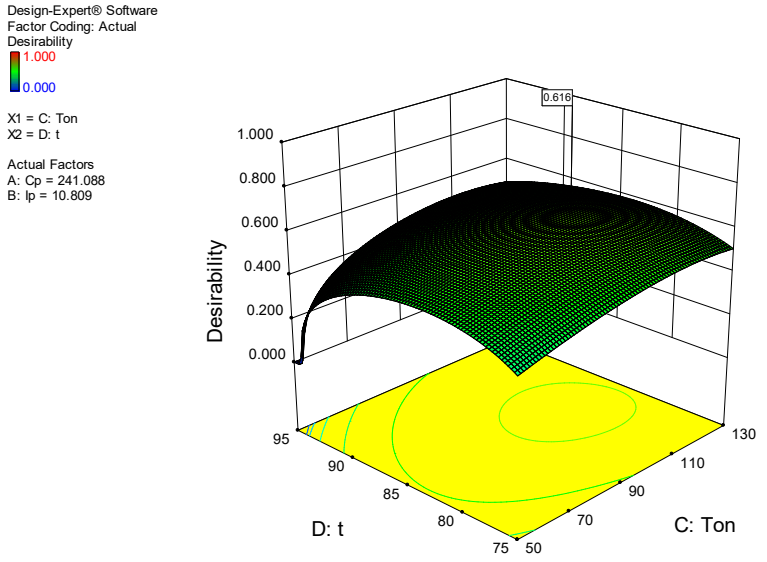

Figure 5.9 (b) 3D surface graph of desirability for MRR, TWR & SR (τ & T_{on})

It is concluded that composite desirability value is lower in the region of low peak current with high compaction pressure. The overall composite desirability was observed higher than 0.61. Similarly, Figure 5.6 (b) indicates the distribution of desirability for duty cycle and pulse on time.

5.2.4 Optimization of MRR, TWR, SR, and MH (equal weight & importance)

The goals and ranges of different input variables such as compaction pressure (C_p), peak current (I_p), pulse on time (T_{on}) and duty cycle (τ) with the response characteristics MRR, TWR, SR, and MH are given in Table 5.13. All the responses (MRR, TWR, SR & MH) have been assigned equal important index levels of 3.

Table 5.13 Constraints of input parameters and responses (MRR, TWR, SR & MH)

Name	Goal	Lower Limit	Upper Limit	Lower Weight	Upper Weight	Importance
A:Compaction Pressure	is in range	125	325	1	1	3
B:Peak Current	is in range	6	18	1	1	3
C:Pulse on Time	is in range	50	130	1	1	3
D:Duty Cycle	is in range	75	95	1	1	3
MRR	maximize	0.1211	0.3032	1	1	3
TWR	is target = 0.0312	0.0238	0.0385	1	1	3
SR	minimize	4.235	10.605	1	1	3
MH	maximize	791	1189	1	1	3

The main objective of the optimization is to obtain an optimal set of process parameters that will able to deliver the desired goal of responses. The value of desirability for individual responses varies from 0 to 1, and the result of the desirability of individual responses mainly depends on how closely the limits (upper and lower) are set compare to the actual optimum. A set of 46 optimal results are obtained for the specified constraints of design space for MRR, TWR, SR, and MH using statistical software Design Expert 10. The set of process parameters possessing maximum desirability is considered as an optimal condition for the desired responses. Table 5.14 indicates the optimal set of input process parameters with desirability required for obtaining an optimum combination of responses under given constraints.

The optimum level of individual process parameters and responses with composite desirability are represented in the form of the dot in the ramp function graph shown in Figure 5.10. The bar graph shown in Figure 5.11, indicates the individual and composite desirability.

Table 5.14 Set of optimum solutions for MRR, TWR, SR, and MH

Sr. No	Cp	Ip	Ton	τ	MRR	TWR	SR	MH	Desirability	
1	125.001	17.971	111.404	75.000	0.230	0.031	8.006	1091.475	0.655	Selected
2	125.000	17.927	110.425	75.000	0.229	0.031	7.979	1090.652	0.655	
3	125.003	17.835	108.790	75.000	0.228	0.031	7.931	1088.684	0.655	
4	125.560	17.918	110.126	75.000	0.229	0.031	7.975	1089.618	0.654	
5	125.005	17.729	107.010	75.001	0.226	0.031	7.879	1086.470	0.654	
6	125.101	17.817	108.413	75.048	0.228	0.031	7.939	1088.021	0.654	
7	125.000	17.626	105.454	75.000	0.225	0.031	7.830	1084.343	0.654	
8	125.000	17.937	107.611	75.000	0.227	0.031	7.932	1094.106	0.654	
9	125.000	18.000	108.022	75.000	0.228	0.031	7.951	1096.180	0.653	
10	125.001	18.000	107.687	75.014	0.228	0.031	7.951	1096.529	0.653	
11	127.085	17.907	109.418	75.001	0.229	0.031	7.970	1087.332	0.653	
12	125.000	18.000	108.938	75.116	0.230	0.031	8.009	1094.723	0.653	
13	125.001	17.366	101.995	75.001	0.222	0.031	7.718	1078.944	0.652	
14	125.000	17.999	105.080	75.003	0.227	0.032	7.902	1099.885	0.652	
15	129.144	18.000	110.668	75.001	0.230	0.031	8.024	1086.453	0.651	
16	126.381	17.787	103.630	75.000	0.225	0.031	7.842	1090.854	0.651	
17	125.003	18.000	104.407	75.063	0.227	0.032	7.912	1100.690	0.651	
18	130.814	17.988	109.895	75.000	0.230	0.031	8.017	1084.090	0.650	
19	125.001	17.998	103.307	75.033	0.226	0.032	7.883	1102.335	0.650	
20	126.127	18.000	114.293	75.000	0.232	0.031	8.072	1088.356	0.649	
21	125.000	18.000	102.242	75.000	0.225	0.032	7.855	1104.149	0.649	
22	130.225	17.454	101.410	75.000	0.223	0.031	7.757	1074.260	0.649	

23	125.003	16.904	96.985	75.029	0.217	0.031	7.547	1069.474	0.648	
24	126.432	17.828	100.573	75.000	0.224	0.032	7.802	1097.182	0.648	
25	125.001	16.720	95.219	75.004	0.215	0.031	7.471	1065.919	0.646	
26	125.000	18.000	120.534	75.148	0.237	0.031	8.242	1086.426	0.641	
27	126.301	17.615	94.147	75.000	0.219	0.032	7.660	1100.438	0.641	
28	125.000	16.731	96.899	76.605	0.230	0.031	8.020	1062.753	0.638	
29	125.000	15.821	84.260	75.000	0.204	0.032	7.106	1057.620	0.629	
30	125.008	8.499	130.000	82.302	0.205	0.031	7.206	1042.858	0.628	
31	125.005	8.521	129.998	82.336	0.205	0.031	7.222	1042.655	0.628	
32	125.000	8.442	129.980	82.209	0.204	0.031	7.165	1043.380	0.628	
33	125.001	8.588	129.999	82.441	0.207	0.031	7.269	1042.075	0.628	
34	125.006	8.515	129.585	82.390	0.205	0.031	7.216	1042.557	0.627	
35	125.000	8.666	130.000	82.557	0.208	0.031	7.323	1041.432	0.627	
36	125.001	8.501	129.311	82.541	0.205	0.031	7.225	1043.878	0.627	
37	125.725	8.486	129.996	82.433	0.205	0.031	7.219	1041.903	0.627	
38	125.017	8.569	129.637	82.658	0.207	0.031	7.284	1043.972	0.627	
39	125.000	8.530	128.207	82.785	0.206	0.031	7.243	1043.853	0.627	
40	125.000	8.601	128.119	82.882	0.207	0.031	7.289	1043.148	0.627	
41	125.001	8.704	125.143	83.140	0.207	0.031	7.290	1039.539	0.626	
42	125.000	8.683	124.674	83.150	0.207	0.031	7.269	1039.491	0.626	
43	125.000	16.393	84.881	76.074	0.218	0.032	7.595	1076.258	0.626	
44	125.001	9.023	125.430	83.467	0.213	0.031	7.497	1037.619	0.626	
45	125.032	8.251	124.461	82.618	0.198	0.031	6.980	1042.785	0.625	
46	125.000	9.275	119.450	84.018	0.215	0.031	7.531	1035.510	0.624	

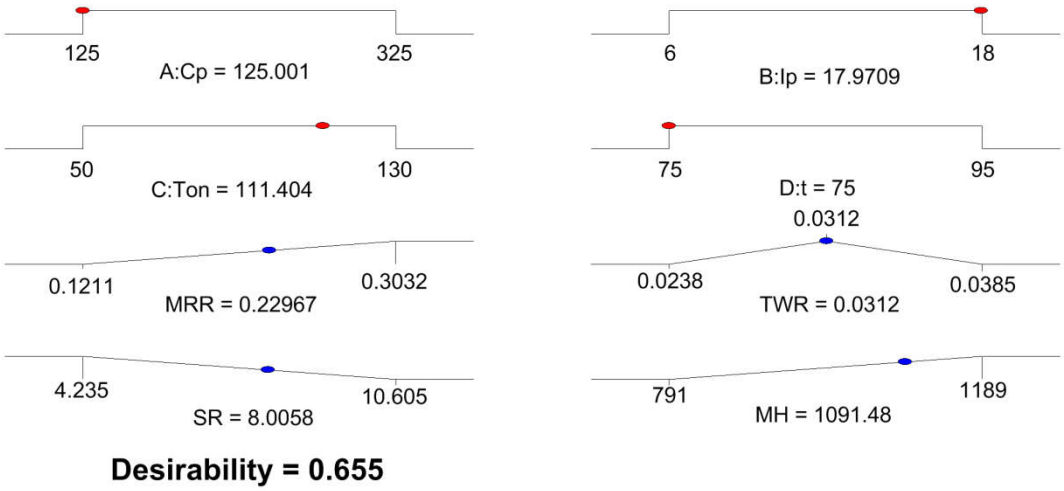

Figure 5.10 Ramp function graph of desirability for MRR, TWR, SR & MH

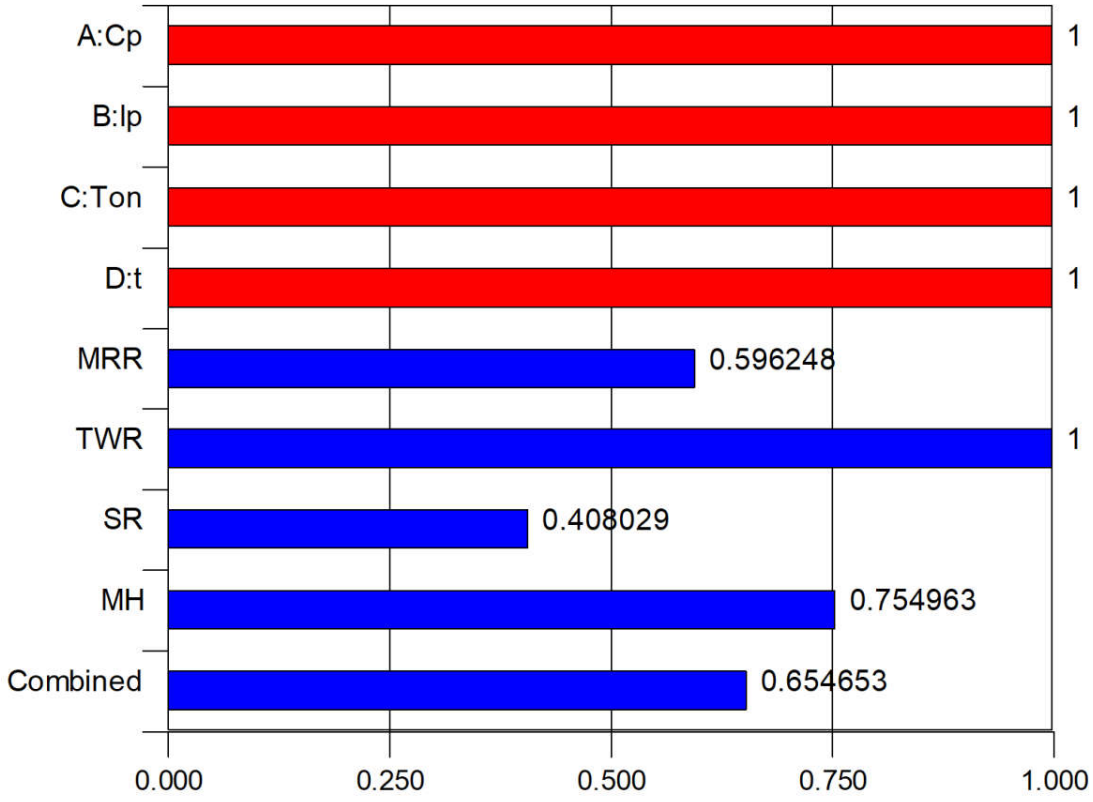

Figure 5.11 Bar graph of desirability for MRR, TWR, SR & MH

Table 5.15 indicates the levels of individual parameters, which considered as an optimal set for optimization of MRR, TWR, SR, and MH with the highest composite desirability. Further, the predicted value of individual responses at 95% of the confidence interval is given in Table 5.16. The predicted value of responses confirmed by performing an experiment on EDM by setting the level of parameters shown in Table 5.15. A good agreement between the predicted value and the experimental value of responses are observed, which strongly validate the predicted model for responses.

Table 5.15 Optimal set of parameters for MRR, TWR, SR, and MH

Factor coding	Name of Factor	Optimum level
A	Compaction Pressure (C_p)	125.001
B	Peak Current (I_p)	17.971
C	Pulse on Time (T_{on})	111.404
D	Duty Cycle (τ)	75.00

Table 5.16 Experimental validations of predicted responses (MRR, TWR, SR & MH)

Responses	Desirability	Predicted value	Experimental value	Prediction Error (%)
MRR (gm/min)	0.5962	0.230	0.239	3.76
TWR (gm/min)	1.00	0.031	0.033	6.06
SR (μm)	0.4080	8.006	8.428	5.00
MH (VHN)	0.7549	1091.475	1032.212	5.42
Overall composite desirability: 0.655				

The 3D surface plots for desirability are developed with keeping the selected parameters in range for maximum MRR and MH with minimum TWR & SR using Design Expert 10. Figure 5.12 (a) indicates the distribution of desirability for P20+Ni steel according to peak current and compaction pressure. It is concluded that composite desirability value is lower in the region of lower peak current with high compaction pressure. The overall composite desirability is observed higher than 0.655. Similarly, Figure 5.12 (b) indicate the distribution of desirability for duty cycle and pulse on time.

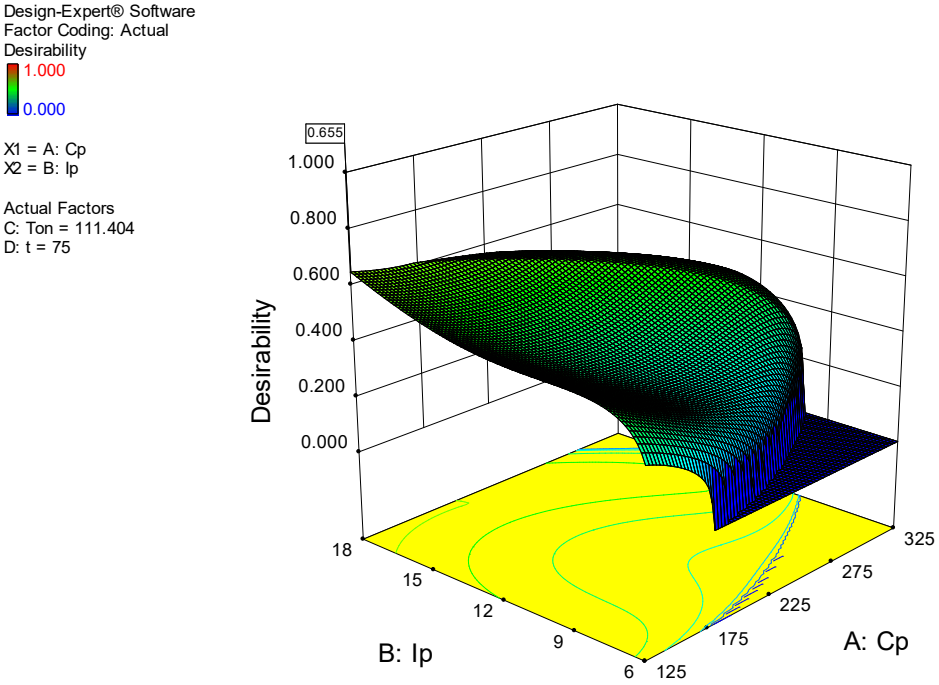

Figure 5.12 (a) 3D surface graph of desirability for MRR, TWR, SR & MH (I_p & C_p)

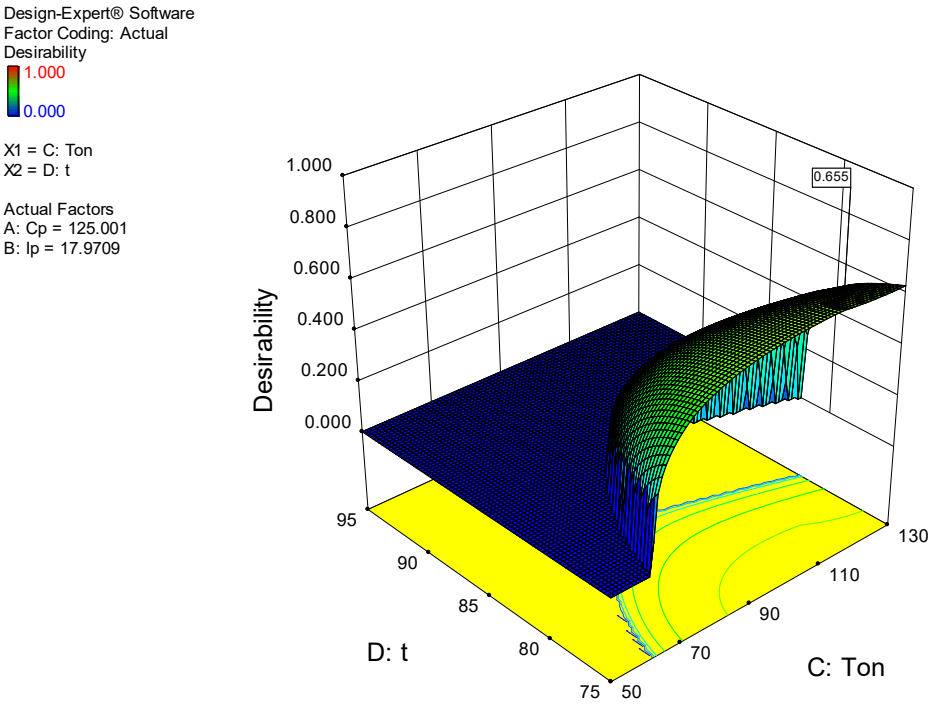

Figure 5.12 (b) 3D surface graph of desirability for MRR, TWR, SR & MH (τ & T_{on})

5.2.5 Optimization of MRR, TWR, SR, and MH (different weight & importance)

The goals and ranges of different input variables such as compaction pressure (C_p), peak current (I_p), pulse on time (T_{on}) and duty cycle (τ) with the response characteristics MRR, TWR, SR, and MH are given in Table 5.17. All the responses (MRR, TWR, SR & MH) have been assigned different importance index level and weight shown in the Table.

Table 5.17 Constraints of input parameters and responses (MRR, TWR, SR & MH)

Name	Goal	Lower Limit	Upper Limit	Lower Weight	Upper Weight	Importance
A:Compaction Pressure	is in range	125	325	1	1	3
B:Peak Current	is in range	6	18	1	1	3
C:Pulse on Time	is in range	50	130	1	1	3
D:Duty Cycle	is in range	75	95	1	1	3
MRR	maximize	0.1211	0.3032	**0.25**	1	**1**
TWR	minimize	0.0238	0.0385	1	**0.25**	**1**
SR	minimize	4.235	10.605	1	**0.5**	**3**
MH	maximize	791	1189	**1**	1	**5**

The main objective of the optimization is to obtain an optimal set of process parameters that will able to deliver the desired goal of responses. The value of desirability for individual responses varies from 0 to 1, and the result of the desirability of individual responses mainly depends on how closely the limits (upper and lower) are set compare to the actual optimum. A set of 44 optimal results are obtained for the specified constraints of design space for MRR, TWR, SR, and MH using statistical software Design Expert 10. The set of process parameters possessing maximum desirability is considered as an optimal condition for the desired responses. Table 5.18 indicates the optimal set of input process parameters with desirability required for obtaining an optimum combination of responses under given constraints.

Table 5.18 Set of optimum solutions for MRR, TWR, SR and MH

Sr. No	Cp	Ip	Ton	τ	MRR	TWR	SR	MH	Desirability	
1	324.990	12.577	50.047	95.000	0.167	0.036	5.864	1189.000	0.883	Selected
2	324.998	12.651	50.600	95.000	0.169	0.036	5.923	1189.019	0.882	
3	324.999	12.735	51.235	95.000	0.171	0.036	5.991	1189.067	0.881	
4	322.038	12.576	50.001	95.000	0.170	0.036	5.935	1188.997	0.881	
5	325.000	12.859	52.197	95.000	0.174	0.036	6.090	1189.000	0.879	
6	325.000	12.820	50.004	94.613	0.173	0.036	6.050	1189.000	0.879	
7	125.000	6.000	107.213	87.877	0.165	0.037	5.849	1189.001	0.878	
8	125.180	6.000	108.555	87.901	0.166	0.036	5.886	1189.000	0.878	
9	179.798	6.000	107.613	95.000	0.149	0.037	5.332	1189.000	0.878	
10	180.013	6.000	106.434	94.997	0.148	0.037	5.293	1189.001	0.878	
11	125.004	6.000	102.270	87.857	0.161	0.037	5.716	1188.997	0.878	
12	180.435	6.000	104.683	95.000	0.147	0.037	5.234	1189.001	0.877	
13	180.575	6.000	104.137	95.000	0.146	0.037	5.216	1189.000	0.877	
14	178.150	6.000	104.353	94.757	0.148	0.037	5.268	1188.998	0.877	
15	125.996	6.000	114.204	87.961	0.170	0.036	6.045	1189.004	0.877	
16	180.984	6.013	102.342	94.999	0.145	0.037	5.166	1189.000	0.877	
17	174.724	6.000	106.879	94.455	0.152	0.037	5.404	1189.001	0.877	
18	180.198	6.096	103.367	94.999	0.148	0.037	5.267	1189.000	0.877	
19	181.094	6.026	101.728	95.000	0.145	0.037	5.156	1189.000	0.877	
20	175.850	6.000	111.841	94.651	0.155	0.037	5.534	1189.002	0.877	
21	173.315	6.000	106.265	94.292	0.152	0.037	5.411	1189.001	0.877	
22	174.900	6.000	104.077	94.412	0.149	0.037	5.320	1189.001	0.877	

23	181.253	6.039	100.955	94.999	0.145	0.037	5.141	1189.000	0.877	
24	169.890	6.001	104.788	93.889	0.152	0.037	5.427	1188.997	0.876	
25	125.000	6.000	97.908	87.797	0.158	0.037	5.601	1189.332	0.876	
26	168.370	6.000	107.521	93.775	0.155	0.037	5.530	1189.002	0.876	
27	133.703	6.000	107.082	89.276	0.165	0.037	5.851	1189.001	0.876	
28	125.004	6.000	96.750	87.759	0.157	0.037	5.570	1189.000	0.876	
29	170.755	6.026	112.577	94.123	0.158	0.037	5.662	1189.001	0.876	
30	135.683	6.000	106.729	89.572	0.164	0.037	5.836	1188.999	0.876	
31	182.228	6.000	99.374	95.000	0.142	0.037	5.054	1188.149	0.876	
32	178.809	6.000	118.191	95.000	0.158	0.037	5.682	1188.997	0.875	
33	160.454	6.000	107.907	92.869	0.159	0.037	5.658	1189.000	0.875	
34	159.651	6.000	105.707	92.739	0.157	0.037	5.604	1188.999	0.875	
35	125.005	6.009	95.387	87.732	0.157	0.037	5.540	1189.000	0.875	
36	140.558	6.000	105.578	90.269	0.163	0.037	5.782	1188.999	0.875	
37	127.632	6.000	120.615	88.043	0.174	0.036	6.230	1188.999	0.875	
38	133.645	6.000	115.452	89.208	0.171	0.036	6.090	1188.999	0.875	
39	153.461	6.000	105.540	91.981	0.159	0.037	5.674	1189.000	0.875	
40	140.951	6.020	104.968	90.336	0.162	0.037	5.776	1188.998	0.875	
41	147.291	6.000	106.650	91.201	0.162	0.037	5.766	1188.999	0.875	
42	178.842	6.002	120.404	95.000	0.160	0.037	5.757	1189.000	0.874	
43	324.999	12.268	50.032	95.000	0.161	0.036	5.648	1175.005	0.874	
44	311.529	12.557	50.000	95.000	0.177	0.037	6.172	1189.000	0.873	

The optimum level of individual process parameters and responses with composite desirability are represented in the form of the dot in the ramp function graph shown in figure 5.13. The level of the dot in ramp function indicates how much desirable individual parameter. The lower and upper weight for the individual parameter with the importance index is assigned for all four process parameters as per Table 5.17. The bar graph shown in Figure 5.14 indicates the individual desirability of responses MRR, TWR, SR and MH with its composite desirability. The composite desirability varies between 0 to 1 and its value mainly depending on how close individual responses (MRR, TWR, SR & MH) towards the target.

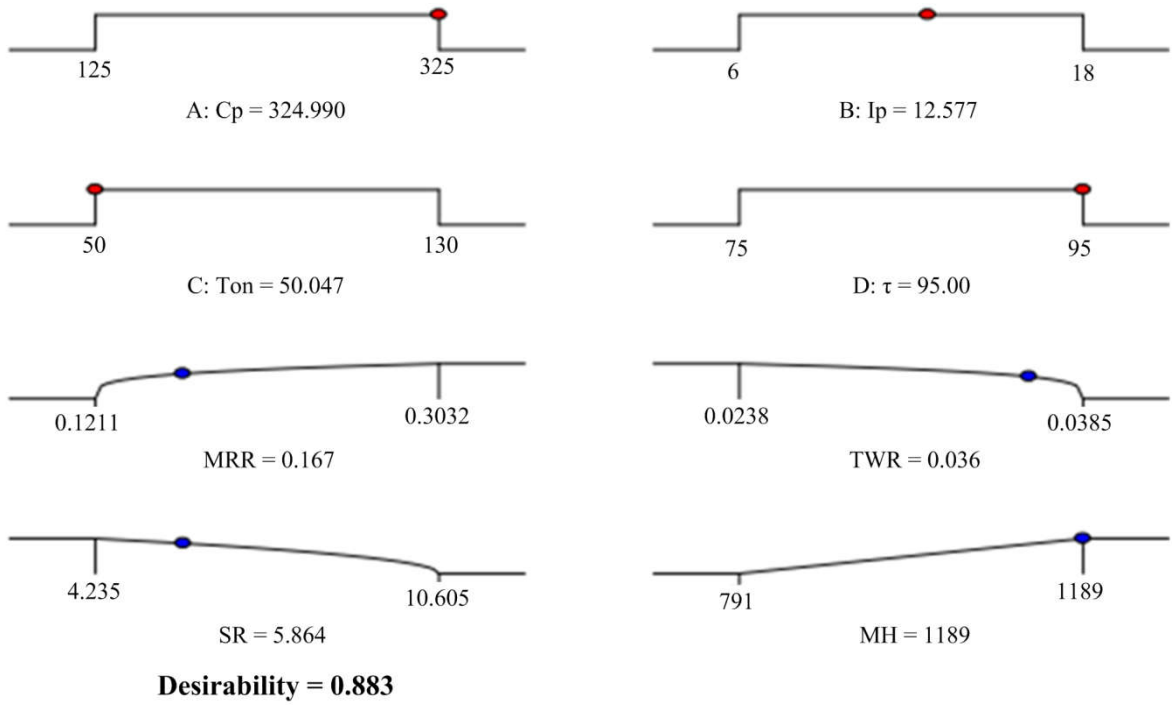

Figure 5.13 Ramp function graph of desirability for MRR, TWR, SR & MH

Table 5.19 indicates the levels of individual parameters, which is considered as an optimal set for optimization of MRR, TWR, SR, and MH with the highest composite desirability. Further, the predicted value of individual responses at 95% of the confidence interval is given in Table 5.20. The predicted value of responses confirmed by performing an experiment on EDM by setting the level of parameters shown in Table 5.19. Good agreement between the predicted value and the experimental value of responses are observed, which strongly validate the predicted model of responses.

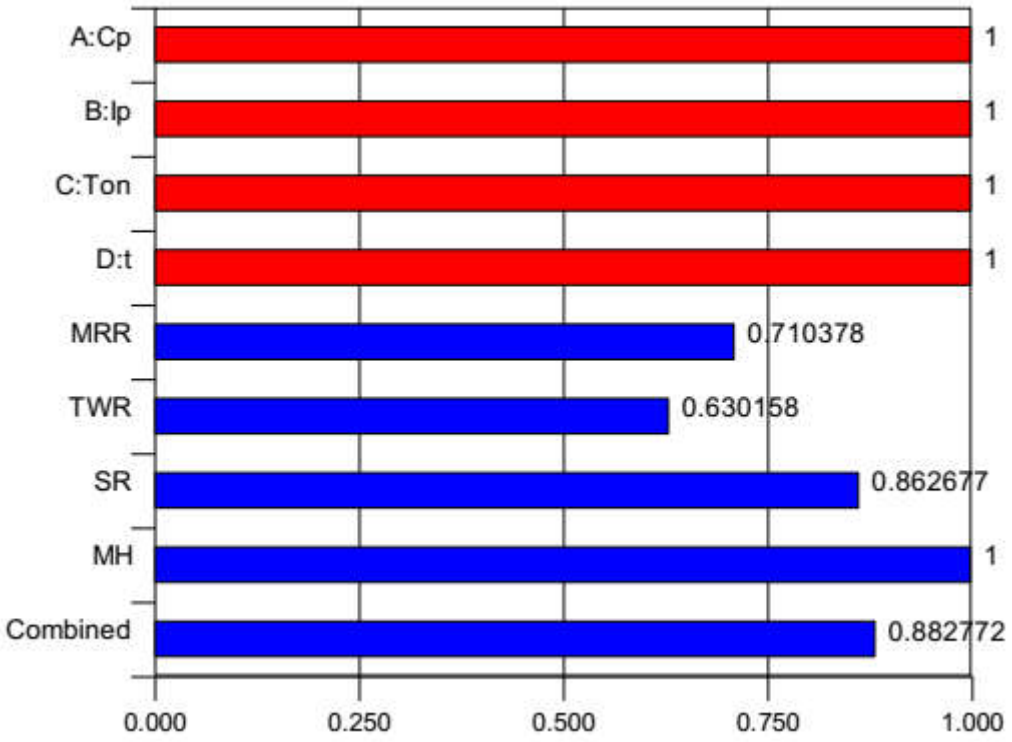

Figure 5.14 Bar graph of desirability for MRR, TWR, SR & MH

Table 5.19 Optimal set of parameters for MRR, TWR, SR, and MH

Factor coding	Name of Factor	Optimum level
A	Compaction Pressure (C_p)	324.990
B	Peak Current (I_p)	12.577
C	Pulse on Time (T_{on})	50.047
D	Duty Cycle (τ)	95.00

Table 5.20 Experimental validations of predicted responses (MRR, TWR, SR & MH)

Responses	Desirability	Predicted value	Experimental value	Prediction Error (%)
MRR (gm/min)	0.7103	0.167	0.174	4.02
TWR (gm/min)	0.6301	0.036	0.0371	2.96
SR (μm)	0.8626	5.864	6.211	5.58
MH (HVN)	1.0000	1189.000	1114.56	6.26
Overall composite desirability: 0.883				

The 3D surface plots for desirability are developed with keeping the selected parameters in range for maximum MRR & MH with minimum TWR & SR using Design Expert 10. Figure 5.15 (a) indicates the distribution of desirability for P20+Ni steel according to peak current and compaction pressure. It is concluded that composite desirability value is higher

in the region of low peak current with high compaction pressure. The overall composite desirability is observed higher than 0.88. Similarly, Figure 5.15(b) indicates the distribution of desirability for duty cycle and pulse on time.

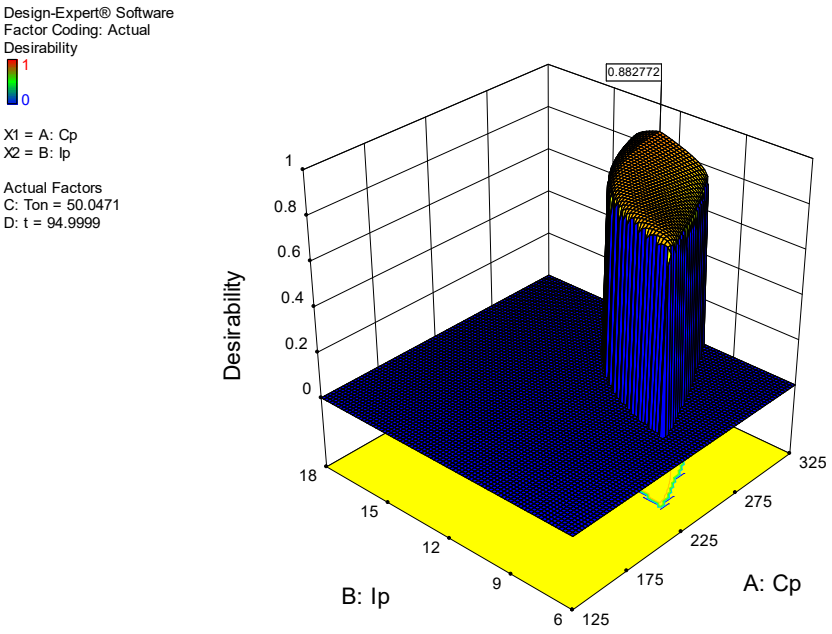

Figure 5.15 (a) 3D surface graph of desirability for MRR, TWR, SR & MH (I_p & C_p)

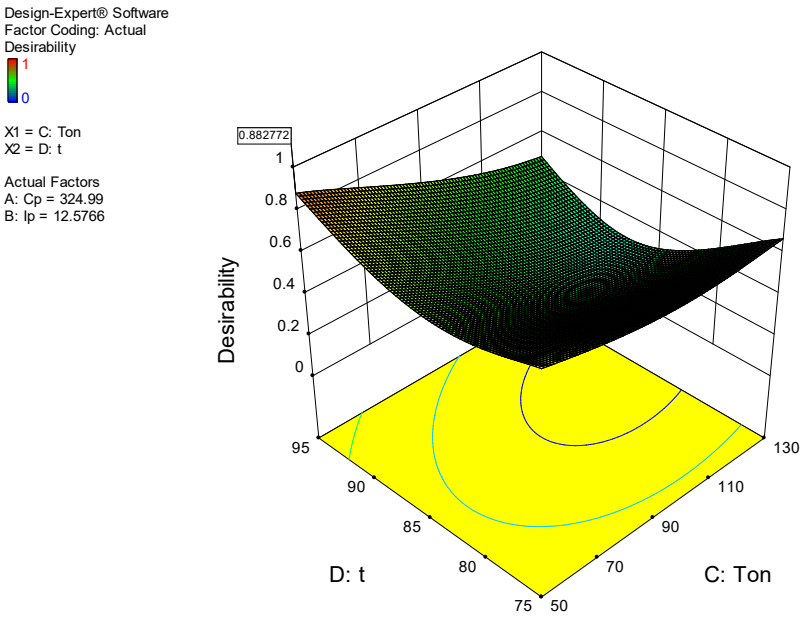

Figure 5.15 (b) 3D surface graph of desirability for MRR, TWR, SR & MH (τ & T_{on})

5.2.6 Optimization of MRR, TWR, SR, and MH (different weight & target)

The goals and ranges of different input variables such as compaction pressure (C_p), peak current (I_p), pulse on time (T_{on}) and duty cycle (τ) with the response characteristics MRR, TWR, SR, and MH are given in Table 5.21. All the responses (MRR, TWR, SR & MH) have been given the desired importance index level, weight, and target value.

Table 5.21 Constraints of input parameters and responses (MRR, TWR, SR & MH)

Name	Goal	Lower Limit	Upper Limit	Lower Weight	Upper Weight	Importance
A:Compaction Pressure	is in range	125	325	1	1	3
B:Peak Current	is in range	6	18	1	1	3
C:Pulse on Time	is in range	50	130	1	1	3
D:Duty Cycle	is in range	75	95	1	1	3
MRR	maximize	0.1211	0.3032	**0.25**	1	**1**
TWR	minimize	0.0238	0.0385	1	**0.25**	**1**
SR	Is Target = 4.5	4.235	10.605	1	**1**	**5**
MH	Is Target = 1189	791	1189	**1**	1	**5**

The main objective of the optimization is to derive an optimal set of process parameters that able to deliver the desired goal of responses. The value of desirability for individual responses varies from 0 to 1, and the result of the desirability of individual responses mainly depends on how closely the limits (upper and lower) are set compare to the actual optimum. A set of 63 optimal results are obtained for the specified constraints of design space for MRR, TWR, SR, and MH using statistical software Design Expert 10. The set of process parameters possessing maximum desirability is considered as an optimal condition for the desired responses. Table 5.22 indicates the optimal set of input process parameters with desirability required for obtaining an optimum combination of responses under given constraints.

Table 5.22 Set of optimum solutions for MRR, TWR, SR, and MH

Sr. No	Cp	Ip	Ton	τ	MRR	TWR	SR	MH	Desirability	
1	187.509	6.000	87.507	95.000	0.132	0.037	4.653	1188.944	0.884	Selected
2	187.640	6.004	87.211	94.999	0.132	0.037	4.646	1188.999	0.884	
3	186.770	6.000	88.786	95.000	0.133	0.037	4.697	1188.983	0.884	
4	187.410	6.000	86.813	94.942	0.132	0.037	4.640	1188.528	0.884	
5	188.446	6.002	86.575	95.000	0.131	0.037	4.616	1187.474	0.884	
6	188.173	6.038	85.991	94.996	0.132	0.037	4.632	1188.999	0.884	
7	189.387	6.000	84.421	95.000	0.129	0.037	4.546	1189.001	0.884	
8	189.545	6.001	84.168	94.999	0.129	0.037	4.538	1188.998	0.884	
9	189.407	6.068	83.899	95.000	0.130	0.038	4.582	1188.999	0.883	
10	185.216	6.008	91.645	95.000	0.136	0.037	4.802	1189.002	0.883	
11	189.965	6.099	82.826	94.998	0.130	0.038	4.570	1188.998	0.882	
12	185.365	6.000	84.479	94.625	0.132	0.038	4.630	1189.000	0.882	
13	191.898	6.175	79.725	95.000	0.129	0.038	4.521	1188.998	0.880	
14	183.362	6.000	79.919	94.143	0.130	0.038	4.575	1188.998	0.877	
15	176.609	6.000	88.164	93.969	0.138	0.037	4.879	1188.999	0.876	
16	179.056	6.000	81.855	93.847	0.134	0.038	4.695	1188.988	0.876	
17	199.695	6.531	72.834	95.000	0.129	0.038	4.501	1177.887	0.873	
18	200.476	6.662	70.395	95.000	0.130	0.038	4.531	1182.341	0.870	
19	174.362	6.003	97.730	94.163	0.145	0.037	5.158	1189.002	0.870	
20	212.474	7.078	63.682	95.000	0.130	0.038	4.500	1166.527	0.865	
21	212.595	7.093	63.244	95.000	0.130	0.038	4.500	1167.914	0.865	
22	217.049	7.277	60.151	95.000	0.130	0.038	4.500	1167.287	0.862	

23	219.858	7.375	58.897	95.000	0.130	0.038	4.500	1164.646	0.862	
24	221.065	7.421	58.205	95.000	0.130	0.038	4.500	1164.353	0.861	
25	156.154	6.000	89.579	91.792	0.148	0.038	5.219	1189.002	0.861	
26	239.320	8.064	50.017	95.000	0.130	0.038	4.500	1160.194	0.859	
27	240.329	8.089	50.000	94.988	0.130	0.038	4.500	1157.679	0.859	
28	125.001	6.000	85.553	87.326	0.150	0.038	5.287	1188.976	0.857	
29	125.000	6.000	86.922	87.395	0.151	0.038	5.321	1188.998	0.857	
30	125.001	6.000	83.251	87.083	0.149	0.038	5.225	1185.811	0.856	
31	125.000	6.000	82.171	86.903	0.148	0.038	5.192	1182.708	0.856	
32	125.001	6.000	83.766	86.936	0.149	0.037	5.228	1181.108	0.856	
33	125.001	6.000	81.493	86.821	0.147	0.038	5.174	1181.630	0.856	
34	144.942	6.000	86.308	90.234	0.149	0.038	5.249	1188.998	0.856	
35	125.000	6.000	80.068	86.633	0.146	0.038	5.134	1179.088	0.855	
36	142.360	6.000	87.533	89.957	0.150	0.038	5.296	1188.998	0.855	
37	125.000	6.000	79.168	86.575	0.146	0.038	5.113	1179.133	0.855	
38	130.367	6.000	86.279	88.195	0.151	0.038	5.309	1188.975	0.855	
39	140.941	6.000	87.013	89.740	0.150	0.038	5.292	1188.998	0.855	
40	130.875	6.000	86.683	88.293	0.151	0.038	5.319	1188.995	0.855	
41	242.351	8.444	50.000	95.000	0.137	0.037	4.719	1157.191	0.855	
42	141.025	6.000	85.732	89.641	0.149	0.038	5.260	1187.623	0.855	
43	139.034	6.000	86.970	89.478	0.150	0.038	5.302	1188.998	0.854	
44	136.903	6.000	86.911	89.177	0.151	0.038	5.310	1188.974	0.854	
45	130.033	6.000	92.863	88.433	0.155	0.037	5.474	1189.002	0.853	
46	125.000	6.000	74.104	85.714	0.142	0.038	4.965	1166.940	0.852	
47	125.037	6.105	81.305	86.941	0.149	0.038	5.238	1182.255	0.852	

48	166.051	6.003	106.998	93.507	0.156	0.037	5.553	1189.002	0.852	
49	153.550	6.001	101.665	91.914	0.157	0.037	5.564	1189.002	0.850	
50	125.000	6.000	70.715	85.137	0.139	0.038	4.867	1160.208	0.850	
51	125.011	6.000	70.338	85.111	0.139	0.038	4.859	1160.391	0.850	
52	325.000	11.724	50.030	95.000	0.151	0.035	5.263	1151.654	0.849	
53	324.809	11.493	50.001	95.000	0.146	0.035	5.103	1142.530	0.849	
54	253.115	8.577	50.000	95.000	0.133	0.036	4.607	1135.979	0.849	
55	130.637	6.000	97.613	88.670	0.158	0.037	5.597	1188.998	0.849	
56	125.000	6.000	68.199	84.679	0.137	0.038	4.793	1155.311	0.847	
57	325.000	12.083	50.000	94.993	0.158	0.035	5.518	1166.842	0.847	
58	321.756	11.206	50.000	95.000	0.143	0.034	4.974	1131.599	0.845	
59	325.000	12.163	50.426	95.000	0.160	0.035	5.579	1167.910	0.845	
60	136.595	6.000	101.260	89.638	0.160	0.037	5.681	1189.002	0.845	
61	321.075	11.108	50.000	95.000	0.141	0.034	4.920	1128.023	0.844	
62	125.000	6.000	64.875	83.918	0.134	0.037	4.685	1146.546	0.843	
63	140.487	6.001	102.885	90.221	0.161	0.037	5.708	1189.002	0.843	

The optimum level of individual process parameters and responses with composite desirability are represented in the form of the dot in the ramp function graph shown in Figure 5.16. The level of the dot in ramp function indicates how much desirable individual parameter. The lower and upper weight for the individual parameter with the importance index assigned for all selected parameters as per Table 5.21. The bar graph shown in Figure 5.17 indicates the individual desirability of responses MRR, TWR, SR and MH with composite desirability. The composite desirability varies between 0 to 1 and its value mainly depending on how the closeness of individual responses (MRR, TWR, SR & MH) towards the target.

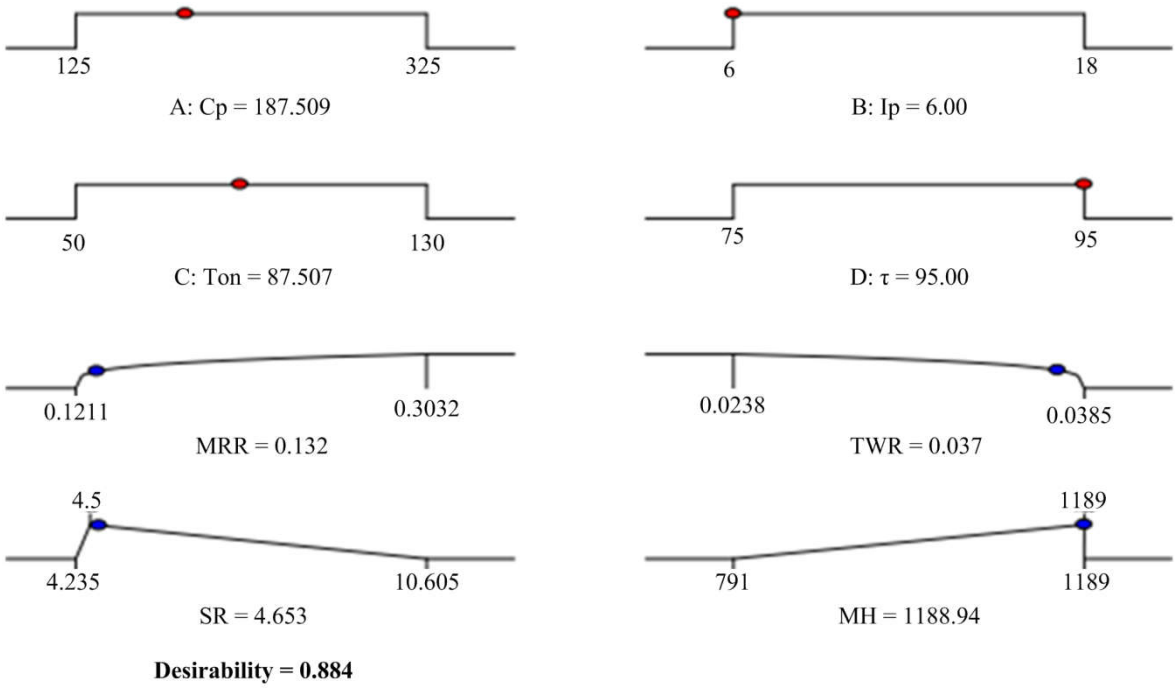

Figure 5.16 Ramp function graph of desirability for MRR, TWR, SR & MH

Table 5.23 indicates the levels of individual parameters, which is considered as an optimal set for optimization of MRR, TWR, SR, and MH with the highest composite desirability. Further, the predicted value of individual responses at 95% of the confidence interval is given in Table 5.24. The predicted value of responses confirmed through performing an experiment on EDM with a setting the level of parameters shown in Table 5.23. Good agreement between the predicted value and the experimental value of responses are observed, which strongly validate the predicted model of responses.

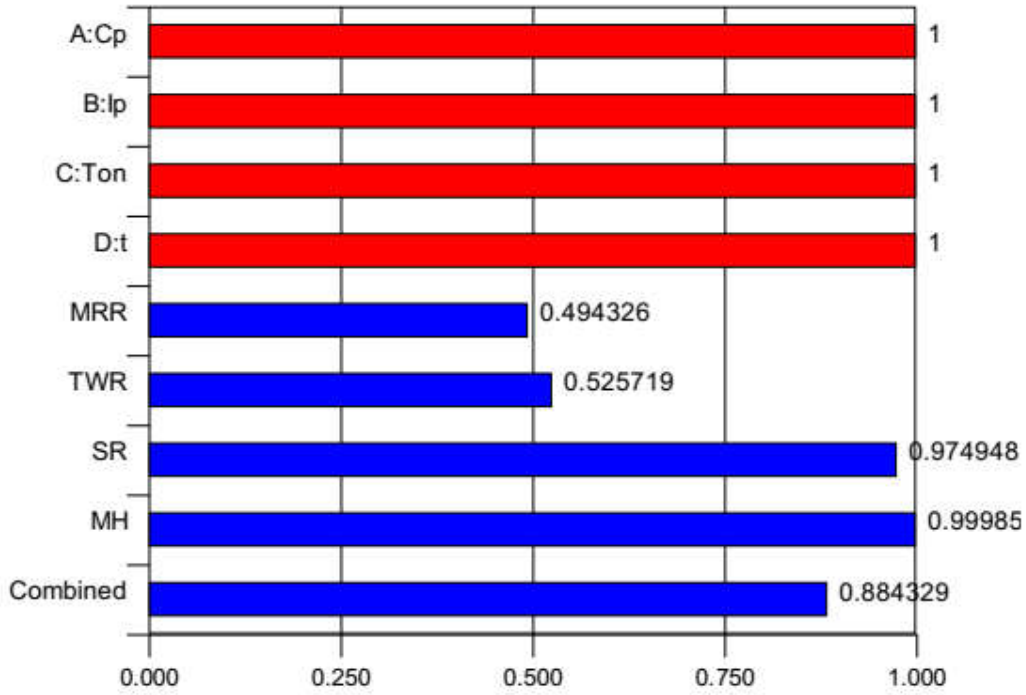

Figure 5.17 Bar graph of desirability for MRR, TWR, SR & MH

Table 5.23 Optimal set of parameters for MRR, TWR, SR, and MH

Factor coding	Name of Factor	Optimum level
A	Compaction Pressure (C_p)	187.509
B	Peak Current (I_p)	6.000
C	Pulse on Time (T_{on})	87.507
D	Duty Cycle (τ)	95.000

Table 5.24 Experimental validations of predicted responses (MRR, TWR, SR & MH)

Responses	Desirability	Predicted value	Experimental value	Prediction Error (%)
MRR (gm/min)	0.4943	0.132	0.127	3.78
TWR (gm/min)	0.5257	0.037	0.0358	3.24
SR (μm)	0.9749	4.653	4.419	5.02
MH (HVN)	0.9998	1188.944	1136.154	4.44
Overall composite desirability: 0.884				

The 3D surface plots for desirability are developed with keeping the selected parameters in range for maximum MRR & MH with minimum TWR & SR using Design Expert 10. Figure 5.18 (a) indicates the distribution of desirability for P20+Ni steel according to peak current and compaction pressure. It is concluded that the composite desirability value is higher in the region of low peak current with high compaction pressure. The overall

composite desirability is observed higher than 0.88. Similarly, Figure 5.18 (b) indicates the distribution of desirability for duty cycle and pulse on time.

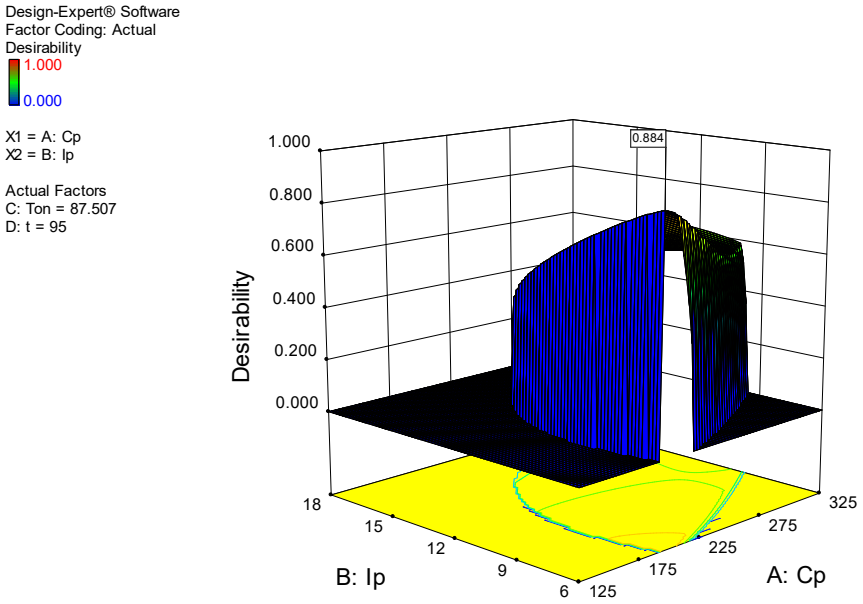

Figure 5.18 (a) 3D surface graph of desirability for MRR, TWR, SR & MH (I_p & C_p)

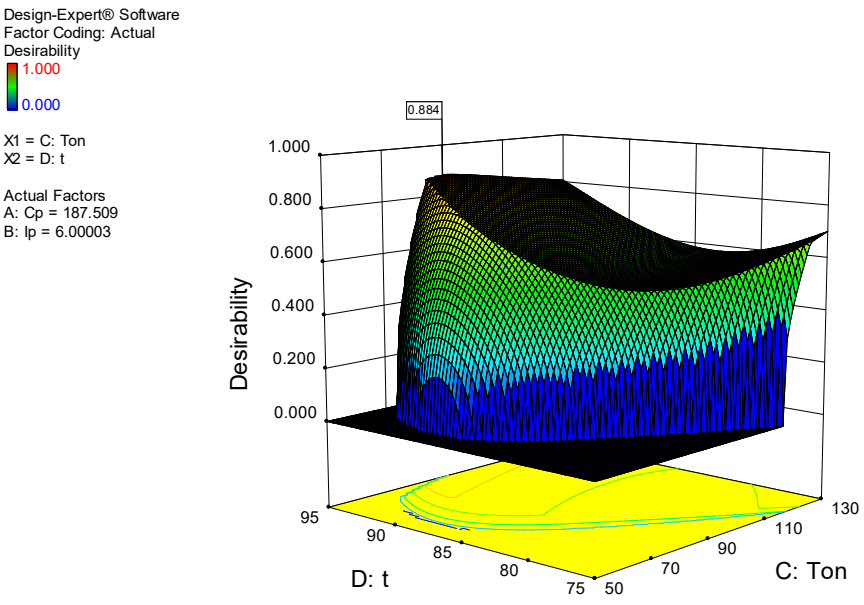

Figure 5.18 (b) 3D surface graph of desirability for MRR, TWR, SR & MH (τ & T_{on})

CHAPTER – 6

CONCLUSION AND SCOPE FOR FUTURE WORK

6.1 CONCLUSION

In the present experimental work, an attempt is made to study the surface modification process performed on P20+Ni die steel using EDM. The process was carried out on EDM using specially manufactured green composite powder metallurgy electrode. Effect of different parameters such as compaction pressure (C_p), peak current (I_p), pulse on time (T_{on}) and duty cycle (τ) was investigated using response surface methodology (RSM). The following inferences can be drawn from the results of experimentation:

1. Surface modification with green P/M composite electrodes using EDM is found to be a promising alternative method to eliminates expensive and time-oriented secondary surface treatments such as PVD, CVD, plasma spraying, etc.
2. The proposed green composite powder metallurgy electrode is capable to improve EDM performance with a substantial increase in microhardness of machined surface.
3. The matching between predicted R^2 and experimental R^2 values for all selected variables are found reasonably well throughout the design space:

Parameter	Pred. R-Squared	R-Squared
MRR	0.9929	0.9984
TWR	0.8172	0.9677
SR	0.9925	0.9986
MH	0.8904	0.9805

4. Peak current is observed most significant parameter contributing 72% for MRR, 25.5% for TWR, 72.8% for SR and 23% for MH during ANOVA analysis. Similarly, duty cycle, pulse on time and compaction pressure also play an important role to meet desired objectives.

5. The second order polynomial regression equation (statistical model) obtained using RSM for MRR = 0.22 – 0.032 * C_p + 0.085 * I_p + 0.022 * T_{on} + 0.033 * τ + 7.850 E-003 * C_pI_p – 0.012 * $C_p\tau$ + 0.024 * $I_p\tau$ – 0.014 * C_p^2 – 0.011 * I_p^2 + 4.658 E-003 * T_{on}^2 – 0.015 * τ^2
6. The second order polynomial regression equation (statistical model) obtained using RSM for TWR = 0.027 – 3.425 E-003 * C_p + 4.258 E-003 * I_p – 3.025 E-003 * T_{on} + 3.575 E-003 * τ + 2.925 E-003 * C_pI_p + 2.375 E-003 *C_pT_{on} – 4.775 E-003 *$C_p\tau$ – 2.125 E–003 * $T_{on}\tau$ + 3.588 E–003 * C_p^2 + 2.838 E-003 * I_p^2 + 3.138 E-003 * T_{on}^2 + 3.888 E-003 * τ^2
7. The second order polynomial regression equation (statistical model) obtained using RSM for SR = 7.63 – 1.08 C_p + 3.01 I_p + 0.77 T_{on} + 1.12 τ + 0.30 C_pI_p– 0.50 $C_p\tau$ + 0.85 $I_p\tau$ + 0.18 $T_{on}\tau$ – 0.46 C_p^2 – 0.30 I_p^2 + 0.19 T_{on}^2 - 0.51 τ^2
8. The second order polynomial regression equation (statistical model) obtained using RSM for MH = 841.17 – 109.92 C_p + 117.92 I_p – 83.92 T_{on} + 111.42 τ + 58.75 C_pI_p– 115.25 $C_p\tau$ – 60.25 I_pT_{on}– 53.25 $T_{on}\tau$ + 119.54 C_p^2 + 117.04 I_p^2 + 57.54 T_{on}^2 + 129.54 τ^2
9. The maximum value of MRR obtained is 0.3032 gm/min during experiment performed at compaction pressure 175 kg/cm^2, peak current 15-A, pulse on time 110 μs and duty cycle 90%. From above result, it can be concluded that higher value of peak current and duty cycle should be selected to obtain maximum MRR.
10. The minimum value of TWR obtained is 0.0238 gm/min during an experiment performed at compaction pressure 225 kg/cm^2, peak current 6-A, pulse on-time 90 μs and duty cycle 85%. P/M electrode with high compaction pressure and minimum value of peak current is desired to lower the TWR.
11. The minimum value of SR obtained is 4.2 μm during an experiment performed at compaction pressure 225 kg/cm^2, peak current 6-A, pulse on-time 90 μs and duty cycle 85%. Experiments performed with a lower value of peak current contributing most to obtain good surface finish.
12. The maximum value of MH obtained is 1189 VHN during an experiment performed at compaction pressure 175 kg/cm^2, peak current 15-A, pulse on-time 70 μs and duty cycle 90%, which shows more than 300% improvements as compared to base material. From the above result, it can be concluded that the higher value of peak current and duty cycle are prominent factors to obtain high microhardness.

13. Composite desirability approach (using RSM) is collectively used to optimize the process parameters to achieve combined objectives of maximum MRR & MH with minimum TWR & SR. The set of parameters at maximum value of composite desirability 88.4% is: compaction pressure = 187.5 kg/cm^2, peak current = 6-A, pulse on-time = 87.5 μs and duty cycle = 95%.
14. The Cu-W-Si green P/M composite electrode is capable to modify the surface of P20+Ni die steel. Under appropriate machining condition a significant amount of copper (24.23%), tungsten (7.51%) and silicon (0.75%) were observed on the machined surface as compared to the base material.
15. The presence of tungsten carbide (WC & W_2C) and silicon carbide (SiC) are observed during XRD analysis of the machined surface indicating migration of silicon and tungsten from P/M electrode and react with dissociated carbon from hydrocarbon oil (dielectric) at very high temperature. The formation of silicon carbide and tungsten carbide leads to significant improvement in microhardness.
16. Presence of a sufficient amount of copper is also observed with tungsten and silicon on the machined surface during the EDS analysis. Migration of copper from P/M electrode forms a solid solution with the ferrite phase, which helps to improve the quality of the machined surface. No adverse effect of copper is observed on die steel surface.
17. No major surface defects such as microcracks, voids, etc. are observed on the EDMed surface during SEM analysis. So, it can be concluded that the surface modification process performed on EDM using P/M electrode does not deteriorate the quality of the machined surface.
18. The process is capable to improve microhardness more than three times as compared to the base material. Improvement in microhardness helps to enhance wear and abrasion resistance and hence the life of die and press tools can be substantially improved by this technique. The presence of tungsten carbide (WC, W_2C) helps to improve the red hardness of die steel and hence, die surface becomes suitable for hot working applications.
19. The EDS analysis reveals that the maximum and minimum amounts of % tungsten by weight possess an inverse relationship with peak current, i.e. 7.51% and 4.47% tungsten by weight is observed while machining at peak current 6-A and 18-A respectively. From the above results, it can be concluded that the lower value of peak current is suitable to transfer a large amount of tungsten on the work material.

6.2 RECOMMENDATION FOR FUTURE WORK

From the result of the present experimental work, it is felt that the surface modification of P20+Ni die steel using green P/M composite electrode is successfully completed. However, the process opens a vast number of avenues for further exploration. One can choose the following different directions for further exploration:

1. AISI P20+Ni die steel (which is widely used die steel for large plastic mould) was chosen for present experimental work. Other plastic mould steels such as corrosion-resistant steel (AISI 420, AISI 440B, AISI 630), pre-heat treated steel (P20), alloyed tool steel (D2, O1, H11, and H13), air hardening cold work die steel (A-series), water hardening die steel (W-series) can be considered for surface modification.
2. Powder metallurgy electrode can be prepared from different alloying elements such as cobalt, molybdenum, chromium, vanadium, and nickel. The composition and powder particle size can be varied to study its effects on surface properties with different compaction pressure and sintering temperature.
3. The cross-sectional area of the P/M electrode was kept constant throughout the experimentation. One can study the effects of the different cross-sectional area of P/M electrode on response characteristics.
4. EDM oil (Pecific-300) was used as a dielectric. Some other dielectric medium can be used to study its effects and role in the surface modification process. The side flushing system was used with constant flushing pressure of 0.75 kg/cm^2. Flushing pressure can be varied to study its influence on surface characteristics.
5. Wear measurement and corrosion test of the machined surface can be considered for predicting improvements in wear and corrosion behavior.

List of References

1. Fuller John E. (1996), "Electrical Discharge Machining", in ASM Machining Handbook, Vol. 16, pp 557-564.
2. Pandey P C and Shan H S (1995), "Modern Machining Processes", Tata McGraw Hill, New Delhi, India, ISBN 0-07-096518-8.
3. Dewes R, Aspinwall D, Simao J and Lee H G (2003), "Electrical Discharge Machining and Surface Alloying – The Process, Parameters and State of Play", Materials World, Vol. 11, No. 5, pp 16-18.
4. Tsukahara H and Sone T (2000), "Surface hardening of titanium using EDM process,' Titan. Japan, Vol. 48 (2), pp 47-49.
5. Lucca D A, Brinksmeirer E and Goch G (1998), "Progress in assessing surface and subsurface integrity", Annals of the CIRP, Vol. 47(2), pp 669-693.
6. Lahiri B N (2001), "Understanding EDM technology", Lecture notes of Summer Programme on Advanced Manufacturing, IIT Kharagpur, pp 61-77.
7. Jain V K (2004), "Advanced Machining Processes", Allied Publishers, New Delhi, India, ISBN 81-7764-294-4.
8. Zolotykh B N (1995), "Modern physical theory of electric erosion of metals- the basis of development of new directions in EDM", Proceedings of ISEM-XI, pp 114-116.
9. K.H. Ho, S.T. Newman, State of the art electrical discharge machining (EDM), Int. J. Mach. Tools Manuf. 43 (2003) 1287–1300.
10. G. Boothroyd, A.K. Winston, Fundamentals of Machining and Machine Tools, CRC Press, Taylor & Francis Group, Boca Raton, 1989.
11. Marafona J. and Wykes C. (2000), "A new method of optimizing material removal rate using EDM with copper tungsten electrodes", Int. J. of Machine tools & manufacture, Vol. 40 (2), pp 153-164.
12. Mohri N, Saito N and Tsunekawa Y (1993), "Metal Surface modification by electrical discharge machining with composite electrodes," Annals of the CIRP, Vol. 42 (1), pp 219-222.
13. ASM Handbook : Surface Engineering (1999), Vol. 5, ASM International, USA, ISBN : 0-87170-384-X.
14. Galerie A, Pons M and Caillet M (1989), "Surface modification using lasers and ion beams", Material Science and Technology, Vol. 5, pp 806-812.
15. Prabhudev K H (2000), "Handbook of Heat Treatment of Steels", Tata McGraw Hill Publishing Company, New Delhi, India. ISBN 0-07-451831-3.
16. Galerie A, Pons M and Caillet M (1989), "Surface modification using lasers and ion beams", Material Science and Technology, Vol. 5, pp 806-812.
17. Ghosh A., Malik A.K. (2009), "Manufacturing Science", East-West Press Private Limited, ISBN-978-81-7671-063-3.
18. Singh G. (2009), "Investigation on improvement of material properties and parametric optimization of MRR, TWR and Roughness using powder mixed EDM", Thesis, Thapar University, Patiala.
19. Kalpakjian S and Schmid S R (2001), "Manufacturing Engineering & Technology", 4th Edition, Pearson Education Inc., USA. ISBN 81-7808-157-1.
20. Schumacher B M (2004), "After 60 years of EDM, the discharge process remains still disputed", Int. Journal of Materials Processing Technology, Vol. 149, pp 376-381.
21. EDM Tech. Manual, Poco Graphite Inc.
22. Popat, Mitesh A.,(2011), "An investigation and analysis of Process Parameters for EDM Drilling machine using Taguchi method", thesis PhD, Saurashtra University.
23. Barash M. (1965), "Effect of EDM on Surface Properties of Tool and Die Steels", Metals Engineering Quarterly, 5/4, 48.
24. Kun Ling Wu, Biing Hwa Yan, Fuang Yuan Huang, Shin Chang Chen (2005), "Improvement of surface finish and surfactant added dielectric", International Journal of Machine Tools and Manufacture, 45, 1195-1201.
25. Guu Y.H., Hocheng H., Chou C.Y., Deng C.S. (2003), "Effect of electrical discharge machining on surface characteristics and machining damage of AISI D2 tool steel", Material Science and Engineering A, 358, 37-43.
26. Lin H.C., Lin K.M., Cheng I.S. (2001), "The electro discharge machining characteristics of Ti Ni shape memory alloys", Journal of Materials Science, 36, 399-404.
27. Gurumurthy T., Arvind B.M., Sudhendra G. (1986), "Development of a Data Bank for Electrical Discharge Machining", Proc. of 12th AIMTDR Conf. IIT Delhi.
28. Ho K H and Newman S T (2003), "State of the art electrical discharge machining", Int. J. of Machine Tools and Manufacture, Vol. 43, pp 1287-1300.

29. George V and Philip P K (1978), “Analysis of EDM Performance and Tool Wear in Cu-Die Steel system – A Review”, Proceedings of the 8th AIMTDR Conference, IIT Bombay.
30. Lazarenko B R (1943), “To invert the effect of wear on electric power contacts”, Dissertation of The All-Union Institute for Electro Technique in Moscow / CCCP (in Russian).
31. Jameson E C (2001), “Description and development of electrical discharge machining”, Society of Manufacturing Engineers, Dearbern, Michigan, USA.
32. McGeough J A (1988), “Advanced Methods of Machining”, Chapman and Hall, USA, 1st Edition, ISBN 0-412-31970-5.
33. Crookall J R and Heuvelman C J (1971), “Electro-discharge machining – the state of the art”, Annals of the CIRP, Vol. 20 (1), pp 113-120.
34. Williams E.M. (1952), “Theory of Electric Spark Machining”, AIEE Trans. (Application and Industry), 71, 105.
35. McGeough J A (1988), “Advanced Methods of Machining”, Chapman and Hall, USA, 1st Edition, ISBN 0-412-31970-5.
36. Crookall J R and Heuvelman C J (1971), “Electro-discharge machining – the state of the art”, Annals of the CIRP, Vol. 20 (1), pp 113-120.
37. Venkatesh V.C., Parasnis S. (1972), “Surface Transformation in High Speed Steel after EDM”, Proc. of 5th AIMTDR Conf., I.I.T. Roorkee, 639.
38. C.P. Khatter (2009) Thesis on “Analysis of surface integrity in electrical discharge machining (EDM) process for tungsten carbide material”.
39. Venkatesh V.C., Parasnis S. (1972), “Surface Transformation in High Speed Steel after EDM”, Proc. of 5th AIMTDR Conf., I.I.T. Roorkee, 639.
40. H.C. Tsai, B.H. Yan, F.Y. Huang, (2003), EDM performance of Cr/Cu-based composite electrodes, International Journal of Machine Tools & Manufacture 43, 245–252.
41. M.S. Shunmugam and P.K. Philip, (1994), Improvement of wear resistance by EDM with tungsten carbide P/M electrode, wear**,** 171, l-5.
42. Balbir Singh, Jatinder Kumar, Sudhir Kumar, (2015), Optimization and surface modification in electrical discharge machining of AA 6061/SiC_p composite using Cu–W electrode , J Materials: Design and Applications 0(0) 1–17.
43. Can Cogun, Ziya Esen, Asim Genc, Ferah Cogun, Nizami Akturk, 2015, Effect of powder metallurgy Cu-B4C electrodes on workpiece surface characteristics and machining performance of electric discharge machining , J Engineering Manufacture 1–14.
44. P. K. Patowari, U. K. Mishra, Partha Saha, P. K. Mishra, (2010), Surface modification of C40 steel using WC-Cu P/M green compact electrodes in EDM , Int. J. Manufacturing Technology and Management, Vol. 21, Nos. 1/2, 83-98.
45. Mohammed B Ndaliman, Ahsan A Khan, Mohammad Y Ali, (2013), Influence of electrical discharge machining process parameters on surface micro-hardness of titanium alloy, Proc IMechE Part B: J Engineering Manufacture, 227(3), 460–464.
46. Mohammed Baba Ndaliman, Ahsan Ali Khan, (2011), Development of Powder Metallurgy (PM) Compacted Cu-TaC Electrodes for EDM, Journal of Mechanics Engineering and Automation, 1, 385-391.
47. B. Jabbaripour, M. H. Sadeghi, Sh. Faridvand, M. R. Shabgard, (2012), Investigating The Effects of EDM Parameters on Surface Integrity, MRR and TWR in Machining of Ti–6Al–4V, Machining Science and Technology, 16:419–444.
48. A. Gangadhar, M. S. Shunmugam, P. K. Philip, (1991), Surface modification in electro discharge processing with a powder compact tool electrode, *Wear,* 143, 45-55.
49. Anirban Bhattacharya, Ajay Batish, Naveen Kumar, (2013), Surface characterization and material migration during surface modification of die steels with silicon, graphite and tungsten powder in EDM process, Journal of Mechanical Science and Technology 27 (1), 133~140.
50. Amoljit Singh Gill, Sanjeev Kumar, (2015), Surface alloying of H11 die steel by tungsten using EDM process, Int J Adv Manuf Technol, 78:1585–1593.
51. Yuan-Feng Chen, Han-Ming Chow, Yan-Cherng Lin, Ching-Tien Lin, (2008), Surface modification using semi-sintered electrodes on electrical discharge machining, Int J Adv Manuf Technol, 36:490–500.
52. Hsin-Jen Chen, Kun-Ling Wu, Biing-Hwa Yan, (2014), Characteristics of Al alloy surface after EDC with sintered Ti electrode and TiN powder additive, Int J Adv Manuf Technol, 72:319–332.
53. A.K. Khanra, B.R. Sarkar, B. Bhattacharya, L.C. Pathak, M.M. Godkhindi, (2007), Performance of ZrB_2–Cu composite as an EDM electrode, Journal of Materials Processing Technology 183, 122–126.

54. Harjot Singh, S.S. Banwait, (2016), Experimental Investigations of Surface Modification of AISI 1045 Die Steel by Electro Discharge Machining Process, American Journal of Mechanical Engineering, 2016, Vol. 4, No. 4, 131-14.
55. Amoljit Singh Gill, Sanjeev Kumar, (2016), Micro-hardness evaluation for surface alloying of H11 die steel with Cu–Cr–Ni powder metallurgy tool in electrical discharge machining , J Engineering Manufacture 1–13.
56. Abhishek Das, Joy Prakash Misra, (2012), Experimental Investigation on Surface Modification of Aluminum by Electric Discharge Coating Process using TiC/Cu Green Compact Tool-Electrode, Machining Science and Technology, 16:4, 601-623, DOI: 10.1080/10910344.2012.731951.
57. M. Eswara Krishna, P. K. Patowari, (2014), Parametric Study of Electric Discharge Coating using Powder Metallurgical Green Compact Electrodes, Materials and Manufacturing Processes, 29:9, 1131-1138, DOI: 10.1080/10426914.2014.930887.
58. P. K. Patowari , U. K. Mishra , P. Saha, P. K. Mishra, (2011), Surface Integrity of C-40 Steel Processed with WC-Cu Powder Metallurgy Green Compact Tools in EDM, Materials and Manufacturing Processes, 26:5, 668-676, DOI: 10.1080/10426914.2010.512652.
59. Yu-Lung Hwang, Chia-Lung Kuo, Shun-Fa Hwang, (2010), The coating of TiC layer on the surface of nickel by electric discharge coating (EDC) with a multi-layer electrode, Journal of Materials Processing Technology, 210, 642–652.
60. J. Simao, H.G. Lee, D.K. Aspinwall, R.C. Dewes, E.M. Aspinwall, (2003), Workpiece surface modification using electrical discharge machining, International Journal of Machine Tools & Manufacture, 43, 121–128.
61. Naveen Beri, Anil Kumar, S. Maheshwari, C. Sharma, (2011), Optimisation of electrical discharge machining process with CuW powder metallurgy electrode using grey relation theory, Int. J. Machining and Machinability of Materials, Vol. 9, Nos. 1/2,103-115.
62. Sanjeev Kumar, Rupinder Singh, (2010), Investigating surface properties of OHNS die steel after electrical discharge machining with manganese powder mixed in the dielectric, Int J Adv Manuf Technol , 50:625–633.
63. N. Mohri, N. Saito, Y. Tsunekawa, (1993), Metal Surface Modification by Electrical Discharge Machining with Composite Electrode, Annals of the ClRP Vol.42/1.
64. Tyagi R, Das AK, Mandal A, (2018), Electrical discharge coating using WS_2 and Cu powder mixture for solid lubrication and enhanced tribological performance, Tribology International, doi: 10.1016/j.triboint.2017.12.023.
65. Yoshiki Tsunekawa, Masahiro Okumiya, Naotake Mohri, (1994), Surface modification of aluminium by electric discharge alloying, Materials Science and Engineering, A174, 193-198.
66. J. S. Soni, G. Chakraverti, (1996), Experimental Investigation on Migration of Material during EDM of Die Steel (T215, Cr12), Journal of Material Processing Technology, 56, 439-451.
67. Eswara Krishna Mussada, P.K. Patowari, (2015), Investigation of EDC parameters using W and Cu powder metallurgical compact electrodes, Int. J. Machining and Machinability of Materials, Vol. 17, No. 1, 65-78.
68. J.W. Murray, R.B. Cook, N. Senin, S.J. Algodi, A.T. Clare , (2017), Defect-free TiC/Si multi-layer electrical discharge coatings. Jmade, doi:10.1016/journal of material design. 2018.06.019.
69. Toshio Moro, Naotake Mohri, Hisashi Otsubo, Akihiro Goto, Nagao Saito, (2004), Study on the surface modification system with electrical discharge machine in the practical usage, Journal of Materials Processing Technology 149, 65–70.
70. B. Mohan, A. Rajadurai, K. G. Satyanarayana, (2002), Effect of SiC and rotation of electrode on electric discharge machining of Al-SiC composite, Journal of Material Processing Technology, 124, 297-304.
71. P. J. Liew, Z. Nurlishafiqa, Q. Ahsan, T. Zhou, J. Yan, (2018), Experimental investigation of RB-SiC using Cu–CNF composite electrodes in electrical discharge machining, The International Journal of Advanced Manufacturing Technology, https://doi.org/10.1007/s00170-018-2417-8.
72. Li Li, Y.S. Wong, J.Y.H. Fuh, L. Lu, (2001), EDM performance of TiC copper-based sintered electrodes, Materials and Design 22, 669- 678.
73. Paras Kumar, Ravi Parkash, (2016), Experimental investigation and optimization of EDM process parameters for machining of aluminium boron carbide (Al–B4C) composite, Machining Science and Technology, 20:2, 330-348, DOI: 10.1080/10910344.2016.1168931.
74. D. Kanagarajan, K. Palanikumar, R. Karthikeyan, (2012), Effect of Electrical Discharge Machining on strength and reliability of WC–30%Co composite, Materials and Design 39, 469–474.
75. S. Chakraborty, S Kar, V Dey, S K Ghosh, (2018), Multi Attribute Decision for Determining Optimum Process Parameters in EDC with Si and Cu Mixed Powders Green Compact Electrode, Journal of Scientific and Industrial Research, vol -77, pp 229-236.

76. Jeykrishnan. J, Vijaya Ramnath. B, Akilesh. S, Pradeep Kumar. R P, (2016), Optimization of process parameters on EN24 Tool steel using Taguchi technique in Electro-Discharge Machining (EDM), IOP Conf. Series: Materials Science and Engineering 149,012022.
77. Nibu Mathew, Dinesh Kumar, (2014), Study of Tool Wear Rate of Different Tool Material during Electric Discharge Machining of H11 Steel at Reverse Polarity, Int. J. Mech. Eng. & Rob. Res. Vol. 3, No. 3, ISSN 2278 – 0149.
78. Parveen Goyal, N M Suri, Sanjeev Kumar, Rajesh Kumar, (2017), Investigating the surface properties of EN-31 die-steel after machining with powder metallurgy EDM electrodes, Materials Today: Proceedings 4, 3694–3700.
79. Amoljit Singh Gill, Sanjeev Kumar, (2015), Surface Alloying by Powder Metallurgy Tool Electrode Using EDM Process, Materials Today: Proceedings 2, 1723 – 1730.
80. Ahad Gholipoor, Hamid Baseri, Mohsen Shakeri, Mohammadreza Shabgard, (2014), Investigation of the effects of magnetic field on near-dry electrical discharge machining performance, Proc IMechE Part B: J Engineering Manufacture, 1–8.
81. Vijaykumar Bhanot, Naveen Beri, Anil Kumar, (2014), Mach inability assessment of Superni-800 during EDM with powder metallurgy processed Cu-Ti electrode using the Taguchi method, All India Manufacturing Technology, Design and Research Conference (AIMTDR 2014), IIT Guwahati, Assam, India.
82. Y.S. Wong , L.C. Lim, Iqbal Rahuman, W.M. Tee, (1998), Near-mirror-finish phenomenon in EDM using powder-mixed dielectric ,Journal of Materials Processing Technology 79, 30–40.
83. Sarabjeet Singh Sidhu, Ajay Batish, Sanjeev Kumar, (2014), Study of Surface Properties in Particulate-Reinforced Metal Matrix Composites (MMCs) Using Powder-Mixed Electrical Discharge Machining (EDM), Materials and Manufacturing Processes, 29: 46–52.
84. Can Cogun, B Ozerkan, T Karacay, (2006), An experimental investigation on the effect of powder mixed dielectric on machining performance in electric discharge machining, J. Engineering Manufacture, 220, 1035-1049.
85. Harmesh Kumar, J. Paulo Davim, (2011), Role of Powder in the Machining of Al10%Sic_p Metal Matrix Composites by Powder Mixed Electric Discharge Machining, Journal of Composite Materials, Vol. 45, 133-151.
86. Banh Tien Long, Ngo Cuong, Nguyen Huu Phan, Pichai Janmanee, (2015), Machining Properties Evaluation of Copper and Graphite Electrodes in PMEDM of SKD61 Steel in Rough Machining, International Journal of Engineering and Advanced Technology, Volume-4, Issue-3, 193-202.
87. Anderson Molinetti, Fred L. Amorim, Paulo César Soares Jr, Tiago Czelusniak, (2015), Surface modification of AISI H13 tool steel with silicon or manganese powders mixed to the dielectric in electrical discharge machining process, Int J Adv Manuf Technol, 10.1007/s00170-015-7613-1.
88. Sanjeev Kumar, Uma Batra, (2012), Surface modification of die steel materials by EDM method using tungsten powder-mixed dielectric, Journal of Manufacturing Processes 14, 35–40.
89. Katsushi Furutani, Hiromichi Sato, Masayuki Suzuki, (2009), Influence of electrical conditions on performance of electrical discharge machining with powder suspended in working oil for titanium carbide deposition process, Int J Adv Manuf Technol, 40:1093–1101.
90. Paulo Pecas, Elsa Henriques, (2008), Effect of the powder concentration and dielectric flow in the surface morphology in electrical discharge machining with powder-mixed dielectric (PMD-EDM), Int J Adv Manuf Technol, 37:1120–1132.
91. Fred L. Amorim, Vitor A. Dalcin, Paulo Soares, Luciano A. Mendes, (2016), Surface modification of tool steel by electrical discharge machining with molybdenum powder mixed in dielectric fluid, Int J Adv Manuf Technol, DOI 10.1007/s00170-016-9678-x.
92. Banh Tien Long, Nguyen Huu Phan, Ngo Cuong, Nguyen Duc Toan, (2016), Surface quality analysis of die steels in powder-mixed electrical discharge machining using titan powder in fine machining Advances in Mechanical Engineering, Vol. 8(7) 1–13.
93. B. Kuriachen, J. Mathew, (2015), Effect of Powder Mixed Dielectric on Material Removal and Surface Modification in Micro Electric Discharge Machining of Ti-6Al-4V, Materials and Manufacturing Processes, DOI: 10.1080/10426914.2015.1004705.
94. Sagar Patel, Dignesh Thesiya, Avadhoot Rajurkar, (2017), Aluminium powder mixed rotary electric discharge machining (PMEDM) on Inconel 718, Australian Journal of Mechanical Engineering, DOI: 10.1080/14484846.2017.1294230.
95. Sanjeev Kumar, Rupinder Singh, T.P. Singh, B.L. Sethi, (2009), Surface modification by electrical discharge machining: A review, Journal of Materials Processing Technology 209, 3675–3687.
96. Min-Seop Han, Byung-Kwon Min, Sang Jo Lee, (2007), Improvement of surface integrity of electro-chemical discharge machining process using powder-mixed electrolyte, Journal of Materials Processing Technology 191, 224–227.

97. H.K. Kansal, Sehijpal Singh, Pradeep Kumar, (2007), Technology and research developments in powder mixed electric discharge machining (PMEDM), Journal of Materials Processing Technology 184, 32–41.
98. Pichai Janmanee, Apiwat Muttamara, (2012), Surface modification of tungsten carbide by electrical discharge coating (EDC) using a titanium powder suspension, Applied Surface Science 258, 7255–7265.
99. Zakaria Mohd Zain, Mohammed Baba Ndaliman, Ahsan Ali Khan, Mohammad Yeakub Ali, (2014), Improving micro-hardness of stainless steel through powder-mixed electrical discharge machining, Proc IMechE Part C: J Mechanical Engineering Science 0(0) 1–7.
100. Kun Ling Wu, Biing Hwa Yan, Fuang Yuan Huang, Shin Chang Chen, (2005), Improvement of surface finish on SKD steel using electro-discharge machining with aluminum and surfactant added dielectric, International Journal of Machine Tools & Manufacture 45, 1195–1201.
101. Gangadharudu Talla, S Gangopadhayay, CK Biswas, (2016), State of the art in powder-mixed electric discharge machining: A review Proc IMechE Part B: J Engineering Manufacture,1–16.
102. Jagdeep Singh, Rajiv K Sharma, (2017), Multi-objective optimization of green powder-mixed electrical discharge machining of tungsten carbide alloy, Proc IMechE Part C: J Mechanical Engineering Science 0(0) 1–13.
103. Anoop Kumar Singh , Sanjeev Kumar, V. P. Singh, (2014), Optimization of Parameters Using Conductive Powder in Dielectric for EDM of Super Co 605 with Multiple Quality Characteristics, Materials and Manufacturing Processes, 29:3, 267-273.
104. Anoop Kumar Singh, Sanjeev Kumar, V. P. Singh, (2014), Effect of the addition of conductive powder in dielectric on the surface properties of superalloy Super Co 605 by EDM process, Int J Adv Manuf Technol, DOI 10.1007/s00170-014-6433-z.
105. Santosh Kumar Sahu, Thrinadh Jadam, Saurav Datta, Goutam Nandi, (2018), Effect of using SiC powder-added dielectric media during electrodischarge machining of Inconel 718 super alloys, Journal of the Brazilian Society of Mechanical Sciences and Engineering, 40:330.
106. Gunawan S. Prihandana,Tutik Sriani, Muslim Mahardika, M. Hamdi, Norihisa Miki, Y. S. Wong, Kimiyuki Mitsui, (2014), Application of powder suspended in dielectric fluid for fine finish micro-EDM of Inconel 718, Int J Adv Manuf Technol DOI 10.1007/s00170-014- 145-4.
107. Chander Prakash, H. K. Kansal, B. S. Pabla, Sanjeev Puri, (2016), Experimental Investigations in Powder Mixed Electric Discharge Machining of Ti-35Nb-7Ta-5Zr β-Titanium Alloy, Materials and Manufacturing Processes, http://dx.doi.org/10.1080/10426914.2016.1198018.
108. Sagar Patel, Dignesh Thesiya, Avadhoot Rajurkar,(2017), Aluminium powder mixed rotary electric discharge machining (PMEDM) on Inconel 718, Australian Journal of Mechanical Engineering, DOI: 10.1080/14484846.2017.1294230.
109. Shalini Mohanty, Vishnu Kumar, Rashi Tyagi, Shakti Kumar, Brij Bhushan, Alok Kumar Das, Amit Rai Dixit, (2018), Surface alloying using tungsten disulphide powder mixed in dielectric in micro-EDM on Ti6Al4V, IOP Conf. Series: Materials Science and Engineering 377, 012040.
110. Marashi Houriyeh, Jafarlou Davoud M, Sarhan Ahmed AD, Hamdi Mohd, (2016), State of the art in powder mixed dielectric for EDM applications. Precision, Engineering http://dx.doi.org/10.1016/j. precision eng, 05.010.
111. Kuang-Yuan Kung, Jenn-Tsong Horng, Ko-Ta Chiang, (2009), Material removal rate and electrode wear ratio study on the powder mixed electrical discharge machining of cobalt-bonded tungsten carbide, Int J Adv Manuf Technol , 40:95–104.
112. Amit Kumar, Amitava Mandal, Amit Rai Dixit, Alok Kumar Das, (2017), Performance Evaluation of Al_2O_3 Nano Powder Mixed Dielectric for Electric Discharge Machining of Inconel 825, Materials and Manufacturing Processes, DOI: 10.1080/10426914.2017.1376081.
113. Murahari Kolli, Adepu Kumar, (2015), Surfactant and graphite powder assisted electrical discharge machining of titanium alloy, Proc IMechE Part B: J Engineering Manufacture,1–17.
114. Pichai Janmanee, Apiwat Muttamara, (2012), Surface modification of tungsten carbide by electrical discharge coating (EDC) using a titanium powder suspension, Applied Surface Science 258, 7255–7265.
115. Mahendra G. Rathi, Deepak V. Mane, (2014), Study on Effect of Powder Mixed dielectric in EDM of Inconel 718, International Journal of Scientific and Research Publications, Volume 4, Issue 11.
116. Nimo Singh Khundrakpam, Gurinder Singh Brar, Dharmpal Deepak, (2018), A Comparative Study on Machining Performance of wet EDM, Near Dry EDM and Powder Mixed Near Dry EDM, International Journal of Applied Engineering Research, ISSN 0973-4562, Volume 13, Number 11, pp. 9378-9381.

117. Bulent Ekmekci, Hamidullah Yasar, Nihal Ekmekci, (2016), A Discharge Separation Model for Powder Mixed Electrical Discharge Machining, Journal of Manufacturing Science and Engineering, Vol-138 / 081006-1.
118. Nihal Ekmekci, Bulent Ekmekci, (2015), Electrical Discharge Machining of Ti6Al4V in Hydroxyapatite Powder Mixed Dielectric Liquid, Materials and Manufacturing Processes, DOI: 10.1080/10426914.2015.1090591.
119. Hamid Baseri, Samin Sadeghian, (2016), Effects of nano powder TiO2-mixed dielectric and rotary tool on EDM, Int J Adv Manuf Technol, 83:519–528.
120. Xue Bai, Qin-He Zhang, Ting-Yi Yang, Jian-Hua Zhang, (2013), Research on material removal rate of powder mixed near dry electrical discharge machining, Int J Adv Manuf Technol DOI 10.1007/ s00170-013-4973-2.
121. Ulas Caydas, Ahmet Hascalik, (2008), Modeling and analysis of electrode wear and white layer thickness in die-sinking EDM process through response surface methodology, Int J Adv Manuf Technol, 38:1148–1156.
122. C. Velmurugan, R. Subramanian, S. Thirugnanam, B. Ananadavel, (2011), Experimental investigations on machining characteristics of Al 6061 hybrid metal matrix composites processed by electrical discharge machining, International Journal of Engineering, Science and Technology Vol. 3, No. 8, pp. 87-101.
123. Nor Ain binti Jamil Hosni, Mohd Amri bin Lajis, Muhammad Ridzuan bin Idris, (2018), Modelling and Optimization of Chromium Powder Mixed EDM Parameter Effect Over the Surface Characteristics by Response Surface Methodology Approach, International Journal of Engineering Materials and Manufacture, 3(2) 78-86.
124. Ramesh S, M.P. Jenarthanan, Bhuvanesh Kanna A.S, (2018), Experimental investigation of powder mixed electric discharge machining of AISI P20 steel using different powders and tool materials, Multidiscipline Modelling in Materials and Structures, https://doi.org/10.1108/MMMS-04-2017-0025.
125. S. Kumar, A. K. Dhingra, (2018), Effects of Machining Parameters on Performance Characteristics of Powder Mixed EDM of Inconel-800, International Journal of Automotive and Mechanical Engineering, Volume 15, Issue 2 pp. 5221-5237.
126. Naveen Beri, Sachin Maheshwari, Chitra Sharma, Anil Kumar, (2014), Surface Quality Modification using Powder Metallurgy Processed CuW Electrode during Electric Discharge Machining of Inconel 718, Procedia Material Science, 5, 2629-2634.
127. S. Assarzadeh, M. Ghoreishi, (2013), A dual response surface-desirability approach to process modeling and optimization of Al2O3 powder-mixed electrical discharge machining (PMEDM) parameters, Int J Adv Manuf Technol, 64:1459–1477.
128. Soumyakant Padhee, Niharranjan Nayak, S. K. Panda, P. R. Dhal, S. S. Mahapatra, (2012), Multi-objective parametric optimization of powder mixed electro-discharge machining using response surface methodology and non-dominated sorting genetic algorithm, Sadhana, Vol. 37, Part 2, pp. 223–240.
129. T. A. El-Taweel, (2009), Multi-response optimization of EDM with Al–Cu–Si–TiC P/M composite electrode, Int J Adv Manuf Technol, 44:100–113.
130. ChittaranjanDas. V, (2016), Response surface Methodology and Desirability Approach to Optimize EDM Parameters, International Journal of Hybrid Information Technology Vol.9, No.4, pp. 393-406.
131. S. Tripathy, D.K. Tripathy, (2016), Multi-attribute optimization of machining process parameters in powder mixed electro-discharge machining using TOPSIS and grey relational analysis, Engineering Science and Technology, an International Journal 19, 62–70.
132. P. Balasubramanian, T. Senthilvelan, (2014), Optimization of Machining Parameters in EDM process using Cast and Sintered Copper Electrodes, Procedia Materials Science 6, 1292 – 1302.
133. Jagdeep Singh, Rajiv Kumar Sharma, (2016), Assessing the effects of different dielectrics on environmentally conscious powder-mixed EDM of difficult-to machine material (WC-Co), Front. Mech. Eng. DOI 10.1007/s11465-016-0388-8.
134. S. Singh, M.F Yeh. (2012), Optimization of Abrasive Powder Mixed EDM of Aluminium Matrix Composites with Multiple Responses Using Gray Relational Analysis, Journal of Materials Engineering and Performance, 21:481–491.
135. Rajiv Kumar Sharma, Jagdeep Singh, (2014), Determination of multi-performance characteristics for powder mixed electric discharge machining of tungsten carbide alloy, Proc IMechE Part B: J Engineering Manufacture,1–10.
136. V Vikram Reddy, P Madar Valli, A Kumar, Ch Sridhar Reddy, (2014), Multi-objective optimization of electrical discharge machining of PH17-4 stainless steel with surfactant-mixed and graphite

powder–mixed dielectric using Taguchi-data envelopment analysis–based ranking method, Proc IMechE Part B: J Engineering Manufacture,1–8.
137. Ramprabhu T, Vimal Savsani, Sohil Parsana, Nishil Radadia, Mohak Sheth, Nisarg Sheth, (2018), Multi-Objective Optimization of EDM Process Parameters by Using Passing Vehicle Search (PVS) Algorithm, Defect and Diffusion Forum, Vol. 382, pp 138-146.
138. Sohil Parsana, Nishil Radadia, Mohak Sheth, Nisarg Sheth, Vimal Savsani, N. Eswara Prasad, T. Ramprabhu, (2018), Machining parameter optimization for EDM machining of Mg–RE–Zn–Zr alloy using multi-objective Passing Vehicle Search algorithm, Archives of Civil and Mechanical Engineering, I-8, 799-817.
139. Huu-Phan Nguyen, Van-Dong Pham, Ngoc-Vu Ngo, (2018), Application of TOPSIS to Taguchi method for multi-characteristic optimization of electrical discharge machining with titanium powder mixed into dielectric fluid, The International Journal of Advanced Manufacturing Technology, https://doi.org/10.1007/s00170-018-2321-2.
140. Anil Kumar , S. Maheshwari , C. Sharma, Naveen Beri, (2010), A Study of Multi objective Parametric Optimization of Silicon Abrasive Mixed Electrical Discharge Machining of Tool Steel, Materials and Manufacturing Processes, 25:10, 1041-1047.
141. Satish Kumar, Ashwani Kumar Dhingra, Sanjeev Kumar, (2017), Parametric optimization of powder mixed electrical discharge machining for nickel based super alloy inconel-800 using response surface methodology, Mechanics of Advanced Materials and Modern Processes, 3:7, 1-17.
142. Ved Raj Khullar, Neeraj Sharma, Sugal Kishore, Renu Sharma, (2017), RSM- and NSGA-II-Based Multiple Performance Characteristics Optimization of EDM Parameters for AISI 5160, Arab J Sci Eng DOI 10.1007/s13369-016-2399-5.
143. D Kanagarajan, R Karthikeyan, K Palanikumar, P Sivaraj, (2008), Influence of process parameters on electric discharge machining of WC/30%Co composites, Proc. IMechE Vol. 222 Part B: J. Engineering Manufacture, DOI: 10.1243/09544054JEM925.
144. Jagdeep Singh, Rajeev Kumar Sharma, (2016), Study of surface modification and characterization of powder mixed electric discharge machining of tungsten carbide, 2016, Indian Journal of Engineering and Material Sciences, vol- 23, 321-335.
145. Dr Xuan-Phuong Dang, (2017), Constrained Multi-Objective Optimization of EDM Process Parameters Using Kriging Model and Particle Swarm Algorithm, Materials and Manufacturing Processes, DOI: 10.1080/10426914.2017.1292037.
146. Sunil Sheshrao Baraskar , S. S. Banwait, S. C. Laroiya, (2013), Multiobjective Optimization of Electrical Discharge Machining Process Using a Hybrid Method, Materials and Manufacturing Processes, 28:4, 348-354.
147. P. Mathan Kumar, K. Sivakumar, N. Jayakumar, (2017), Multi objective optimization and analysis of copper–titanium diboride electrode in EDM of monel 400 alloy, Materials and Manufacturing Processes, DOI: 10.1080/10426914.2017.1415439.
148. Farhad Kolahan, Mohammad Bironro, (2008), Modeling and Optimization of Process Parameters in PMEDM by Genetic Algorithm, proceeding of world academy of science, engineering and technology vol-36, ISSN-2070-3740.
149. Bikramjit Singh, Chandan Deep Singh, Jaswinder Singh, (2015), Optimization of Chromium Mixed Powder EDM parameters using Response Surface Methodology for H13 Tool steel Machining, International Journal of Multidisciplinary and Scientific Emerging Research, Vol.4, No.2.
150. Kanwal Jit Singh, (2018), Optimization of process parameters of powder mixed EDM for high carbon high chromium alloy steel (D2 steel) through GRA approach, Grey Systems: Theory and Application, https://doi.org/10.1108/GS-01-2018-0001.
151. Ross, P.J. (1988), "Taguchi techniques for quality engineering", McGraw-Hill Book Company, New York.
152. Roy, R.K. (2001), "Design of Experiments Using the Taguchi approach" Canada John Wiley & Sons.
153. Roy, R.K. (1990), "A primer on Taguchi method", Van Nostrand Reinhold, New York.
154. Singh, H. and Kumar, P. (2006), "Optimizing multi-machining characteristics through Taguchi‟s approach and utility concept", Journal of Manufacturing Technology Management, 17, 36-45.
155. Dr. S. S. Khandare and Mitesh a. Popat (2009), Experimental Investigations of EDM to optimize Material Removal Rate and Surface Roughness through Taguchi's Technique of Design of Experiments. IEEE explore, ICETET-09, pg 476 – 482 Print ISBN: 978-1-4244-5250-7.
156. Mahapatra, S. and Patnaik, A. (2006), "Parametric optimization of wire electrical discharge machining (wedm) process using Taguchi method", J. of the Braz. Soc. of Mech. Sci. & Eng., 28, 422-429.

157. Mahapatra, S. S. and Patnaik, A. (2007), “Optimization of wire electrical discharge machining (WEDM) process parameters using Taguchi method”, International Journal of Advanced Manufacturing Technology, 34, 911-925.
158. Sanjeev Kumar and Rupinder Singh, (2010), Investigating surface properties of OHNS die steel after electrical discharge machining with manganese powder mixed in the dielectric, Int J Adv Manuf Technol (2010) 50:625–633
159. Rudorff, D.W. (1957), “Principles and Applications of Spark Machining”, Proc. Instrumentation Mechanical Engineering, London, 171/14, 495.
160. S.T. Jilani and P.C.Pandey. Analysis and modeling of edm parameters. Precision Engg., pages 215{221, 1982.
161. Bhattacharya S., Kanshawy M.E., Carber S., Wallbank J. (1981), “A Correlation between Machining Parameters and Machinability in EDM”, Int. J. Prod. Res., 19/2, 111.
162. Lee S. H., Li, S.P. (2001), “Study l of the effect of machining parameters on the machining characteristics in Electrical Discharge Machining of Tungsten Carbide”, J. of materials processing technology, 115, 344-358.

List of Publications

1. J. L. Ramdatti, A. V. Gohil, (2016), "Trends in surface modification of cold work die steel using electrical discharge machining: A review", International Journal of Engineering Applied Sciences and Technology, Vol. 1, Issue 10, ISSN NO. 2455-2143, pp. 120-126. (UGC Approved Journal)
2. J. L. Ramdatti, A. V. Gohil, (2019), "A Grey Relational Analysis Approach for Multi-objective Optimization of EDM Process of P20+Ni Die Steel Using P/M Composite Electrode", International Journal of Research and Analytical Reviews, Vol. 6, Issue 1, ISSN NO. 2348-1269, pp. 1-6. (UGC Approved Journal)
3. J. L. Ramdatti, A. V. Gohil, (2019), "Performance Evaluation of Composite Powder Metallurgy Electrode on P20+Ni Steel Using Electric Discharge Machining", International Journal of Technical Innovation in Modern Engineering & Science (IJTIMES), Vol. 5, Issue 3, ISSN NO. 2455-2585, pp. 251-256. (UGC Approved Journal)
4. Ramdatti J. L., Gohil A. V. (2020), "Optimization of Surface Modification Phenomenon for P20+Ni Die Steel Using EDM with P/M Composite Electrode". Advances in Intelligent system and Computing, Vol 949. pp 689-697.https://doi.org/10.1007/978-981-13-8196-6_60. Springer, Singapore.
5. J. L. Ramdatti, A. V. Gohil (2018), "Optimization of surface modification phenomenon for P20+Ni die steel using EDM with P/M composite electrode" proceedings of international conference on Advanced Engineering Optimization through Intelligent Techniques (AEOTIT), August 3-5, S. V. National Institute of Technology, Surat.
6. J. L. Ramdatti, A. V. Gohil, K. G. Dave (2019), "Experimental investigation on electro-discharge surface modification phenomenon of P20+Ni die steel using green P/M composite electrode", Journal of Mechanical Engineering and Sciences, Universiti Malaysia Pahang, Malaysia. Scopus indexed journal. (Under review)
7. Ramdatti J. L., Gohil A. V., Jain Vineet and Dave K. G. (2020) 'Performance Evaluation of Cu-W-Si Green P/M Composite Electrode for Surface Modification of P20+Ni Steel using Electrical Discharge Machine', *Int. J. Machining and Machinability of Materials*, Inderscience Publications (Accepted for publication).

APPENDIX – A
TECHNICAL SPECIFICATION OF THE EDM MACHINE

Experimental work related to surface modification was performed on die sinker EDM model M25-6040 (Make: Maruti machine tools, Baroda, India). The EDM machine was installed at work shop of Government Engineering College, Bhavnagar, Gujarat, India. The die sinker EDM has following specifications:

Size of Oil Container	:	650 X 400 X 300 mm
Table Size	:	400 X 250 mm
X Axis travel	:	250 mm
Y Axis travel	:	150 mm
Z Axis travel	:	150 mm
Maximum job height	:	165 mm
Maximum job weight	:	150 kg
Maximum current	:	25 Amp
Best MMR	:	140 mm^3
Connected load	:	2 KVA
die electric tank capacity	:	200 ltr
Supply Volts	:	415 V, 3 Ø, 50 Hz
Maximum Table-Quill distance	:	340 mm
Minimum Table-Quill distance	:	190 mm

APPENDIX – B

IMPORTANT PROPERTIES OF ELEMENTS INVOLVED IN EXPERIMENTATION

(All values at 25°C)

Element	Atomic Number	Atomic Weight	Density (g/cm^3)	Melting Point (°C)	Thermal Conductivity (W/cm °C)	Electrical Resistivity (μΩ cm)	Specific Heat (J/g °C)
Copper	29	63.55	8.96	1083.4	3.98	1.673	0.385
Tungsten	74	183.85	19.35	3410	1.78	5.65	0.133
Silicon	14	28.09	2.33	1410	0.835	10.0	0.703
Carbon	6	12.011	2.25	3550	0.238	1375	0.712
Iron	26	55.84	7.86	1535	0.803	9.71	0.444

APPENDIX – C
IMPORTANT SPECIFICATIONS OF MEASURING INSTRUMENTS USED IN EXPERIMENTATION

1. Computerized Vickers microhardness tester:

Make and model	:	Vaisesika, Model No. 7005 – B
Hardness measuring range	:	5-3000HV
Test Loads	:	10, 20, 50, 100, 200, 300, 500 gf
Maximum Test Height	:	30 mm with clamping vice
Sample Stage (XY stage) with micrometer heads of 0.01 LC	:	10mm movement in each axis
Clamping vice capacity	:	40mm max.
Scale least count	:	0.0001 mm
Machine dimensions	:	L 450 X W 275 X H 535 mm (Aprox)
Weight (approx.)	:	48 kgs
Measuring Range	:	0.01 to 0.2 mm

2. Laboratory High Precision Balance:

Make and model	:	WENSAR, HPB 1000H
Capacity	:	1000 gm
Readability	:	0.001 gm
Pan size	:	120 mm
Display	:	Large Backlight Display
Calibration	:	Auto external

3. Surface Roughness Measurement Tester:

Make and model	:	ITI- India, Surf test RS-232
Measuring range	:	17.5 mm
Measuring speed	:	0.25, 05, 0.75 mm/s
Detector Range	:	360µ
Measuring methods	:	Skidded
Measuring force	:	0.75mN
Stylus tip		Diamond, 90° / 5µmR

4. X-Ray Diffractometer System:

Make and model	:	BRUKER, D2 PHASER
Geometry	:	Theta / Theta
Max. useable angular range	:	-3 … 160 ° 2Theta (depending on detector)
Accuracy	:	± 0.02° throughout the entire measuring range
Achievable peak width	:	< 0.05°
X-ray wavelengths	:	Cr / Co / Cu, standard ceramic sealed tube
X-ray generation	:	30 kV / 10 mA
Radiation level	:	<< 1mSv/h
Detectors	:	Scintillation counter, XFlash® detector, 1-dimensional LYNXEYE
Sample motion	:	Spinner
Instrument type	:	Portable, desktop
Exterior Dimension	:	61 x 60 x 70 cm (h x d x w), 24.02” x 23.62” x 27.56”
Weight	:	95 kg
Power supply	:	90 – 250 V
Computer	:	Built-in, optional additional PC connected via LAN interface

5. Scanning Electron Microscope:

Make and model	:	JEOL, JSM-6010 LA
Secondary electron image resolution	:	0.8 nm (Accelerating voltage 15kv)
Magnification	:	X25 to X1000000
Accelerating voltage	:	0.1 to 30 kv
Specimen holder	:	12.5 mm diameter x 10 mm thick
Image observation LCD	:	Screen size: 23 inch wide Maximum resolution: 1280 x 1024 pixels
SEM control system	:	PC: IBM PC/AT compatible computer with window-7
Ultimate pressure	:	Gun chamber: 10^{-7} pa Specimen chamber: 10^{-4} pa

6. EDM oil:

Make and type	:	Make: Pacific, USA, Type: EDM 300 oil
Specific gravity at 30 °C	:	0.757
Flash point °C	:	108
Pour point °C	:	0
Viscosity cSt at 40 °C	:	3.1
Di-electric strength	:	40

APPENDIX – D

STANDARD L30 ORTHOGONAL ARRAY AS PER CENTRAL COMPOSITE DESIGN OF RESPONSE SURFACE METHODOLOGY

Experiment No.	Process Parameters			
	C_p	I_p	T_{on}	τ
1	-1	-1	-1	-1
2	1	-1	-1	-1
3	-1	1	-1	-1
4	1	1	-1	-1
5	-1	-1	1	-1
6	1	-1	1	-1
7	-1	1	1	-1
8	1	1	1	-1
9	-1	-1	-1	1
10	1	-1	-1	1
11	-1	1	-1	1
12	1	1	-1	1
13	-1	-1	1	1
14	1	-1	1	1
15	-1	1	1	1
16	1	1	1	1
17	-2	0	0	0
18	2	0	0	0
19	0	-2	0	0
20	0	2	0	0
21	0	0	-2	0
22	0	0	2	0
23	0	0	0	-2
24	0	0	0	2
25	0	0	0	0
26	0	0	0	0
27	0	0	0	0
28	0	0	0	0
29	0	0	0	0
30	0	0	0	0